The Role of the Proneural Transcription Factor ASCL1 in Neuroblastoma Cell Division and Differentiation

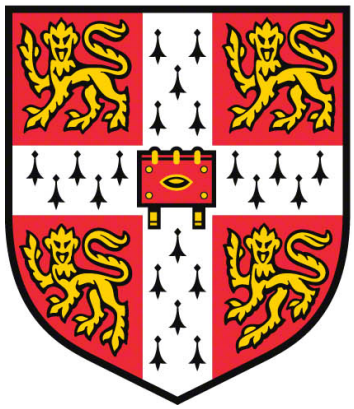

Lydia Mary Parkinson

Department of Oncology

University of Cambridge

This Thesis is submitted for the degree of

Doctor of Philosophy

Clare College

September 2021

Declaration

This thesis is the result of my own work and includes nothing which is the outcome of work done in collaboration except as declared in the Preface and specified in the text. I further state that no substantial part of my thesis has already been submitted, or is being concurrently submitted for any such degree, diploma or other qualification at the University of Cambridge or any other University or similar institution except as declared in the Preface and specified in the text. It does not exceed the prescribed word limit of 60,000 words.

Lydia Parkinson

September 2021

Acknowledgements

Firstly, I would like to thank my supervisor, Professor Anna Philpott. I will never be able to thank you enough for giving me this opportunity. Thank you for your support and guidance over the past four years - of course you were right about everything; I should have written my figure legends as I was going along and yes, I should have read all those papers years ago! Thank you for always encouraging me to speak my mind and stick up for what I think is right!

I would like to thank everyone in the Philpott lab for their support and friendship over the past four years. I am especially thankful to Daniel for his incredible teaching and continuous patience in my first year and Lewis for all the ideas, advice and for being the friend every PhD student needs. I would like to thank Laura for all her bioinformatics help and Clara, Roberta, Lidiya, Fahad, Will and Fani for making my time in the lab enjoyable.

Thank you to the Cambridge Cancer Centre for generously funding my work. I would like to thank the core facilities teams at both the Hutchison Research Centre and the Jeffry Cheah Biomedical Centre – Shout out to Terry for always having a brilliant story to share.

I would like to thank my family; my Mum and sister Charlotte for your endless support and interest into everything I do, I really do appreciate it. Also, my Dad and Paula and Sally and Chris. Special thanks to my Nan and Grandad for always telling me (and all your friends!) how proud you are of me, remembering this really does keep me going. You can all read this and finally understand what I have spent the last four years going on about!

I would like to thank my friend Laura for always being there, for listening to my excitement when things were going well and never complaining when I just needed a walk and a rant. Cheers for always knowing when a cold bottle of Chenin would make everything better. Also thanks to Jonathan and Jonty for their friendship and for being brilliant social distractions.

Lastly I would like to thank my partner, Luke. You have been my absolute rock over the last four years. Sticking with me through a PhD and three lockdowns? I don’t know how you have done that and still maintained the ability to make me laugh when everything seemed terrible. I absolutely couldn’t have done this without your unfaltering support (emotionally and financially!).

Abstract

Neuroblastoma is the most common solid childhood cancer and typically has a very poor prognosis. Neuroblastoma is a 'cancer of improper development' and is thought to arise from sympathetic neuroblast precursors that fail to engage the neuronal differentiation programme; instead they are locked in a pro-proliferative developmental state. Neuroblastomas are epigenetically regulated, a core regulatory circuit (CRC) of transcription factors maintaining their highly proliferative, developmental state. In subtype MS neuroblastoma, tumours can spontaneously regress, in which case children are cured for life. The mechanisms behind spontaneous regression are poorly understood, but the main hypothesis is that the cells enter a terminal differentiation programme. Thus, harnessing the latent differentiation capacity of neuroblasts provides an exciting therapeutic avenue for drug induced cell differentiation and tumour clearance in neuroblastoma.

ASCL1 is a master transcriptional regulator which modulates both proliferation and differentiation of sympathetic neuroblast precursor cells. During development, ASCL1 is transiently expressed and is downregulated as cells differentiate into mature sympathetic neurones. In high-risk neuroblastomas, the levels of ASCL1 remain high, supporting proliferation. The aim of this project was to understand the effect of ASCL1 deletion on neuroblastoma cell behaviour. CRISPR technology was used to remove ASCL1 from three different neuroblastoma cell lines to study the effect of losing ASCL1 in different cellular contexts.

It was found that ASCL1 deletion results in slower cell growth, a phenotype consistent in all neuroblastoma cell lines tested. Studies show no difference in the transcription and expression of the CRC transcription factors, but instead their ability to bind to regulatory regions of chromatin is compromised. RIME analysis shows that ASCL1 binds components of the CRC on the chromatin suggesting ASCL1 could be directly recruiting targets. ASCL1 is considered a pioneer factor and ATAC-Seq analysis shows that chromatin accessibility is reduced in the ASCL1 knock-out lines, suggesting ASCL1 could be limiting both chromatin accessibility and directly recruiting transcription factors to the chromatin. In addition to these findings, when analysing RNA-Seq and ATAC-Seq data it appears ASCL1 maintains neuroblastoma cells in a state which is primed for differentiation. Taken together these results suggest ASCL1 has a dual role in neuroblastoma, supporting both the proliferative state and also poising cells for differentiation.

Table of Contents

List of Figures

Chapter 1 Introduction

Chapter 2 Successful Knockout of ASCL1 in Three Neuroblastoma Lines

Chapter 3 The Effect of Losing ASCL1 on the Core Regulatory Circuit

Chapter 4 Genome Wide Changes Following ASCL1 Knockout

Chapter 5 Reintroducing ASCL1 into Knockout Lines

Chapter 6 Conclusions and Future Work

Chapter 7 Materials and Methods

List of Tables

Abbreviations

°C	Degrees Centigrade
ADRN	Adrenergic
ASCL1	Achaete-Scute Family bHLH Transcription Factor 1
ATAC	Assay for Transposase-Accessible Chromatin
BCA	Bicinchoninic Acid
bHLH	Basic Helix Loop Helix
BMP	Bone Morphagenetic Protein
BSA	Bovine Serum Albumin
CDK	Cyclin Dependant Kinase
CDKi	Cyclin Dependant Kinase Inhibitor
cDNA	Complementary DNA
ChIP	Chromatin Immunoprecipitation
CRC	Core Regulatory Circuit
CRISPR	Clustered Regularly Interspaced Short Palindromic Repeats
DBH	Dopamine-β-Hydroxylase
ddH2O	Double Distilled H2O
DMSO	Dimethyl Sulfoxide
DNA	Deoxynucleic Acid
E-box	Ephrussi-box
EMT	Epithelial to Mesenchymal Transition
FACS	Fluorescence Activated Cell Sorting
FBS	Fetal Bovine Serum
FDR	False Discovery Rate
GBM	Glioblastoma
gDNA	Genomic DNA
GFP	Green Fluorescent Protein
GO	Gene Ontology
H3K27ac	Histone H3 Lysine27 Acetylation
bHLH	Basic Helix-Loop-Helix
IF	Immunofluorescence
INRG	International Neuroblastoma Risk Group
IP	Immunoprecipitation
kb	Kilobase
kDA	Kilodalton
KO	Knockout
LDS	Lithium Dodecyl Sulfate
LN2	Liquid Nitrogen
LogFC	Log Fold Change
mAB	Monoclonal Antibody
MES	Mesenchymal

MIBG	Meta-Iodobenzylguanidine
µl	Microlitre
mM	Millimolar
MOI	Multiplicity of Infection
mRNA	Messenger RNA
NCC	Neural Crest Cell
NEPC	Neuroendocrine Prostate Carcinoma
PAC	Prostate Adenocarcinoma
PBS	Phosphate Buffered Saline
PCA	Principal Component Analysis
PCR	Polymerase Chain Reaction
Pen-Strep	Penicillin-Streptomycin
PHOX2A	Paired Like Homeobox 2A
PHOX2B	Paired Like Homeobox 2B
PI	Propidium Iodide
PIC	Protease Inhibitor Cocktail
qPCR	Quantitative Polymerase Chain Reaction
RA	Retinoic Acid
RIME	Rapid immunoprecipitation mass spectrometry of endogenous protein
RNA	Ribonucleic Acid
RNase	Ribonuclease
RT-PCR	Reverse Transcriptase Polymerase Chain Reaction
S-A	Serine to Alanine (Phosphomutant ASCL1)
SCLC	Small Cell Lung Cancer
sgRNA	Single Guide RNA
SNS	Sympathetic Nervous System
SP	Serine Proline
TBS	Tris Buffered Saline
TCT	Tetracycline Controlled Transactivator
TE	Tris EDTA
TERT	Telomerase Reverse Transcriptase
TF	Transcription Factor
TH	Tyrosine Hydroxylase
TRE	Tetracycline Response Element
TSS	Transcriptional Start Site
WT	Wildtype

Chapter 1

Introduction

1.1 Introduction to Neuroblastoma

1.1.1 Neuroblastoma Background

Neuroblastoma is a paediatric cancer that affects the sympathetic nervous system (Johnsen et al., 2019; Matthay et al., 2016). In developed countries, neuroblastoma is the most frequently diagnosed extracranial solid cancer in children younger than one year, approximately 100 children in the UK are diagnosed with neuroblastoma annually (Maris, 2010; Childhood Cancer Statistics, England Annual report 2018). Neuroblastomas exhibit a wide range of clinical features and prognosis can vary hugely. Some neuroblastomas are capable of spontaneous regression and require no treatment whereas the high-risk forms of neuroblastoma can be devastating (Maris, 2010). Despite improvements in understanding, therapies and treatment, neuroblastoma is still responsible for 15% of paediatric cancer deaths (Johnsen et al., 2019).

At diagnosis, patients can present with a variety of symptoms. Some patients will be asymptomatic, and some will have mild symptoms such as body aches or constipation. In some cases, patients may have severe abdominal pain and visible tumour masses (Maris, 2010). At diagnosis, tumours commonly present in the adrenal glands, but as neuroblastoma is a cancer of the sympathetic nervous system, tumours can arise at various locations in the body (Matthay et al., 2016).

Many factors are believed to impact the prognosis of neuroblastoma. MYCN amplification in neuroblastomas was first reported in the 1980s and was associated with poor prognosis and advanced disease (Brodeur et al., 1984; Seeger et al., 1985). Today, MYCN amplification is observed in around 20% of neuroblastomas and is still used as a marker associated with high-risk disease (Matthay et al., 2016). In addition to this, children who are diagnosed before the age of 1 year have a much higher survival rate and tumours are much more likely to undergo spontaneous regression, than those who are diagnosed later (Childhood Cancer Statistics, England Annual report 2018; Nakagawara et al., 2018). The site of origin of neuroblastoma has also been shown to be important

in neuroblastoma status. Adrenal tumours are the most common and have the worst overall survival rates compared to tumours which arise at other sites (Sung et al., 2009; Vo et al., 2014). Neuroblastomas with an adrenal origin are more likely to have features associated with a poorer outcome, such as MYCN amplification, higher rates of metastasis and a less differentiated phenotype (Vo et al., 2014).

As mentioned, not all neuroblastomas are high risk. Some neuroblastomas are capable of spontaneous regression and require no treatment. These are known as MS (historically 4S) neuroblastomas. MS neuroblastoma was first reported in 1971 and was described as "spontaneous differentiation and regression of tumours with no need for chemotherapy or other treatment" (D'Angio et al., 1971). This phenomenon only occurs in patients that are less than one year old and long-term survival is nearly 100% if the tumours undergo spontaneous regression (Spix et al., 2006). MS neuroblastoma patients have multiple tumours which arise at multiple sites across the sympathetic nervous system, including the adrenal gland, skin and liver but patients do not have tumours in the bone marrow (van Noesel, 2012). Other cancers also exhibit the regression phenomenon, but neuroblastoma shows the highest rate of regression of any human cancer (Ratner et al., 2016).

Mechanisms behind spontaneous regression are poorly understood. Theories include differentiation, apoptosis, epigenetic regulation or immune system clearance. For example, TrkA is a receptor involved in the development of the sympathetic nervous system (SNS) and high TrkA expression is found on low-risk neuroblastomas (Brodeur et al., 1997). *In Vitro* studies show TrkA expressing cells will differentiate if exposed to neuronal growth factor, or die via apoptosis if this is removed, supporting differentiation or apoptosis as potential pathways behind neuroblastoma regression (Brodeur and Bagatell, 2014).

The role of the immune system in clearing neuroblastoma is not well understood. In some patients, neuroblastoma regression follows an infection and immune system activation, and in some cases, the presence of immune cells and anti-tumour antibodies have been identified. In addition to this, high-risk neuroblastomas have very low levels of HLA antigens on their surface which could help them escape recognition by the immune system (Raffaghello et al., 2005). In contrast, the levels of these antigens in MS neuroblastoma cells are comparable to the levels observed on adrenal tissues (Squire et al., 1990).

The epigenetic landscape of neuroblastoma may also play a role in tumour regression. The methylation profiles of high-risk tumours and those that undergo spontaneous regression are very distinct. For example, in neuroblastomas that regress, genes that are associated with differentiation are hypo-methylated. This means they will be less methylated, so more accessible and therefore transcribed and expressed at a higher level (Decock et al., 2016). There are many potential mechanisms and pathways underlying spontaneous regression and could be more than one occurring. Understanding the reasons why spontaneous regression occurs and exploiting it could be very promising for future treatments.

1.1.2 Neuroblastoma Diagnosis and Screening

Neuroblastoma is commonly diagnosed using radiolabelled meta-iodobenzylguanidine (MIBG). MIBG is detected and taken up by the noradrenaline receptor on sympathetic neurones and stored within cells. Neuroblastoma cells express the noradrenaline receptor and MIBG screening detects neuroblastomas with high sensitivity and specificity (Rufini et al., 2006; Vik et al., 2009). Detection of catecholamine metabolites in the urine is another way of screening for neuroblastoma. Catecholamine is a metabolite of neurones, and neuroblastoma cells will often have defects in the catecholamine synthesis pathway. This results in neuroblastoma patients exhibiting an increased level of the catecholamine metabolites vanillylmandelic acid and homovanillic acid in the urine. This is not true for all neuroblastoma patients but is a quick and non-invasive way of screening for neuroblastoma (Nakagawara et al., 2018; Smith et al., 2010).

In Japan, Canada and Germany, catecholamine screening of babies less than one year old has been trialled with the aim of detecting high-risk neuroblastoma patients at an early stage, before tumours progress to the advanced disease (Ajiki et al., 1998.; Schilling et al., 2002; Woods et al., 2002). However, the screening mostly identified low risk neuroblastomas, with a good prognosis and no need for medical intervention. Some children involved in the study who tested negative, later went on to develop high-risk neuroblastoma. When they were diagnosed, they had presence of catecholamine in their urine, suggesting catecholamine metabolites are only detectable when high-risk neuroblastomas are clinically apparent (Schilling et al., 2002; Woods et al., 2002). These studies propose that there are two forms of neuroblastoma, they are either high or low risk. Low risk tumours do not progress to a more lethal form, so detecting low risk patients at an early stage has no effect on the mortality of high-risk patients (Woods et al., 1996).

These studies gave insights about the occurrence of neuroblastoma and neuroblastoma regression. It is estimated the screening programmes identified 50% more children with neuroblastomas than in control groups, but these children presented with low-risk neuroblastomas which had a good prognosis. Many of the neuroblastomas identified in this study never became clinically apparent and would have otherwise gone undetected, indicating a higher incidence of neuroblastoma and potentially a higher rate of spontaneous regression than is recorded (Nakagawara et al., 2018; Woods et al., 1996). The results of these studies show that children who were diagnosed with neuroblastomas, that may have otherwise spontaneously regressed, were likely to be at more risk from the side effects of treatments administered after diagnosis (Schilling et al., 2002). The increased risk to these children far outweighed any small benefits that would be gained from routine neuroblastoma screening (Ajiki et al., 1998). Since ending the screening programme in Japan there has been a reduction in overall cases of neuroblastoma detected, but no significant increase in the number children diagnosed with high-risk neuroblastoma, further supporting the belief that mass screening does not benefit or improve overall survival of high-risk patients (Ioka et al., 2016).

1.1.3 Neuroblastoma Classification

A new neuroblastoma classification system was introduced in 2008, the 'International Neuroblastoma Risk Group (INRG) Staging System' studied children from Europe, America and Japan to produce a scale of neuroblastoma risk (Monclair et al., 2009). One of the main drivers of this was to standardise neuroblastoma classification across the world, to enable clinical trial comparisons to be made across different regions. The traditional neuroblastoma staging system was largely based around post-surgical observations and the same tumour could be categorised as multiple different stages depending on the initial surgery (Monclair et al., 2009).

The INRG staging system classifies patients at diagnosis based on histological features, imaging and age of diagnosis. Bone marrow involvement, imaging of the tumour sites and MIBG testing are all required in order for a patients neuroblastoma to be categorised using the new system. There are 4 stages in the new classification; L1, L2, M and MS and these are described in Table 1.1. L1 and L2 are considered low/intermediate risk, M is the high-risk form and MS is the form capable of spontaneous regression (Monclair et al., 2009).

Stage	Description
L1	Tumours are localised and located in only one area of the body.
L2	Tumours have not spread beyond neighbouring tissue of where they started. Presence of one or more image-defined risk factors.
M	Distant metastatic disease with bone marrow involvement and tumours found on both sides of the body. If MIBG staining identifies two distant tumours neuroblastoma is described as metastatic.
MS	Previously known as 4S neuroblastoma, tumours have a promising prognosis and are likely to undergo spontaneous regression. If tumours do regress, survival rate is nearly 100%. Only observed in children younger than 18 months at diagnosis who have tumour metastases restricted to skin, liver and/or bone marrow, although the tumour cells must account for less than 10% of total cells of the bone marrow.

Table 1.1: Neuroblastoma Classification System. (Monclair et al., 2009; CRUK). The current neuroblastoma staging system based on factors such as age of diagnosis, location of tumours and bone marrow involvement.

1.1.4 Neuroblastoma Treatment

1.1.4.1 Low and Intermediate Risk Patients

Efforts are underway to reduce intensive treatments for children with low and intermediate risk neuroblastomas as they can lead to negative effects later in life (Laverdière et al., 2009). For children with low-risk neuroblastomas, surgery to remove the tumour mass was the standard method of treatment. Even when the whole tumour mass is not totally removed, surgery alone leads to very high overall survival rates (Strother et al., 2012). For intermediate risk patients, treatment with chemotherapy and surgery to remove the tumour mass is very successful and has good overall survival rates. Studies have been completed with the aim of reducing the dose and duration of chemotherapy for low and intermediate risk patients without affecting survival rates. Sample sizes in these studies have been small, but results are promising (Baker et al., 2010; Kim et al., 2018).

Surgery in young children comes with many risks, so trials are underway to determine if children with small, localised tumours require surgery at all (Hero et al., 2008; Nuchtern et al., 2012; Oue et al., 2005). In initial trials, if children were diagnosed under six months of age and had small tumours located in the adrenal glands, parents were offered two treatment options; surgery or ‘expectant

observation'. Expectant observation consisted of frequent sonograms to check tumour size, and urine screening to check the levels of catecholamine metabolites. If either tumour size or catecholamine metabolites increased, the children were referred for surgery. This study showed 80% of patients required no surgery and overall survival rate was 100% (Nuchtern et al., 2012). Observation is becoming the standard treatment for low-risk neuroblastoma, a long-term study is currently underway which includes children who are up to one year of age at diagnosis with low-risk neuroblastoma (trial reference NCT02176967).

1.1.4.2 High Risk Patients

Despite intensive treatment regimes, the survival rate for patients with high-risk neuroblastoma is only 10% due to patients not responding to therapy or tumours relapsing (Johnsen et al., 2019). Patients with high-risk neuroblastoma usually go through multiple stages of treatment beginning with an induction phase, followed by a consolidation phase and finally a maintenance phase (Smith and Foster, 2018). Patients initially go through the induction phase which is typically multiple rounds of chemotherapy followed by surgery. Many patients respond well to this initial treatment; however, a large proportion of patients will relapse and around 20% will not respond at all. Following chemotherapy, patients normally have surgery to remove the tumour mass. The consolidation phase follows, this includes myeloablative therapy and autologous bone marrow transplantation which improves outcome compared to patients who just receive chemotherapy (Matthay et al., 2009, 1999). Patients usually also receive radiation therapy at this point to try and eradicate residual disease. However, despite this rigorous treatment protocol, many patients still suffer relapse (Whittle et al., 2017).

To try and prevent relapse following chemotherapy, surgery and radiotherapy, patients embark on the maintenance phase where they will continue to receive treatment to try and remove any residual tumour cells. A standard treatment in this phase is differentiation therapy, commonly 13-cis-retinoic acid. This is to control proliferation of any remaining tumour cells and attempt to initiate their differentiation. This has been shown to improve overall survival rates following myeloablative treatment and stem cell transplantation (Matthay et al., 2009, 1999). Other more specific treatments are being developed to try and improve survival whilst minimising off target interactions, reducing side effects. The first approved immunotherapy to treat neuroblastoma targets disialoganglioside (GD2), an antigen that is present on all neuroblastoma cells (Wu et al., 1986). GD2 monoclonal antibodies are used in combination with immune stimulating drugs with the aim of increasing their efficiency and improving overall survival in comparison to traditional treatments

(Smith and Foster, 2018; Yu et al., 2010). Maintenance treatment using retinoic acid and anti-GD2 antibodies in combination with immune activating compounds show an improvement in survival (Cheung et al., 2012). However, the additional use of immune stimulating drugs can result in toxicities (Blom et al., 2021; Landenstein et al., 2021).

1.2 Development of the Sympathetic Nervous System and Neuroblastoma

Neuroblastoma is a developmental malignancy and is believed to arise due to a deregulation of the differentiation of sympathetic neuroblast precursors of the neural crest. Neuroblastoma cells resemble immature, undifferentiated sympathetic precursors (Maris, Hogarty et al. 2007; Johnsen et al., 2019). In addition to this, cell surface markers found on cells in the developing nervous system are found on neuroblastoma tumour cells. For example, GD2, the antigen targeted by neuroblastoma immunotherapy, is expressed on neural stem cells and TrkA and TrkB, markers of neuroblastoma pathogenesis, are expressed on cells of the developing peripheral nervous system (Johnsen et al., 2019; Brodeur et al., 1997; Wu et al., 1986).

1.2.1 Overview of Sympathetic Nervous System Development

During early development, the ectoderm is comprised of three parts: the neural plate, the non-neural ectoderm and the region between the two, the neural plate border. Neurulation occurs when the neural plate border rises to first form a fold, then the neural plate groove, then the cells at the top of the groove will meet to form an enclosed structure, the neural tube, comprised of the cells that initially formed the neural plate (Shyamala et al., 2015; Simões-Costa and Bronner, 2015). The cells of the neural tube are now located in the centre of the embryo and will form the central nervous system, whereas the cells of the non-neural ectoderm which were not involved in neural tube formation, will now surround the embryo and form the epidermis. The neural plate border gives rise to cells which become both neural tube and the non-neural ectoderm, and a small percentage of these border cells will lose their tight cell-cell contacts and delaminate. These cells will then undergo epithelial to mesenchymal transition (EMT) and will become the multipotent population of neural crest cells (NCCs). Following EMT, NCCs will migrate to various locations of the embryo. Initially, NCCs will migrate together before splitting to form four different domains; cranial, trunk, cardiac and vagal, each will give rise to different specialised cell populations. The trunk NCCs can take one of two fates; they can become melanocytes or form the dorsal root ganglia which gives

rise to the sympathetic nervous system, adrenal medulla and aortic nerves (Bhatt et al., 2013; Shyamala et al., 2015).

Once NCCs reach the dorsal aorta they will be subject to BMP signalling which induces the SNS differentiation pathway. Inhibiting BMP signalling using the antagonist NOGGIN in chick and mouse embryos leads to a total lack of differentiation and cells undergo apoptosis, showing the requirement for the BMP pathway in the differentiation of sympathetic neurones (Schneider et al., 1999). BMP-2, BMP-4 and BMP-7 are expressed in the dorsal aorta, and their signalling induces a downstream signalling cascade that has many roles in the development of the SNS, from the survival and maintenance of the precursor population to inducing differentiation. At the dorsal aorta, BMP signalling induces the expression of transcription factors PHOX2B and ASCL1, which maintain the proliferation of precursor cells (Morikawa et al., 2009; Schneider et al., 1999). PHOX2B is then able to regulate the expression of PHOX2A, HAND2 and GATA2/3, transcription factors which promote the expression of both Dopamine-β-Hydroxylase (DBH) and Tyrosine Hydroxylase (TH), enzymes involved in the synthesis of noradrenaline, a sympathetic neuron marker (Martik and Bronner, 2017; Morikawa et al., 2009).

1.2.2 Sympathetic Nervous System Development and Neuroblastoma

During development, cells will transition from a highly proliferative precursor to a differentiated neuron, so signalling pathways must be tightly controlled and regulated during this process. Many of the genes and pathways that play a role in the maintenance of sympathetic precursors and development of sympathetic neurones are implicated in neuroblastoma.

1.2.2.1 Epithelial to Mesenchymal Transition

The process of EMT involves cells losing their cell-cell contacts and taking on a more migratory phenotype. So, it is logical that the deregulation of genes and proteins involved in this process would lead to a set of tumour cells that are capable of invasion and metastasis (Ribatti et al., 2020). Many genes involved in the EMT process are implicated in neuroblastoma including the transcription factor SNAI2 and the kinase ROCK2 (Barrallo-Gimeno and Nieto, 2005; Dyberg et al., 2017). SNAI2 can induce EMT and aids both the survival and motility of migratory NCCs. Removing SNAI2 from neuroblastoma cells results in the downregulation of anti-apoptotic genes and the upregulation of genes associated with neuronal differentiation (Vitali et al., 2008; Vrenken et al., 2020). Deletion of SNAI2 also reduces the ability of cells to metastasize, reiterating the importance of SNAI2 on the

invasive ability of neuroblastoma cells and the importance of this on metastasis (Vitali et al., 2008; Vrenken et al., 2020).

Rho signalling is another important component during the EMT process and is involved in both the induction of a migratory phenotype and during the migration processes (Johnsen et al., 2019). A target of Rho signalling is ROCK2 a protein that aids the rearrangement of the actin cytoskeleton, contributing to cellular migration. High levels of ROCK2 in neuroblastoma are associated with poor prognosis (Dyberg et al., 2017). Inhibiting ROCK2 results in a slower proliferative rate and cells that are less able to migrate (Dyberg et al., 2017). This again underlines the importance of components of the EMT process in the invasiveness of neuroblastomas.

1.2.1.1 MYCN

MYCN is expressed at high levels in developing sympathetic neuroblasts where it supports their proliferation and the downregulation of MYCN is followed by a rise in pro-neural factors and differentiation (Kramer et al., 2016; Otte et al., 2021; Thomas et al., 2004). MYCN overexpression in neural crest cells leads to the development of tumours resembling neuroblastomas in mice (Olsen et al., 2017; Weiss et al., 1997). Silencing MYCN in neuroblastoma cells with a MYCN amplification results in slower growth, apoptosis and downregulation of the anti-apoptotic WNT signalling pathway (Wang et al., 2018). In addition to this, MYCN KO results in a lower association of histone H3K27ac with chromatin, indicating MYCN is a key regulator of chromatin accessibility in neuroblastoma cells (Zeid et al., 2018).

MYCN works alongside, and is reliant on, several other factors to maintain its own expression and to drive neuroblastoma aggressiveness. This includes the MYCN driven upregulation of proteins such as N-CYM, OCT4 and TWIST, which have pro-tumorigenic effects and roles in sustaining MYCN expression. For example, MYCN transcribes a cis-antisense version of itself, N-CYM, which is always present alongside MYCN in human neuroblastomas. Cellular levels of MYCN are controlled by GSK3β which phosphorylates MYCN leading to recognition and degradation by the proteasome. NCYM prevents GSK3β phosphorylating MYCN, inhibiting recognition and degradation, stabilising the MYCN protein (Suenaga et al., 2014). Removing NCYM from MYCN amplified neuroblastomas results in apoptosis of the cells, demonstrating the importance of NCYM on the maintenance of MYCN and the survival and progression of MYCN amplified neuroblastomas (Suenaga et al., 2014). OCT4 is involved in the MYCN/NCYM maintenance loop. Patients who have OCT4 expression alongside MYCN amplification in neuroblastoma have a poorer prognosis (Kaneko et al., 2015).

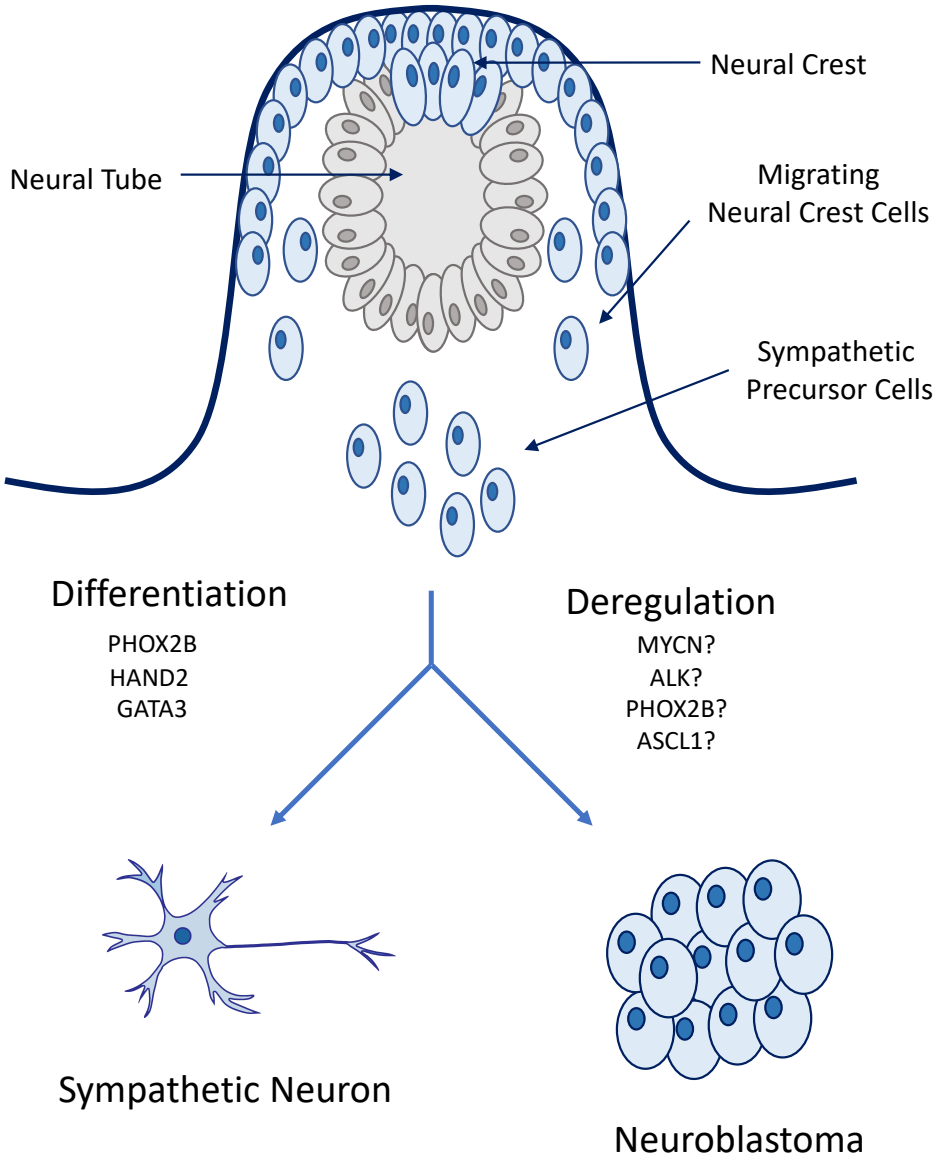

Figure 1.1: Sympathetic Neuron Development and Neuroblastoma. During development, cells of the neural tube will delaminate and form neural crest cells. These neural crest cells will migrate to the dorsal aorta where they will be subject to signalling molecules such as BMP-4 and begin to differentiate into sympathetic neurones. It is widely accepted that neuroblastoma arises due to a deregulation in this process. The neuronal precursors are highly proliferative and this whole process should be tightly controlled. (Adapted from Johnsen et al., 2019).

MYCN amplified neuroblastomas also show high levels of TWIST. TWIST prevents apoptosis by inhibiting ARF activity which would induce apoptosis in response to high levels of MYCN (Valsesia-Wittmann et al., 2004). TWIST also assists MYCN chromatin binding and knockdown of TWIST results in slower growth (Zeid et al., 2018).

In addition to upregulating proteins that support its expression, MYCN also overcomes factors which would have a negative effect on its expression. The let-7 family of miRNA sequesters MYCN mRNA before it produces MYCN protein. However, in MYCN amplified neuroblastomas there is a very high amount of MYCN mRNA present in cells. This means that there is sufficient mRNA for some to be acquired by let7 whilst enough remains to produce protein at high levels (Powers et al., 2016). There are other non-MYCN specific ways neuroblastoma cells overcome let-7, for example chromosome 11q is frequently affected close to the let7 locus, disrupting its production. In addition to this, LIN28B is frequently overexpressed in neuroblastomas and inhibits the maturation of let-7, therefore reducing its effectiveness (Molenaar et al., 2012). One study showed MYCN can upregulate LIN28B itself although this has not been reproduced (Cotterman and Knoepfler, 2009). Neuroblastomas have multiple ways to overcome let7 indicating its important role as a tumour suppressor in neuroblastoma by dampening the expression of MYCN (Powers et al., 2016).

1.2.1.2 PHOX2B

Germline mutations in PHOX2B were the first to be associated with a predisposition to neuroblastoma (Trochet et al., 2004). Mutations of the PHOX2B gene are most likely to be missense or substitution mutations leading to truncated proteins or defects in the DNA binding domain affecting the function (Mosse et al., 2004; Trochet et al., 2004). In normal development, PHOX2B has a tumour suppressive role; overexpression of PHOX2B in neuroblastoma cells leads to a reduction of proliferation and apoptosis and knockdown of PHOX2B increases the metastatic ability of neuroblastoma cells (Naftali et al., 2016; Raabe et al., 2008). PHOX2B variants associated with neuroblastoma appear to have a growth promoting role when expressed in sympathetic neurones (Reiff et al., 2010). PHOX2B has recently been identified as part of a network that maintains the highly proliferative state of neuroblastoma cells and the silencing of PHOX2B slows growth rates (Boeva et al., 2017). In addition to this, upon retinoic acid treatment of neuroblastoma cells, PHOX2B mRNA levels are downregulated, indicating PHOX2B supports the proliferation of neuroblastoma cells and must be downregulated before cells can differentiate (di Lascio et al., 2016).

Other pro-neural proteins such as ASCL1 (Wang et al., 2019; Wylie et al., 2015), GATA3 and HAND2 have also been implicated in neuroblastoma (Boeva et al., 2017; van Groningen et al., 2017). This will be described in more detail in section 1.3.2.

1.2.3 Neuroblastoma Cell of Origin

The tissues neuroblastoma arises in and the genes and pathways that are implicated in neuroblastoma led to the hypothesis that neuroblastoma originates from precursors of sympathetic neurones. Initial experiments used mRNA microarray analysis to identify the developmental origin of neuroblastoma and these early experiments confirmed neuroblastomas were transcriptionally similar to neuroblasts (de Preter et al., 2007).

Recently, the possibility of single cell sequencing has enabled a greater insight into the cell type neuroblastoma might arise from. Single cell and single nucleus RNA-Seq has been completed on foetal adrenal medulla cells, which identified the presence of four cell types and deconvoluted their developmental trajectories. Schwann cell precursors will give rise to the bridge cell population. The bridge cells will then develop into chromaffin cells or neuroblasts (sympathoblasts) (Jansky et al., 2021; Kildisiute et al., 2021). Neuroblastoma tumours were then sequenced, and transcriptomes compared to the developing adrenal medulla cells. All neuroblastomas sequenced resemble neuroblasts. However, the degree of similarity varied between tumours. It was found that the most high-risk neuroblastomas represent a less differentiated, more proliferative neuroblast, whereas the low-risk neuroblastomas resemble a more differentiated neuroblast cell (Jansky et al., 2021; Kildisiute et al., 2021). It is maybe surprising that a cancer with such a high level of genetic heterogeneity is believed to arise from a single cell type.

1.3 Epigenetic Landscape of Neuroblastoma

As described, neuroblastomas display a high level of genetic heterogeneity and few predisposing genes have been identified. Despite this, it has been shown that genetically diverse neuroblastoma cells will cluster into distinct groups, determined by their epigenetic landscape.

1.3.1 Methylation

Investigating the methylation profiles of neuroblastomas show they vary hugely between high risk, low risk and tumours that spontaneously regress (Henrich et al., 2016; Decock et al., 2016).

Hypomethylated promoters are non-methylated and therefore accessible to transcription factors (TFs) whereas hypermethylated promoter regions are heavily methylated, and the ability of TFs to bind these targets is reduced (Henrich et al., 2016). In high-risk neuroblastomas, genes that are known to drive the cell cycle are transcribed as they are associated with hypomethylated promoters, whereas genes associated with neuronal differentiation and apoptosis are typically hyper-methylated and inaccessible (Henrich et al., 2016). It has been shown that inhibiting demethylase activity in cells has an anti-tumour effect, and mice treated with GSK-J4, a demethylase inhibitor, exhibited slower growth and tumour regression. Inhibiting demethylation also led to a decrease in pro-proliferative genes, an increase in differentiation associated genes and made the cells susceptible to the differentiation agent retinoic acid (Lochmann et al., 2018). In addition to this, the methylation profile of tumours that spontaneously regress is different to other subtypes. In 4S/MS neuroblastoma, the TERT gene is hypermethylated, leading to a lower level of TERT expression than in other, higher risk neuroblastomas (Decock et al., 2016). The differences between the epigenetics of a tumour that will spontaneously regress when compared to a high-risk neuroblastoma could be hugely important in understanding the pathways involved in neuroblastoma and aid therapeutics.

1.3.2 Super-Enhancer Landscape of Neuroblastoma Cells

Transcription factors bind DNA at enhancer regions, stretches of DNA that are hundreds of base pairs in length. Super-enhancers are clusters of enhancers, associated with a high amount of TF binding and multiple marks of accessible chromatin. The chromatin in a super-enhancer will be transcriptionally active and super-enhancer associated genes will be transcribed at a much higher rate than those not associated with a super-enhancer (Whyte et al., 2013). Super-enhancers are cell type specific, and a differentiated cell may have thousands of specific super-enhancers. Super-enhancers have also been identified around key oncogenes in cancers and it is thought that these are acquired during the cancer initiation process to support transcription and expression of genes that ultimately drive tumour development (Hnisz et al., 2013; Whyte et al., 2013). Neuroblastomas can be grouped as determined by their super-enhancer landscape (Boeva et al., 2017; van Groningen et al., 2017).

Two publications that pioneered this idea were Van Groningen et al., 2017 and Boeva et al., 2017. Van Groningen *et al* initially took a patient neuroblastoma tumour sample and showed presence of two very distinct cell populations. Following this observation, RNA-Seq analysis of patient cells and neuroblastoma cell lines was completed and showed they cluster into two groups based on gene expression. These two neuroblastoma cell types were termed mesenchymal (MES) and adrenergic

(ADRN). The MES subtype are less differentiated and have an mRNA signature that resembles a neural crest cell like state. MES-type cells express high levels of transcription factors such as PRRX1. MES cells also express proteins such as SNAI2, VIM and FN1, mesenchymal cell markers which are upregulated and involved in EMT and the migration process. The ADRN subtype resemble a more differentiated and specified cell type and are more tumorigenic than MES cells. ADRN-type cells show high levels of PHOX2B, HAND2 and GATA3, transcription factors which are involved in initiating the differentiation process and sympathetic neuronal cell specification (Howard, 2005). ADRN cells also express enzymes such as DBH and TH which are expressed in mature sympathetic neurones. After identifying the two groups of cells, H3K27ac chromatin immunoprecipitation and sequencing (ChIP-Seq) was completed to identify super-enhancers present in the MES and ADRN cells. The super-enhancers were very distinct between the two subtypes and transcription factors associated with a super-enhancer were very highly expressed. It was proposed that these transcription factors are what drives neuroblastoma progression (van Groningen et al., 2017).

Similarly, Boeva et al used H3K27ac ChIP-Seq data to group neuroblastoma cell lines depending on their super-enhancer landscape. Using the super-enhancer landscapes, neuroblastoma cells cluster into three groups; Type I cells, Type II and a set of intermediate cells which have features of both subtypes. TFs associated with a super-enhancer were used to define a core regulatory circuitry (CRC) of transcription factors specific for each cell type. The CRC is the network of transcription factors, marked by H3K27ac signal, that keeps neuroblastoma cells in their highly proliferative state. Type I cells are similar to the ADRN subtype described and have a CRC comprising of TFs such as PHOX2B, HAND2 and GATA3. Type II are similar to the MES subtype, and their super-enhancers and CRC closely resembles that of NCCs. Type II cells show high levels of FOS and JUN, transcription factors typically found in undifferentiated NCCs, and Type II do not express markers of more mature sympathetic neurones, again indicating they resemble earlier stage of development (Boeva et al., 2017). I will now refer to Type I/ADRN cells as ADRN and Type II/MES as MES.

The TF networks and proteins expressed are very distinct between the two subtypes. The TFs are self-promoting and self-sustaining, driving the transcription and expression of themselves and other members of the CRC (Boeva et al., 2017; Wang et al., 2019). Binding motifs for CRC TFs are found in their own enhancers and the enhancers of other members of the CRC. ChIP-Seq analysis confirms CRC transcription factors bind at the same location in enhancer elements of each TF (Boeva et al., 2017; Wang et al., 2019). Following the initial description of the two cell types, many other groups

have identified members of ADRN CRCs, such as ASCL1, ISL1 and TBX2 (Decaesteker et al., 2018; Durbin et al., 2018; Wang et al., 2019).

A single tumour will likely comprise of cells of both subtypes, and tumours usually have a larger proportion of ADRN-type cells than MES cells (Boeva et al., 2017; van Groningen et al., 2017). Neuroblastoma cells aren't confined to one particular state and are able to switch between the two subtypes. MES cells are more resistant to chemotherapy and following treatment, the tumour cell population has a larger proportion of MES cells (Boeva et al., 2017; van Groningen et al., 2017). It has not been established whether the ADRN cells are dying following treatment and therefore population is enriched for MES, or whether ADRN are switching to the MES state as a survival mechanism (Boeva et al., 2017). If a patient relapses, the tumours are not comprised of only MES cells, showing the dynamic nature of neuroblastoma cells and the ability to switch between the two subtypes. This also underlines the need to target both types of neuroblastoma cell to prevent relapse (Boeva et al., 2017; van Groningen et al., 2017).

Multiple groups have shown the ability of ADRN to switch to MES *In Vitro*, and identified key genes involved in the process. Initially this was achieved by inducing PRRX1, a MES specific transcription factor which can induce EMT on its own. By expressing PRRX1 in the ADRN line SK-N-BE(2)c, cells undergo a phenotypic change, downregulate ADRN markers, upregulate MES markers and acquire a H3K27ac ChIP-Seq profile that resembles a MES phenotype (van Groningen et al., 2017). More recently it has been shown that the knockout of ADRN genes GATA3, RET or ARID1A is enough to cause a phenotypic change and induce MES-like RNA-Seq signature (Shi et al., 2020; Siaw et al., 2021). In addition to this, the forced expression of MES genes such as NOTCH3 or a combination of TNFα and EGF results in a MES phenotype and the upregulation of MES markers (Huang et al., 2021; van Groningen et al., 2019). The MES transition induced by NOTCH3 was validated by H3K27ac ChIP-Seq which shows reprogramming of the super-enhancer landscape to a MES state (van Groningen et al., 2019). The ADRN to MES switch has been demonstrated by both knock-out and knock-in experiments. *In Vitro*, the ability to reprogramme MES to ADRN has not been achieved, with multiple groups reporting knocking in a panel of ADRN genes or knocking out a panel of MES genes has no effect on the MES cell line SHEP (Huang et al., 2021).

Initial observations showed a mixed population of ADRN and MES cells in tumours *In Vivo*. However, this has recently been disputed. The reprogramming of multiple MES lines to ADRN *In Vivo* has not been achieved, which raises the possibility of mesenchymal like cells being a culture-specific

phenomenon. Thirant poses the possibility that MES cells may not be tumour associated MES cells and instead a transient group of cells that arise during therapy (Thirant et al., 2021).

1.4 Achaete-Schute Homolog 1

1.4.1 The Role of ASCL1 in Normal Development

Achaete-Schute Homolog 1 (ASCL1) is a pro-neural basic helix-loop-helix (bHLH) transcription factor that has a role in normal development. bHLH transcription factors are comprised of a basic domain and two α-helices which are joined by a loop region. The basic domain recognises ASCL1 consensus sequences CANNTG, known as E-boxes, and facilitates DNA binding (Bertrand et al., 2002). In order for ASCL1 to bind DNA, it must heterodimerize with E-proteins, an interaction that occurs via the α-helices (Bertrand et al., 2002; Wang and Baker, 2015). As a pro-neural transcription factor, ASCL1 is expressed in development before precursor cells are committed to their neuronal fate, and ASCL1 can drive cells out of the cell cycle and initiate differentiation (Guillemot and Hassan, 2017).

ASCL1 is essential for the proper development of the sympathetic nervous system. ASCL1 is found at low levels in migrating NCCs, upregulated in neural progenitor cells as they gather at the dorsal aorta, and remains at high levels during the initiation of differentiation, indicating a role in the transition from a migratory to differentiating NCC (Lee et al., 2020; Wylie et al., 2015). ASCL1 is downregulated upon initiation of the differentiation process and mature neurones will not express ASCL1 (Figure 1.2) (Wylie et al., 2015). As ASCL1 is downregulated when cells differentiate, ASCL1 is only expressed in regions where there is neurogenesis. This means that in healthy adults, ASCL1 expression is limited to the brain, spinal cord and areas where there are developing neuroendocrine cells (Altree et al., 2016).

Ectopic ASCL1 expression in Xenopus embryos leads to the presence of transcription factors required for neuronal differentiation (Parlier et al., 2008). Mice lacking ASCL1 through development will die at birth. ASCL1 knockout mice will have neuronal precursors but lack mature sympathetic neuronal markers, such as TH and DBH, indicating ASCL1 is required for the maturation of sympathetic neurones (Guillemot et al., 1993; Sommer et al., 1995).

Many groups have shown ASCL1 expression along with two other factors, MYT1 and BRN2, can efficiently convert fibroblasts into neurones. ASCL1 is an integral part of this combination, and

induction of ASCL1 alone can re-programme fibroblasts into mature neurones (Pang et al., 2011; Torper et al., 2013; Wapinski et al., 2017, 2013). ASCL1 is regarded as a pioneer factor as it has the ability to bind and remodel closed chromatin allowing transcription of previously inaccessible genes (Raposo et al., 2015; Wapinski et al., 2013). The DNA targeting basic domain of ASCL1 is located next to the first a-helix of ASCL1, this helix is much shorter compared to other bHLH transcription factors. This means ASCL1 is able to target, and bind to much shorter sequences of DNA, aiding DNA binding when target genes are compacted and silenced by nucleosomes (Soufi et al., 2015). It is thought that ASCL1 recognises and targets closed chromatin marked by H3K27ac, H3K4Me1, H3K9Me3 (Wapinski et al., 2013). ASCL1 binds primarily open and accessible chromatin in proliferating cells. When cells begin to differentiate, ASCL1 targets neuronal specification genes which are typically associated with closed chromatin in proliferating precursors (Aydin et al., 2019; Raposo et al., 2015). ASCL1 is able to remodel closed chromatin. ASCL1 binding to neuronal genes is associated with the recruitment of H3K27ac, resulting in a more accessible chromatin state. This occurs around genes associated with sympathetic neuronal fate, and ASCL1 will shape the chromatin landscape so downstream transcription factors can access target genes (Aydin et al., 2019).

Initially the only role of ASCL1 was believed to be pro-differentiation as the overexpression in neuronal precursors leads to the generation of mature neurones. However, it now known ASCL1 is involved in both the proliferation and maintenance of the neural progenitor cell pool before being an integral part in initiating the differentiation process (Castro et al., 2011).

1.4.2 ASCL1 Mechanisms of Control

1.4.2.1 Phospho-Regulation

As is the case with other bHLH transcription factors, ASCL1 can be regulated by its phosphorylation status. Human ASCL1 has five serine-proline (SP) sites which can be targeted by CyclinA/cyclin-dependant kinase (CDK) 2 for phosphorylation. ASCL1 phosphorylation by CDKs allows it to be controlled in response to the cell cycle (Ali et al., 2014). The importance of the phosphorylation status of ASCL1 can be assessed by using mutant forms of the ASCL1 protein, where the serine residues in the SP sites are mutated to alanine (S-A ASCL1) which prevents CDK mediated phosphorylation (Ali, 2014). The S-A protein can be compared to the wild-type (WT) form to identify any differences in activity. The S-A form of the protein is more stable and has a longer half-life than WT ASCL1 (Hindley, unpublished). Using the phospho-mutant protein, it was shown that the S-A form is not affected by CDK overexpression, unlike WT which upregulates pro-proliferation and cell cycle progression genes when CDKs are overexpressed (Ali, 2014).

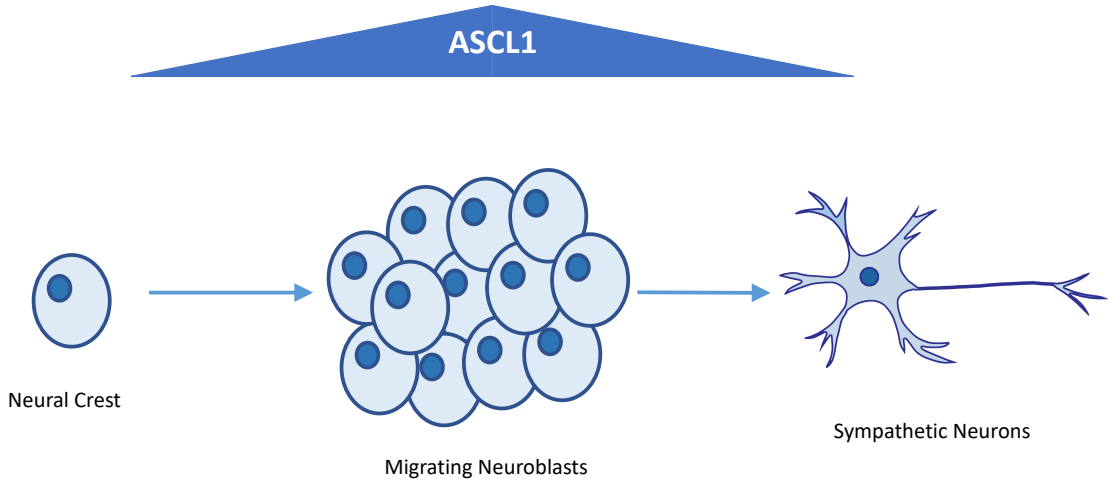

Figure 1.2: ASCL1 is expressed transiently in development. ASCL1 is at low levels in neural crest cells, transiently upregulated in migrating, proliferating neuroblasts and then downregulated in order for terminal differentiation to occur (Wylie et al., 2014; Lo et al., 1991).

Both forms of the protein can induce differentiation, but in Xenopus embryos, S-A ASCL1 is much more efficient at inducing mature neurones and upregulating genes involved in differentiation (Figure 1.3). In addition to this, expressing S-A ASCL1 along with BRN1 and MYT1 in fibroblasts produces more mature neurones than WT ASCL1 (Ali et al., 2014). It has been proposed that the difference in DNA binding of the phospho-forms is mediated by the stability of the protein-DNA interaction, similarly to what is observed for Ngn2, a bHLH whose activity is also controlled by phosphorylation (Ali et al., 2011). Genes associated with proliferation are typically accessible allowing the phosphorylated form of ASCL1 to bind and transcribe targets (Figure 1.4 A). Genes associated with mature sympathetic neurones, such as Myt1 and β-Tubulin, are often found in nucleosome rich, highly compacted areas of DNA (Vasconcelos et al., 2016; Raposo et al., 2015). ASCL1 is a pioneer factor and able to alter the structure of chromatin around less accessible genes, but to do this, requires a more stable interaction, or a higher level of transcription factor binding. S-A ASCL1 could have a higher affinity for DNA allowing a longer DNA association. Alternatively, there could be a build-up of less phosphorylated ASCL1. As cells prepare to differentiate, the cell cycle lengthens and the levels of cyclin dependant kinase inhibitors (CDKi) increase, leading to the accumulation of dephosphorylated ASCL1, which is able to bind and transcribe DNA at differentiation targets (Figure 1.4 B) (Ali et al., 2011, 2014).

1.4.2.2 Ubiquitination

ASCL1 protein has a short half-life of around 30 minutes (Gillotin et al., 2018). Cellular ASCL1 levels are controlled by ubiquitylation and proteasomal degradation. HUWE1, an E3 ubiquitin ligase, adds ubiquitin to cytoplasmic ASCL1 forming long chains of ubiquitin which are recognised by the proteasome, leading to ASCL1 degradation (Gillotin et al., 2018). Silencing HUWE1 leads to an increase in the levels of ASCL1, a decrease in ubiquitin tagged ASCL1 and doubles the half-life of ASCL1 (Urbán et al., 2016). Treating cells with proteasomal inhibitors increases the amount of ubiquitin tagged ASCL1 present (Gillotin et al., 2018). This tagging and degradation method is limited to the cytoplasm, while chromatin bound ASCL1 is associated with shorter ubiquitin chains and a longer half-life than cytoplasmic ASCL1. Stabilising cellular ASCL1 levels by silencing HUWE1 or the proteasome leads to an increased amount of chromatin bound ASCL1, showing the importance of controlling cytoplasmic levels to regulate ASCL1 mediated transcription (Gillotin et al., 2018).

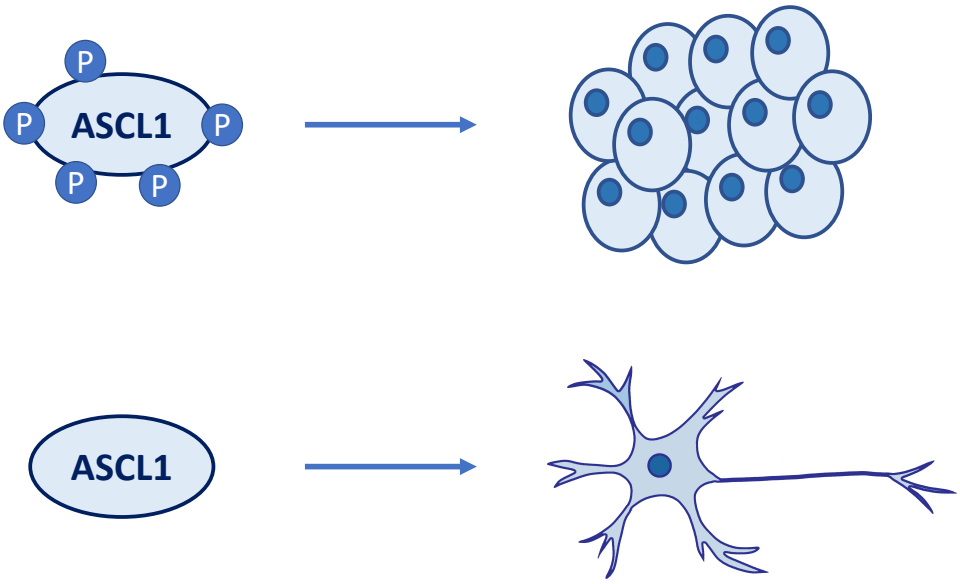

Figure 1.3: ASCL1 activity is regulated by phosphorylation. The phosphorylated form of ASCL1 drives proliferation and the de-phosphorylated form of ASCL1 favours differentiation (Ali et al., 2014).

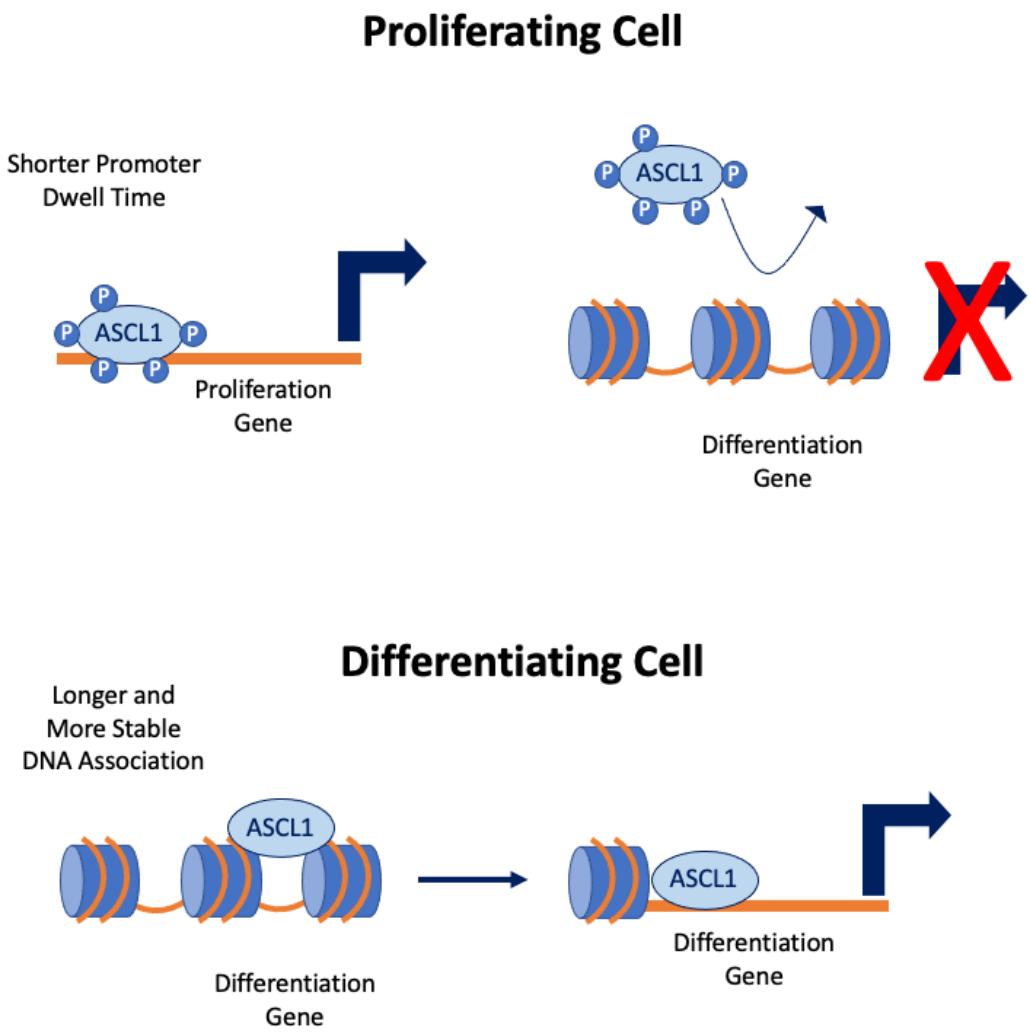

Figure 1.4: Schematic to show the differences between WT and S-A ASCL1 binding. The phosphorylated form of ASCL1 will bind and transcribe open regions of DNA, typically associated with pro-proliferative targets (A). The dephosphorylated form of ASCL1 has a longer promoter dwell time and is able to bind and form a more stable interaction with closed chromatin. This allows the recruitment of proteins that are able to remodel the chromatin landscape resulting in a permissive state for differentiation (Ali et al., 2011, 2014; Raposo et al., 2015).

1.4.3 ASCL1 and Cancer

As described, ASCL1 has an important role in promoting proliferation and ASCL1 transcribes proteins that have a positive effect on the progression of multiple phases of the cell cycle. ASCL1 promotes the expression of E2F1 and FOXM1, proteins which drive the G1/S transition and G2/M transition respectively (Castro et al., 2011). ASCL1 also targets Tead1/2 and ID2, aiding the proliferation of progenitors whilst having a negative effect on their differentiation. ASCL1 also upregulates VEGF, important in angiogenesis and invasion (Castro et al., 2011). As ASCL1 displays many pro-oncogenic traits it is unsurprising that deregulated or sustained expression of ASCL1 leads to cell cycle progression and tumour expansion.

In contrast, overexpressing ASCL1 in fibroblasts or neural stem cells leads to a differentiated phenotype and upregulation of genes that regulate cell cycle exit and differentiation (Chanda et al., 2014; Wapinski et al., 2017). Sustained expression of ASCL1 in the central nervous system, or overexpression of ASCL1 in peripheral nervous system precursors leads to asymmetric cell division and promotion of neurogenesis (Imayoshi et al., 2013). ASCL1 has contrasting roles in development, and has been described to have growth promoting, and also growth inhibiting roles in multiple human cancers.

1.4.3.1 Neuroblastoma

Neuroblastomas with high levels of ASCL1 are associated with poor prognosis regardless of MYCN status showing the importance of the transcription factor (Kasim et al., 2016; Wang et al., 2019). ASCL1 is expressed at high levels in neuronal precursors and should be downregulated when sympathetic neurones have differentiated. However, ASCL1 has been shown to persist at a high level in neuroblastomas (Wylie et al., 2015). This supports the theory that neuroblastoma arises from a deregulation in normal development, leading to cells that are trapped in a developmentally immature, and highly proliferative state. In neuroblastomas ASCL1 could fail to be downregulated, or precursor cells could be stalled at a stage of development when ASCL1 is at high levels (Wylie et al., 2015).

Neuroblastoma cell lines express the phosphorylated form of ASCL1 associated with cell cycle progression and proliferation (Wylie et al., 2015). The phospho-mutant form of ASCL1 shown to promote differentiation in development has a similar function when induced in neuroblastoma cells. ChIP-Seq and RNA-Seq analysis have shown the phospho-mutant form of ASCL1 can effectively bind and downregulate members of the ADRN CRC, MYC and proliferative targets, whilst having a positive

effect on the expression of differentiation targets. This leads to slower growth of neuroblastoma cells and morphology indicative of differentiation (Ali et al., 2020).

In neuroblastoma, ASCL1 maintains the proliferative phenotype and ASCL1 expression is associated with genes involved in cell cycle progression. ASCL1 has recently been described as a member of the CRC in ADRN neuroblastoma (Kasim et al., 2016; Wang et al., 2019). The ASCL1 locus is associated with H3K27ac and H3K4me1 active chromatin marks, and the enhancer region is bound by other members of the ADRN CRC, supporting its transcription and expression. In addition to this, ASCL1 binds chromatin at the same locations as other members of the CRC in the regulatory regions of itself and other members of the CRC, cooperating to sustain high expression of these critical transcription factors (Wang et al., 2019). ASCL1 expression in neuroblastoma is negatively correlated with genes involved in neuronal differentiation and associated processes (Kasim et al., 2016). ASCL1 levels are diminished when neuroblastoma cells are differentiated by retinoic acid, emphasising the inhibitory effect high levels of ASCL1 have on neuroblastoma cell differentiation. Elevated levels of ASCL1 render neuroblastoma cells insensitive to retinoic acid differentiation and downregulating high levels of ASCL1 before retinoic acid treatment results in a more differentiated phenotype (Ichimiya et al., 2001; Kasim et al., 2016). In addition to this, other treatments, such as the demethylase inhibitor GSK-J4, that make cells more susceptible to differentiation also result in ASCL1 downregulation, showing the anti- differentiation effect ASCL1 has on neuroblastoma cells (Lochmann et al., 2018).

1.4.3.2 Glioblastoma

ASCL1 has been reported to play both tumour promoting and tumour suppressive roles in glioblastoma (GBM). ASCL1 has been described as a promoter of glioblastoma progression and ASCL1 levels increase with the severity of the tumour (Rheinbay et al., 2013). ASCL1 can induce the transcription of genes involved in cell cycle progression and growth (Vue et al., 2020). In addition to this, ASCL1 is expressed in GBM cancer stem cells (CSCs), where it promotes the activity of the WNT pathway through blocking the expression of DKK1, a WNT pathway inhibitor. ASCL1 binds upstream of the DKK1 promoter region, silencing its transcription. DKK1 inhibition permits the WNT pathway to be constitutively active, driving the proliferation of GBM CSCs (Rheinbay et al., 2013). The loss of ASCL1 in mouse models of GBM will still result in the formation tumours, but the survival of these mice is increased (Vue et al., 2020).

Conversely, most studies show that high levels of ASCL1 in GBM lead to a better survival rate (Narayanan et al., 2019; Park et al., 2017). GBM with high levels of ASCL1 have high expression of genes associated with a pro-neural phenotype and differentiation, whereas low levels of ASCL1 have a more mesenchymal phenotype and are associated with anti-apoptotic pathways (Park et al., 2017). The WNT and NOTCH pathway are important at maintaining the tumorigenic state of glioblastoma and play important roles in sustaining the CSC population. GBM with high levels of ASCL1 are susceptible to differentiation through inhibition of the NOTCH and/or the WNT pathway (Park et al., 2017; Rajakulendran et al., 2019). In cells expressing low levels of ASCL1, or in lines where ASCL1 has been removed, treating with the same inhibitors will not lead to a differentiated phenotype, underlining the importance of ASCL1 in inducing differentiation in glioblastomas (Park et al., 2017; Rajakulendran et al., 2019).

Studies show the role of ASCL1 is dependent on the genetic background of the glioblastoma cell. The differentiation promoting effects of ASCL1 overexpression are only observed in glioblastoma cells that have a pro-neural phenotype. In the mesenchymal phenotype, where ASCL1 is not typically expressed, overexpressing ASCL1 leads to a more aggressive and malignant phenotype (Narayanan et al., 2019). This underlines the importance of understanding the GBM tumour type and ASCL1 status before targeting the transcription factor or treating with agents to drive differentiation, as outcome will likely be dependent on cell type (Narayanan et al., 2019; Park et al., 2017).

1.4.3.3 Small Cell Lung Cancer

In small cell lung cancer (SCLC), ASCL1 is upregulated in 70% of diagnosed cases and is at a high level in most SCLC cell lines (Rudin et al., 2019; Sato et al., 2020). There are two main subtypes of SCLC; neuroendocrine and mesenchymal, ASCL1 is associated with the neuroendocrine subtype where it is found to be expressed at high levels (Baine et al., 2020). ASCL1 is thought to be important in the maintenance of the neuroendocrine state as ASCL1 actively represses MES-type genes, such as SOX9, and the loss of ASCL1 results in the transition to a MES-type cell (Olsen et al., 2021). In ASCL1 high SCLC, the ASCL1 gene is associated with a super-enhancer, leading to a high level of expression (Borromeo et al., 2016). ASCL1 is able to drive the expression of other genes associated with super-enhancers, such as genes associated with tumour progression, inhibition of apoptosis and lung development (Borromeo et al., 2016).

ASCL1 knockdown in SCLC lines results in slower growth, due to cells being stalled at the G2-M phase, and results in apoptosis of tumour cells (Jiang et al., 2009; Osada et al., 2005). ASCL1 plays an

important role in the initiation of SCLC tumours. Some studies have found ASCL1 is required for the formation of SCLC tumours in xenografts and mouse models and even in heterozygous knockouts, there is a much lower than expected rate of tumour formation (Borromeo et al., 2016). Others have found tumours still arise despite the loss of ASCL1, but tumours arise at a much slower rate (Olsen et al., 2021).

1.4.3.4 Prostate Cancer

The standard treatment methods for prostate adenocarcinomas (PAC) target the androgen receptor, resulting in the cancer cells becoming androgen deprived. Prostate cancers can evolve to become non-reliant on androgen to evade therapy and as a result take on a neuroendocrine phenotype (Fraser et al., 2019). Neuroendocrine prostate cancer (NEPC) is a high-risk, highly aggressive and therapy resistant phenotype associated with the upregulation of genes which are typically associated with neuronal and neuroendocrine differentiation (Gupta and Gupta, 2017; Yamada and Beltran, 2021). Currently around 30% of men who have prostate cancer are diagnosed with NEPC (Gupta and Gupta, 2017). ASCL1 is not present in PAC but is highly expressed and nuclear localised in NEPC cells (Fraser et al., 2019; Rapa et al., 2008). Following androgen deprivation treatment, cells upregulate ASCL1 and take on the neuroendocrine phenotype (Fraser et al., 2019). Silencing ASCL1 before treatment inhibits their ability to transition to the neuroendocrine phenotype, highlighting the importance of ASCL1 in this process (Rapa et al., 2013). In NEPC, the ASCL1 locus is also associated with high levels of H3K27ac supporting its transcription and therefore high expression (Baca et al., 2021).

FOXA1 plays an important role in NEPC. Expressing ASCL1 and NKX2-1 in PAC results in the change of the H3K27ac landscape to a NEPC state and is accompanied by FOXA1 binding targets associated with the NEPC subtype. ASCL1 also colocalises with FOXA1 at its binding sites (Baca et al., 2021). It has recently been proposed targets such as ASCL1 are already marked for activation in PAC due to the presence of H3K4me3 and H3K27me3 (Baca et al., 2021).

1.5 Aims

During development, ASCL1 is initially involved in maintaining the highly proliferative state of neuronal precursors and is subsequently required to induce their differentiation into sympathetic neurones. ASCL1 should be downregulated in order for neurones to fully differentiate, but ASCL1 has been shown to remain at high levels in high-risk neuroblastomas. ASCL1 is part of the core network of transcription factors in neuroblastoma and plays an important role in neuroblastoma progression and pathogenesis. Modulation of the phosphorylation status of ASCL1 can influence the growth and differentiation of neuroblastoma cells.

The aim of this project was to complete CRISPR knockout of ASCL1 in multiple neuroblastoma cell lines to evaluate the importance of ASCL1 in neuroblastoma. I tested the hypothesis that ASCL1 presence is integral to maintain the high level of proliferation of neuroblastoma cells and without ASCL1, the cells will increase in number at a slower rate. I also anticipated the loss of ASCL1 would lead to differences in the prominence and activity of members of the core regulatory circuitry.

Project Aims

i. Use CRISPR/Cas9 technology to produce and validate neuroblastoma cell lines which harbour a stable ASCL1 knockout.
ii. Assess differences in growth and proliferation following ASCL1 removal from neuroblastoma cells.
iii. Establish effects on both the levels and functionality of the core regulatory circuitry transcription factors when ASCL1 is no longer present.
iv. Use RNA-Sequencing and ATAC-Sequencing to determine the effect on the global transcriptome and changes to the chromatin accessibility landscape following ASCL1 knockout.
v. Re-introduce ASCL1 into ASCL1 knockout cells to restore any parental phenotypes that are lost following knockout.

Chapter 2

Successful Knockout of ASCL1 in Three Neuroblastoma Lines

2.1 Introduction

ASCL1 is capable of encouraging proliferation during the development of the sympathetic nervous system (SNS) and in also some cancer cell types. During development, ASCL1 is present in neural progenitor cells where it upregulates genes involved in cell cycle progression to promote proliferation (Castro et al., 2011; Raposo et al., 2015). In addition to this, ASCL1 has a growth promoting role in cancers such as glioblastoma, where its expression is associated with proliferation markers and genes involved in promoting cell cycle progression (Vue et al., 2020).

The expression of ASCL1 during development of the SNS should be transient. However, ASCL1 remains at high levels in high-risk neuroblastomas (Wang et al., 2019; Wylie et al., 2015). The Philpott lab have a plethora of data on the role of ASCL1 in normal neuronal development and also on understanding how ASCL1 contributes to neuroblastoma proliferation and progression. A highly phosphorylated form of ASCL1 predominates in neuroblastomas (Wylie et al., 2015). Work thus far has largely focussed on how both expression levels and post-transcriptional modifications of ASCL1 affect its function. Previous work has identified differences resulting from overexpression of the wildtype (WT) and phospho-mutant (S-A) forms of the protein. When the S-A form of ASCL1 is expressed, it is more efficient at causing neuroblastoma cells to grow more slowly, leads to inhibition of pro-proliferative genes and upregulates differentiation targets (Ali et al., 2020). Complementing our previous work on the outcome of upregulating ASCL1 expression and activity in neuroblastoma cells, this project was aimed at gaining a deeper understanding of the role of endogenous ASCL1 in neuroblastoma, focussing on what happens when ASCL1 is deleted from neuroblastoma cells.

As ASCL1 has an important role in promoting proliferation and maintaining the stem cell pool during development and also supports cancer cell growth, it was hypothesised that the removal of ASCL1

from neuroblastoma cell lines would result in slower growth. This chapter will describe the process in which the ASCL1 knockout (KO) lines were established. Initially, neuroblastoma cell lines were screened to determine ASCL1 expression level and MYC status. Cell lines were then selected to undergo ASCL1 KO, lines were chosen that represented a range of ASCL1 levels. ASCL1 was then permanently deleted from these cell lines using CRISPR-Cas9 technology. These cell lines were then validated by sequencing and western blot to ensure successful KO of ASCL1, and the effects of ASCL1 KO on growth were assessed.

2.2 Results

2.2.1 ASCL1 is Expressed in Multiple Neuroblastoma Cell Lines

To determine which neuroblastoma cell lines express ASCSL1, and therefore which cell lines might be sensitive to ASCL1 activity, a western blot was run using twelve different neuroblastoma cell lines (Figure 2.1). Eleven of the neuroblastoma cell lines tested; Kelly, SK-N-BE(2), NGP, SK-N-F1, NB1643, NBEBC1, SK-N-BE(2)c, IMR32, SH-SY5Y, SK-N-SH and SK-N-AS show ASCL1 expression. Only the SHEP cell line tested did not have detectable ASCL1. With the exception of SK-N-SH, all cell lines which showed ASCL1 protein presence were adrenergic (ADRN) neuroblastoma cells and as ASCL1 has been previously described as a member of the ADRN core regulatory circuitry (CRC), the presence of ASCL1 is to be expected in these lines (Wang et al., 2019). SK-N-SH is a mixed population of cells, comprising both ADRN and mesenchymal (MES) cells, the lower expression of ASCL1 reflecting this.

For the ASCL1 CRISPR KO, cells were chosen that had different levels of ASCL1 protein, and to determine the effect of losing ASCL1 in varying genetic backgrounds, cell lines with different MYC statuses were also desirable.

2.2.2 Most Neuroblastoma Cell Lines are MYCN Amplified

As described previously, the cell lines exhibiting ASCL1 protein expression are all ADRN cell lines, so the proliferative state is maintained by the same network of transcription factors. To ensure there was genetic variation in the cell lines chosen to use for ASCL1 CRISPR KO, the MYC protein present in the neuroblastoma cell lines was determined. Western blots for MYC and MYCN were run to confirm which MYC protein was present in the different neuroblastoma lines (Figure 2.2 and 2.3). Only one of the cell lines, SH-SY5Y, was shown to express ASCL1 and MYC so was chosen for this reason. All the other cell lines that express ASCL1 were MYCN amplified. The cell lines SK-N-BE(2)c and IMR32 were chosen as they have very different ASCL1 levels, and were supported by MYCN.

The neuroblastoma cell lines chosen to complete CRISPR KO of ASCL1 were SH-SY5Y, IMR32 and SK-N-BE(2)c. They show different levels of ASCL1 expression and by choosing these lines, the role of ASCL1 in different genetic backgrounds could be interrogated.

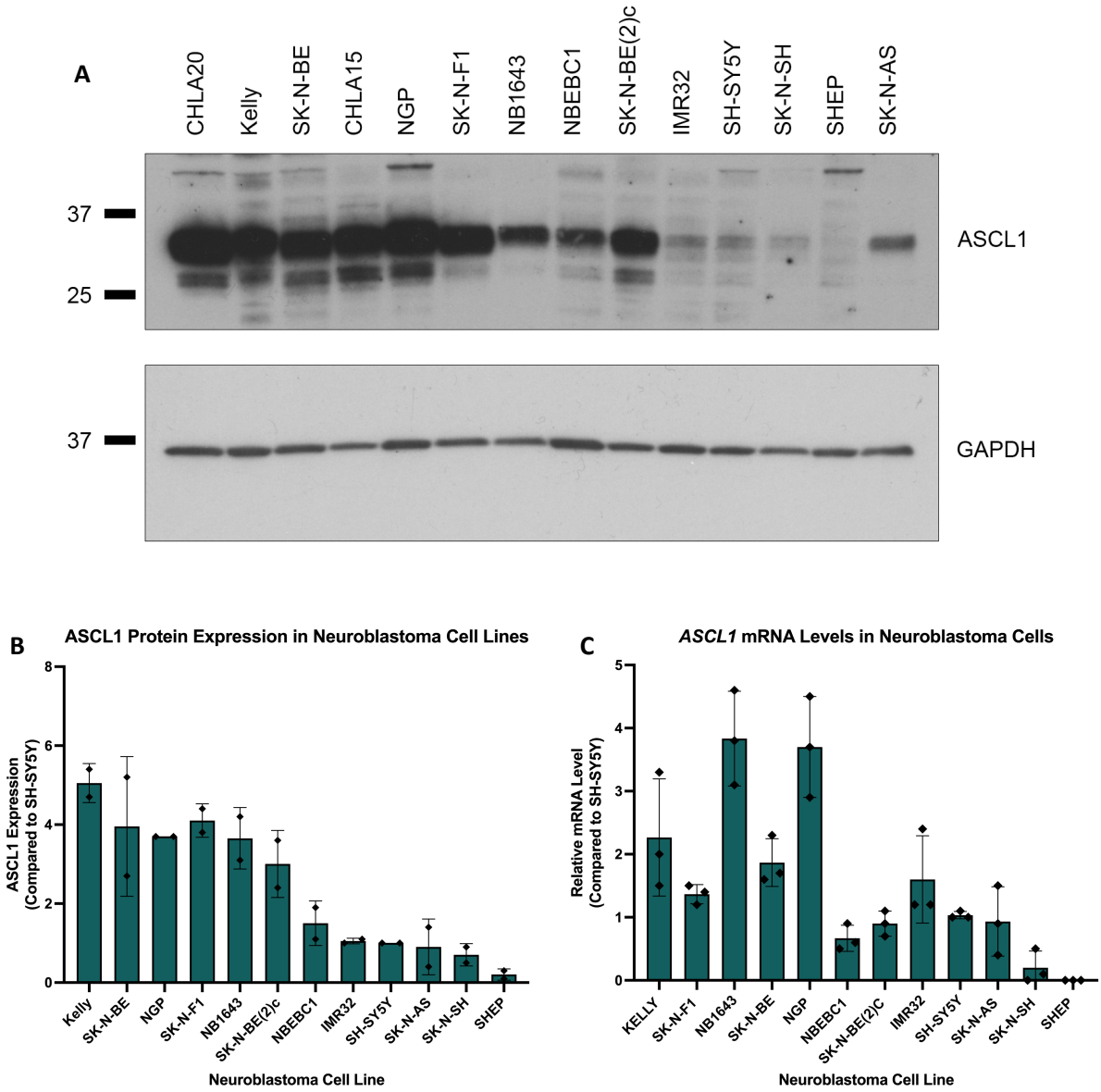

Figure 2.1: ASCL1 protein and mRNA are expressed in multiple neuroblastoma cell lines. ASCL1 expression in neuroblastoma cell lines confirmed by western blot (A, quantitation shown in B) and qPCR (C). Expression and transcript levels have been normalised to the SH-SY5Y cell line. Graphs show all data points (n=3), bars represent the mean value and +/- SEM is shown.

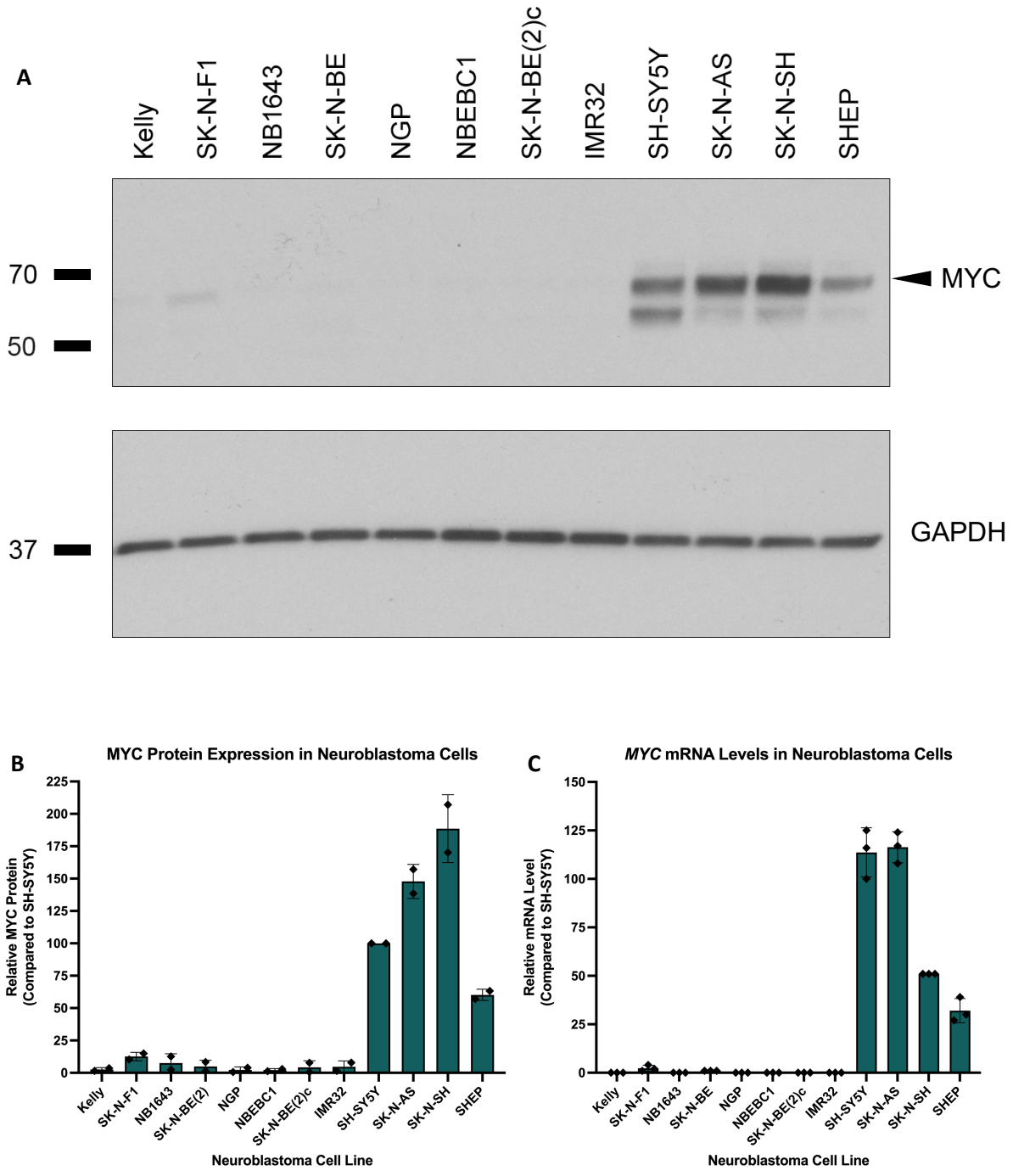

Figure 2.2: Four neuroblastoma cell lines express MYC. MYC expression in neuroblastoma cell lines confirmed by western blot (A, quantitation shown in B) and qPCR (C). Expression and transcript levels have been normalised to the SH-SY5Y cell line. Graphs show all data points (n=3), bars represent the mean value and +/- SEM is shown.

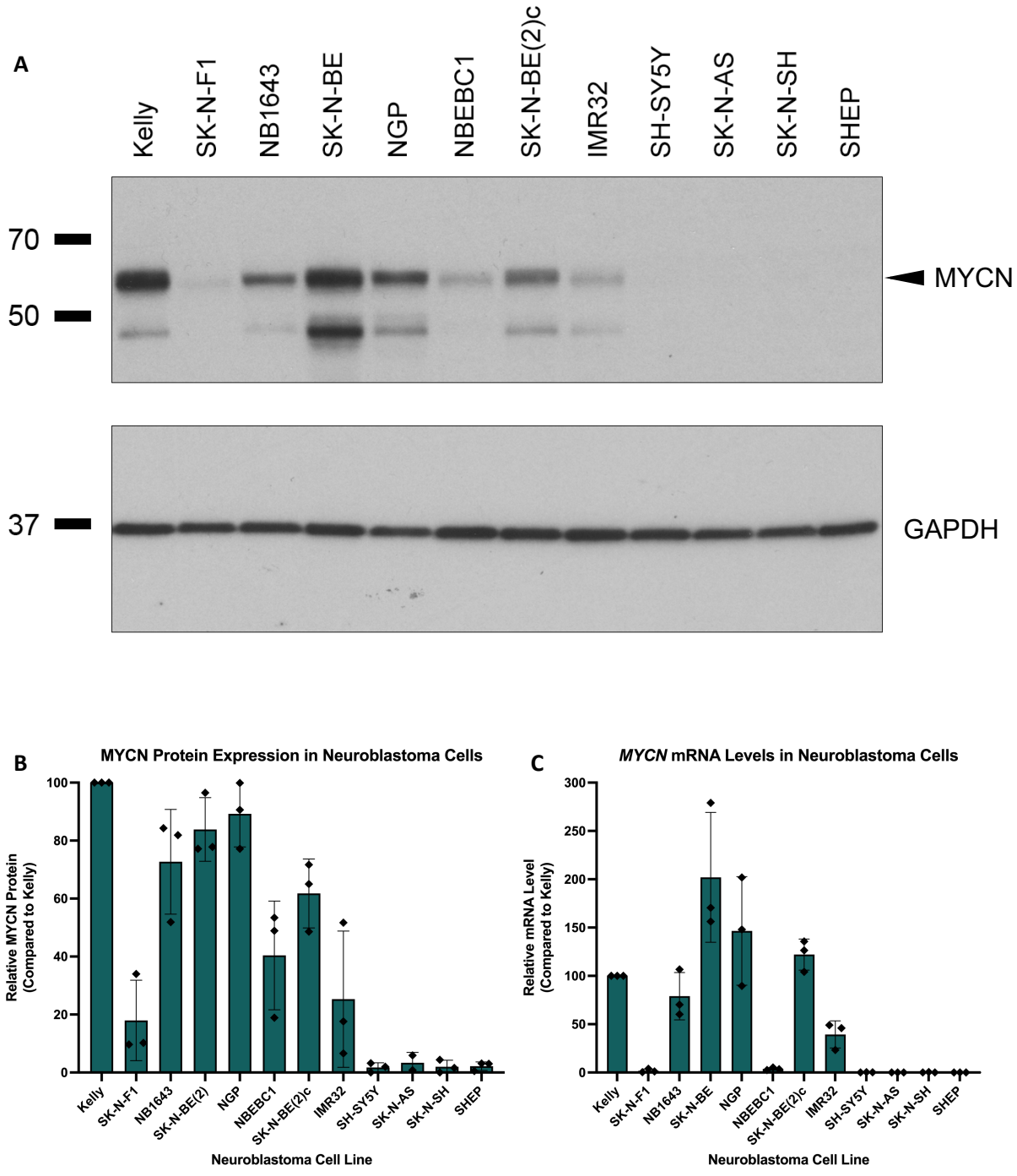

Figure 2.3: Most neuroblastoma cell lines are MYCN amplified. MYCN expression in neuroblastoma cell lines confirmed by western blot (A, quantitation shown in B) and qPCR (C). Expression and transcript levels have been normalised to the Kelly cell line. Graphs show all data points (n=3), bars represent the mean value and +/- SEM is shown.

2.2.3 ASCL1 CRISPR KO was Successful

CRISPR KO of ASCL1 was completed on the three cell lines SH-SY5Y, SK-N-BE(2)c and IMR32, which were confirmed by western blot and qPCR to have ASCL1 expression. CRISPR KO of ASCL1 was achieved using two CRISPR plasmids. One plasmid contained the Cas9 protein, responsible for the exonuclease activity and non-homologous recombination and also contained a GFP marker. The second plasmid contained the sgRNA responsible for targeting Cas9 to the ASCL1 locus. Cells were simultaneously transfected with both plasmids.

Following the transfection of the two CRISPR plasmids, cells were analysed for the expression of GFP, indicating transfection had been successful. For all three cell lines, expression of GFP was observed and cells were FACS sorted. GFP positive cells were single cell sorted into 96 well plates. Cells were maintained for four weeks and then observed for the presence of colonies. At this point, at least twenty colonies from each cell line were chosen and expanded. To determine whether CRISPR gene deletion of ASCL1 had been successful, cells that had formed colonies following the single cell sort were analysed by sanger sequencing and western blot. This process is summarised in Figure 2.4.

Sanger sequencing of the ASCL1 locus in parental and ASCL1 KO clones was completed to ensure a homozygous KO had been achieved. The sequence changes identified were located within or closely around the Cas9 target DNA site, typical of the cleavage and repair mechanism of the Cas9 enzyme. All identified sequence changes would cause a frameshift in the DNA, resulting in either an mRNA template that would be unstable and degraded, or if the mRNA was translated, the result would be a truncated form of the ASCL1 protein. The sequence differences in comparison with parental are described in Table 2.1. Once sequence changes had been confirmed, western blot of potential ASCL1 KO clones was completed to ensure the full length, functional ASCL1 protein was not present. Western blots were run using the parental cell lines and the chosen ASCL1 KO lines. As expected, the parental lines show presence of ASCL1, whereas the chosen ASCL1 KO lines have no detectable ASCL1 (Figure 2.5). The sequence analysis together with the western blot results confirm absence of ASCL1 in the KO lines.

2.2.4 The Morphology of Parental and ASCL1 Knockout Lines is the Same

Following confirmation of ASCL1 KO by CRISPR, cell morphology was observed. ASCL1 is known to play a role in the ADRN CRC, and as ADRN and MES cells are known to have different appearances, the result of removing ASCL1 on cell morphology was investigated. SH-SY5Y parental and ASCL1 KO

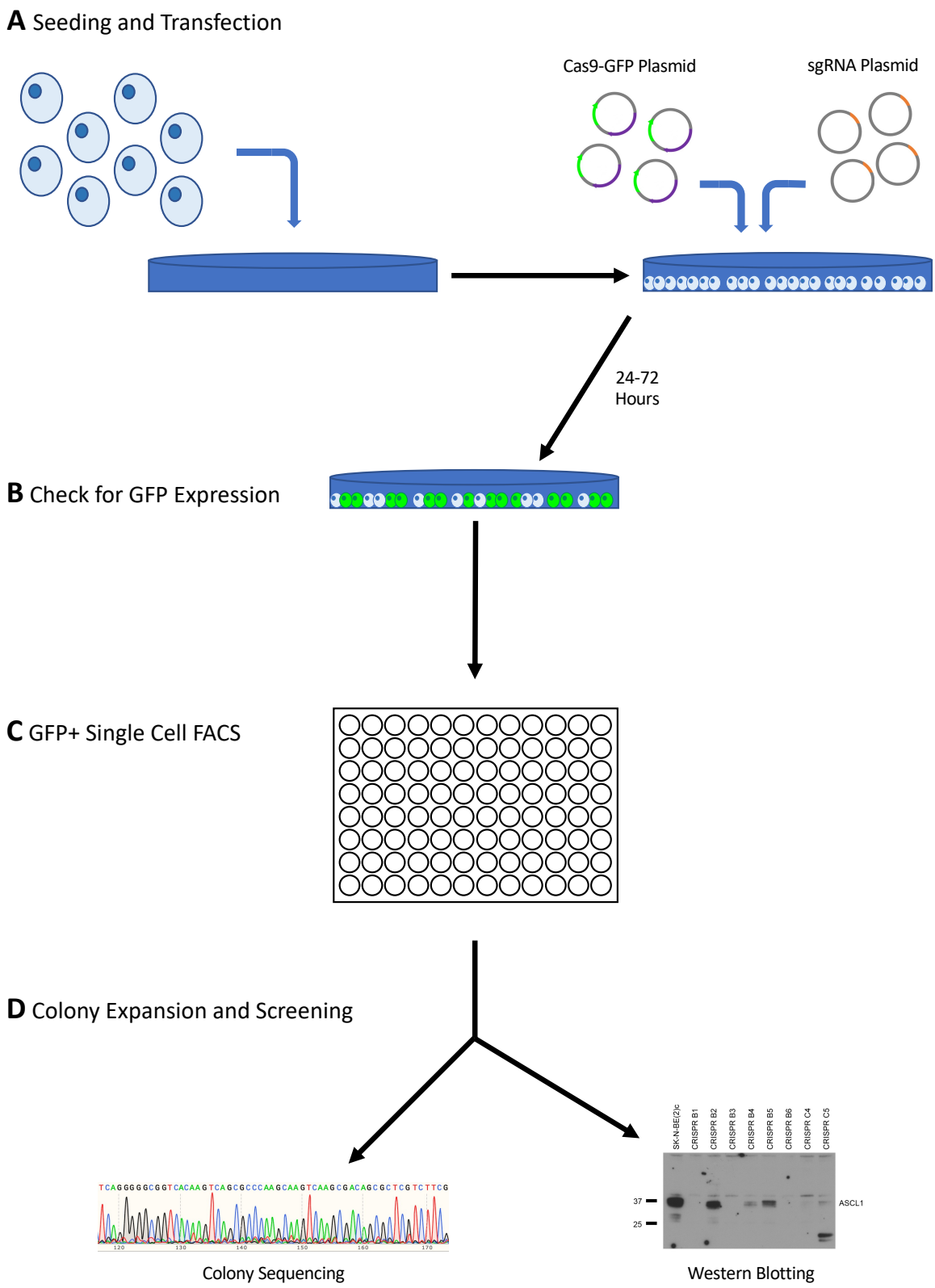

Figure 2.4: Schematic of ASCL1 knockout. The process of ASCL1 KO, beginning with seeding of cells and transfection of the CRISPR plasmids (A). Transfected cells were left for between 24 and 72 hours and checked for GFP expression (B). GFP positive cells were then single cell sorted into 96 well plates (C), colonies were expanded before colony screening by sequencing and western blot (D).

CRISPR Line	Mutation	Difference to Wildtype
SH-SY5Y CRISPR 1	c.825_826insCA	2 base pair insertion – homozygous mutation
	c.825_826insCA	
SH-SY5Y CRISPR 2	c.873_892del	20 base pair deletion
	c.870_871	2 base pair deletion
IMR32 CRISPR 1	c.869_989del	121 base pair deletion
	c912_915del	4 base pair deletion
IMR32 CRISPR 2	c.834_835insA	1 base pair insertion
	c.813_833del	21 base pair deletion resulting in a Stop Codon
SK-N-BE(2)c CRISPR 1	c.883delC	1 base pair deletion
	c.793_794insG	1 base pair insertion
SK-N-BE(2)c CRISPR 2	c.883delC	1 base pair deletion
	c.882_883insGC	2 base pair insertion

Table 2.1: Identification of sequence mutations in ASCL1 knockout cells. Genomic DNA was extracted from parental and ASCL1 KO cells and multiple regions around the expected Cas9 cut site were amplified by PCR. The PCR product was sent for Sanger sequencing to identify sequence differences between parental and KO cells.

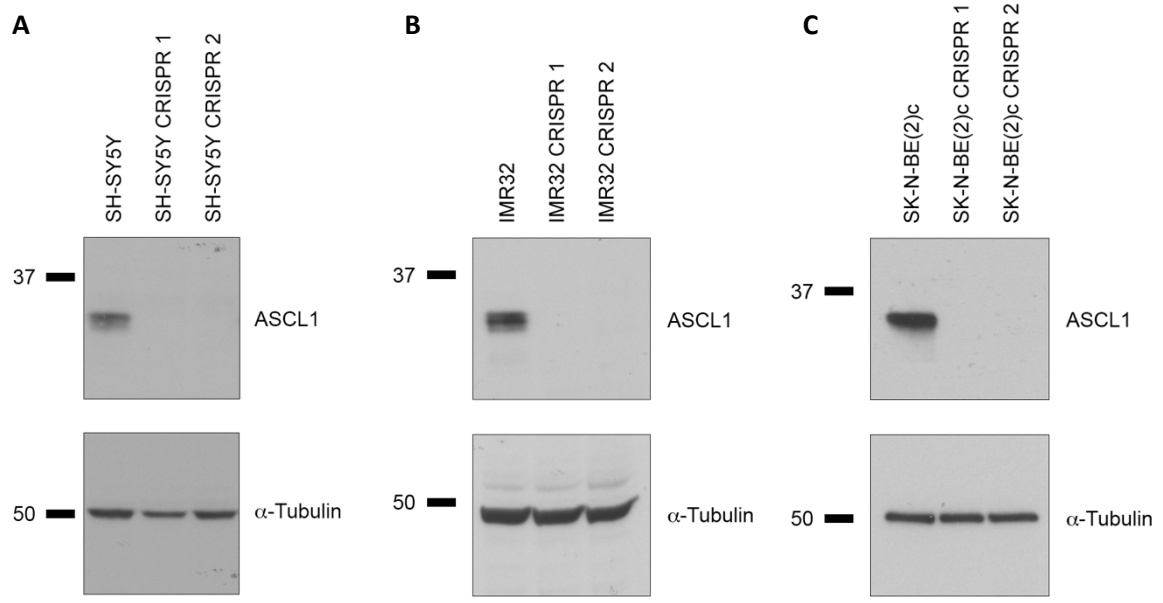

Figure 2.5: ASCL1 protein is undetectable in ACSL1 KO Lines. Parental and ASCL1 KO lines were analysed by western blot to confirm ASCL1 knockout. SH-SY5Y (A), IMR32 (B) and SK-N-BE(2)c (C) parental lines are shown alongside their two chosen CRISPR clones.

cells look very similar morphologically, and their distribution on the plate looks the same (Figure 2.6). IMR32 parental cells and ASCL1 KO cells again, look very similar morphologically, but their growth is different. IMR32 parental cells grow in clusters, whereas the IMR32 ASCL1 KO cells are much more dispersed when they grow (Figure 2.7). The SK-N-BE(2)c parental cells looks very similar to the ASCL1 KO cells, and the growth is similar (Figure 2.8).

2.2.5 ASCL1 Knockout Cells Grow Slower

It has been shown that ASCL1 maintains the pro-proliferative state by targeting and upregulating genes involved in cell cycle progression (Castro et al., 2011). In addition to this, as a member of the ADRN CRC, ASCL1 is part of the network of transcription factors that cooperate to maintain the high level of neuroblastoma proliferation. It has also been observed that silencing of ASCL1 by shRNA in Kelly and SH-SY5Y cells results in slower growth (Wang et al., 2019).

Following the successful CRISPR knockout of ASCL1, the growth of parental and ASCL1 KO cells was analysed to determine if losing ASCL1 resulted in a slower growth phenotype. Cells were analysed by

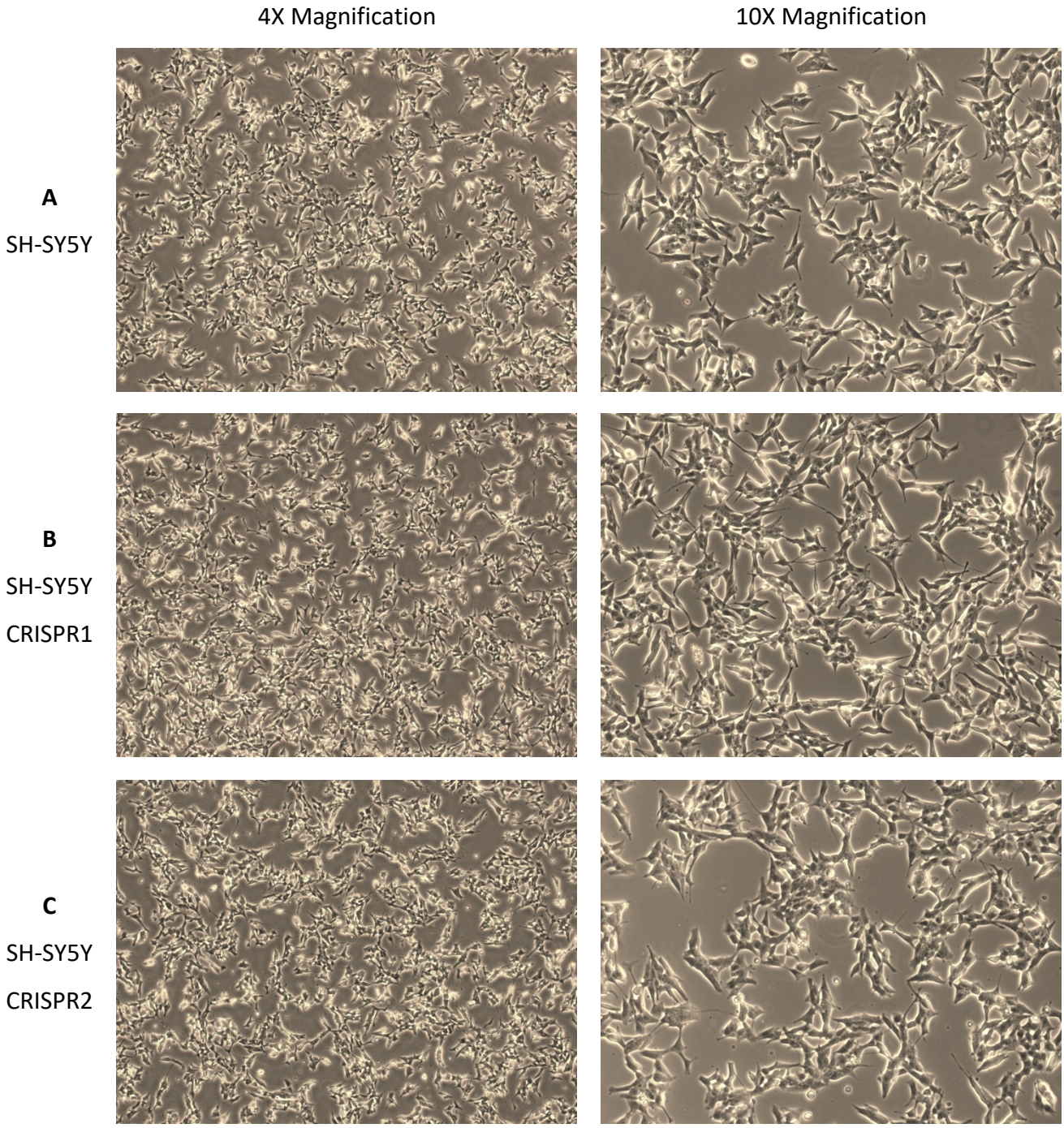

Figure 2.6: The morphology of SH-SY5Y parental and SH-SY5Y ASCL1 knockout lines is similar. SH-SY5Y parental and ASCL1 KO lines were observed to determine morphological changes after ASCL1 KO. Phase-contrast microscopy images of SH-SY5Y (A), SH-SY5Y CRISPR 1 (B) and SH-SY5Y CRISPR 2 (C).

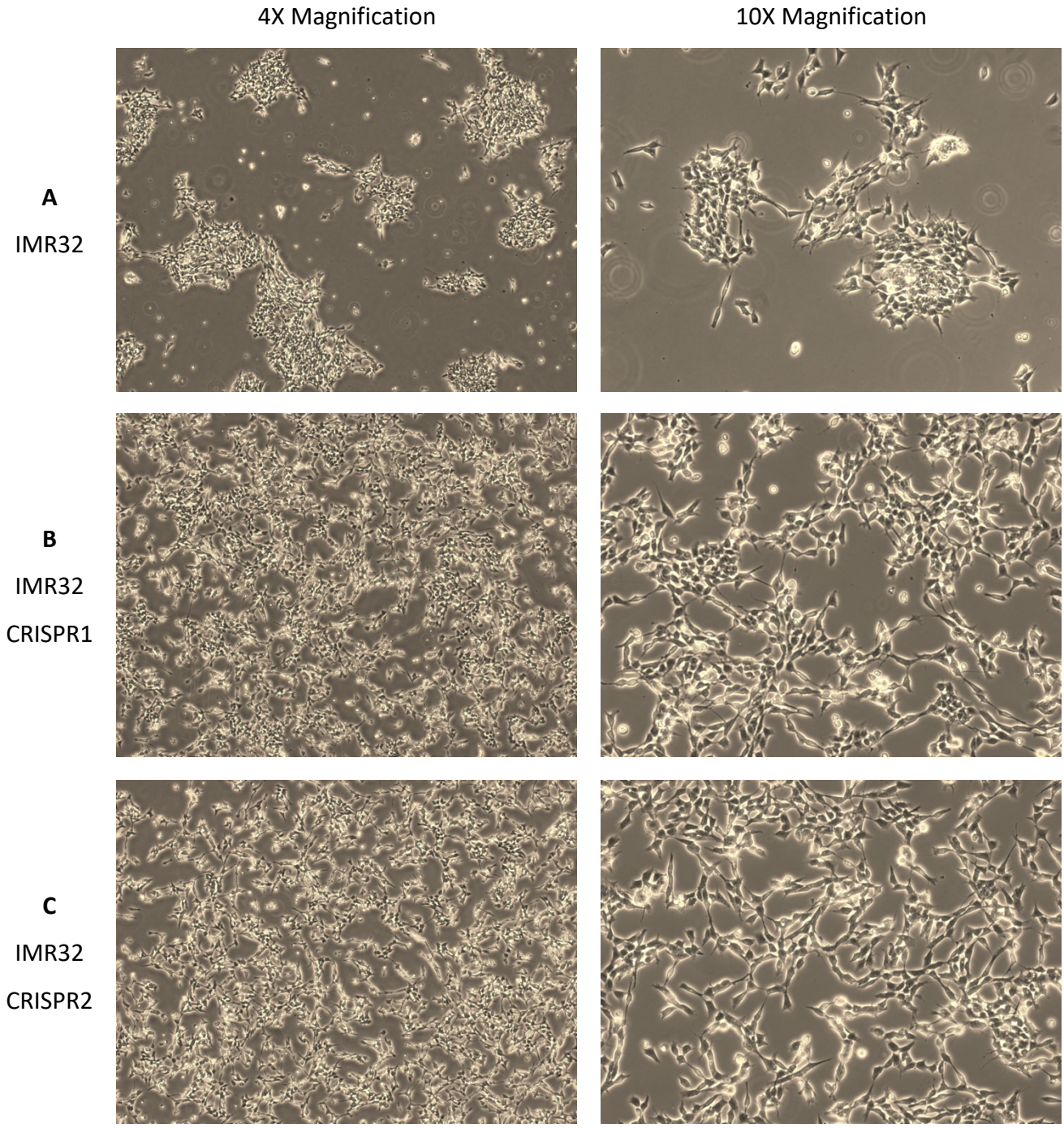

Figure 2.7: The morphology of IMR32 Parental and IMR32 ASCL1 knockout lines is similar. IMR32 parental and ASCL1 KO lines were observed to determine morphological changes after ASCL1 KO. Phase-contrast microscopy images of IMR32 (A), IMR32 CRISPR 1 (B) and IMR32 CRISPR 2 (C).

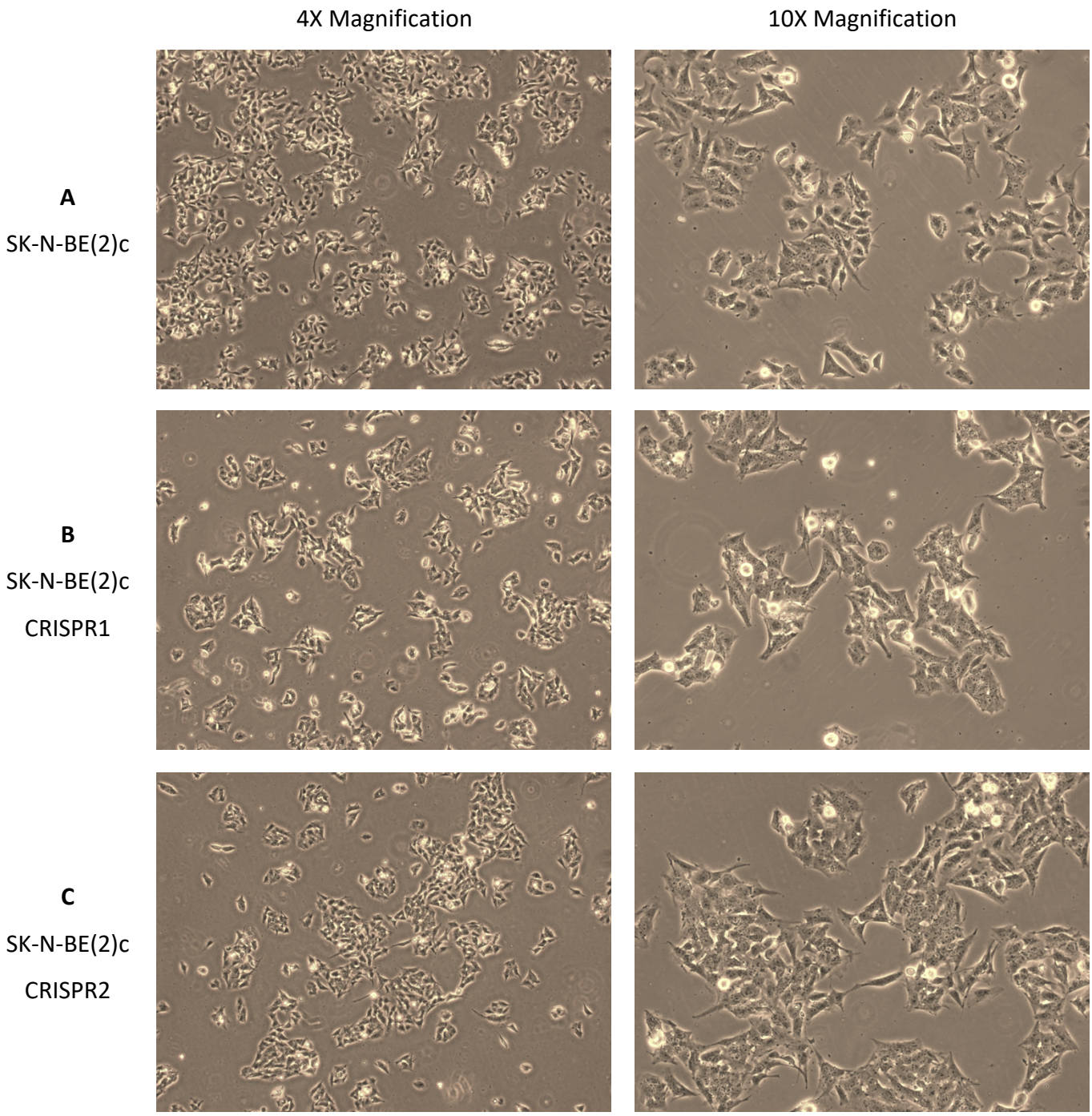

Figure 2.8: The morphology of SK-N-BE(2)c Parental and SK-N-BE(2)c ASCL1 knockout lines is similar. SK-N-BE(2)c parental and ASCL1 KO lines were observed to determine morphological changes after ASCL1 KO. Phase-contrast microscopy images of SK-N-BE(2)c (A), I SK-N-BE(2)c CRISPR 1 (B) and SK-N-BE(2)c CRISPR 2 (C).

cell count and Incucyte (confluency) analysis. For both the cell count and confluency analysis, parental and ASCL1 KO cells were counted, and the same number of cells were plated. The cell count was completed every 24 hours for a total of 96 hours and at each time point, cells were collected and counted using the Cell Countess. For the confluency analysis, cells were analysed using the Incucyte over a 96 hour period.

For all cell lines tested, the ASCL1 KO cells increase in number at a slower rate than the parental cells (Figure 2.9). Cell count and confluency analysis of the SH-SY5Y lines showed both ASCL1 KO cell lines to grow at a slower rate to the parental, the CRISPR 1 line in particular showed a much slower increase in cell number (Figure 2.9 A). The IMR32 ASCL1 KO lines also increase in number at a slower rate compared to parental, shown in both the results of the cell count and confluency analysis (Figure 2.9 B). The slower increase in confluency of IMR32 ASCL1 KO cells is maybe surprising. Confluency analysis measures the coverage of the plate and as IMR ASCL1 KO cells tend to grow in a less clustered manner than the parental cells, this could have confounded the analysis. The SK-N-BE(2)c ASCL1 KO lines also grow at a slower rate compared to the parental lines (Figure 2.9 C).

2.2.6 ASCL1 Knockout Affects the Cell Cycle

Following the observation that ASCL1 KO cells grow at a slower rate compared to the parental cells, cell cycle analysis was completed. This was done to identify whether there was a cell cycle dependant cause of the slower growth, and to determine if the lack of ASCL1 meant cells were struggling to progress through the cell cycle or were taking longer to advance through a particular stage. Cells were harvested and fixed, then stained with propidium iodide (PI) and analysed using flow cytometry. PI intercalates with DNA, so the signal detected from each cell is relative to the amount of DNA present in a cell. This allowed deduction of the particular stage of the cell cycle each cell was in when harvested, based on DNA content per cell.

The PI analysis shows that removal of ASCL1 results in different cell cycle effects in different cell lines (Figure 2.10). For SH-SY5Y, the loss of ASCL1 protein results in a larger proportion of cells in G1 than in the parental line, and there are less cells in both S phase and G2 than in the parental line. This indicates in SH-SY5Y cells ASCL1 is important for the G1/S transition. The PI staining shows that IMR32 Parental and CRISPR cells have a similar proportion of cells in G1. However, parental cells have more cells in G2 than S phase, whereas ASCL1 KO cells show more cells are in S phase than G2. This result implies that in IMR32 cells, ASCL1 is more important for the S/G2 transition. When SK-N-BE(2)c cells are analysed, there is no significant difference between the proportion of cells in each

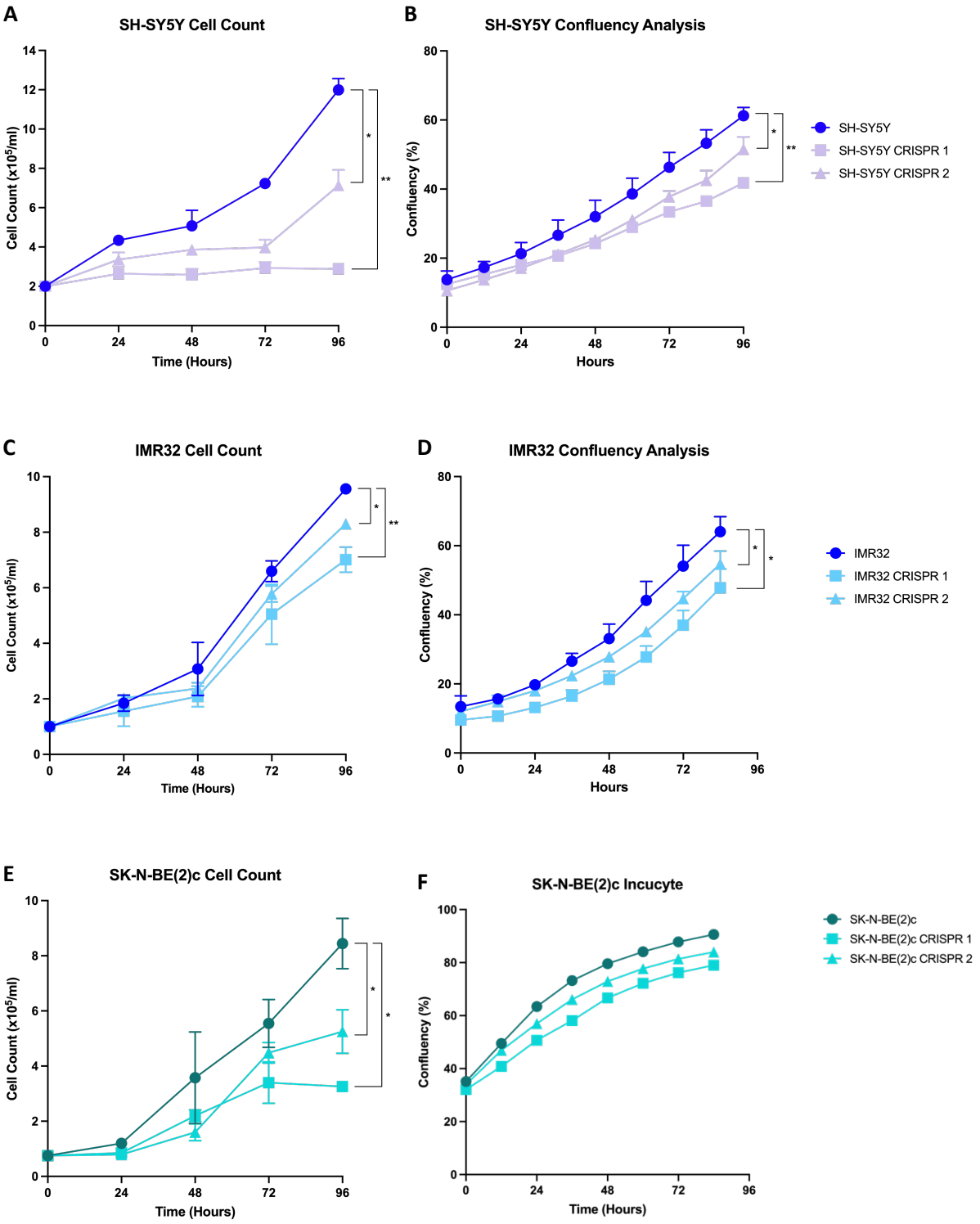

Figure 2.9: ASCL1 knockout cells grow slower. Cell count and Incucyte confluency analysis were completed over a period of 96 hours to analyse growth differences of parental and ASCL1 KO cells. SH-SY5Y parental and CRISPR cell count (A) and confluency analysis (B), IMR32 parental and CRISPR cell count (C) and confluency analysis (D), and SK-N-BE(2)c parental and CRISRPR cell count (E) and confluency analysis (F) are shown. Graphs show the mean value (n=3) and SEM (* = $p < 0.05$, ** = $p < 0.005$).

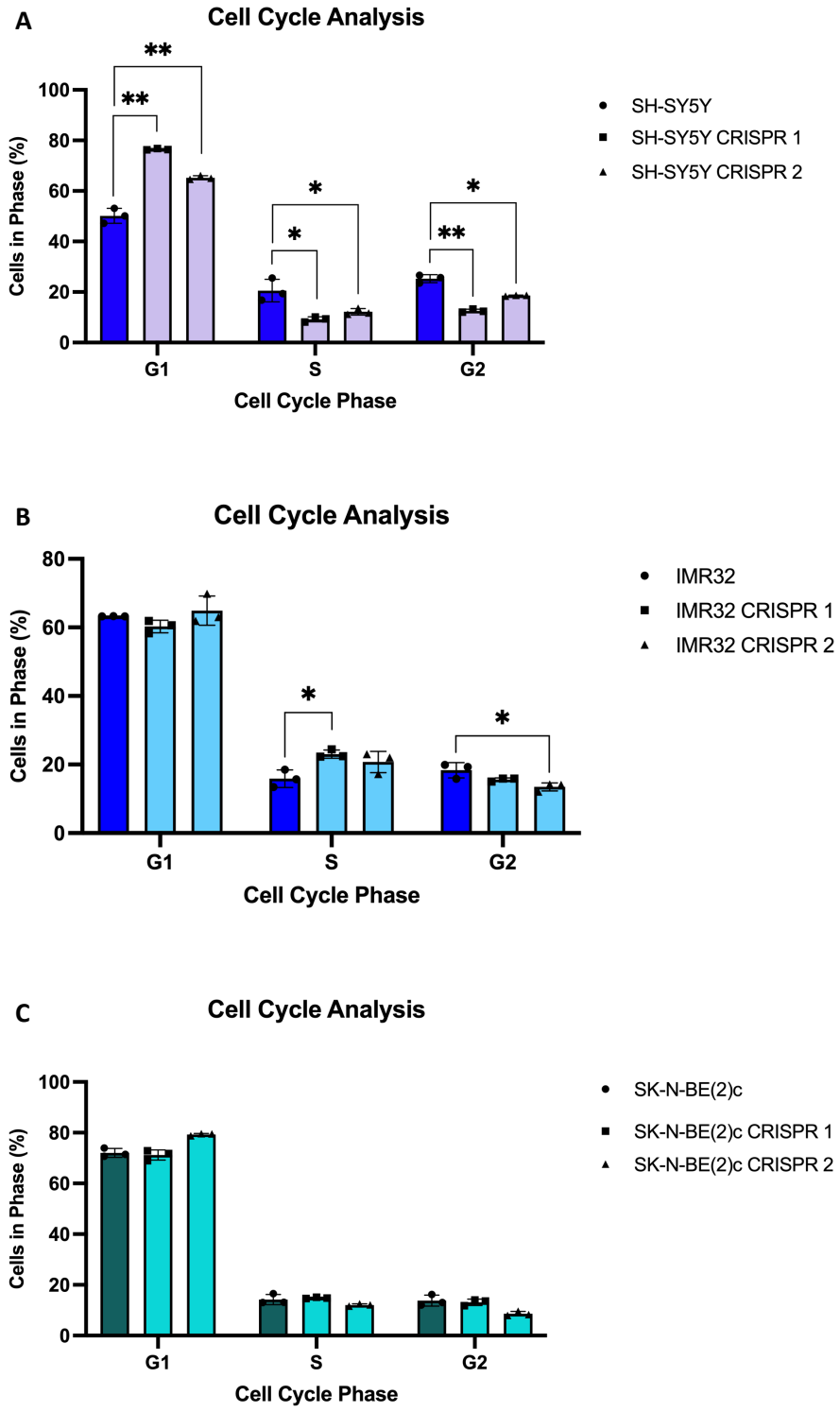

Figure 2.10: ASCL1 knockout effects progression through the cell cycle. Cells were harvested whilst in the exponential growth stage, at no more than 60% confluency. Cells were stained with propidium iodide and then analysed using flow cytometry. Parental and ASCL1 KO lines of SH-SY5Y (A), IMR32 (B) and SK-N-BE(2)c (C) were analysed. The proportion of cells in each phase is displayed as a percentage of the whole cell population for that cell line. Graphs show all data points, n=3, the mean value and +/- SEM (ns = $p \geq 0.05$, * = $p < 0.05$, ** = $p < 0.005$).

phase of the cell cycle, implying ASCL1 is not having an effect on a specific phase of the cell cycle in these cells. These results indicate removal of ASCL1 causes different effects on the cell cycle, these effects likely to be dependent on other genetic factors within the cells.

2.3 Discussion

The aim of this project was to determine the effect of ASCL1 knockout on a variety of neuroblastoma cell lines. ASCL1 has been shown to remain upregulated and highly phosphorylated in high-risk neuroblastoma (Wylie et al., 2014). It was hypothesised that the permanent removal of ASCL1 from neuroblastoma cells would make neuroblastoma cells grow at a slower rate. The aim of this chapter was to produce and validate ASCL1 knockout cells and perform growth analysis to determine overall effects on cell proliferation.

2.3.1 Summary of Results

ASCL1 was successfully knocked out of the neuroblastoma cell lines SH-SY5Y, IMR32 and SK-N-BE(2)c using CRISPR-Cas9 technology. The CRISPR KO was completed, colonies were grown from a single cell and potential KO clones were validated by sequencing and western blot (Figure 2.5). The mutations of the ASCL1 gene following Cas9 cleavage and repair were all small insertions or deletions and located closely to the Cas9 sgRNA target site (Table 2.1). This is typical following CRISPR-Cas9 genome editing; a large proportion of mutations will be close to the PAM target site and commonly mutations will be less than 10 base pairs in length (Zhang et al., 2020). Removing ASCL1 had little effect on the morphology of neuroblastoma cells and all ASCL1 KO cells retained the neuronal phenotype (Figure 2.6-2.8). ASCL1 KO resulted in the cells growing more slowly (Figure 2.9).

2.3.2 ASCL1 Expression Level is Variable Between Cell Lines

Western blots and qPCR analysis were run to investigate the level of ASCL1 expression in neuroblastoma cells. The results of showed that although most of the cell lines expressed ASCL1, the level of ASCL1 protein expressed is not the same between cell lines (Figure 2.1). This is in line with previous observations of ASCL1 expression in neuroblastoma cell lines (Wylie et al., 2015). The MYCN expression level is also variable between cell lines. The ASCL1 enhancer region contains a MYCN consensus sequence (Watt et al., 2007). If MYCN is able to bind, transcribe and therefore encourage expression of ASCL1, it is consistent that cell lines which exhibit MYCN amplification will have higher ASCL1 expression too.

The variation in ASCL1 and MYCN expression between neuroblastoma cell lines could be related to the point in development at which the neuroblastoma arose. ASCL1 and MYCN are both important factors during the normal neuronal development process, but levels of the transcription factors

change over developmental time (Otte et al., 2021; Guglielmi et al., 2014; Wylie et al., 2014). ASCL1 and MYCN both need to be present in precursor cells to drive the cell cycle, encourage proliferation and to maintain the precursor pool. In addition to this, despite having a pro-proliferative role, both proteins must be present at the initial stages of differentiation (Guglielmi et al., 2014). Following the onset of differentiation, ASCL1 and MYCN are then downregulated to allow cells to fully differentiate (Otte et al., 2021). Neuroblastomas are known to be stalled in a developmental precursor state, some of the neuroblastoma cells could have arisen from a point in development where ASCL1 and MYCN levels are high, and others from a cell type where expression levels have started to decrease.

All the neuroblastoma cell lines tested that express ASCL1 are ADRN lines. ASCL1 has been shown to be an important member of the ADRN CRC, so expression is expected in these lines (Wang et al., 2019). The one cell line that did not express ASCL1 mRNA or protein was SHEP, a MES type cell. MES cells are supported by a different network of transcription factors that does not include ASCL1, so the absence of ASCL1 protein in these lines is to be expected (Van Groningen et al., 2017).

2.3.3 ASCL1 KO Slows Neuroblastoma Proliferation

ASCL1 is known to have a growth promoting role in development (Castro et al., 2011), neuroblastoma (Wylie et al., 2014) and in other cancers, such as glioblastoma (Vue et al., 2020). Therefore, removal of ASCL1 resulting in a slower proliferative rate is unsurprising. The effects on neuroblastoma cell growth are in line with previous publications, where silencing ASCL1 using shRNA results in slower growth of Kelly and SH-SY5Y cells (Wang et al., 2019).

Interestingly, cells show different effects on the cell cycle following ASCL1 removal (Figure 2.10). ASCL1 target genes include those involved in the G1/S transition such as E2F1, as well as genes involved in the G2/M transition such as FOXM1. ASCL1 is known to transcribe genes responsible for cell cycle progression, so loss of ASCL1 and therefore lower transcription of these targets results in cells becoming stalled during the cell cycle. The difference between cells being stuck in G1 or S phase could be due to other genetic factors within the cells. It is interesting that the PI staining didn't underline an obvious cell cycle difference between SK-N-BE(2)c parental and ASCL1 KO. The cells grow at a different rate, so there must be a cell cycle dependant cause, the PI assay was not specific enough to establish it.

There are other reasons cells may exhibit a slower growth phenotype. There is the possibility that losing ASCL1 could lead to an increase in cell death. However, the cell count assay uses the Trypan

Blue cell viability dye to determine the amount of live and dead cells in a population. The proportions of live and dead were very similar between parental and ASCL1 KO lines and there were no visible differences in dead cells. These observations taken together indicate the lower cell count in ASCL1 KO lines was not a result of excess cell death. In addition to this, the differences in growth in the IMR32 parental and ASCL1 KO lines could be related to the lower amount of cell-to-cell contact observed which could lead to slower growth.

Following the observation the cells grow at a slower rate, the next step was to understand the mechanism behind this. Chapter 3 will investigate the effects on the CRC following ASCL1 removal and whether components of the CRC are contributing to the slower growth.

The work in this thesis focusses on the role of ASCL1 in neuroblastoma, specifically trying to understand why cells lacking functional ASCL1 protein grow at a slower rate. The ASCL1 cell lines are a valuable resource and are being used by many members of Professor Anna Philpott's lab. Currently there are multiple projects underway in which the role of ASCL1 is being evaluated. These include; the role of ASCL1 in Palbociclib mediated differentiation, the activity of ASCL1 during the cell cycle and identifying ASCL1 binding partners.

We have shown that the cyclin dependant kinase inhibitor (CDKi), Palbociclib is capable of differentiating neuroblastoma cells. The role of ASCL1 in Palbociclib mediated differentiation is being interrogated, using the ASCL1 KO cells to determine if ASCL1 is required for this process. Current data shows that cells lacking ASCL1 do not differentiate as efficiently as parental lines following Palbociclib treatment. In addition to this, the presence and activity of ASCL1 in different stages of the cell cycle is being analysed, using the FUCCI system to induce ASCL1 at specific stages of the cell cycle. The ASCL1 KO cells are being used for this project to look at the effect of inducing ASCL1 at G1, S and G2 without any endogenous protein present. This project will also take a more in-depth look at the relationship between ASCL1 and cell cycle proteins which will help to understand why removing ASCL1 results in different effects on the cell cycle in different lines. In addition to this, proteomics techniques are being used to study ASCL1 binding partners, the knockout cells are being used in this project as the negative control. The cells that have ASCL1 deletion have been instrumental in validating these projects as they are being used to ensure the results obtained are directly attributed to ASCL1.

Chapter 3

The Effect of Losing ASCL1 on the Core Regulatory Circuit

3.1 Introduction

Neuroblastoma cells are supported by a network of transcription factors (TFs) known as the core regulatory circuit (CRC). In adrenergic (ADRN) neuroblastoma cells, this network includes transcription factors such as PHOX2B, GATA3, HAND2, ASCL1, ISL1, TBX2 (Boeva et al., 2017; van Groningen et al., 2017).

It is known that the CRC supports proliferation and members of the CRC have an important role in neuroblastoma development and progression. PHOX2B, ASCL1, ISL1 and GATA3 promote growth and repress differentiation, and high levels of these transcription factors are associated with poor neuroblastoma prognosis (Almutairi et al, 2019, Viprey et al., 2014, Peng et al., 2014). The network is self-sustaining, each member of the network binds the enhancer regions of itself and other members of the network promoting their expression (Figure 3.1 A) (van Groningen et al., 2017; Boeva et al., 2017) Silencing of members of the CRC such as GATA3, ISL1 or PHOX2B slows cell proliferation (Almutairi et al., 2019, Boeva et al., 2017, Zhang et al., 2019). Silencing PHOX2B downregulates ASCL1 and GATA3, demonstrating the reliance of the TFs on other members of the network and underlining the importance of all TFs being present (Yang et al., 2016). These results implicate members of the ADRN CRC as potential targets for neuroblastoma therapies. High throughput screening has been completed to identify drugs that specifically target PHOX2B resulting in slowing of neuroblastoma cell growth and induction of apoptosis (Zanni et al., 2017).

Retinoic acid (RA) is used to treat high-risk neuroblastoma as it decreases the proliferative capacity and initiates a differentiation programme in neuroblastoma cells. Overall survival rates are improved when chemotherapy is followed by RA treatment (Matthay et al., 1999). RA treatment is only effective against ADRN neuroblastoma cells in culture and leads to a decrease in proliferation and

neuronal differentiation (Higashi et al., 2015; Thiele, 1998; van Groningen et al., 2021). Genes such as PHOX2B and GATA3 are decreased after RA treatment (Peng et al., 2014, Di Lascio et al., 2016). Recently, this has been shown to be a result of ADRN CRC repression. Following RA treatment, the H3K27ac landscape is changed so the transcription of ADRN targets is no longer promoted and instead, genes involved in differentiation are associated with super-enhancer marks (Zimmerman et al., 2020). This again underlines the importance of the ADRN CRC in maintaining the proliferative, undifferentiated state of neuroblastoma cells (Figure 3.1 B).

As ASCL1 knockout (KO) causes cells to grow more slowly (described in Chapter 2), it was hypothesised that this was due to effects on the TFs that are part of the CRC. As described, ASCL1 is a member of this self-sustaining CRC network and so it was expected that when an integral component of this network is removed, the expression levels of other proteins in the network would be reduced. This chapter focusses on what happens to the CRC TFs and MYC following ASCL1 KO. Overall expression and transcription of the CRC proteins was analysed and then their sub-cellular localisation was assessed. ASCL1 binding partners were also be evaluated to explore the possibility that ASCL1 is recruiting or co-binding members of the CRC.

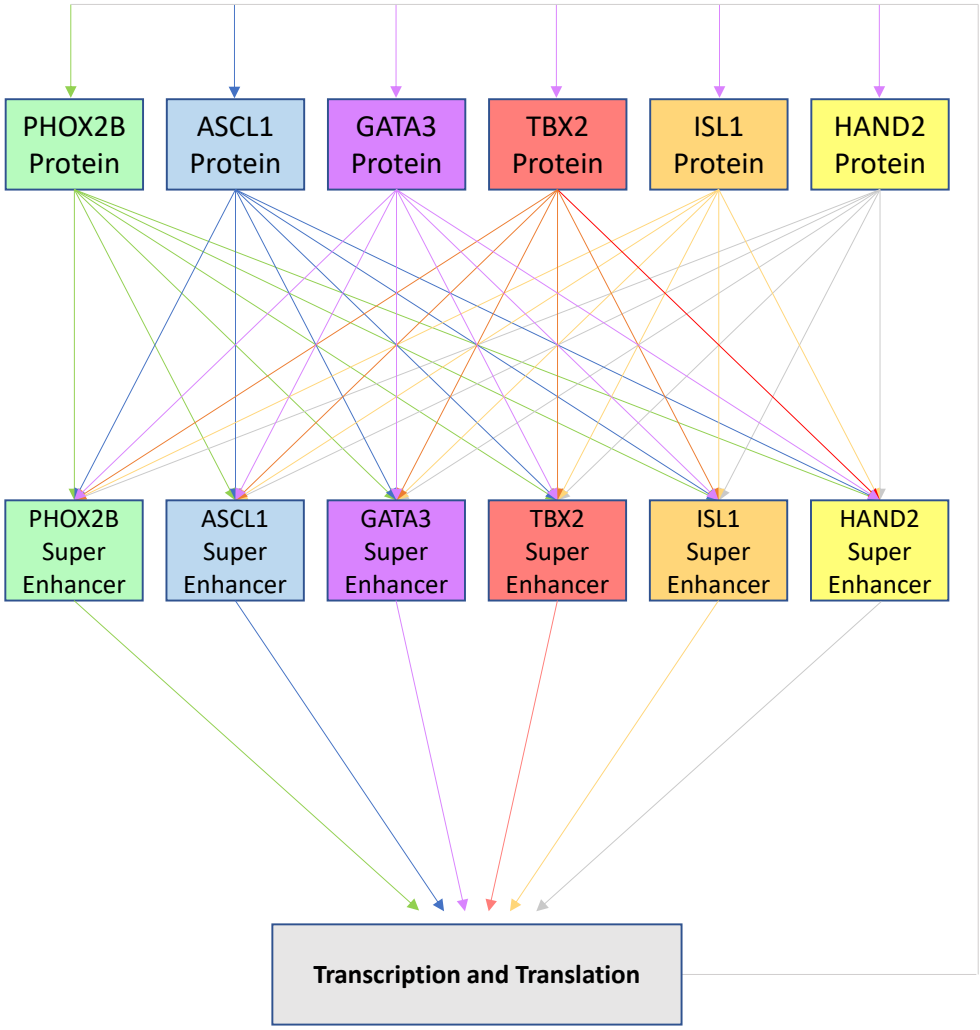

Figure 3.1 A: Schematic of the role of ADRN transcription factors in neuroblastoma. The super enhancer network of transcription factors maintains the proliferative capacity of neuroblastoma cells. The network is self-supporting, each member binds the enhancer regions of other members and promotes the expression of itself and other members of the network. (van Groningen et al., 2017; Boeva et al., 2017, Wang et al., 2019).

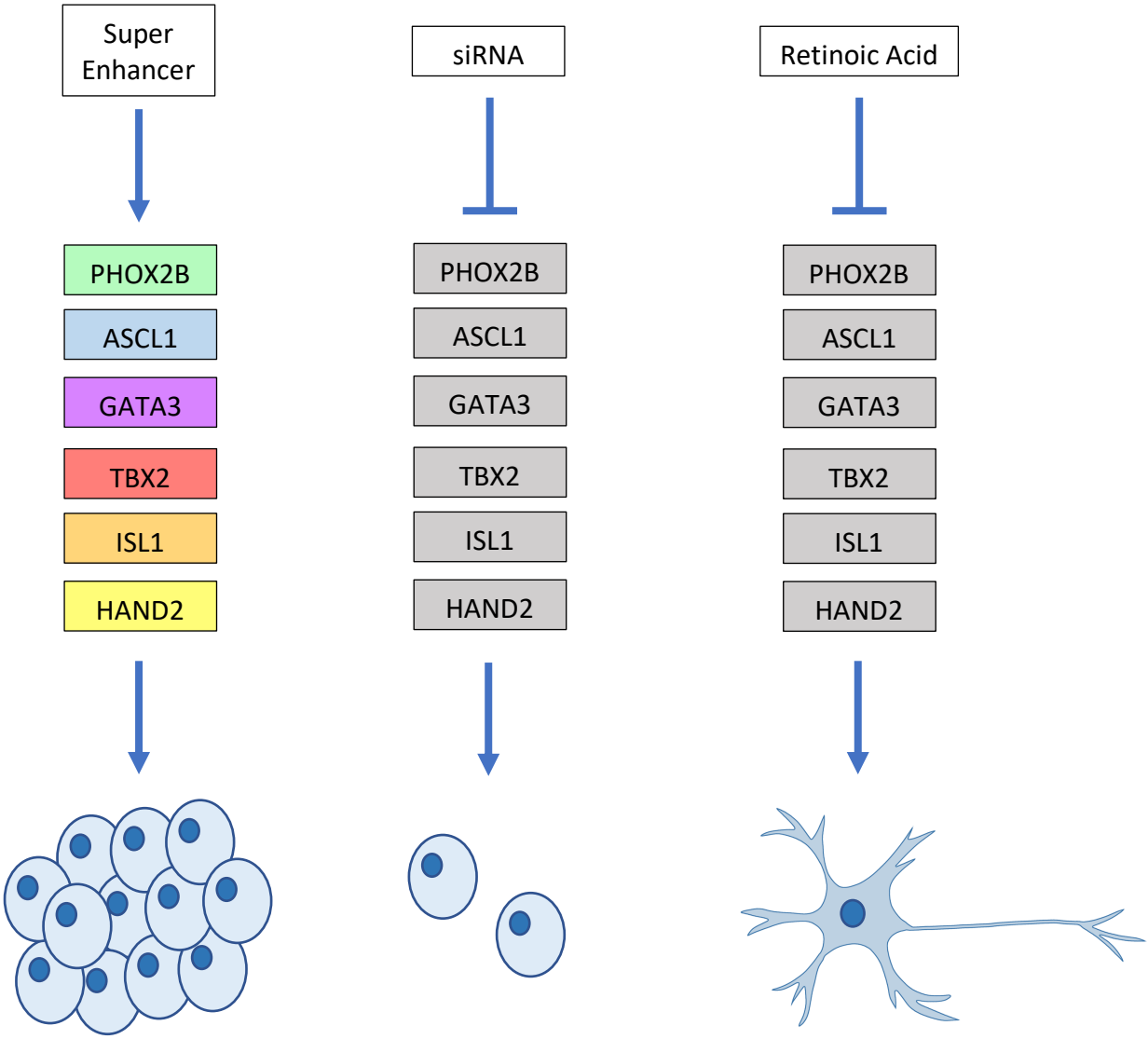

Figure 3.1 B: Schematic of the role of ADRN transcription factors in neuroblastoma. The super enhancer network of transcription factors maintains the proliferative capacity of neuroblastoma cells (A). Silencing members of the CRC leads to slower growth and cell death (B). Treating cells with Retinoic Acid shuts down the CRC and results in differentiation (C) (van Groningen et al., 2017; Zhang et al., 2019; Yang et al., 2016; Zanni et al., 2017; Zimmerman et al., 2020).

3.2 Results

3.2.1 Levels of ADRN Transcription Factors are Largely Unchanged in ASCL1 KO Cells

ASCL1 KO cells grow more slowly than parental cell lines (described in Chapter 2). As previously described, neuroblastoma cells are maintained in their highly proliferative state by the core regulatory network of TFs, so the effect of removing ASCL1 on this network was investigated. Firstly, the overall protein and mRNA levels of PHOX2A, PHOX2B and GATA3 in parental and ASCL1 KO cells were explored by western blot and qPCR.

The protein levels of PHOX2A are comparable between parental and ASCL1 KO cells for SH-SY5Y, IMR32 and SK-N-BE(2)c (Figure 3.2 A-F) and there is no significant difference in PHOX2A mRNA levels (Figure 3.2 G-I). The protein levels of PHOX2B in SH-SY5Y parental and ASCL1 KO cells, and in IMR32 parental and ASCL1 KO cells are again very similar (Figure 3.3 A-B, D-E). This is mirrored in the mRNA levels (Figure 3.3 G-H). However, there is more variability in the SK-N-BE(2)c ASCL1 KO cells. It is believed that PHOX2A and PHOX2B are able to compensate for each other, so the lower amount of PHOX2B in the SK-N-BE(2)c CRISPR lines could be compensated for by PHOX2A, which is still present at high levels. There is little difference between GATA3 protein levels (Figure 3.4 A-F) and average transcription levels (Figure 3.4 G-I) between parental and ASCL1 KO cells.

These results suggest that removing ASCL1 from neuroblastoma cells is not affecting the overall levels of key ADRN targets, as the protein and mRNA levels are similar between parental and ASCL1 KO cells. Following this observation, the effect on MYC was then examined.

3.2.2 MYC Levels are similar in ASCL1 KO Cells

As described, MYC is important in driving the proliferation of neuroblastoma cells so the effect of removing ASCL1 on MYC protein and mRNA levels was explored. The MYC protein levels in SH-SY5Y parental and ASCL1 KO cells are very similar, as are the MYCN levels in both IMR32 and SK-N-BE(2)c parental and ASCL1 KO cells (Figure 3.5 A-F). Similarly, the level of transcription of MYC and MYCN is largely unchanged between parental and ASCL1 KO cells (Figure 3.5 G-I). There is a difference in MYC transcription for the SH-SY5Y CRISPR 1 line, although this isn't reflected in the protein levels of MYC in this line. These results indicate that removing ASCL1 does not affect the overall levels of MYC in cells. These were interesting observations, ASCL1 KO cells grow more slowly but there seems to be minimal effect on the levels of key drivers of neuroblastoma cell proliferation; members of the ADRN core transcriptional network and MYC.

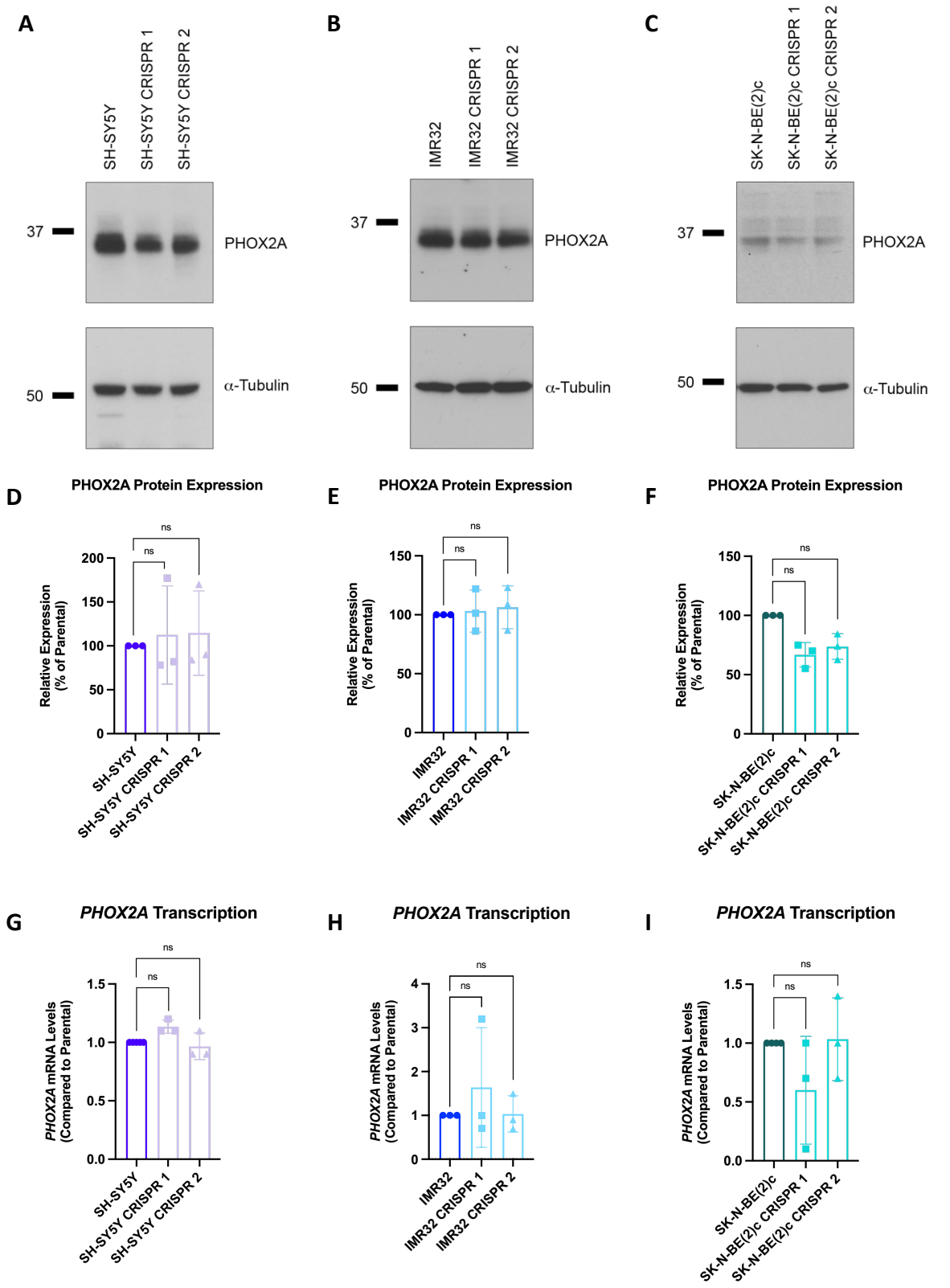

Figure 3.2: PHOX2A levels in parental and ASCL1 KO cells are very similar. Cells were cultured under normal conditions and harvested for western blot and qPCR. Western blot for PHOX2A was completed for the parental and associated ASCL1 KO lines of SH-SY5Y, IMR32 and SK-N-BE(2)c (A-C respectively), and quantitated (n=3) (D-F). qPCR was also completed to show the level of PHOX2A transcription in the parental and ASCL1 KO lines (G-I). Graphs show all data points (n=3), the mean value and +/- SEM (ns = p = > 0.05, * = p < 0.05, ** = p < 0.005).

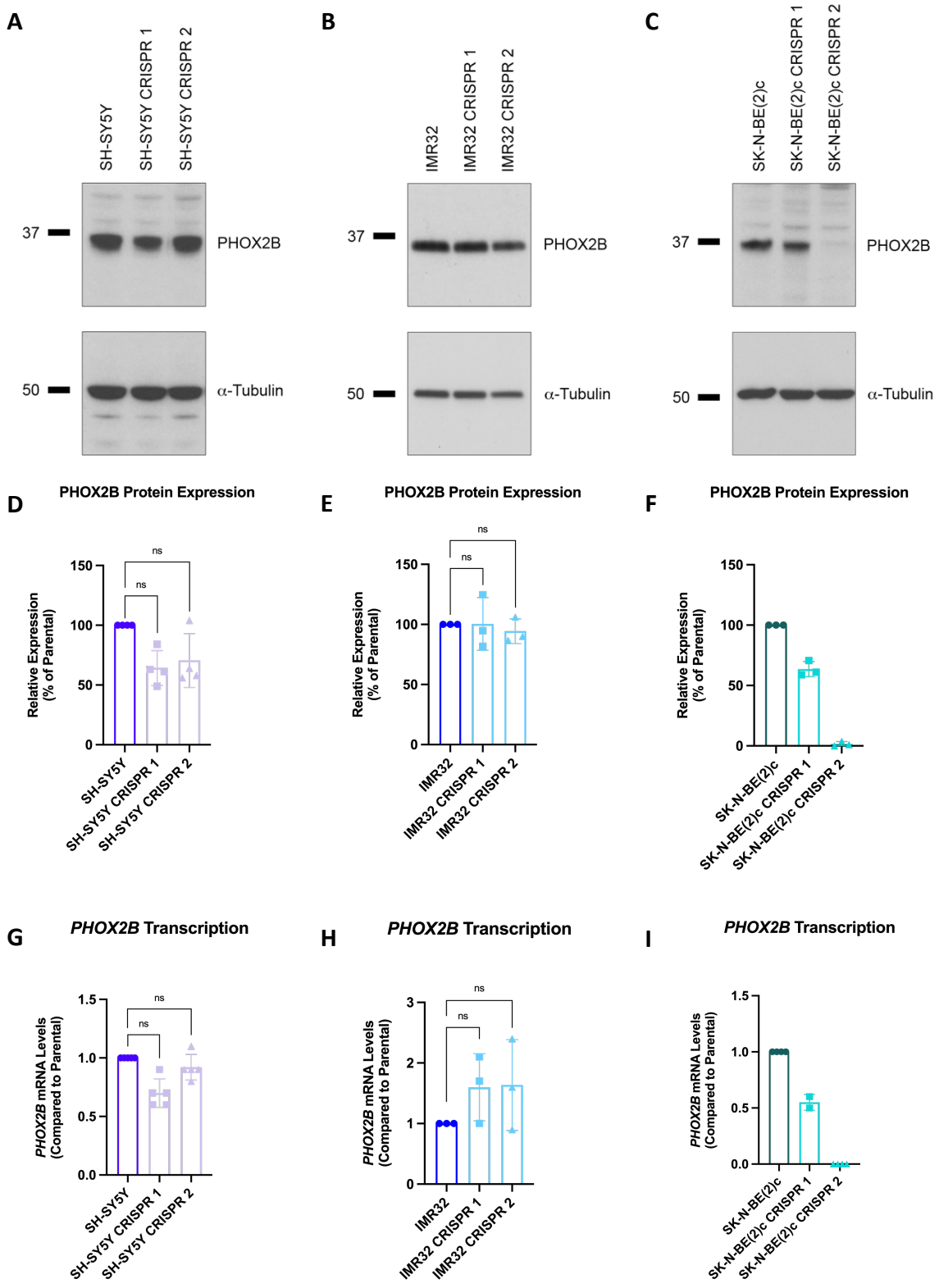

Figure 3.3: PHOX2B levels in parental and ASCL1 KO cells are very similar. Cells were cultured under normal conditions and harvested for western blot and qPCR. Western blot for PHOX2B was completed for the parental and associated ASCL1 KO lines of SH-SY5Y, IMR32 and SK-N-BE(2)c (A-C respectively), and quantitated (n=3) (D-F). qPCR was also completed to show the level of PHOX2B transcription in the parental and ASCL1 KO lines (G-I). Graphs show all data points (n=3), the mean value and +/- SEM (ns = p = > 0.05, * = p < 0.05, ** = p < 0.005).

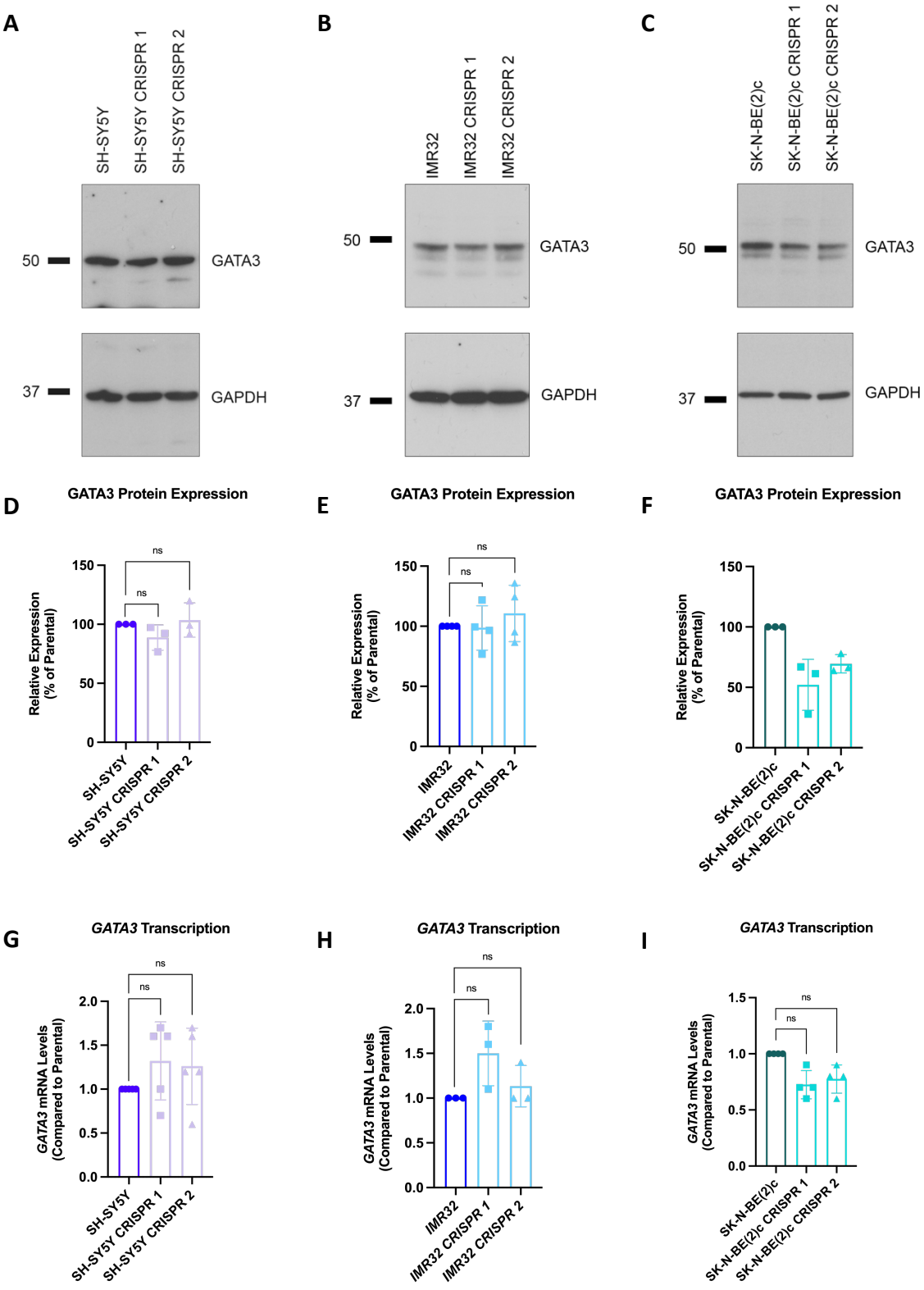

Figure 3.4: GATA3 levels in parental and ASCL1 KO cells are very similar. Cells were cultured under normal conditions and harvested for western blot and qPCR. Western blot for GATA3 was completed for the parental and associated ASCL1 KO lines of SH-SY5Y, IMR32 and SK-N-BE(2)c (A-C respectively), and quantitated (n=3) (D-F). qPCR was also completed to show the level of GATA3 transcription in the parental and ASCL1 KO lines (G-I). Graphs show all data points (n=3), the mean value and +/- SEM (ns = p = > 0.05, * = p < 0.05, ** = p < 0.005).

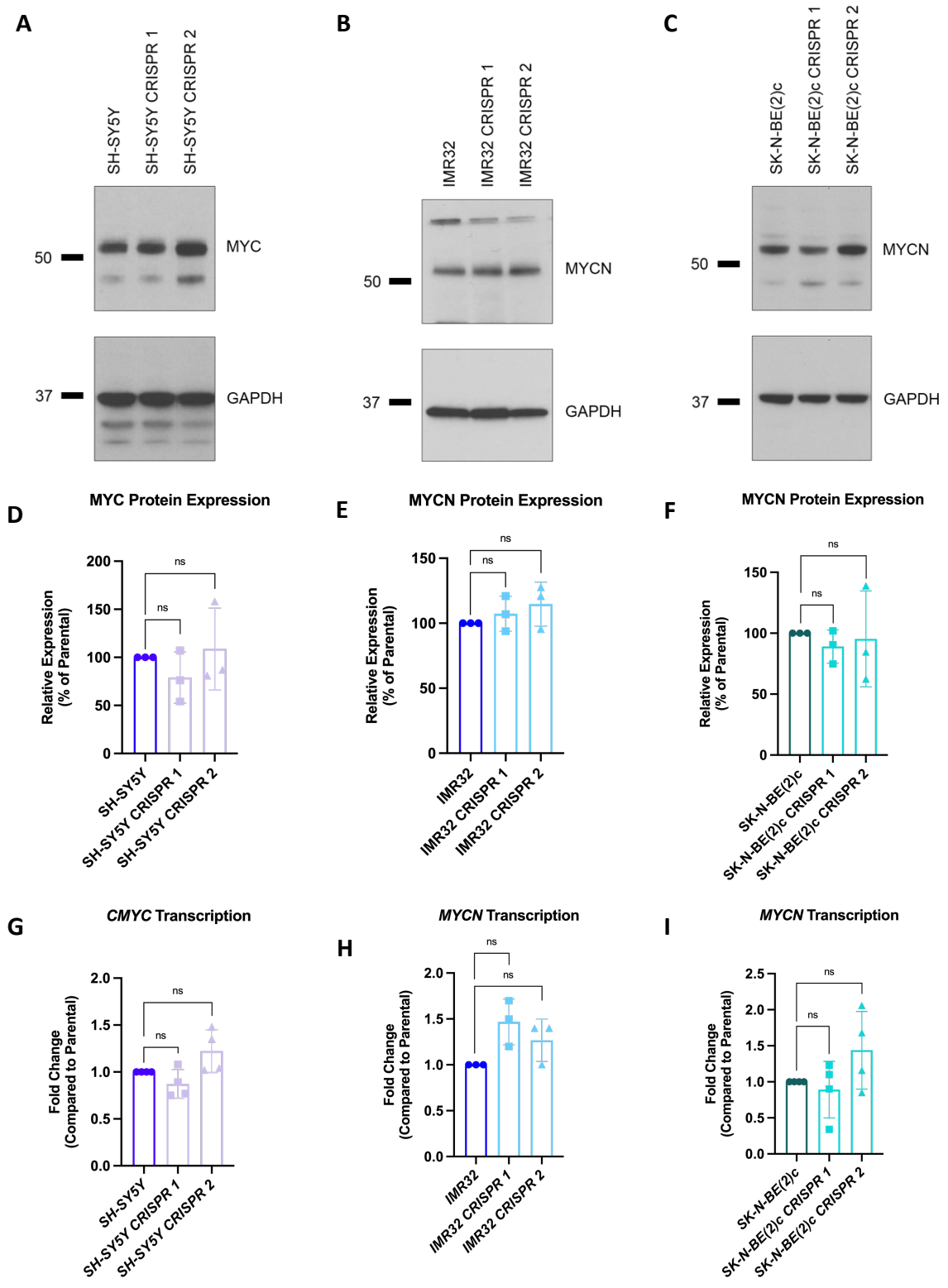

Figure 3.5: MYC levels in parental and ASCL1 KO cells are very similar. Cells were cultured under normal conditions and harvested for western blot and qPCR. Western blot for MYC was completed for the parental SH-SY5Y and the ASCL1 KO lines (A), western blot for MYCN was completed for IMR32 and SK-N-BE(2)c and their associated ASCL1 KO lines (B and C respectively). Western blots were quantitated (n=3) (D-F). qPCR was also completed to show the level of MYC transcription in SH-SY5Y parental and ASCL1 KO lines (G) and the level of MYCN transcription for IMR32 and SK-N-BE(2)c and their associated ASCL1 KO lines (H and I). Graphs show all data points (n=3), the mean value and +/- SEM (ns = p = > 0.05, * = p < 0.05, ** = p < 0.005).

3.2.3 ADRN TFs and MYC are Located in the Nucleus in Parental and ASCL1 KO Cells

Following the observation that the levels of PHOX2A, PHOX2B and MYC protein are similar between parental and ASCL1 KO cells, their cellular localisation was next interrogated. TFs should be most abundant in the nucleus in order to carry out their function, so the localisation was investigated to determine if the lack of ASCL1 is resulting in TFs not being correctly located in the nucleus. Nuclear fractionation followed by western blot was completed on parental and ASCL1 KO cells to identify the localisation of the TFs and detect if there was a difference following the deletion of ASCL1.

PHOX2A (Figure 3.6), PHOX2B (Figure 3.7) and GATA3 (Figure 3.8) are still nuclear localised in parental and ASCL1 KO cells; the levels look to be very similar, and when quantitated there is no significant difference between the abundance of these ADRN TFs in the nucleus of parental and ASCL1 KO cells. MYC is also present in the nucleus. Again, the levels look very similar and when quantitated, there is no significant difference between parental and ASCL1 KO cells (Figure 3.9).

Immunofluorescence (IF) staining and imaging of PHOX2A, PHOX2B and MYCN was then completed to ensure that the TFs were present in the nucleus of every cell. IF analysis shows that PHOX2A (Figure 3.10-3.12), PHOX2B (3.13-3.15) and MYCN (3.16-3.17) are located in the nucleus in both parental and ASCL1 KO cells.

3.2.4 Chromatin Binding of ADRN Transcription Factors is Reduced in ASCL1 KO Cells

After confirming that PHOX2A, PHOX2B, GATA3 and MYC are nuclear localised in parental and ASCL1 KO cells, the next step was to identify whether they were still bound to the chromatin. TFs must be in the nucleus, but also chromatin-bound to carry out their function. In order to study this, chromatin fractionation followed by western blot was completed to determine the levels of chromatin binding of these key TFs.

PHOX2A binding to chromatin is reduced in ASCL1 KO cells relative to parental cells. In SH-SY5Y and IMR32 ASCL1 KO cells, the levels of PHOX2A binding to chromatin drops to below 50% of the amount bound in parental cells. For SK-N-BE(2)c CRISPR 1 cell line there is 20% PHOX2A binding to chromatin compared to parental, and in the CRISPR 2 cell line there is 50% of the amount of PHOX2A bound to chromatin compared to parental cells (Figure 3.18).

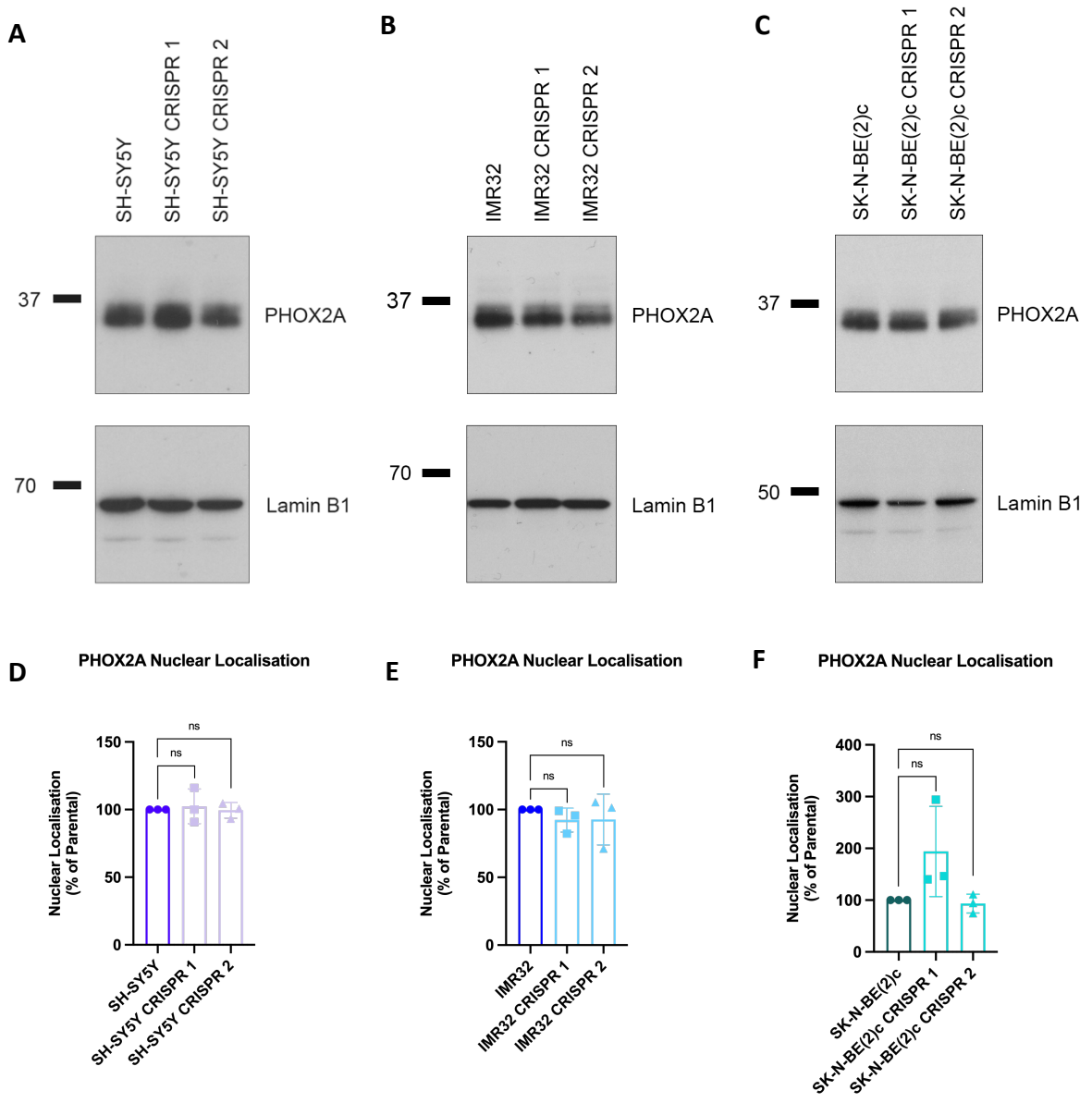

Figure 3.6: PHOX2A is located in the nucleus in Parental and ASCL1 KO cells. Cells were harvested and subject to the subcellular fractionation protocol, followed by western blot. Soluble nuclear fractions of both the parental and ASCL1 KO lines of SH-SY5Y, IMR32 and SK-N-BE(2)c were run on a western blot and analysed for PHOX2A present in the nucleus (A-C respectively). The western blots were quantitated, and the amount of PHOX2A in the nucleus was calculated as a percentage of the nuclear localised PHOX2A in parental cells (D-F). Graphs show all values (n=3), the mean value and +/- SEM (ns = $p > 0.05$).

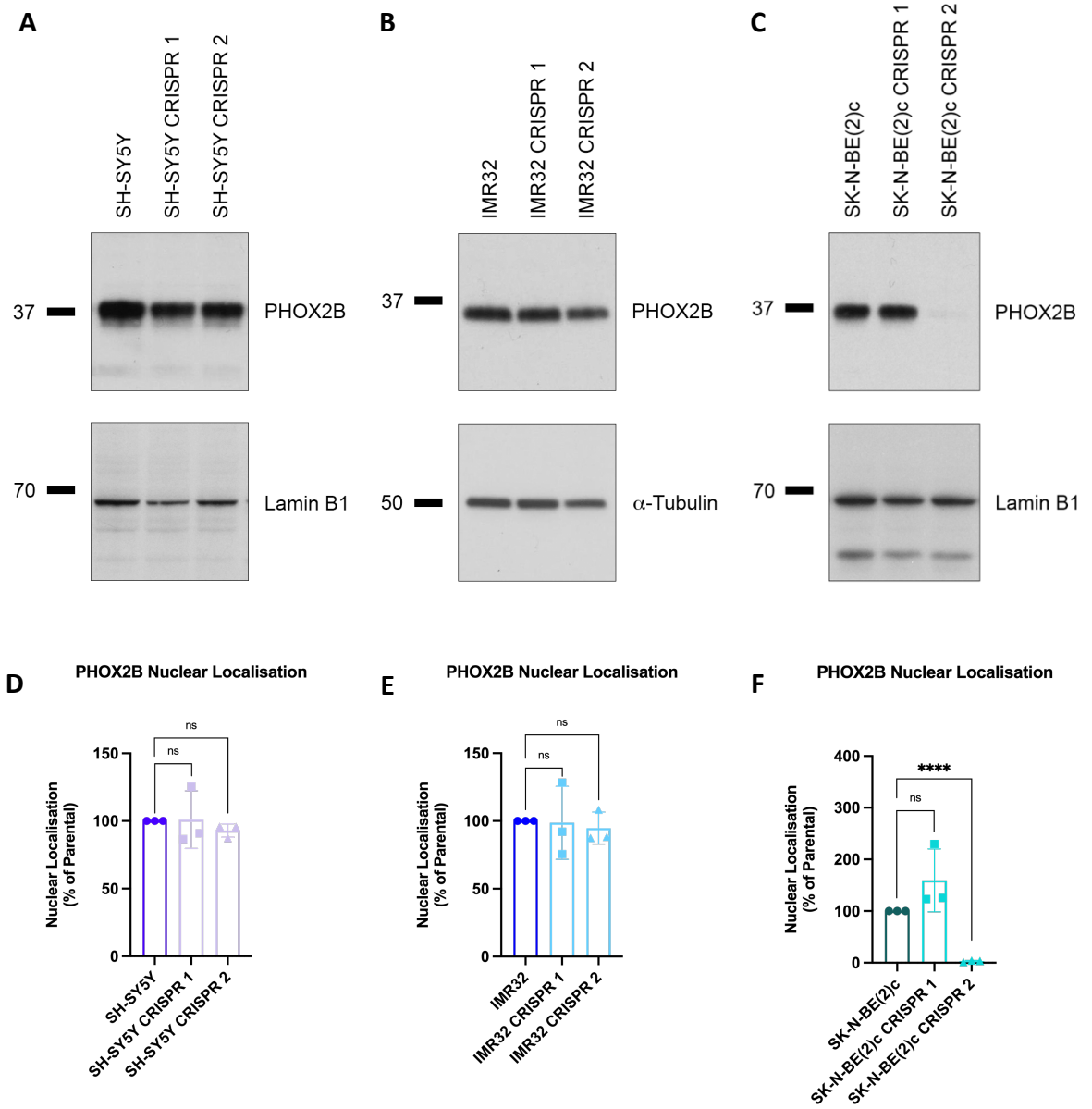

Figure 3.7: PHOX2B is located in the nucleus in ASCL1 KO cells. Cells were harvested and subject to the subcellular fractionation protocol, followed by western blot. Soluble nuclear fractions of both the parental and ASCL1 KO lines of SH-SY5Y, IMR32 and SK-N-BE(2)c were run on a western blot and analysed for PHOX2B present in the nucleus (A-C respectively). The western blots were quantitated, and the level of PHOX2B in the nucleus was calculated as a percentage of the nuclear localised PHOX2B in parental cells. Graphs show all values (n=3), the mean value and +/- SEM (ns = $p > 0.05$, **** $p = < 0.0001$).

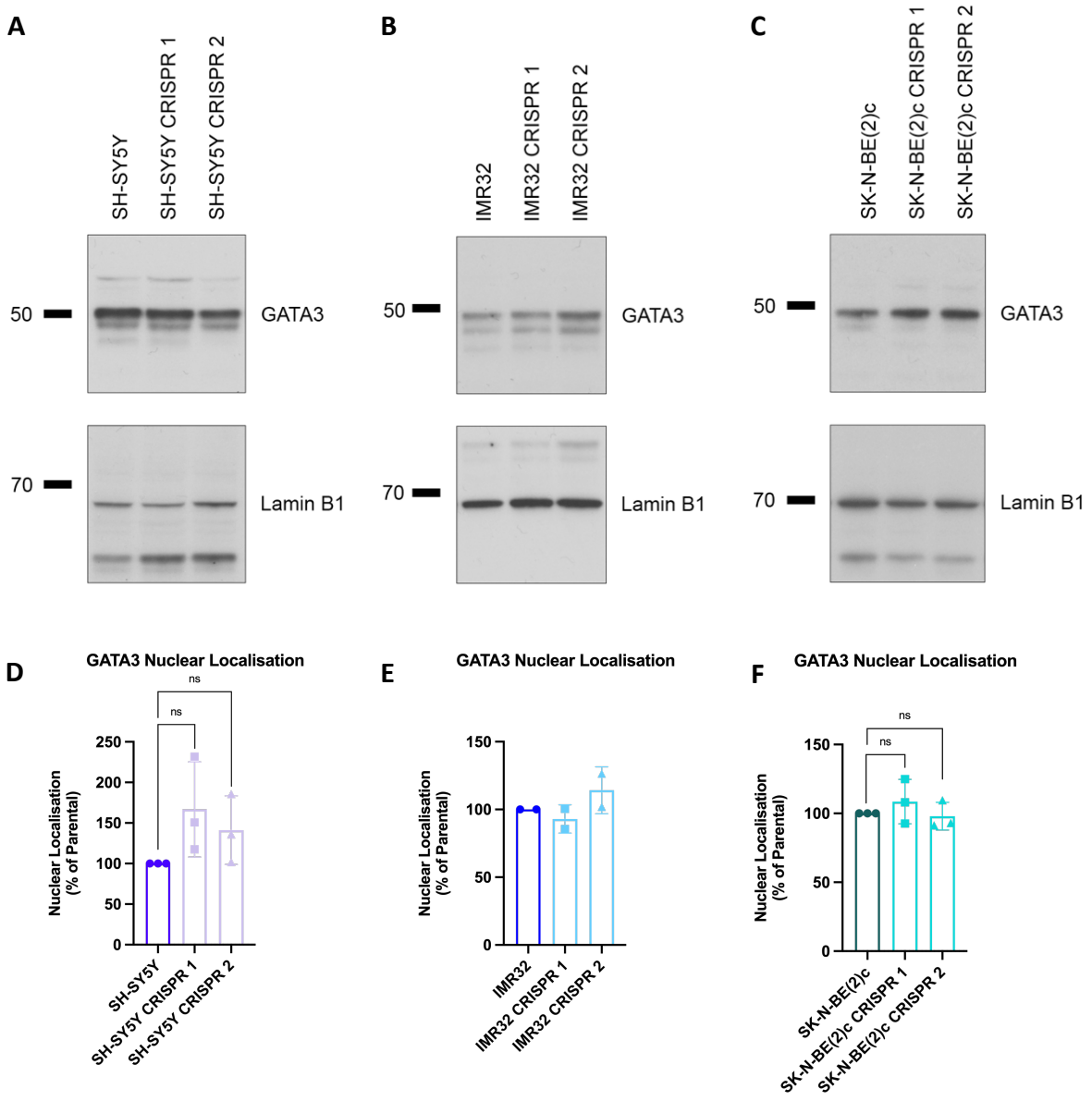

Figure 3.8: GATA3 is located in the nucleus in ASCL1 KO cells. Cells were harvested and subject to the subcellular fractionation protocol, followed by western blot. Soluble nuclear fractions of both the parental and ASCL1 KO lines of SH-SY5Y, IMR32 and SK-N-BE(2)c were run on a western blot and analysed for GATA3 present in the nucleus (A-C respectively). The western blots were quantitated, and the level of GATA3 in the nucleus was calculated as a percentage of the nuclear localised GATA3 in parental cells. Graphs show all values (n=3), the mean value and +/- SEM (ns = $p > 0.05$).

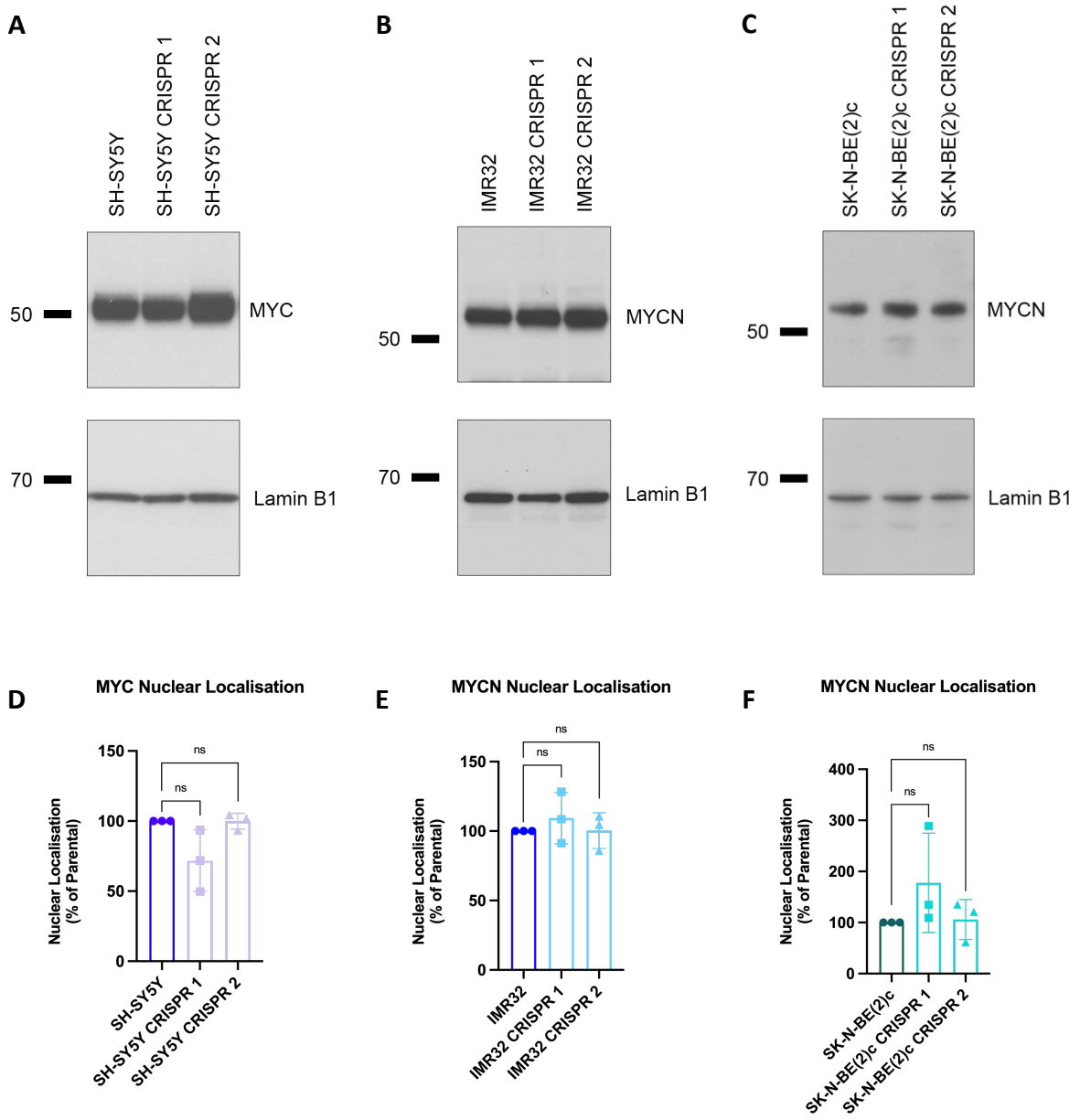

Figure 3.9: MYC and MYCN are located in the nucleus in parental and ASCL1 KO cells. Cells were harvested and subject to the subcellular fractionation protocol, followed by western blot. Soluble nuclear fractions of both the parental and ASCL1 KO lines of SH-SY5Y, IMR32 and SK-N-BE(2)c were run on a western blot and analysed for nuclear localised MYC (SH-SY5Y, A) or MYCN (IMR32 and SK-N-BE(2)c, B and C). The western blots were quantitated, and the abundance of MYC/MYCN was calculated as a percentage of the nuclear localised MYC/MYCN in parental cells. Graphs show all values (n=3), the mean value and +/- SEM (ns = $p > 0.05$).

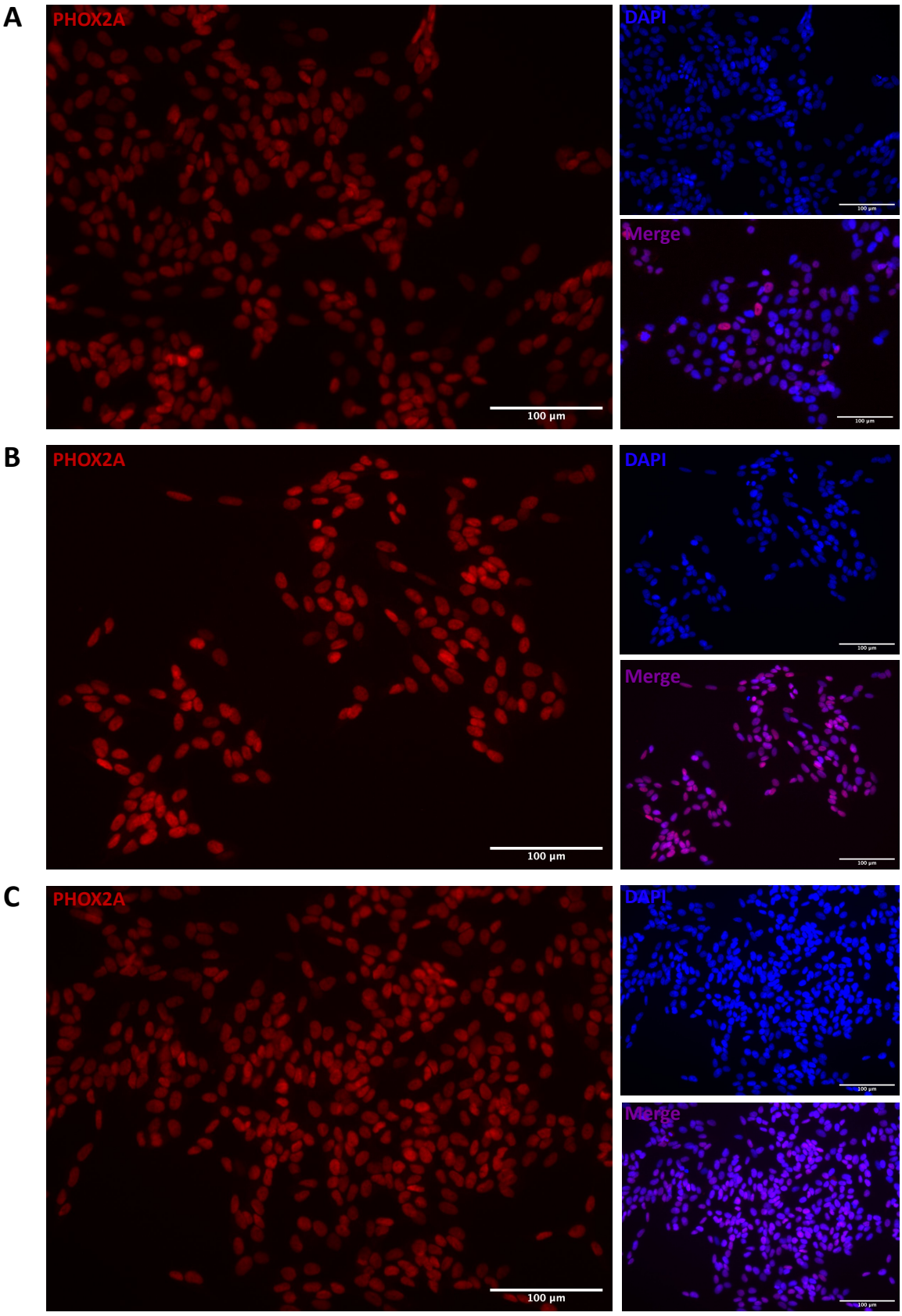

Figure 3.10: The Localisation of PHOX2A in SH-SY5Y and CRISPR cells. Immunofluorescence staining and imaging to show the localisation of PHOX2A in SH-SY5Y parental (A), CRISPR 1 (B) and CRISPR 2 (C) cells. Cells were immunostained with PHOX2A (red) and DAPI (blue). Images were taken on the Zeiss 4000 microscope at 20X magnification.

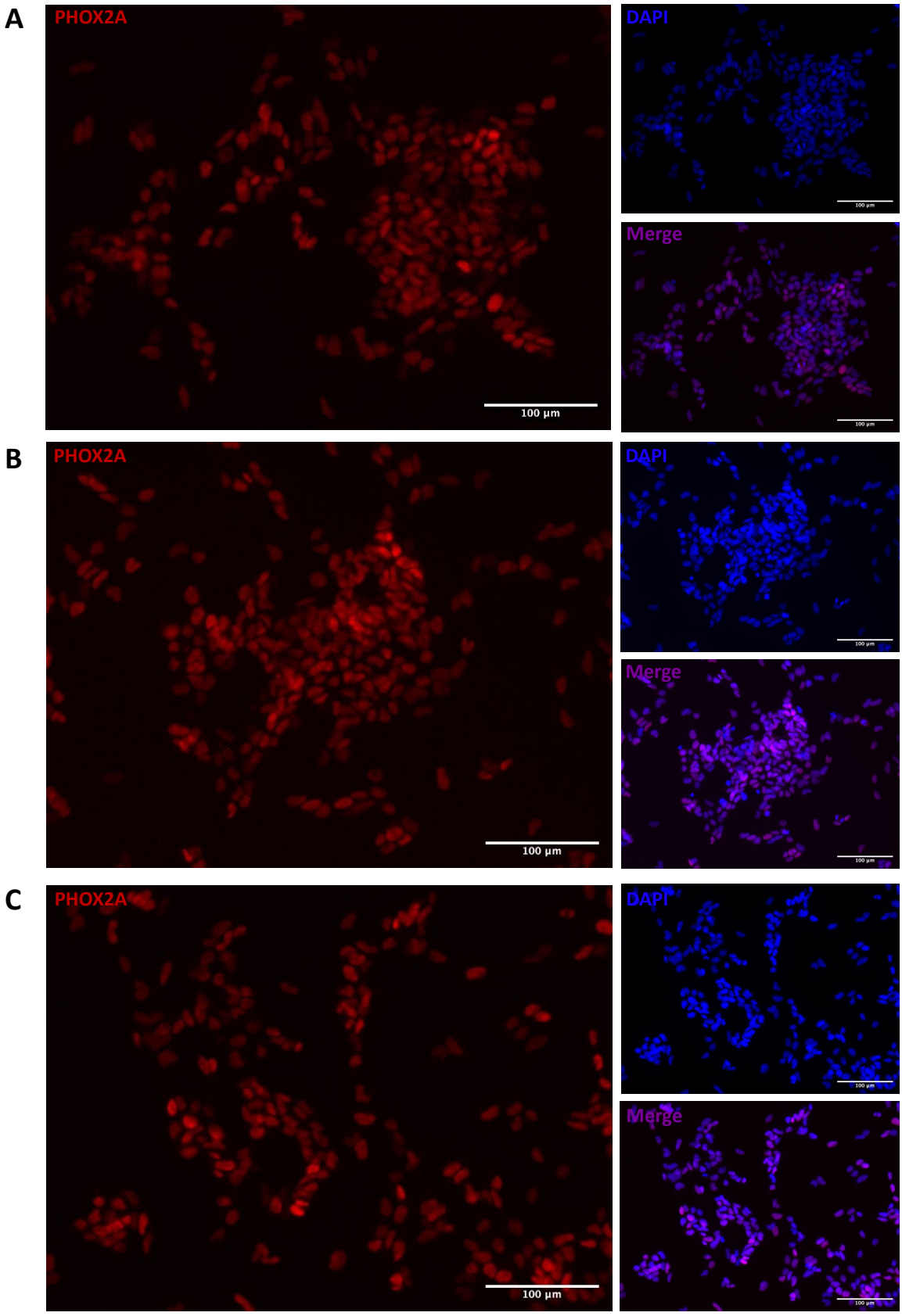

Figure 3.11: The Localisation of PHOX2A in IMR32 and CRISPR cells. Immunofluorescence staining and imaging to show the localisation of PHOX2A in IMR32 parental (A), CRISPR 1 (B) and CRISPR 2 (C) cells. Cells were immunostained with PHOX2A (red) and DAPI (blue). Images were taken on the Zeiss 4000 microscope at 20X magnification.

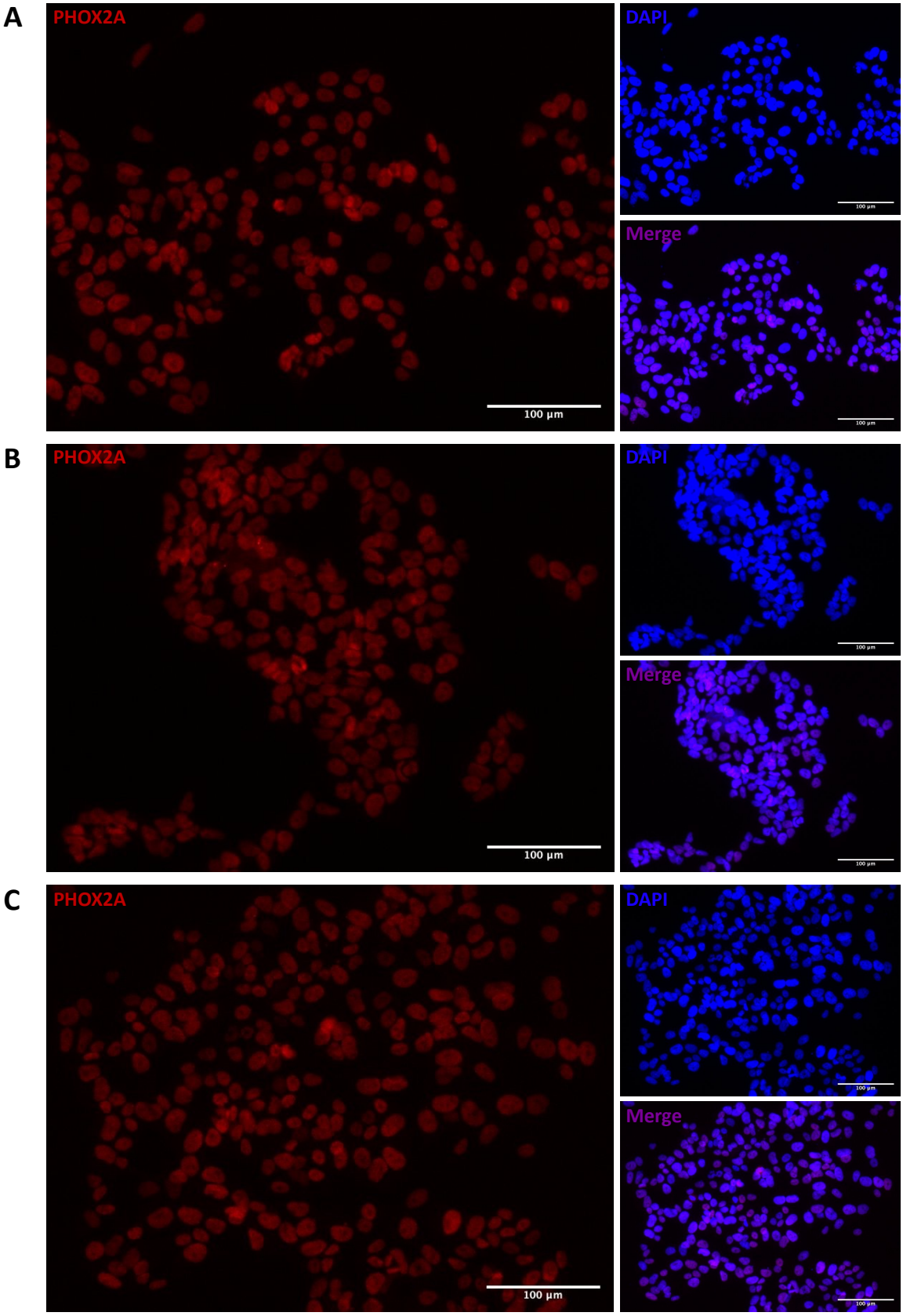

Figure 3.12: The localisation of PHOX2A in SK-N-BE(2)c parental and CRISPR cells. Immunofluorescence staining and imaging to show the localisation of PHOX2A in SK-N-BE(2)c parental (A), CRISPR 1 (B) and CRISPR 2 (C) cells. Cells were immunostained with PHOX2A (red) and DAPI (blue). Images were taken on the Zeiss 4000 microscope at 20X magnification.

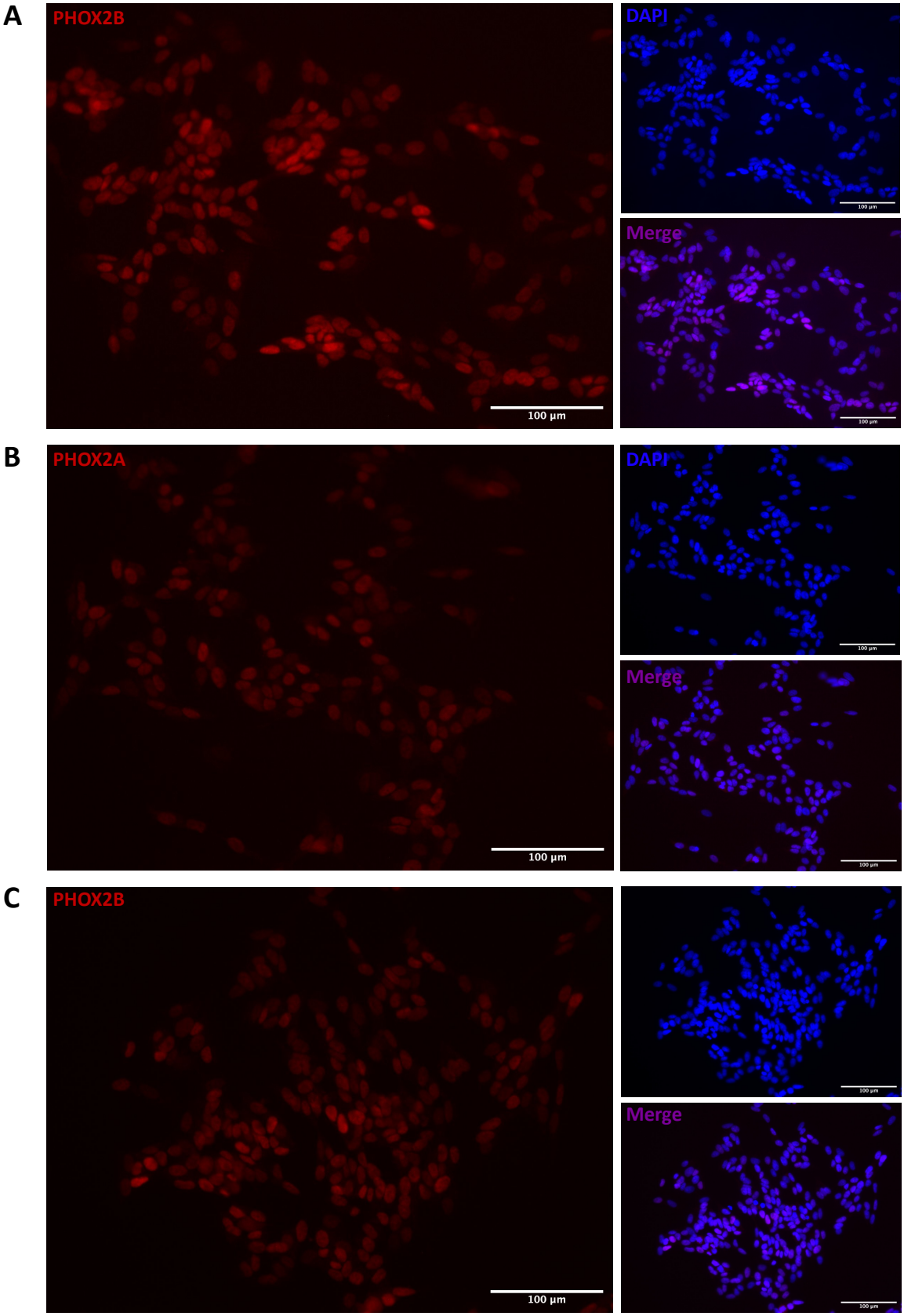

Figure 3.13: The Localisation of PHOX2B in SH-SY5Y and CRISPR cells. Immunofluorescence staining and imaging to show the localisation of PHOX2B in SH-SY5Y parental (A), CRISPR 1 (B) and CRISPR 2 (C) cells. Cells were immunostained with PHOX2B (red) and DAPI (blue). Images were taken on the Zeiss 4000 microscope at 20X magnification.

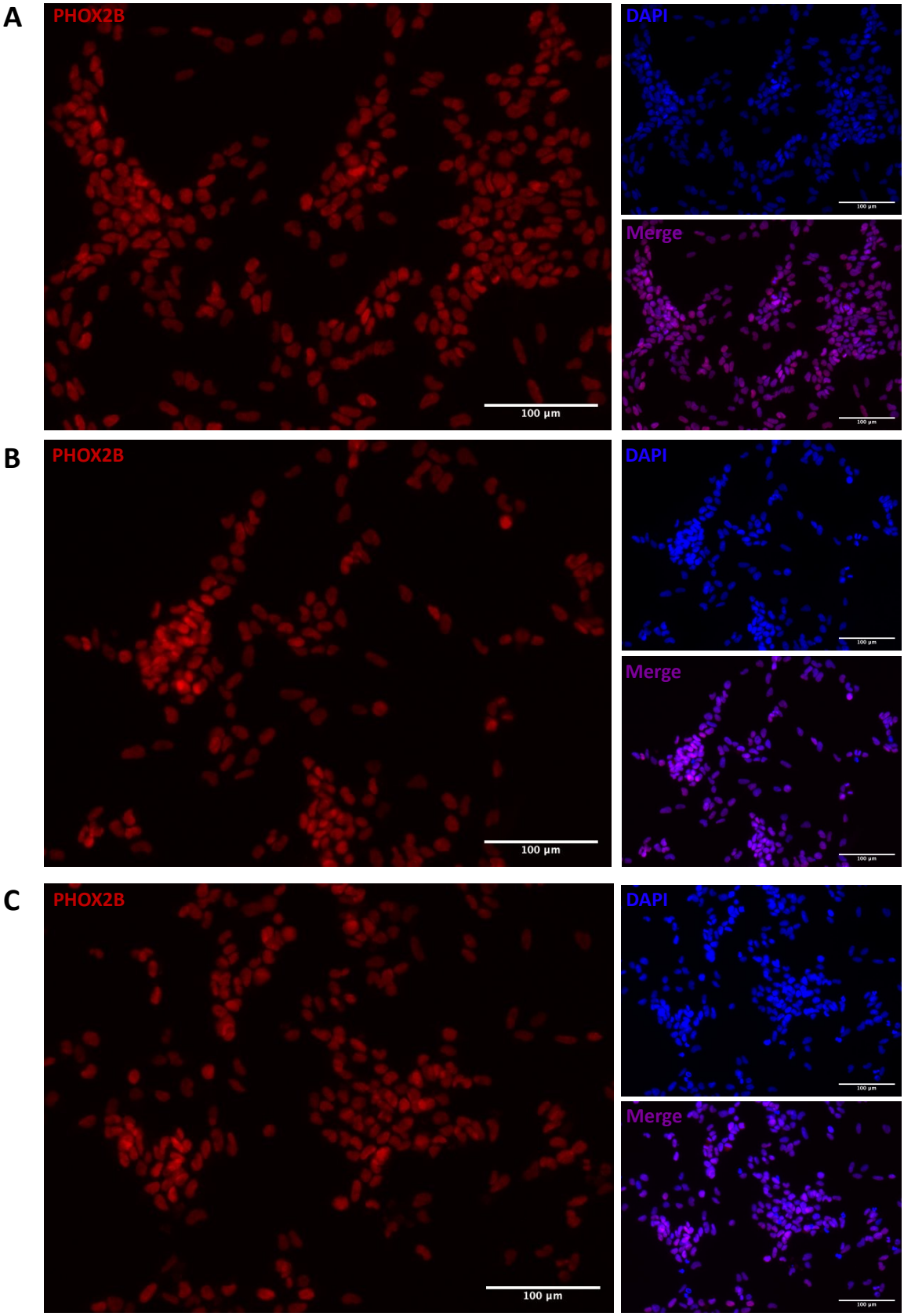

Figure 3.14: The localisation of PHOX2B in IMR32 parental and ASCL1 KO cells. Immunofluorescence staining and imaging to show the localisation of PHOX2B in IMR32 parental (A), CRISPR 1 (B) and CRISPR 2 (C) cells. Cells were immunostained with PHOX2B (red) and DAPI (blue). Images were taken on the Zeiss 4000 microscope at 20X magnification.

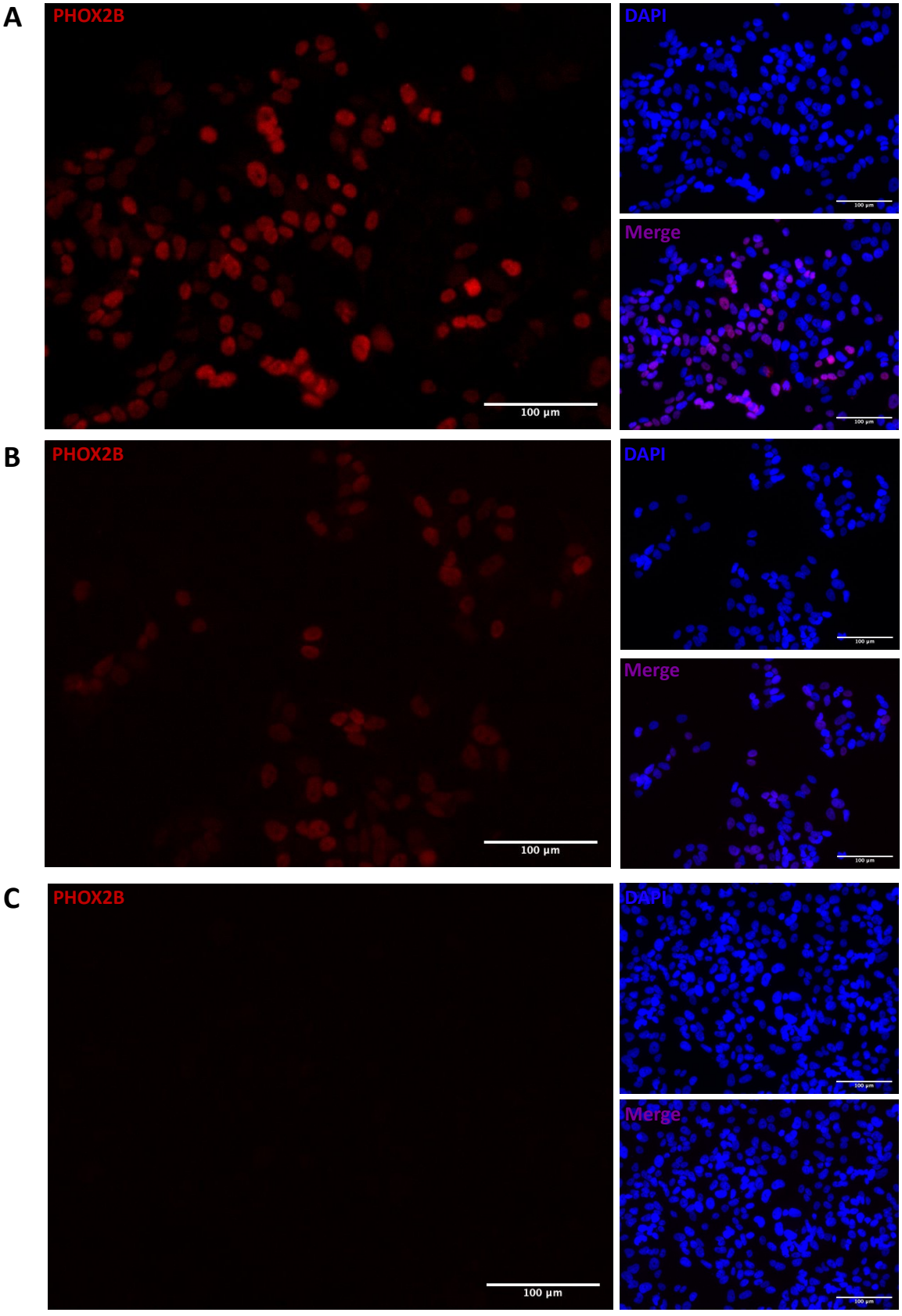

Figure 3.15: The localisation of PHOX2B in SK-N-BE(2)c parental and ASCL1 KO cells. Immunofluorescence staining and imaging to show the localisation of PHOX2B in SK-N-BE(2)c parental (A), CRISPR 1 (B) and CRISPR 2 (C) cells. Cells were immunostained with PHOX2B (red) and DAPI (blue). Images were taken on the Zeiss 4000 microscope at 20X magnification.

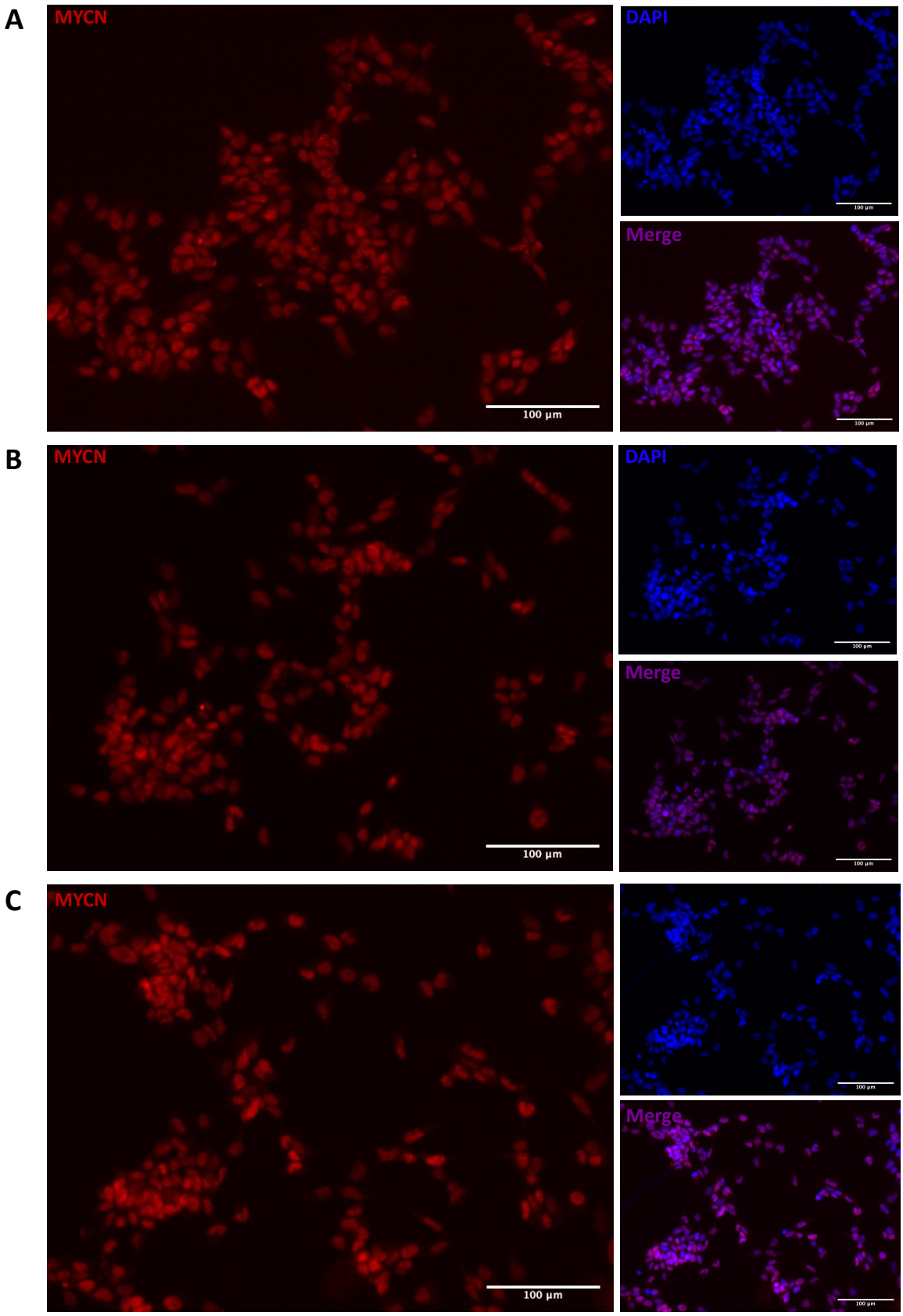

Figure 3.16: The Localisation of MYCN in IMR32 and IMR32 ASCL1 KO Cells. Immunofluorescence staining and imaging to show the localisation of MYCN in IMR32 parental (A), CRISPR 1 (B) and CRISPR 2 (C) cells. Cells were immunostained with MYCN (red) and DAPI (blue). Images were taken on the Zeiss 4000 microscope at 20X magnification.

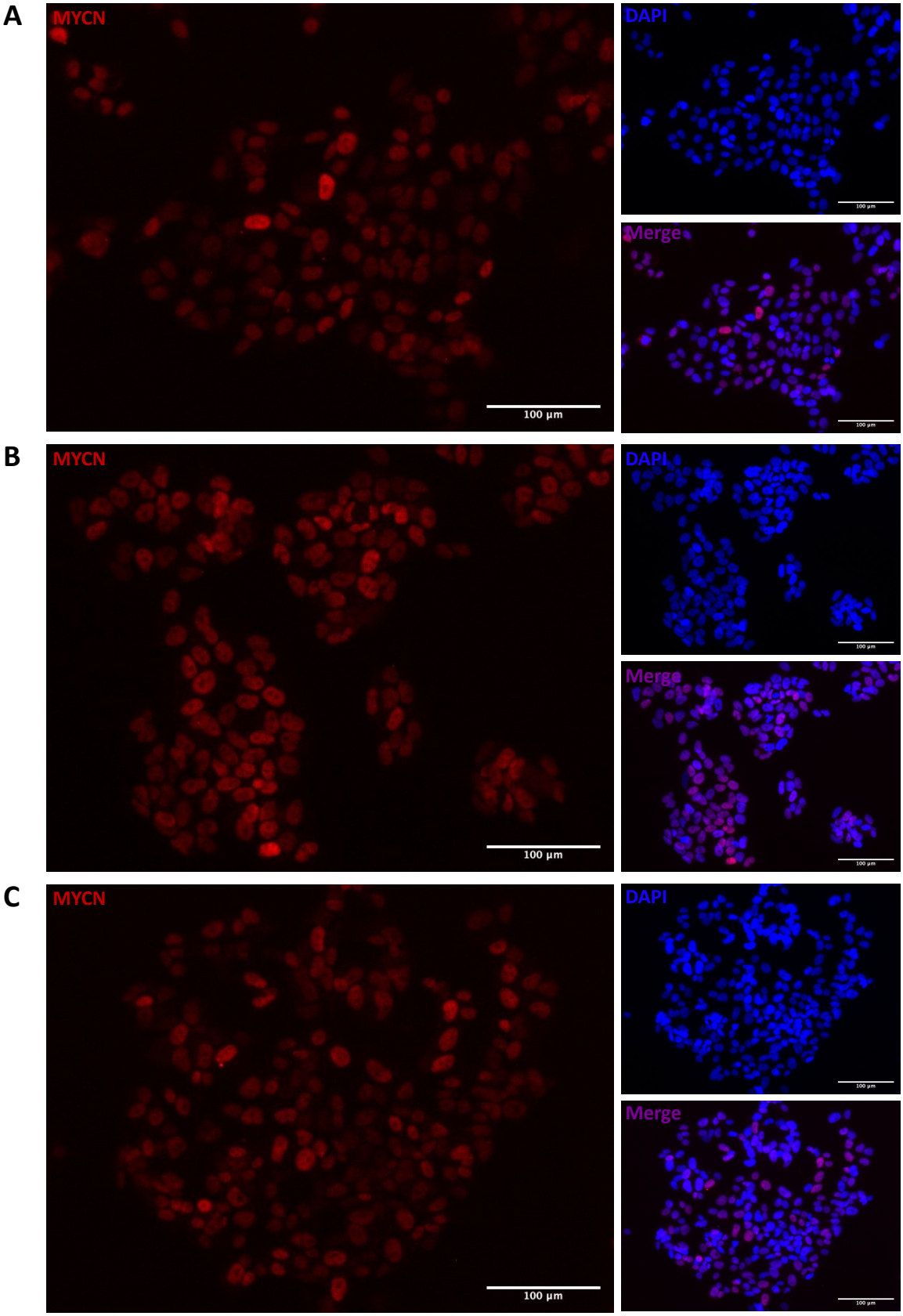

Figure 3.17: The Localisation of MYCN in SK-N-BE(2)c Parental and ASCL1 KO Cells. Immunofluorescence staining and imaging to show the localisation of MYCN in SK-N-BE(2)c parental (A), CRISPR 1 (B) and CRISPR 2 (C) cells. Cells were immunostained with MYCN (red) and DAPI (blue). Images were taken on the Zeiss 4000 microscope at 20X magnification.

PHOX2B binding to chromatin is also reduced in ASCL1 KO cells relative to parental controls. In SH-SY5Y and IMR32 ASCL1 KO cells, the levels of PHOX2B binding to chromatin drops to below 50% of the levels seen in the parental lines. For SK-N-BE(2)c ASCL1 KO cells, the levels are much lower, around 20% of the PHOX2B chromatin binding seen in parental lines. For the CRISPR 2 line this is to be expected, as the levels of PHOX2B overall are much lower (Figure 3.19). Similarly, the amount of GATA3 protein bound to chromatin is lower in ASCL1 KO cells compared to the parental controls. (Figure 3.20). All ASCL1 KO lines show less than 50% of the level of GATA3 bound to the chromatin compared to their parental counterparts.

A similar phenotype is observed for the chromatin association of MYC. The average levels of MYC binding to chromatin in SH-SY5Y ASCL1 KO cells is 80% lower than the amount of chromatin bound MYC in SH-SY5Y parental lines. For the IMR32 ASCL1 KO lines, chromatin binding of MYCN is 50% lower than the levels seen in parental lines, and for SK-N-BE(2)c, the MYCN chromatin binding is 70% lower (Figure 3.21).

Despite the overall protein levels of PHOX2A, PHOX2B, GATA3 and MYC being generally the same in parental and CRISPR lines, and the proteins being localised in the nucleus, the chromatin binding of these key TFs in ASCL1 KO lines is significantly reduced. The importance of these TFs in driving the proliferation of neuroblastoma cells has been described, and the lower chromatin binding could explain why the ASCL1 KO cells grow more slowly. The lack of ASCL1 is having a clear effect on the ability of these TFs to bind chromatin, understanding the mechanisms behind this could help gain a greater understanding of the role of ASCL1 in neuroblastoma.

3.2.6 ASCL1 interacts with PHOX2A and PHOX2B on the Chromatin

After the observation that removing ASCL1 is reducing the binding of key TFs to the chromatin, the mechanism by which ASCL1 could be affecting chromatin binding was then hypothesised. ASCL1 could be involved in recruiting TFs to the chromatin, or ASCL1 could be altering chromatin accessibility.

In order to investigate the possibility of ASCL1 recruiting TFs, Rapid Immunoprecipitation Mass spectrometry of Endogenous proteins (RIME) data was interrogated. RIME involves formaldehyde fixation of proteins to the chromatin, followed by immunoprecipitation (IP) of the protein of interest. The IP product is then broken down into peptides and run through the Mass-Spec to identify proteins bound to the protein of interest (Mohammed et al., 2016). Fahad Ali completed

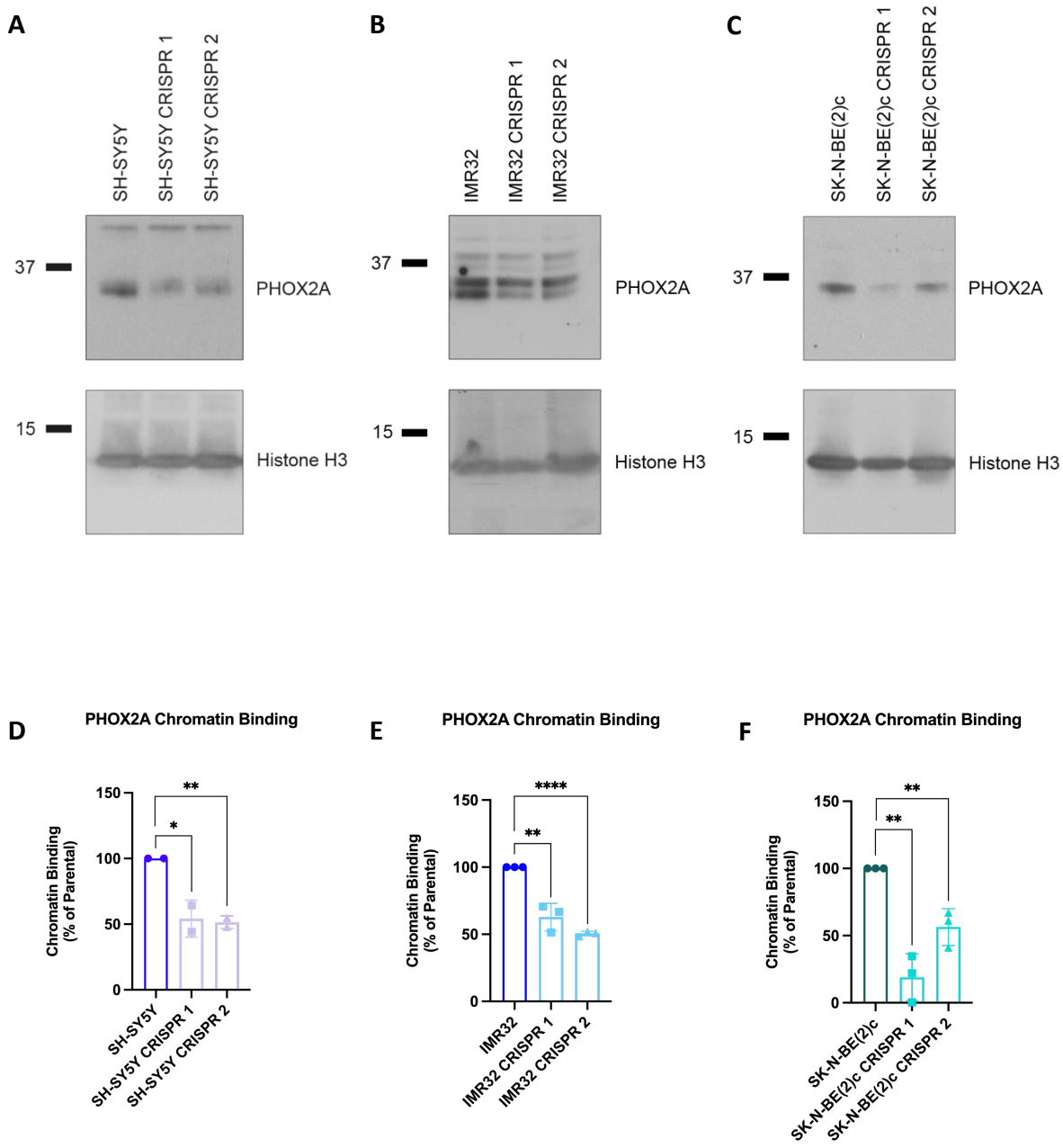

Figure 3.18: Chromatin binding of PHOX2A in ASCL1 KO cells is reduced. Cells were harvested and subject to the subcellular fractionation protocol, followed by western blot. Chromatin fractions of both the parental and ASCL1 KO lines of SH-SY5Y, IMR32 and SK-N-BE(2)c were run on a western blot and analysed for chromatin bound PHOX2A (A-C respectively). The western blots were quantitated, and the amount of chromatin bound PHOX2A was calculated as a percentage of the chromatin bound PHOX2A in parental cells (D-F). Graphs show all data points (n=3), bars represent the mean value and +/- SEM is shown (** = $p < 0.005$, *** = $p < 0.0005$, **** $p = < 0.0001$).

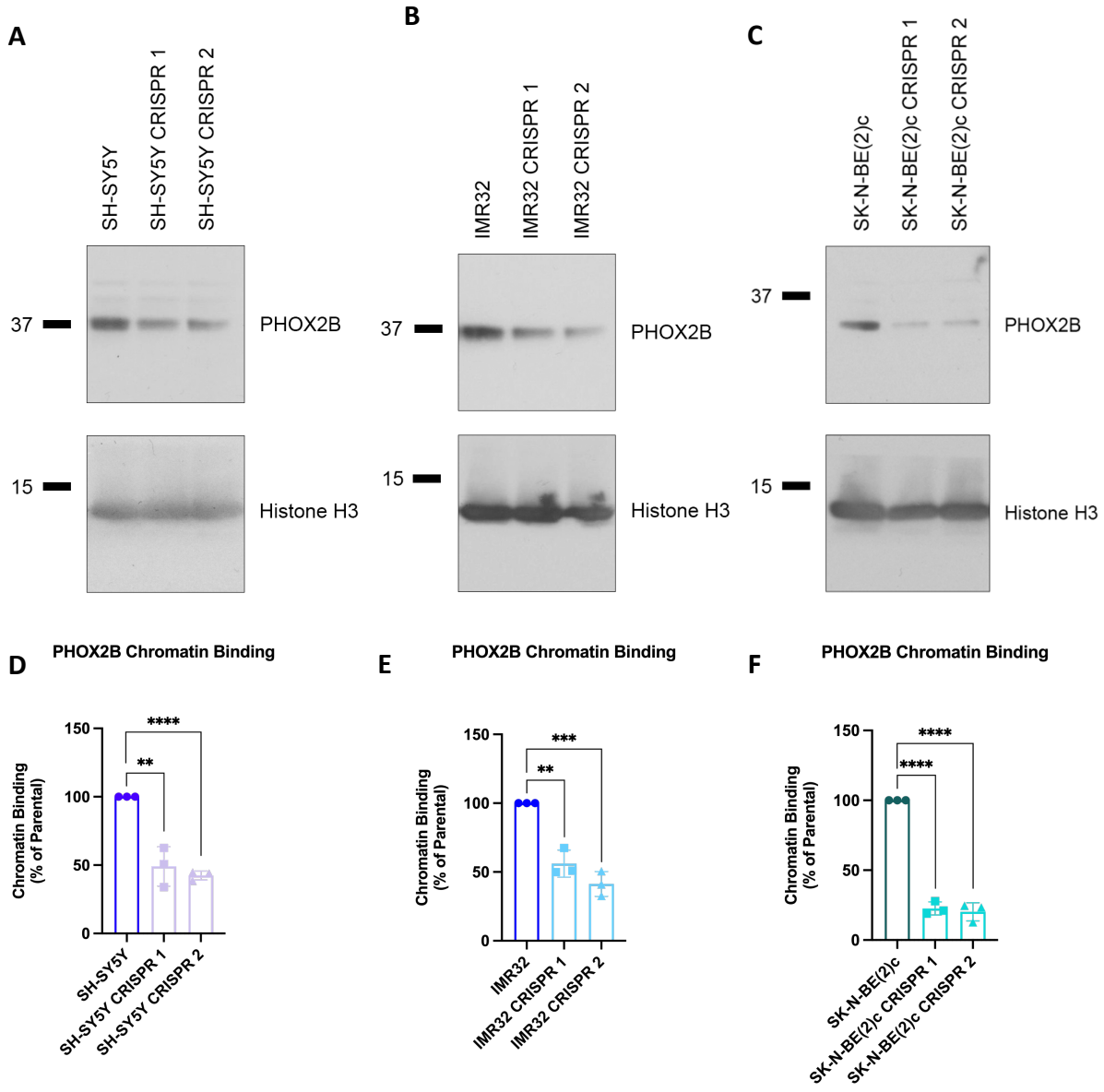

Figure 3.19: Chromatin binding of PHOX2B in ASCL1 KO cells is reduced. Cells were harvested and subject to the subcellular fractionation protocol, followed by western blot. Chromatin fractions of both the parental and ASCL1 KO lines of SH-SY5Y, IMR32 and SK-N-BE(2)c were run on a western blot and analysed for chromatin bound PHOX2B (A-C respectively). The western blots were quantitated, and the amount of chromatin bound PHOX2B was calculated as a percentage of the chromatin bound PHOX2B in parental cells (D-F). Graphs show all data points (n=3), bars represent the mean value and +/- SEM is shown (** = $p < 0.005$, *** = $p < 0.0005$, **** $p = < 0.0001$).

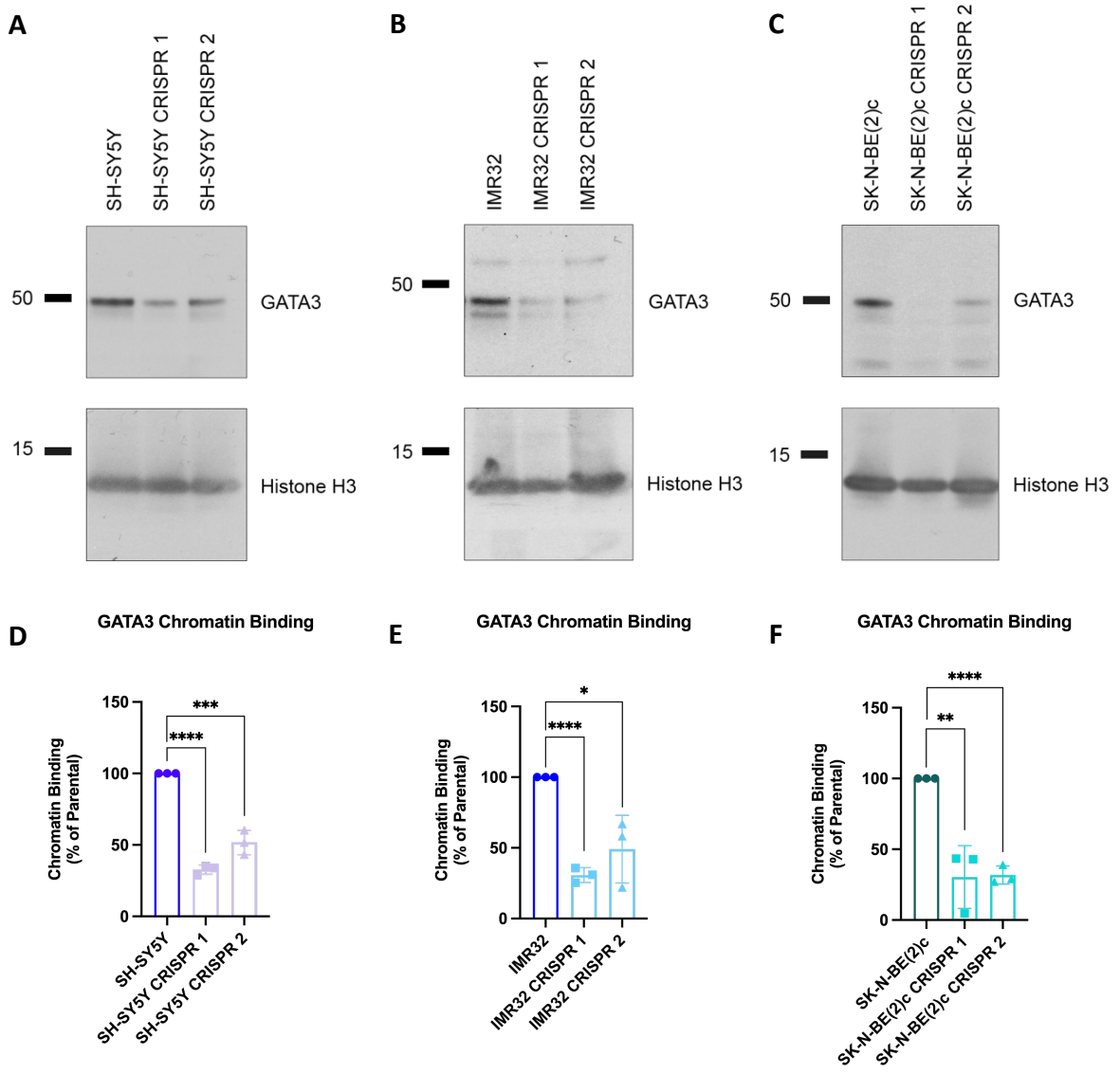

Figure 3.20: Chromatin binding of GATA3 in ASCL1 KO cells is reduced. Cells were harvested and subject to the subcellular fractionation protocol, followed by western blot. Chromatin fractions of both the parental and ASCL1 KO lines of SH-SY5Y, IMR32 and SK-N-BE(2)c were run on a western blot and analysed for chromatin bound GATA3 (A-C respectively). The western blots were quantitated, and the amount of chromatin bound GATA3 was calculated as a percentage of the chromatin bound GATA3 in parental cells (D-F). Graphs show all values and the mean (n=3) (** = $p < 0.005$, *** = $p < 0.0005$, **** $p = < 0.0001$).

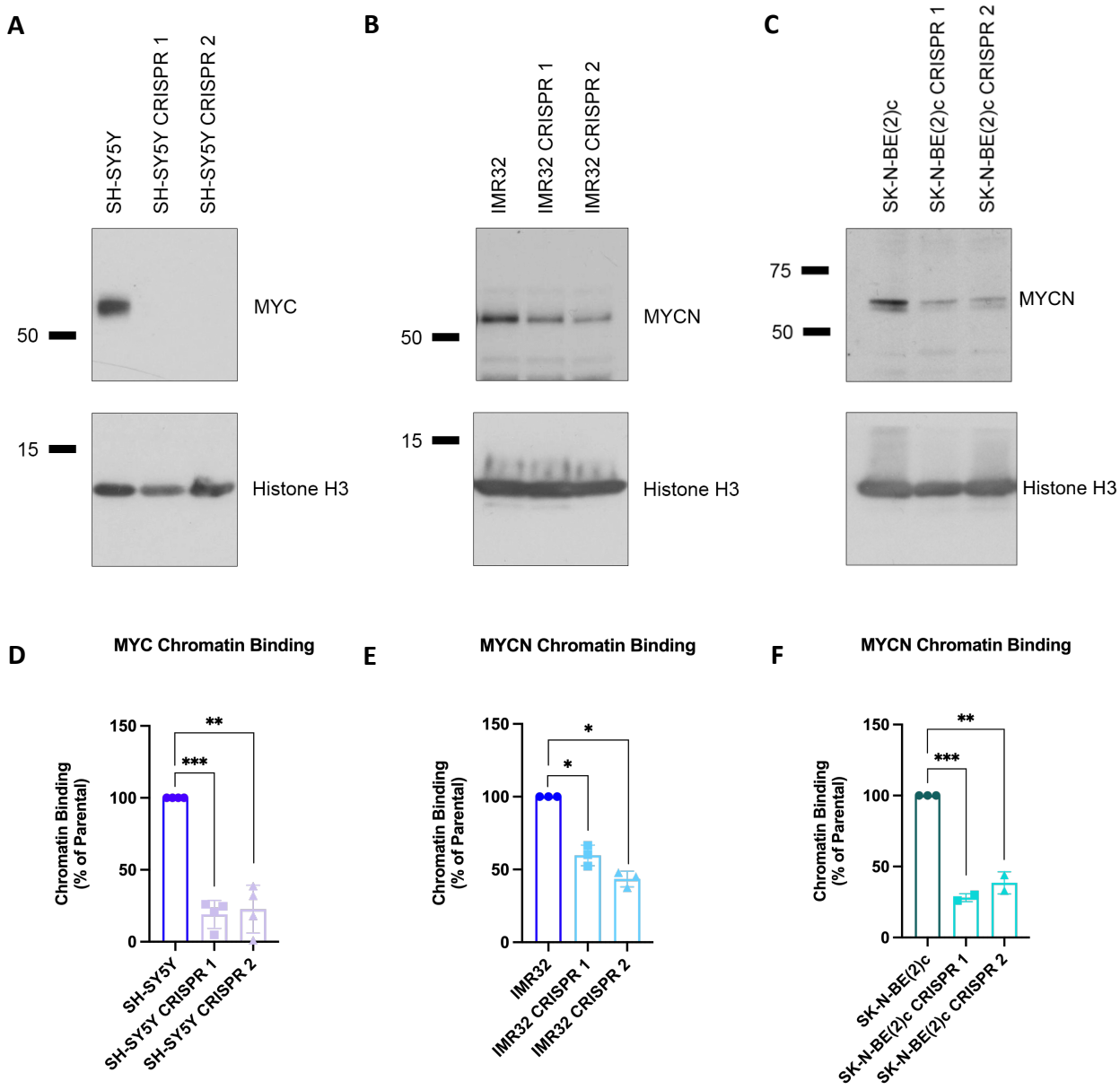

Figure 3.21. Chromatin binding of MYC in ASCL1 KO cells is reduced. Cells were harvested and subject to the subcellular fractionation protocol, followed by western blot. Chromatin fractions of both the parental and ASCL1 KO lines of SH-SY5Y, IMR32 and SK-N-BE(2)c were run on a western blot and analysed for chromatin bound MYC (SH-SY5Y, A) or MYCN (IMR32 and SK-N-BE(2)c, B-C respectively). The western blots were quantitated, and the amount of chromatin bound MYC was calculated as a percentage of the chromatin bound MYC in parental cells (D-F). Graphs show all data points (n=3), bars represent the mean value and +/- SEM is shown (** = $p < 0.005$, *** = $p < 0.0005$, **** $p = < 0.0001$).

RIME on SH-SY5Y cells to identify binding partners of chromatin bound ASCL1. The proteins identified as ASCL1 binding partners were compared to the Van Groningen ADRN gene set of 369 genes. When selecting for only ADRN targets, 47 proteins that associate with ASCL1 on the chromatin were also ADRN associated genes (Figure 3.22 A, Table 4.1). Importantly, PHOX2A and PHOX2B are identified using this method of selection (Figure 3.22 B). This shows ASCL1 is interacting with PHOX2A and PHOX2B on the chromatin, so ASCL1 could be recruiting these proteins or assisting their chromatin binding. However, there are many ADRN targets, including GATA3, that do not appear as binding partners in the RIME analysis, and MYC is not identified as an ASCL1 interactor either, indicating another mechanism behind the lower levels of chromatin binding of TFs in ASCL1 KO cells.

Following interrogation of RIME data and the observation that ASCL1 and PHOX2B interact on the chromatin, it was next determined if the proteins interact elsewhere in the cell. To investigate this, immunoprecipitations (IP) and co-IPs were run on whole cell samples as well as the cytoplasmic, nuclear and chromatin cellular fractions to confirm the interaction. Firstly, the IP was completed with ASCL1 and PHOX2B and the products run on a western blot. ASCL1 is at the highest level in the nucleus and can also be detected in the chromatin fraction. PHOX2B can also be detected in the nucleus and chromatin and levels are similar between the two cellular compartments. Following confirmation the two proteins could be detected, a co-IP was run to confirm interaction. ASCL1 IP was completed, followed by a western blot to detect PHOX2B. The sample using protein from the whole cell confirms ASCL1 and PHOX2B interaction in the cell. When testing the cellular fractions, PHOX2B-ASCL1 interaction can only be detected in the chromatin fraction (Figure 3.23). Despite the levels of the two TFs being higher in the nucleus they do not interact there, indicating recruitment or co- binding occurring.

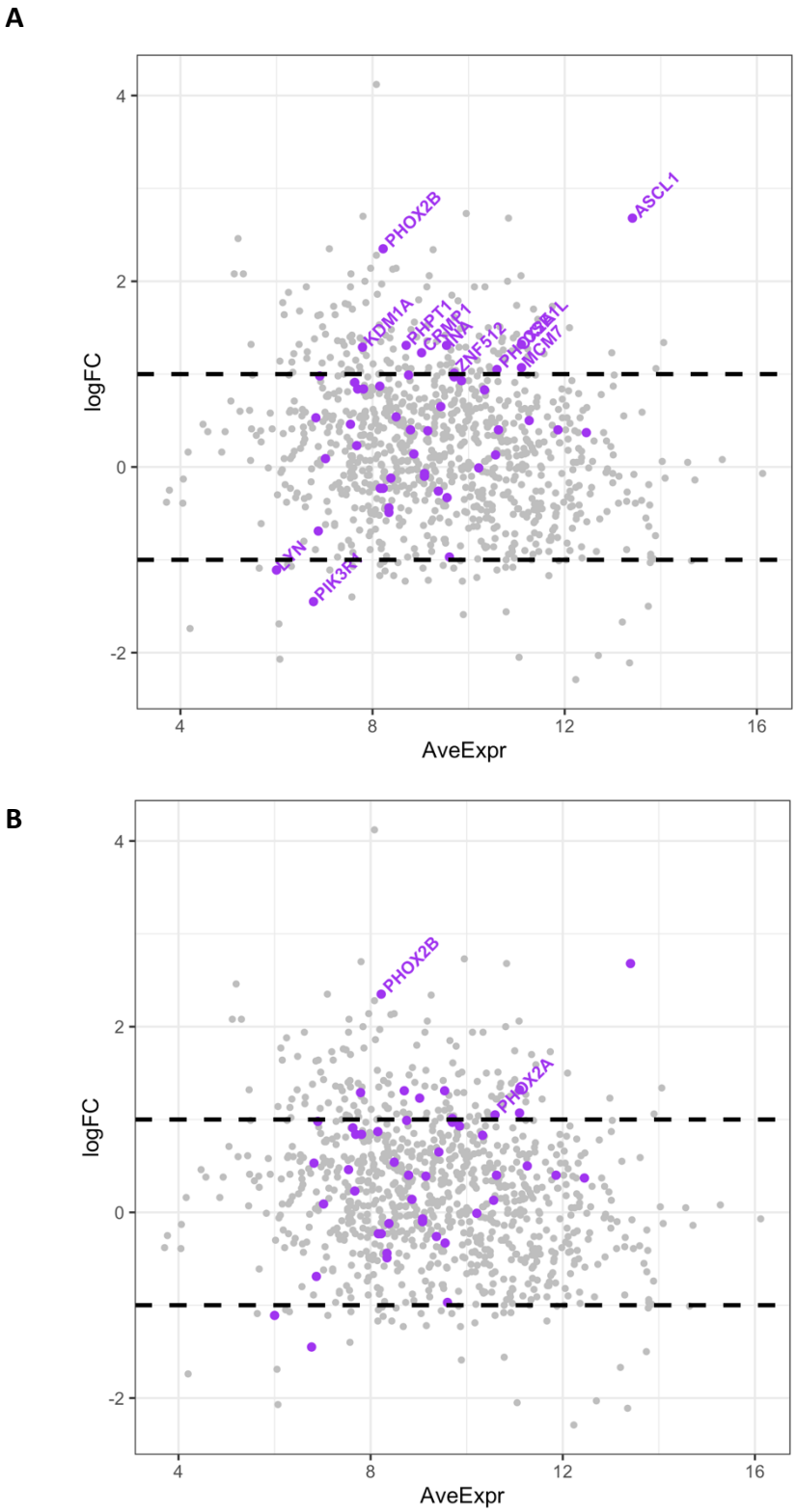

Figure 3.22: RIME analysis shows PHOX2A and PHOX2B interact with ASCL1 on the chromatin. Fahad Ali completed RIME analysis on SH-SY5Y cells to identify ASCL1 binding partners. The total list of ASCL1 binding partners was filtered to identify members of the ADRN CRC that are interacting with ASCL1 on the chromatin, these proteins are labelled as purple points. All the significantly bound ADRN targets are labelled (A), and PHOX2A and PHOX2B are shown (B).

Gene Symbol	Description
ACOT7	Cytosolic acyl coenzyme A thioester hydrolase
ANP32A	Acidic leucine-rich nuclear phosphoprotein 32 family member A
ASCL1	Achaete-scute homolog 1
CKB	Creatine kinase B-type
CRMP1	Dihydropyrimidinase-related protein 1
CSE1L	Exportin-2
DDX39A	ATP-dependent RNA helicase DDX39A
DNAJB1	DnaJ homolog subfamily B member 1
DNAJC9	DnaJ homolog subfamily C member 9
DPYSL2	Dihydropyrimidinase-related protein 2
DPYSL3	Dihydropyrimidinase-related protein 3
DPYSL5	Dihydropyrimidinase-related protein 5
EEF1A2	Elongation factor 1-alpha 2
ELAVL4	ELAV-like protein 4
EML4	Echinoderm microtubule-associated protein-like 4
FIGNL1	Fidgetin-like protein 1
FKBP4	Peptidyl-prolyl cis-trans isomerase FKBP4
GATA2	Endothelial transcription factor GATA-2
H1FX	Histone H1x
HMGA1	High mobility group protein HMG-I/HMG-Y
HNRNPA0	Heterogeneous nuclear ribonucleoprotein A0
INA	Alpha-internexin
KDM1A	Lysine-specific histone demethylase 1A
LSM4	U6 snRNA-associated Sm-like protein LSm4
LYN	Tyrosine-protein kinase Lyn
MAP1B	Microtubule-associated protein 1B
MCM2	DNA replication licensing factor MCM2
MCM6	DNA replication licensing factor MCM6
MCM7	DNA replication licensing factor MCM7
MSH6	DNA mismatch repair protein Msh6
MYEF2	Myelin expression factor 2
OLA1	Obg-like ATPase 1
PHOX2A	Paired mesoderm homeobox protein 2A
PHOX2B	Paired mesoderm homeobox protein 2B
PHPT1	14 kDa phosphohistidine phosphatase
PIK3R1	Phosphatidylinositol 3-kinase regulatory subunit alpha
PRC1	Protein regulator of cytokinesis 1
RANBP1	Ran-specific GTPase-activating protein
RBP1	Retinol-binding protein 1
STXBP1	Syntaxin-binding protein 1
SYNPO2	Synaptopodin-2
TMOD1	Tropomodulin-1
TMOD2	Tropomodulin-2
TUBB3	Tubulin beta-3 chain
TUBB4B	Tubulin beta-4B chain
ZNF24	Zinc finger protein 24
ZNF512	Zinc finger protein 512

Table 3.1: ADRN proteins that are identified as ASCL1 binding partners. Fahad Ali completed RIME analysis on SH-SY5Y cells to identify ASCL1 binding partners. The total list of ASCL1 binding partners was filtered to identify members of the ADRN CRC that are interacting with ASCL1 on the chromatin. The 47 ADRN proteins that bind ASCL1 on the chromatin are shown in the table.

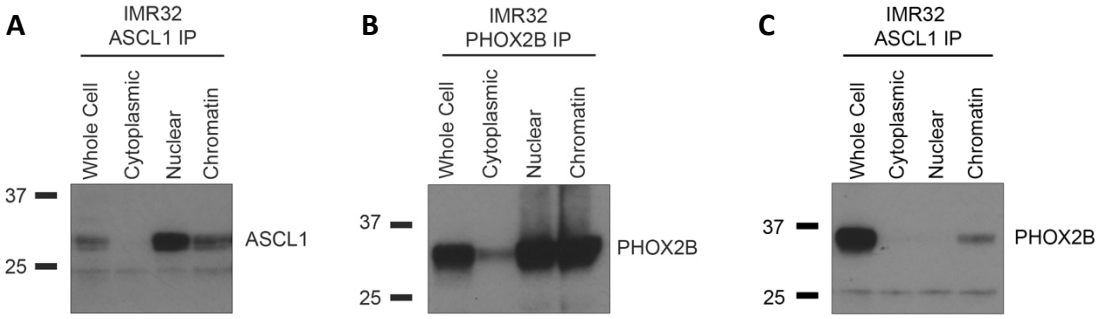

Figure 3.23: Co-immunoprecipitation confirms ASCL1 and PHOX2B binding. IPs were run to detect ASCL1 (A) and PHOX2B (B) in IMR32 parental whole cell lysates and cellular fractions. ASCL1 IP was run followed by PHOX2B western blot to identify where in the cell the binding occurs (C).

3.3 Discussion

When ASCL1 is removed from cells, the cells grow at a slower rate than parental counterparts. The aim of this chapter was to determine what happens to key ADRN TFs in the absence of ASCL1. As mentioned, these ADRN targets are part of the neuroblastoma CRC, working together to support neuroblastoma growth and identity. These TFs sustain their own expression and transcription as well as cooperating with other members of the CRC to maintain the high expression levels of all transcription factors in the network (Van Groningen et al., 2017, Boeva et al., 2017). As ASCL1 is a part of this network, it was expected that in the absence of ASCL1, the transcription and translation of the proteins in the network may decrease (Wang et al., 2019).

3.3.1 Summary of Results

Following the removal of ASCL1, ADRN targets and MYC are still expressed within the cells. The overall mRNA and protein levels of PHOX2A, PHOX2B, GATA3 and MYC/MYCN are very similar to parental lines (Figure 3.2-3.5). In addition to this, the proteins are all localised in the nucleus in parental and ASCL1 KO lines (Figure 3.6-3.9). However, all ASCL1 KO cell lines showed less chromatin bound PHOX2A, PHOX2B, GATA3 and MYC/MYCN when comparing to the parental cell lines (Figure 3.18-3.21). RIME analysis identified ASCL1 binding partners and shows ASCL1 interacts with some ADRN TFs on the chromatin (Figure 3.22).

3.3.2 ASCL1 Knockout Does Not Change the Abundance of the CRC Proteins

As a member of the ADRN CRC, ASCL1 is part of the self-sustaining network of transcription factors which have been shown to be mutually activating. It would therefore have been expected that following the removal of ASCL1, the transcription of other members of this network would have been suppressed. However, the mRNA and protein levels of the different members of the CRC in ASCL1 KO cells is comparable to parental lines. Despite the overall levels being the same, and the observation that the TFs were still present in the nucleus, the binding of these transcription factors to the chromatin is lower. The members of the CRC were determined as they are marked by super enhancers, regions of the genome which has a high amount of H3K27ac and other open chromatin marks. It is a possibility that the CRC TFs such as PHOX2A, PHOX2B and GATA3 have a high affinity for these transcriptionally active areas, so even though overall chromatin binding is lower, these TFs are still able to bind at the CRC genes and therefore able to maintain their expression.

The maintenance of transcript levels of CRC genes following the deletion of ASCL1 may also explain why ASCL1 KO only has a small effect on the ADRN neuroblastoma phenotype. Following KO, cells still morphologically resemble ADRN cells, they just grow at a slower rate. This indicates that, despite the CRC network being self-sustaining and reliant on each protein within the group, there may also be an element of redundancy of proteins in the network when all others are expressed at a high level. The CRC TFs binding less to the chromatin, coupled with the observation that the cells grow at a slower rate could indicate that binding of these TFs at genes associated with cell cycle progression is lower. Another function of ASCL1 or the CRC TFs could be to bind enhancer regions of cell cycle activating genes, promoting their expression and driving the cell cycle.

To confirm where the CRC TFs are binding chromatin following ASCL1 KO, Chromatin Immunoprecipitation (ChIP) followed by qPCR could be completed for the CRC TFs. ChIP involves fixing proteins to chromatin and then utilises antibodies to determine where specific proteins are bound. qPCR can then be completed to investigate protein binding at different regions of interest. ChIP with antibodies targeting the CRC proteins could be followed by qPCR of enhancer regions of CRC genes and genes associated with proliferation. The qPCR on the enhancer regions of members of the CRC would determine if CRC proteins are still able to bind at these regions, maintaining the high level of protein expression observed. The qPCR on genes associated with proliferation and cell cycle progression would inform whether CRC TF binding is lower around these regions leading to lower expression and therefore slower growth. This could help explain three of the observations following ASCL1 deletion; lower chromatin binding of CRC TFs, CRC TFs expression maintained at the same level as parental cells and the slower rate of growth of ASCL1 KO cells.

3.3.3 ASCL1 Could be Recruiting TFs to the Chromatin

There may be multiple reasons to explain why the CRC TFs bind to chromatin less following ASCL1 KO. One possibility is that in the parental cell lines ASCL1 could be recruiting TFs to chromatin. ASCL1 has been shown to assist the chromatin binding of transcription factors during neuronal development and neuronal reprogramming. The TGFβ signalling cascade in developing neurones of the CNS will lead to SMAD3 chromatin binding. ASCL1 and SMAD3 bind the chromatin at the same location and also bind each other on the chromatin. ASCL1 knockdown results in less SMAD3 binding and transcription following TGFβ signalling, indicating it is actively recruiting SMAD3 (Fueyo et al., 2018). Fibroblasts can be reprogrammed to neurones using ASCL1, BRN2 and MYT1. ASCL1 binds the chromatin at the same location as BRN2, has a role in recruiting BRN2 during the reprogramming

process and the loss of ASCL1 results in less BRN2 binding (Wapinski et al., 2013). These examples show the ability and importance of ASCL1 in recruiting TFs in developing neurones.

ChIP-Seq analysis shows that ASCL1 and ADRN TFs such as PHOX2B, HAND2 and GATA3 bind the chromatin at the same location around key genes, so there is the possibility ASCL1 could be binding and also recruiting other TFs to the chromatin (Boeva et al., 2017, Wang et al., 2019). Rapid Immunoprecipitation and Mass Spectrometry of Endogenous proteins (RIME) is a way of deducing which proteins are bound on the chromatin. RIME was completed for ASCL1 by Fahad Ali in the Philpott lab, and it was seen that ASCL1 binds many ADRN proteins on the chromatin, including the transcription factors PHOX2A and PHOX2B (Ali et al., unpublished). Considering ASCL1 binds the chromatin in the same location as key TFs and also binds these TFs on the chromatin, ASCL1 could be recruiting or aiding the chromatin binding of PHOX2A and PHOX2B (Figure 3.24). ASCL1 could be acting in a similar manner here to when it assists the chromatin binding of SMAD3 in CNS development and BRN2 in reprogramming. However, ASCL1 doesn't bind GATA3 or MYC/MYCN on the chromatin so there must be another mechanism to explain the lower chromatin binding of these transcription factors.

To investigate what is happening to a transcription factor such as MYC which does not bind ASCL1, immunoprecipitation followed by mass spectrometry could be completed on the non-chromatin bound protein in parental and ASCL1 KO cells. This would detect proteins associated with MYC when it is not bound to the chromatin. Differences in binding partners of non-chromatin bound MYC in parental and ASCL1 KO cells could identify proteins restricting MYC binding in the ASCL1 KO lines.

ASCL1 is a pioneer factor and alters chromatin accessibility. If ASCL1 is maintaining the chromatin in an open and permissive state in neuroblastoma, then removing the protein could result in less accessible chromatin and therefore less transcription factor binding (Figure 3.24). The effect of ASCL1 KO on chromatin accessibility will be explored in Chapter 4.

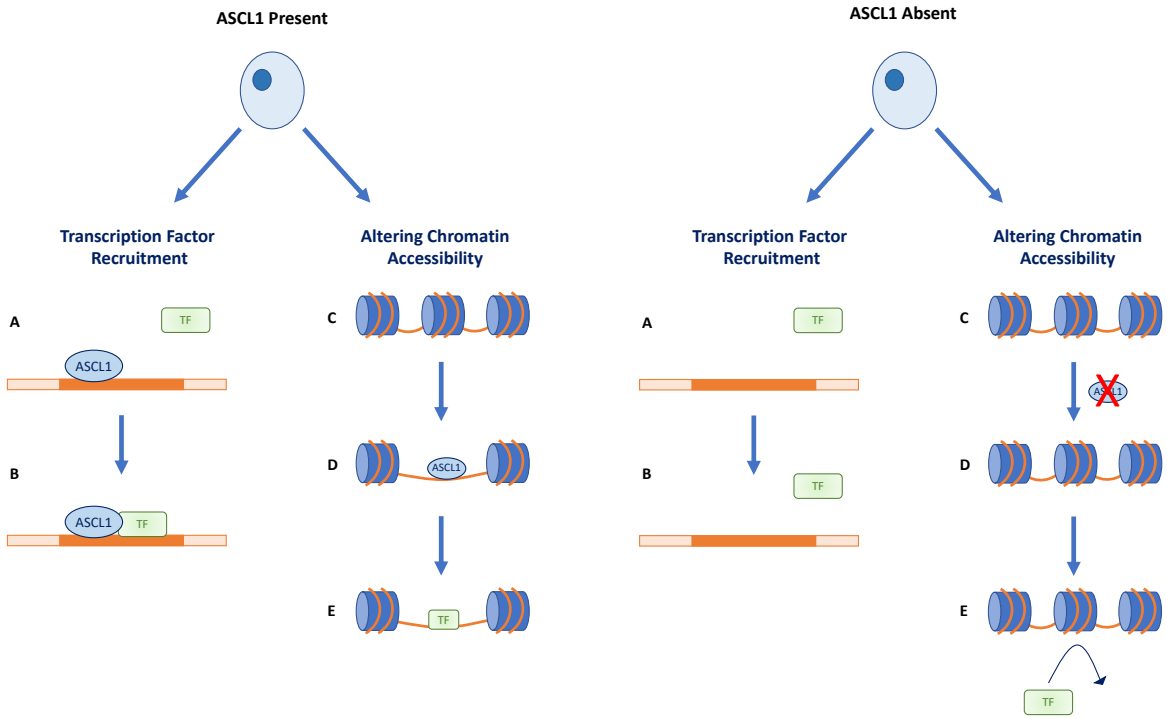

Figure 3.24: Possible Mechanisms Leading to Lower TF Binding in ASCL1 KO cells. The panel on the left shows what could be happening in parental cells; ASCL1 could be recruiting TFs to the chromatin or assisting their binding (A,B). ASCL1 could also be remodelling the chromatin resulting in a more accessible chromatin landscape (C-E). The panel on the right shows what could be happening when ASCL1 is removed. There is no ASCL1 available to assist binding or recruit TFs so they bind the chromatin less (A,B). In addition to this, if ASCL1 is altering chromatin accessibility then the lack of ASCL1 would result in highly compacted, non-accessible chromatin (C-E).

Chapter 4

Genome Wide Changes Following ASCL1 Knockout

4.1 Introduction

ASCL1 is a transcription factor (TF) that has a diverse array of transcriptional targets. As described in Chapter 2, ASCL1 contributes to the proliferation of neural stem cells and target genes include those involved in cell growth and cell cycle progression (Andersen et al., 2014; Chanda et al., 2014). In contrast to this, ASCL1 targets also include genes that are associated with differentiation. When ASCL1 is induced in neuroblastoma cells or fibroblasts, genes associated with a more differentiated neuronal subtype are upregulated (Ali et al., 2020; Chanda et al., 2014).

ASCL1 is regarded as an on-target pioneer factor. ASCL1 is able to bind nucleosome dense, closed chromatin and recruit proteins involved in remodelling in order to make the chromatin more accessible for other TFs to bind (Raposo et al., 2015; Wapinski et al., 2013). For instance, ASCL1 is able to bind the CDH7 locus leading to its transcription and expression. CDH7 is a chromatin modifier important in neurogenesis. This shows one example of how ASCL1 is able to influence chromatin accessibility, in this case by inducing proteins that are capable of chromatin remodelling (Rao et al., 2021). The pioneer factor activity of ASCL1 has been documented in many contexts, such as during the reprogramming of fibroblasts to neurones and during the differentiation of neural stem cells. Transducing ASCL1 into fibroblasts or neural stem cells quickly results in the chromatin landscape changing to one permissive of neural differentiation, leading to the upregulation of neuronal development associated genes and a differentiated morphology (Wapinski et al., 2017; Raposo et al., 2015).

As ASCL1 has been described as a transcriptional regulator, a pioneer factor and may play a central role in determining a neurogenic identity, the aim of this chapter was to determine the effects on both global transcription and chromatin accessibility following ASCL1 knockout (KO). To investigate this, RNA-Seq and ATAC-Seq were completed. RNA-Seq determines the overall transcriptional landscape of a cell and was used to investigate how the loss of ASCL1 changes the transcriptome.

ATAC-Seq identifies regions of accessible chromatin by utilising a transposase to cleave the DNA at open regions. These regions are then amplified and sequenced so the difference in chromatin accessibility between parental cells and ASCL1 KO cells could be explored.

It was predicted that the transcriptional landscape would be changed following ASCL1 KO. ASCL1 has a diverse spectrum of target genes including those involved in proliferation and regulating the cell cycle. After removing ASCL1 from neuroblastoma cells, cells exhibit slower growth (described in Chapter 2) so it was expected that these pro-proliferation genes will be downregulated in ASCL1 KO cells. In addition to this, following the observation that TFs such as PHOX2B, GATA3 and MYC show reduced chromatin binding following ASCL1 KO (described in chapter 3), it was anticipated that the chromatin would be less accessible in ASCL1 KO lines.

4.2 RNA-Seq Results

4.2.1 Visualisation of Differentially Expressed Genes following ASCL1 KO

RNA-Seq of SH-SY5Y, IMR32, SK-N-BE(2)c and their associated ASCL1 KO lines was completed to determine genome wide transcriptional changes following the removal of ASCL1. All cell lines were sequenced at the same time to allow comparisons between parental and ASCL1 KO lines and also between different cell lines. DESeq2 was used to identify differentially expressed genes between the groups and then the genes identified as significantly different were used for downstream analysis (Love et al., 2014).

Following DESeq2 analysis, principal component analysis (PCA) plots were produced to visualise how the different cell lines compare to each other. When comparing all parental and all ASCL1 KO lines three distinct clusters can be observed; SH-SY5Y and ASCL1 KO lines, IMR32 and ASCL1 KO lines, and SK-N-BE(2)c and ASCL1 KO lines. The parental and ASCL1 KO lines are more similar to each other following ASCL1 KO than they are to the other cell lines. Removing ASCL1 from neuroblastoma cells does not result in a shared transcriptome between cell lines (Figure 4.1 A).

When comparing each of the parental lines to their own ASCL1 KO lines, there are three distinct clusters in all cell lines. The replicates of the parental line cluster together and each of the ASCL1 KO lines forms its own distinct cluster. This shows that removing ASCL1 results in cell lines that are different from the parental, but there are also some differences between the ASCL1 KO lines (Figure 4.1 B-D).

The amount of variation between conditions can be visualised using an MA plot. MA plots show the log fold change (logFC) on the Y-axis and mean counts on the X-axis. More points clustered around 0 mean there is less variation, more points further away from 0 indicates more variation between parental cells and ASCL1 KO cells. For all the cell lines, there are a large number of points that are not clustered around zero, indicating changes to the transcriptome following ASCL1 KO (Figure 4.2).

4.2.2 ASCL1 KO Lines are Transcriptionally Similar to Each Other and Distinct from Parental

The DESeq2 analysis produces a list of significantly different genes between experimental conditions, in this case parental and ASCL1 KO lines. The significantly changed genes were ranked in order of most variable between the two conditions, parental and ASCL1 KO, and then this data set

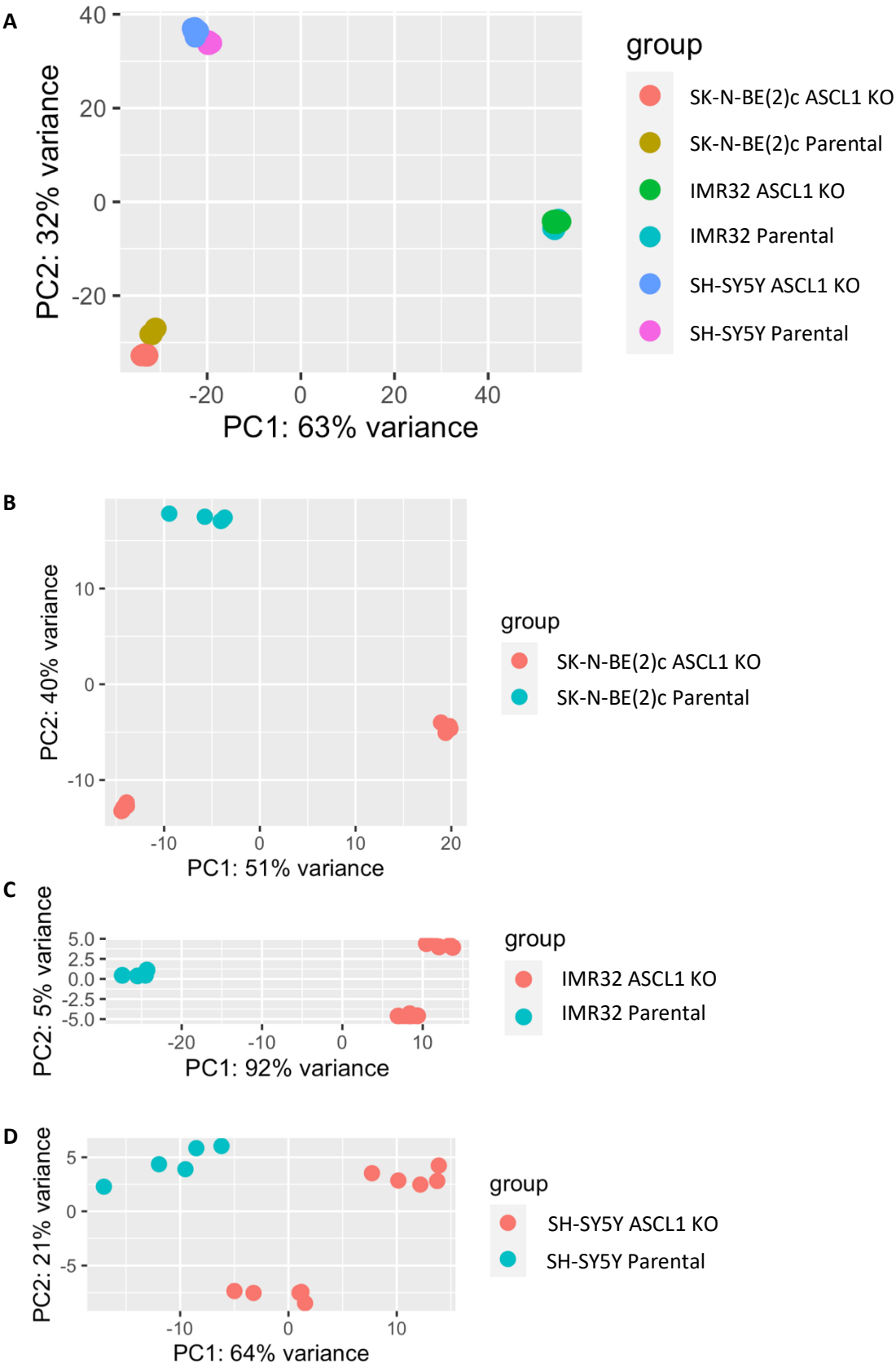

Figure 4.1: PCA Plots showing clustering of RNA-Seq data from parental and ASCL1 KO lines. PCA plots to show the variation and clustering between all cell lines (A), SK-N-BE(2)c parental and ASCL1 KO (B), IMR32 parental and ASCL1 KO (C) and SH-SY5Y parental and ASCL1 KO (D).

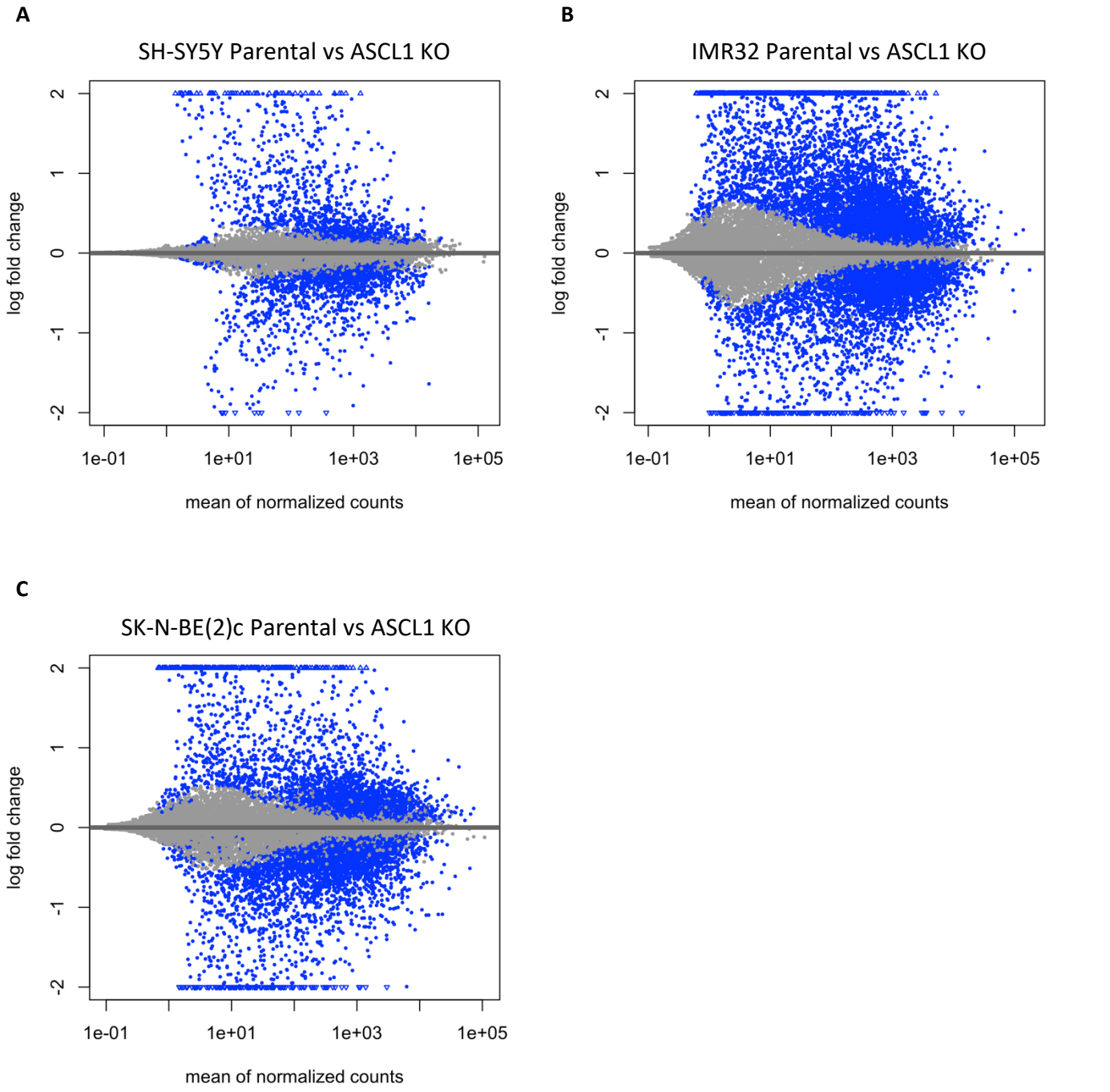

Figure 4.2: MA plots of parental and ASCL1 KO RNA-Seq data. MA plots were produced to show the difference in transcription following ASCL1 KO. SH-SY5Y (A), IMR32 (B) and SK-N-BE(2)c are all shown. MA plots show the mean normalised count of a particular gene vs logFC. Blue points represent significantly changed values ($p < 0.05$).

was used to produce heatmaps of differentially expressed genes. Each distinct parental line clusters together and in all cases the ASCL1 KO lines are more similar to each other than the parental line. There are two heatmaps shown for each parental cell line and associated ASCL1 KO line. The first shows the top 50 differentially expressed genes with the genes labelled and the second shows the top 500 genes to visualise how the cell lines cluster together (Figure 4.3-4.5). Looking at the heatmaps, the proportion of transcripts with higher expression (shown in red) is much larger in the parental lines than the KO lines. ASCL1 has been described as a 'master regulator of transcription', so it is understandable that removing ASCL1 would result in lower transcription.

4.2.3 Downregulation of Transcription of Neuronal Targets in ASCL1 KO Cells

Following the observation that the ASCL1 KO cells are transcriptionally more similar to each other than parental cells, and that the ASCL1 KO cells have similar genes with higher and lower expression compared to the parental, the gene sets and pathways that are most affected following the removal of ASCL1 were investigated. In order to do this, the Bioconductor package clusterProfiler was used. The clusterProfiler programme takes the list of differentially expressed genes identified from the DESeq2 analysis and defines pathways and functions associated with the gene sets. The output of clusterProfiler analysis can then be used to compare upregulated and downregulated gene sets and associated functions following ASCL1 KO. For this analysis, the genes associated with a negative logFC value were chosen. These are the genes transcribed at a lower rate following ASCL1 KO.

For SH-SY5Y, when comparing parental and ASCL1 KO lines, the genes that are expressed at a lower level following ASCL1 deletion are genes associated with neuronal development. These include genes associated with neuron projection, the axon, the synapse and synaptic signalling (Figure 4.6). For IMR, it is a similar phenotype. IMR32 ASCL1 KO cells show a lower level of transcription of genes involved in nervous system development such as neuron projection, axon development and synapse associated genes (Figure 4.7). This indicates that the removal of ASCL1 in SH-SY5Y and IMR32 is causing downregulation of genes associated with a neuronal phenotype.

When compared to parental cells, SK-N-BE(2)c ASCL1 KO cells have a different genes which are expressed at a lower rate. There are no specific terms associated with neuronal development, and instead the downregulated genes are associated with transcription factor binding, DNA replication and RNA splicing (Figure 4.8).

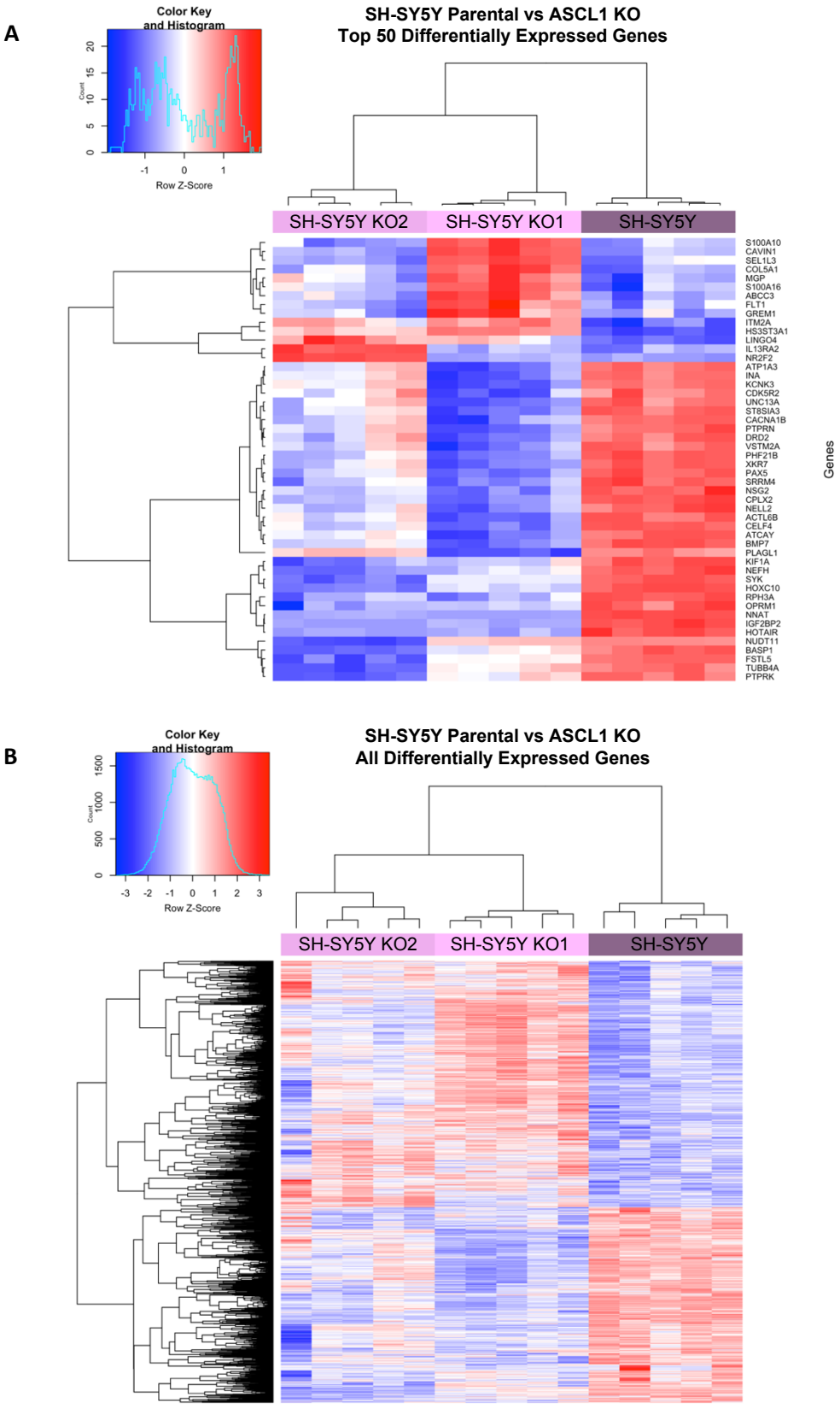

Figure 4.3: Heatmaps to show differential gene expression in SH-SY5Y parental and ASCL1 KO cells. The DESeq list of differentially expressed genes was ranked in order of most variable. The top 50 most variable genes (A) and top 500 genes are shown (B). Upregulated genes in the cell line are shown in red and downregulated genes shown in blue.

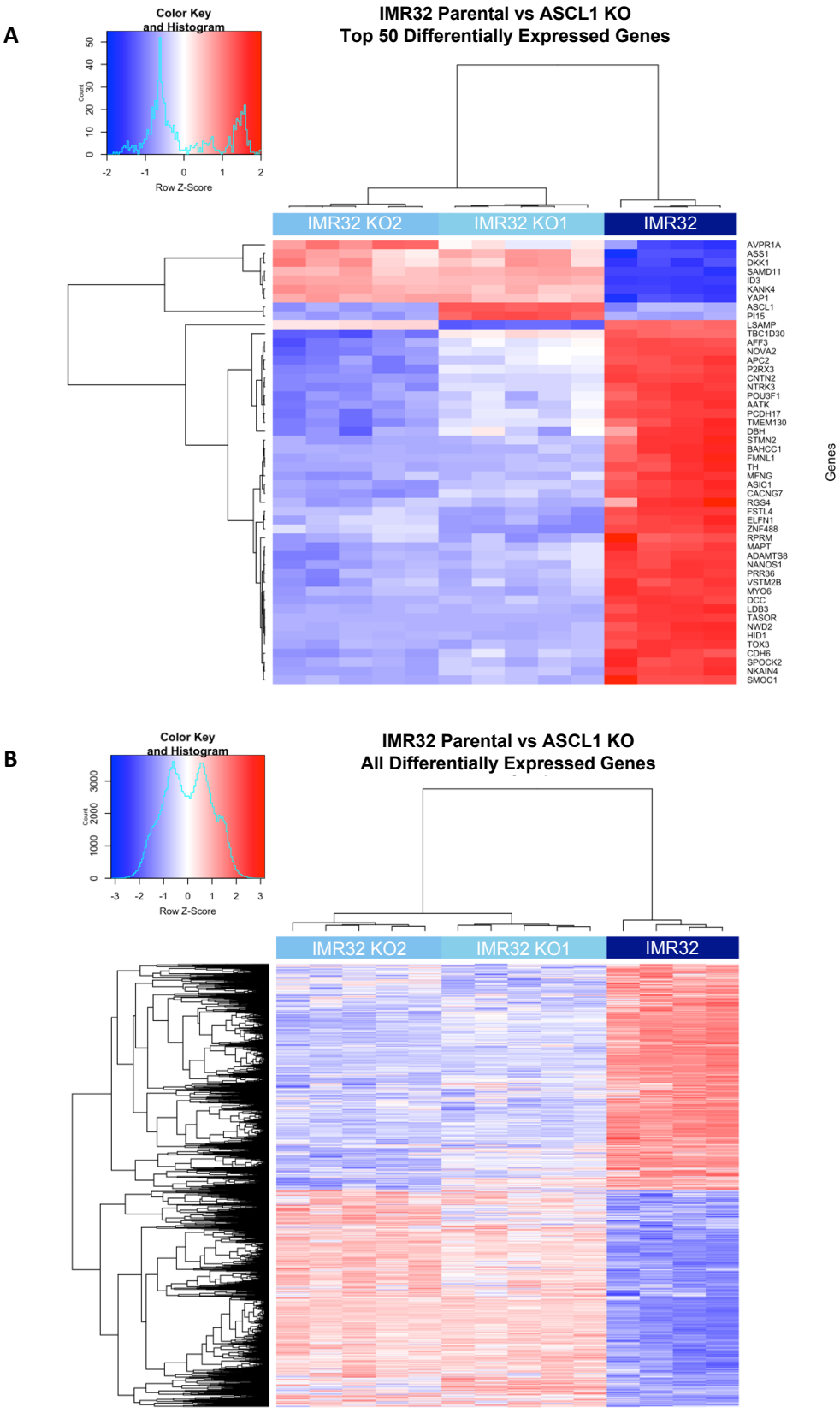

Figure 4.4: Heatmaps to show differential gene expression in IMR32 parental and ASCL1 KO cells. The DESeq list of differentially expressed genes was ranked in order of most variable. The top 50 most variable genes (A) and top 500 genes are shown (B). Upregulated genes in the cell line are shown in red and downregulated genes shown in blue.

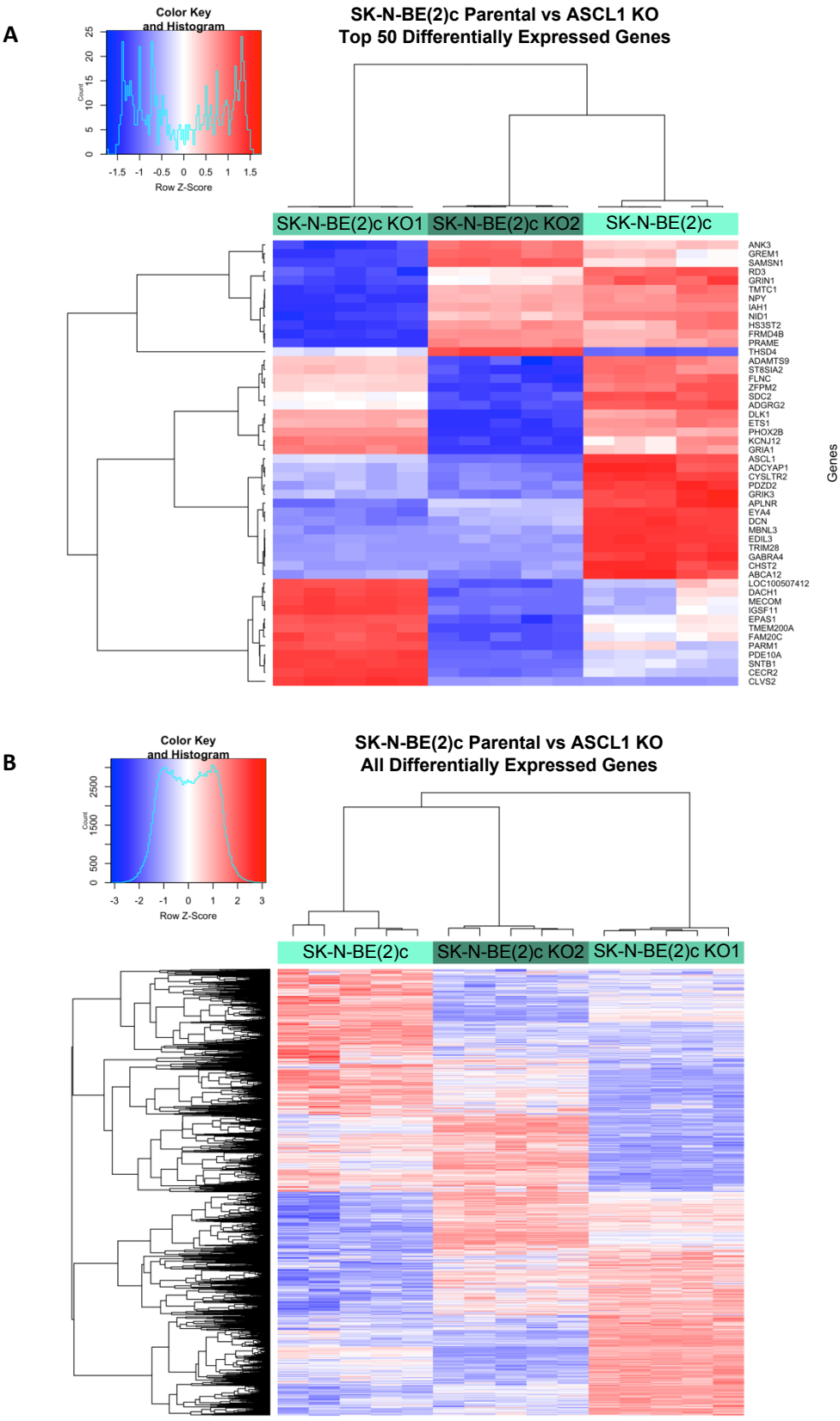

Figure 4.5: Heatmaps to show differential gene expression in SK-N-BE(2)c parental and ASCL1 KO cells. The DESeq list of differentially expressed genes was ranked in order of most variable. The top 50 most variable genes (A) and top 500 genes are shown (B). Upregulated genes in the cell line are shown in red and downregulated genes shown in blue.

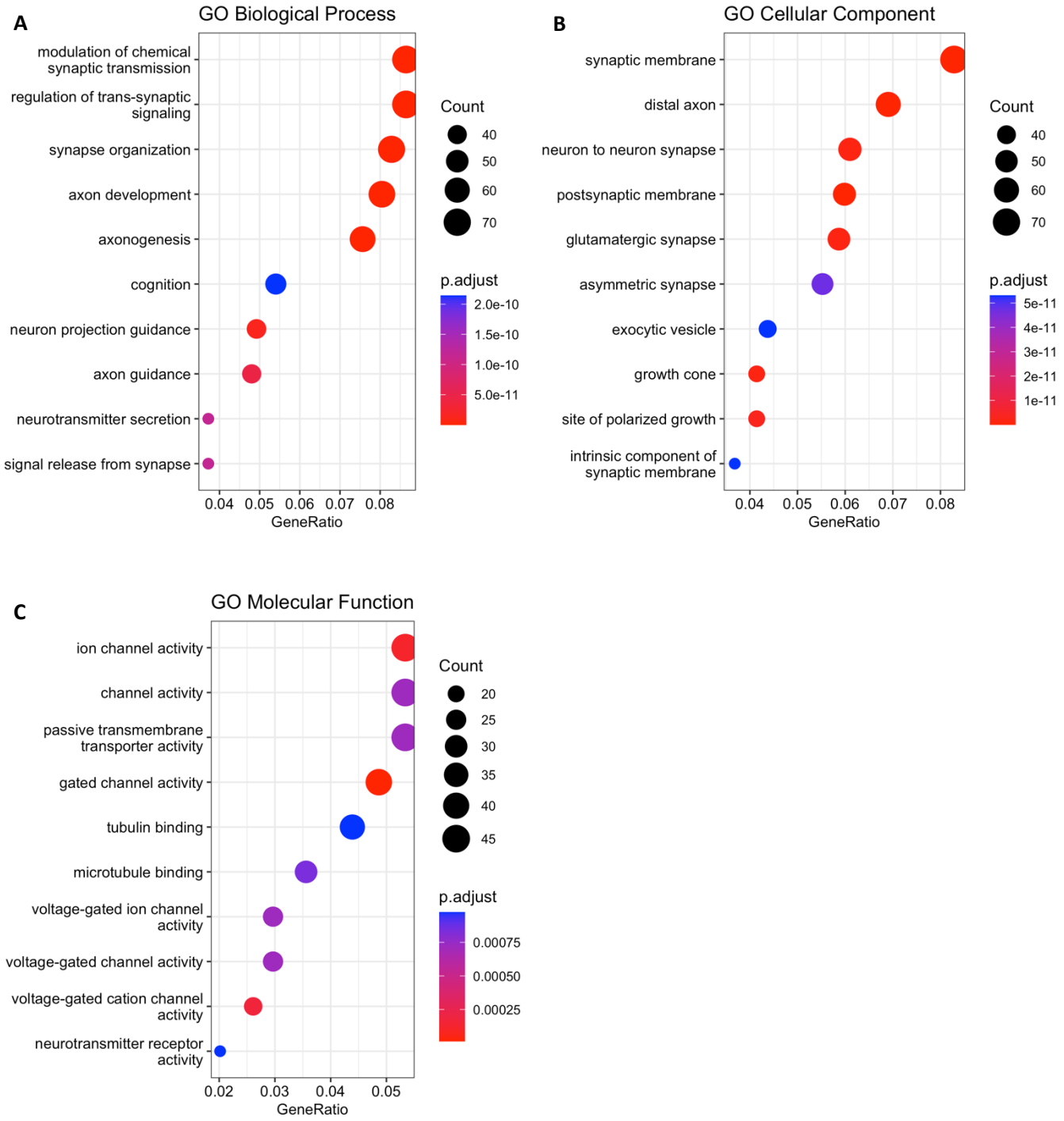

Figure 4.6: Genes associated with neuronal development are downregulated following ASCL1 KO in SH-SY5Y cells. The DESeq2 list of significantly downregulated genes was used for GO analysis. The GO analysis was split into three categories; Biological Process (A), Cellular Component (B) or Molecular Function (C). The top 10 downregulated (less transcribed following ASCL1 KO) GO terms in each category are shown.

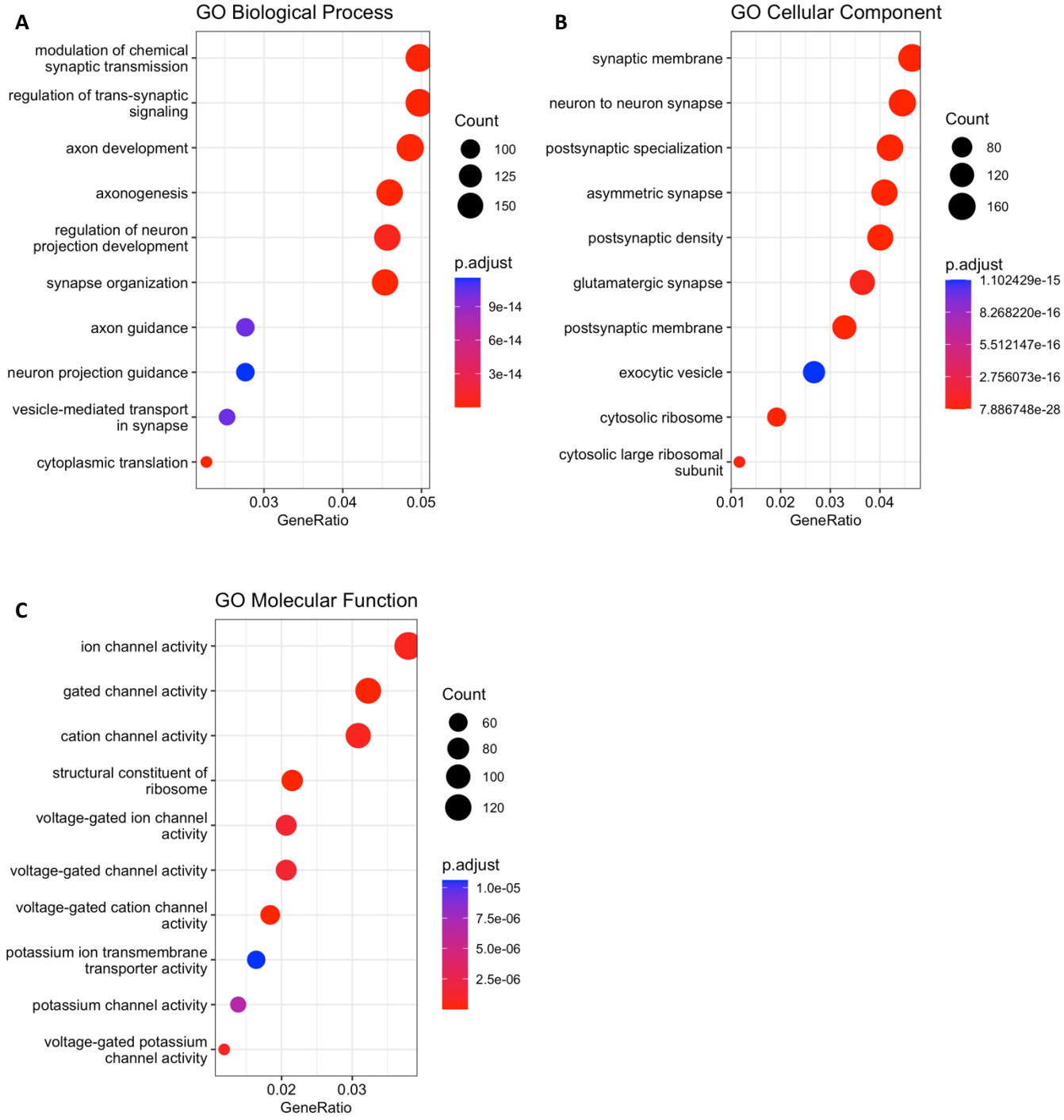

Figure 4.7: Genes associated with neuronal development are downregulated following ASCL1 KO in IMR32 cells. The DESeq2 list of significantly downregulated genes was used for GO analysis. The GO analysis was split into three categories; Biological Process (A), Cellular Component (B) or Molecular Function (C). The top 10 downregulated (less transcribed following ASCL1 KO) GO terms in each category are shown.

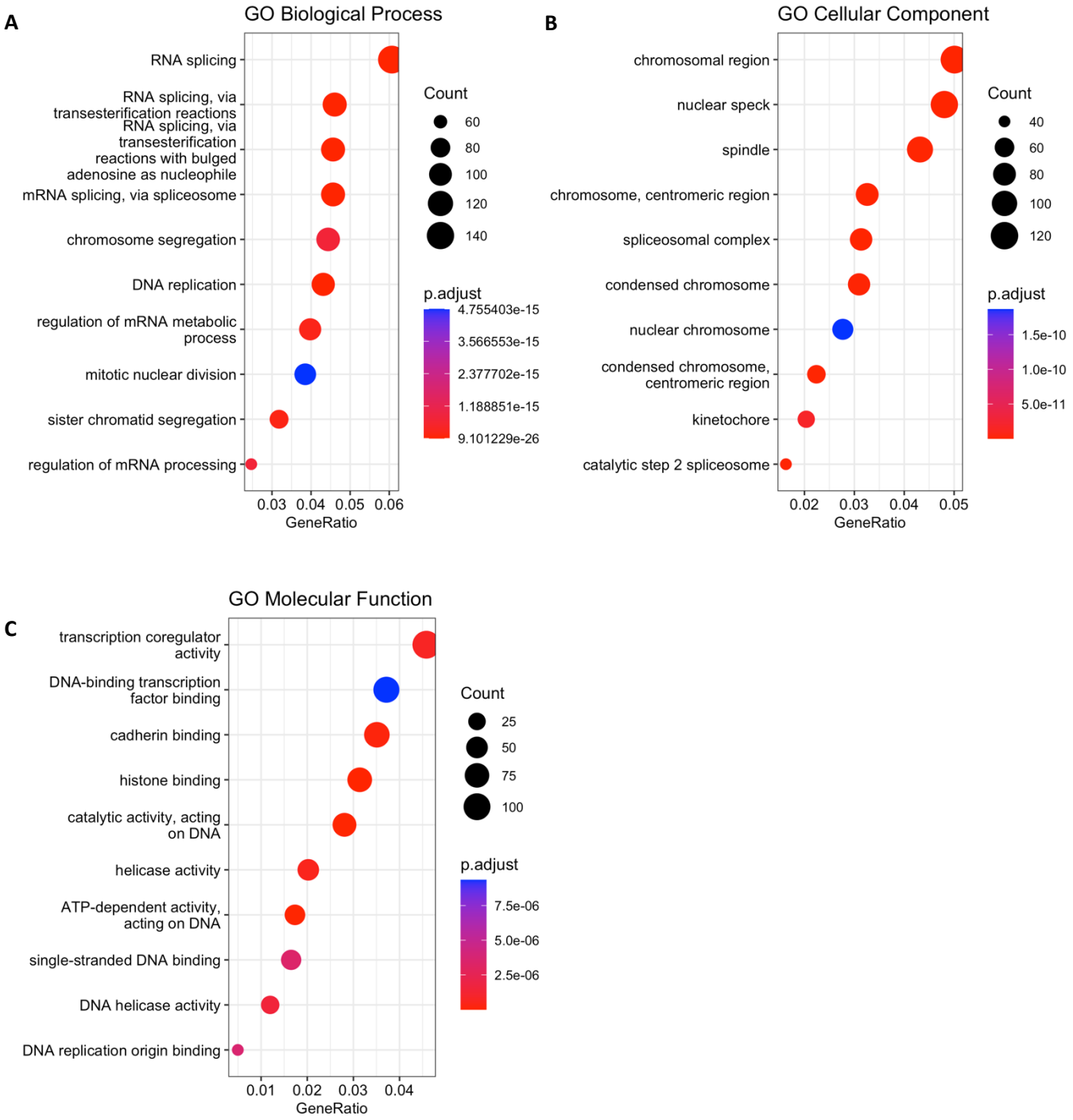

Figure 4.8: GO analysis comparing SK-N-BE(2)c parental and ASCL1 KO RNA-Seq. The DESeq2 list of significantly downregulated genes was used for GO analysis. The GO analysis was split into three categories; Biological Process (A), Cellular Component (B) or Molecular Function (C). The top 10 downregulated (less transcribed following ASCL1 KO) GO terms in each category are shown.

4.2.4 RNA-Seq Molecular Signatures

The RNA-Seq data can be interrogated further using the Molecular Signatures Database (Subramanian et al., 2005). This database takes a list of genes and analyses for commonalities in the gene set. In this case, the genes that were downregulated across all cell lines following ASCL1 KO were analysed for shared transcription factor binding sites. The most common consensus sequence found in the downregulated genes is CAGCTG, a known ASCL1 binding site (Bertrand et al., 2002). It makes sense that following the deletion of a master regulator of transcription its target genes are downregulated. In addition to this, the binding sequence of the E-proteins E47 and E12 are identified. As described in section 1.4.1, in order for ASCL1 to bind DNA, ASCL1 must heterodimerise with an E-protein and it has been shown that E12 and E47 bind ASCL1 and aid differentiation (Le Dreau et al., 2018). The MYC/MAX binding site is also a feature in a subset of the downregulated genes. It was observed that MYC binding to chromatin is lower following ASCL1 KO, so it is logical that less MYC binding leads to a downregulation of MYC target genes.

4.3 ATAC-Seq Results

4.3.1 Visualisation of Chromatin Accessibility Data following ASCL1 KO

To determine the effects of ASCL1 KO on chromatin accessibility, ATAC-Seq was completed on the parental and ASCL1 KO lines. ATAC-Seq uses the TN5 transposase to cut DNA at open regions. These open regions are then amplified and sequenced. The open regions will form the sequencing reads and multiple reads at a certain location will pile up resulting in peaks (Buenrostro et al., 2015). These peak sets can then be used to compare the open regions between samples, in this case the differences in open chromatin between parental and ASCL1 KO lines were analysed. This was achieved by doing differential analysis, which was completed using the Bioconductor package DiffBind (Stark and Brown, 2011). Diffbind uses the peaks identified following MACS2 peak calling, quantifies these and produces a set of peaks that differ significantly between parental and ASCL1 KO lines. DiffBind analysis identified a large number of sites which are significantly different between the parental and ASCL1 KO cells. There are 20,273 identified between SH-SY5Y and ASCL1 KO, 8,258 between IMR32 and ASCL1 KO and 40,816 between SK-N-BE(2)c parental and ASCL1 KO lines.

Following DiffBind analysis, PCA plots were created to visualise the variation between cell lines. Similarly to the clustering of RNA-Seq data, parental SH-SY5Y and SK-N-BE(2)c form a cluster and each ASCL1 KO line forms its own distinct cluster. For IMR32, again the parental replicates cluster together, but the ASCL1 KO lines are more similar and form one cluster containing both the cell lines (Figure 4.9 A-C).

When setting up the parameters for the DiffBind analysis, the parental lines were chosen to be the condition to compare to, so all analysis will be in relation to the parental cells. If a region of the genome has less reads present in the ASCL1 KO line than the parental line, meaning there is less open DNA at this point, it will receive a negative logFC value. If a region receives a positive logFC value, it means that there are more reads present in the ASCL1 KO cells than the parental, indicating chromatin is more open in the ASCL1 KO cells. This data can be visualised by MA plots (Figure 4.9 DF) and Volcano plots (Figure 4.9 G-I).

MA plots show the normalised number of reads (log concentration) against the logFC value. The points in pink are regions where chromatin accessibility is significantly changed between the parental and ASCL1 KO lines. There are a large proportion of pink points and therefore a large amount of regions which have a significantly different number of reads present. Volcano plots show

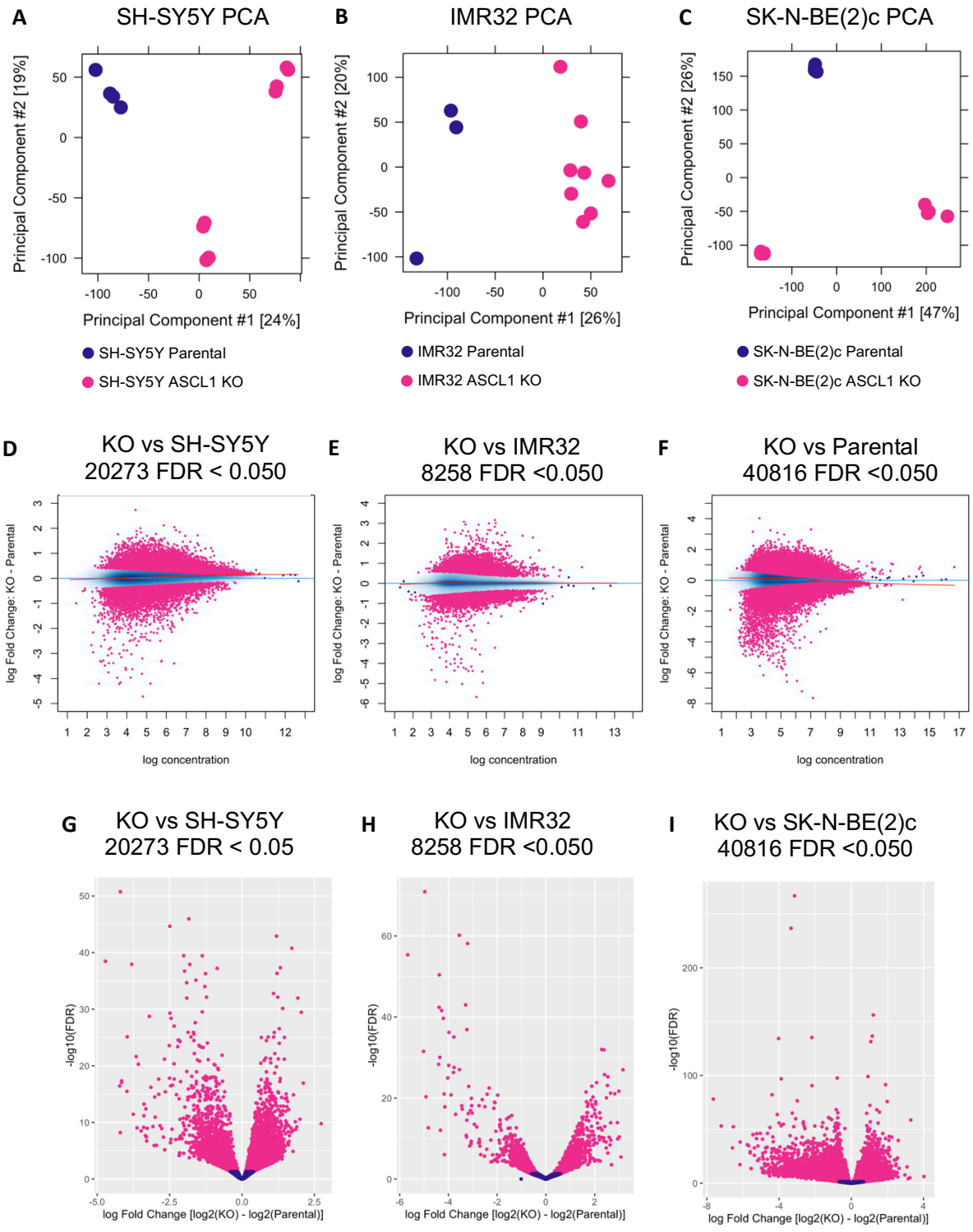

Figure 4.9: Visualisation of parental and ASCL1 KO ATAC-Seq data. PCA plots to show the variation and clustering of ATAC-Seq data between SH-SY5Y parental and ASCL1 KO (A), IMR32 parental and ASCL1 KO (B) and SK-N-BE(2)c parental and ASCL1 KO (C). MA plots were produced to show the difference in chromatin accessibility following ASCL1 KO. SH-SY5Y (D), IMR32 (E) and SK-N-BE(2)c are all shown (F). MA plots show the mean normalised count of a particular gene vs logFC. Pink points represent significantly changed values ($p < 0.05$). Volcano plots show the logFC value against the false discovery rate. Pink points represent significantly altered regions (FDR < 0.05). The further from 0 on the X-axis, the more the accessibility has changed. Volcano plots for SH-SY5Y (G), IMR32 (H) and SK-N-BE(2)c (I) are all shown.

the logFC against the false discovery rate (FDR). Again, the points in pink are identified as being significantly changed between parental and ASCL1 KO lines. For all cell lines, there are a large number of points identified as being significantly different. Points that are further from 0 on the X axis have a larger logFC change value and shows the chromatin accessibility differs more between the two conditions (Figure 4.9 D-I). There are a large number of regions in the ASCL1 KO lines that have a negative logFC value and so are less accessible than in the parental. There are also a similar number of genes that have a positive logFC value and are therefore more accessible following ASCL1 KO.

Heatmaps were produced to show the overall accessibility changes between parental and ASCL1 KO lines. For all cell lines, the parental repeats cluster together and the ASCL1 KO lines are more similar to each other than the parental lines (Figure 4.10). The regions shown in green are more accessible in the parental cells compared to the ASCL1 KO cells, and regions in red are less accessible in parental cells compared to the ASCL1 KO cells. The heatmaps show a large proportion of regions that are more accessible in parental lines, but there is also a distinct set of regions that are more accessible once ASCL1 has been removed.

4.3.2 Accessible Chromatin is Largely in Distal Intergenic and Intronic Regions and Around TSS

Using the Bioconductor package ChIPSeeker, the MACS2 peaks file can be utilised to identify genomic features associated with the location of the peaks. For all parental and ASCL1 KO lines, around 40% of open chromatin was found in distal intergenic regions and 20% found in intronic regions. 20% of accessible DNA is located within 1kb of a TSS and less than 5% between 2kb and 3kb of a TSS (Figure 4.11).

4.3.3 Neuronal Targets are Associated with Less Accessible Chromatin in ASCL1 KO Cells

Following DiffBind analysis to identify differentially accessible areas of the genome, GREAT software was used to identify gene sets/pathways that were changed (McLean et al., 2010). The regions identified following ATAC-Seq are likely to be non-coding, GREAT takes these regions and assigns them to the nearest gene. GREAT will then predict the biological process and cellular component these genes are associated with. Biological process refers to pathways and functions of the cell and cellular component relates to specific parts within a cell.

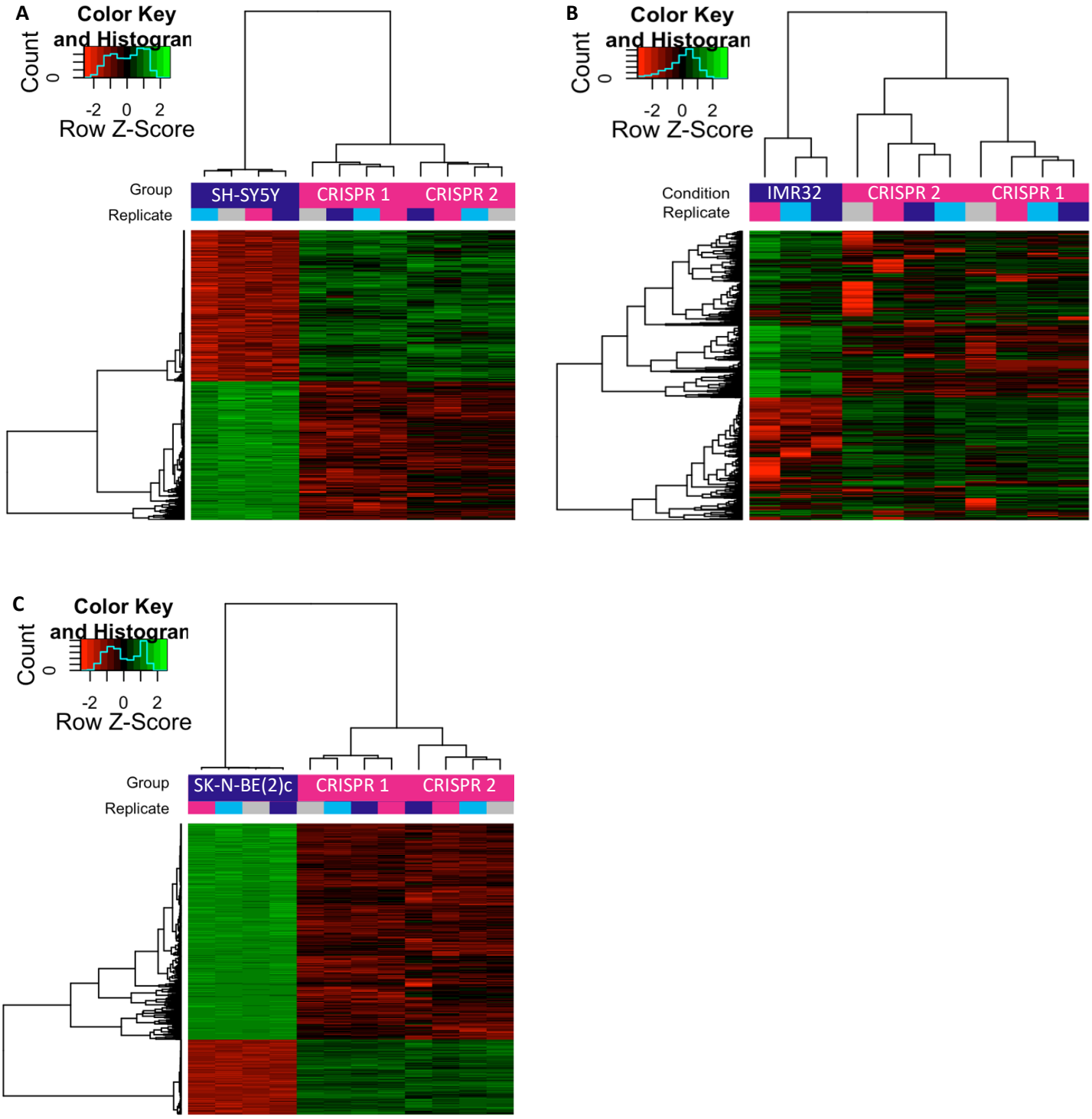

Figure 4.10: Heatmaps to show the difference in accessible regions between parental and ASCL1 KO cells. Heatmaps to show [the difference in accessibility between parental and ASCL1 KO cells. SH-SY5Y (A), IMR32 (B) and SK-N-BE(2)c (C) are shown alongside their respective ASCL1 KO lines. Regions that are more accessible are shown in green and less accessible regions are shown in red.

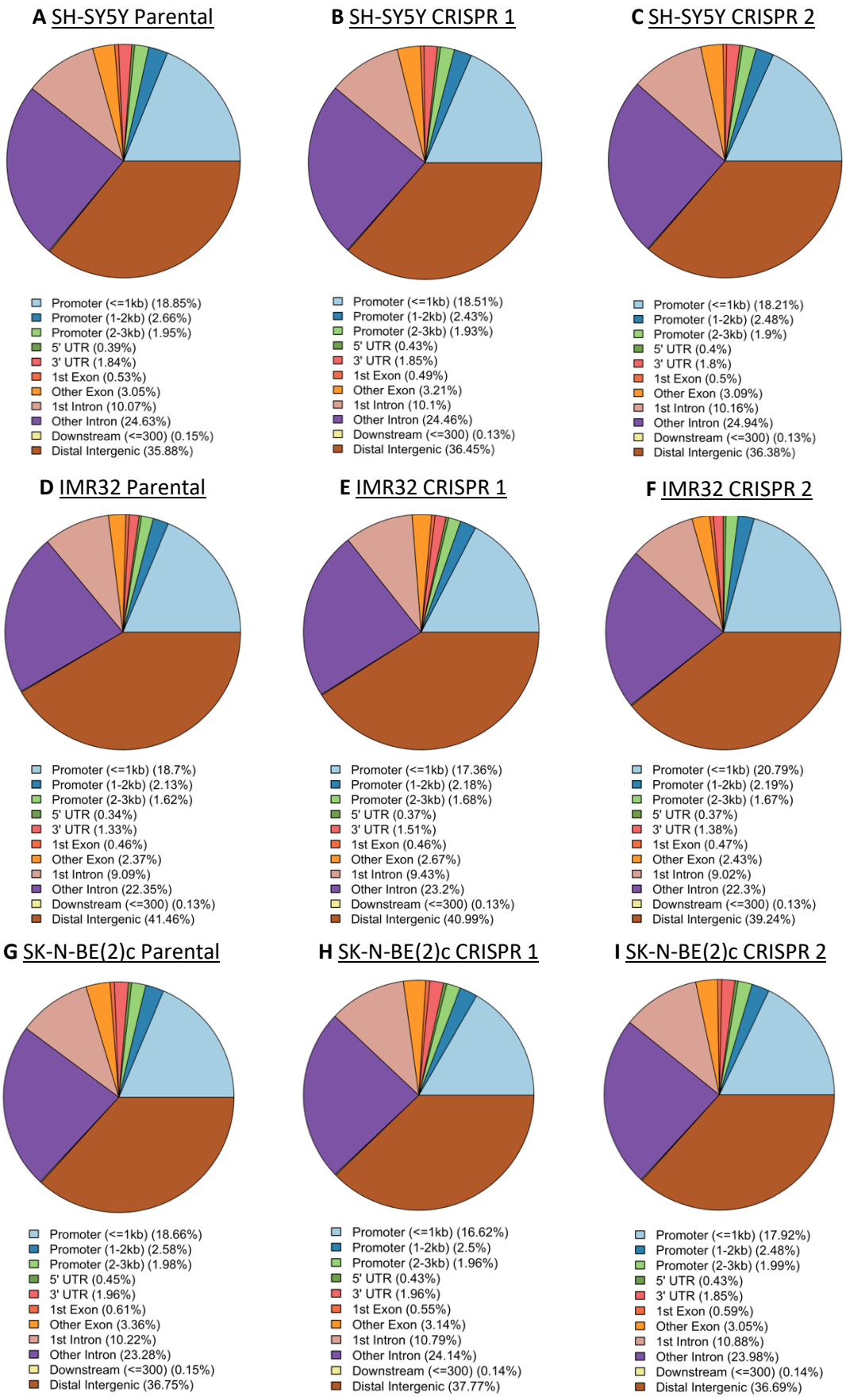

Figure 4.11: Peak annotation shows most open regions are intergenic and intronic. Open chromatin regions were assigned a genomic annotation, these regions were quantitated and visualised as a pie chart. SH-SY5Y and ASCL1 KO lines (A-C), IMR32 and ASCL1 KO lines (D-F) and SK-N-BE(2)c and ASCL1 KO lines (G-I) are shown.

As there was a large number of regions that had a negative logFC value, these were filtered to the top 4000 regions before GREAT analysis. GREAT analysis was performed on the top regions that have a negative logFC which identified areas that are less accessible once ASCL1 has been removed. This analysis showed that many of the regions that were less accessible after ASCL1 KO are associated with neuronal development and differentiation. Following ASCL1 deletion from SH-SY5Y cells, eight of the top 20 terms are specifically related to neuronal processes, such as axon extension and guidance and synaptic associated functions. Other functions include hormone and peptide secretion and transport. Of the six cellular component-related terms, five are associated with neuronal composition (Figure 4.12). When ASCL1 is deleted from IMR32 cells, functions associated with nerve development and innervation are decreased, as well as perception and detection of temperature stimulus (Figure 4.13). When comparing SK-N-BE(2)c and the ASCL1 KO lines, there are many neuronal differentiation processes identified. Functions that also relate to neuroblastoma development include noradrenergic differentiation, adrenal gland development, autonomic nervous system development and sympathetic nervous system development. In addition to this, there are many other processes identified that are involved in development and differentiation of other types of neurones (Figure 4.14).

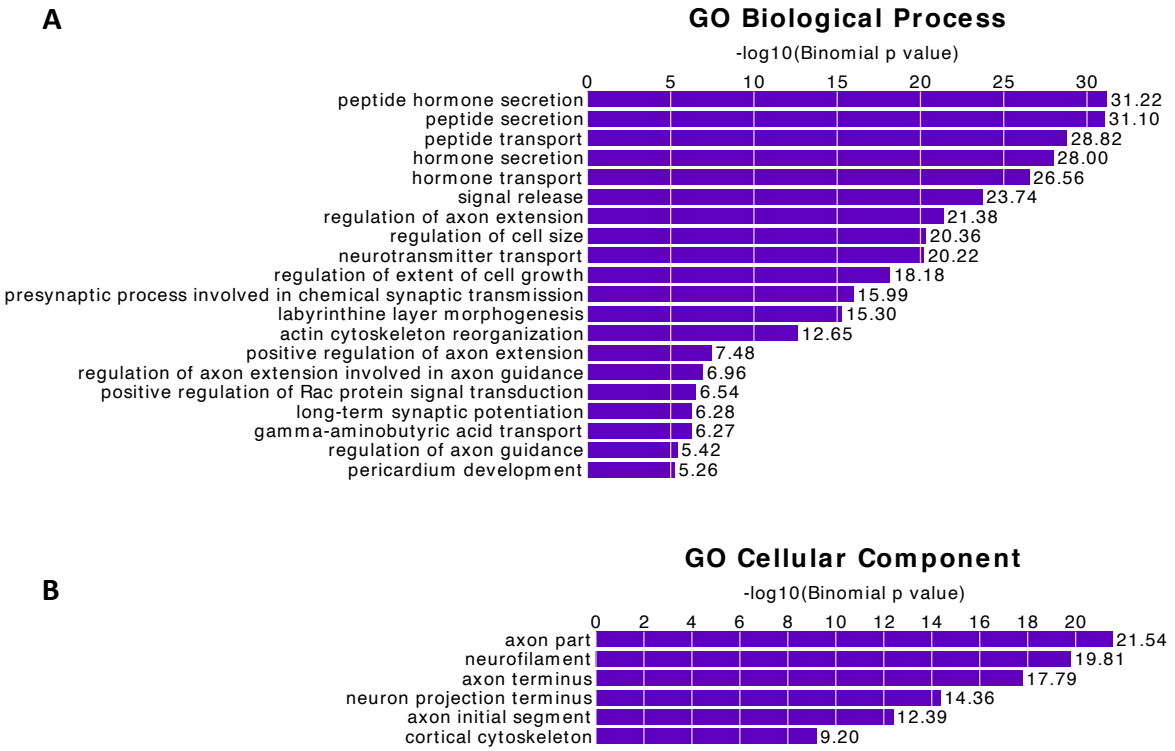

Figure 4.12: Neuronal regions are less accessible in SH-SY5Y ASCL1 KO cells. GREAT software was utilised to perform GO analysis on the top regions that were recognised as less accessible in ASCL1 KO cells. GREAT analysis identified biological processes (A) and cellular components (B) associated with the genomic regions.

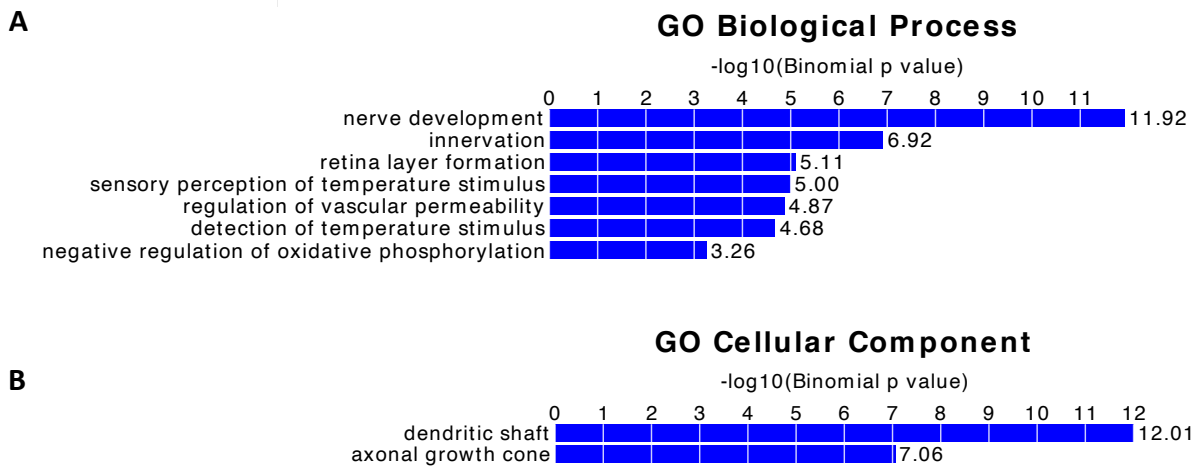

Figure 4.13: Neuronal regions are less accessible in IMR32 ASCL1 KO cells. GREAT software was utilised to perform GO analysis on the top regions that were recognised as less accessible in ASCL1 KO cells. GREAT analysis identified biological processes (A) and cellular components (B) associated with the genomic regions.

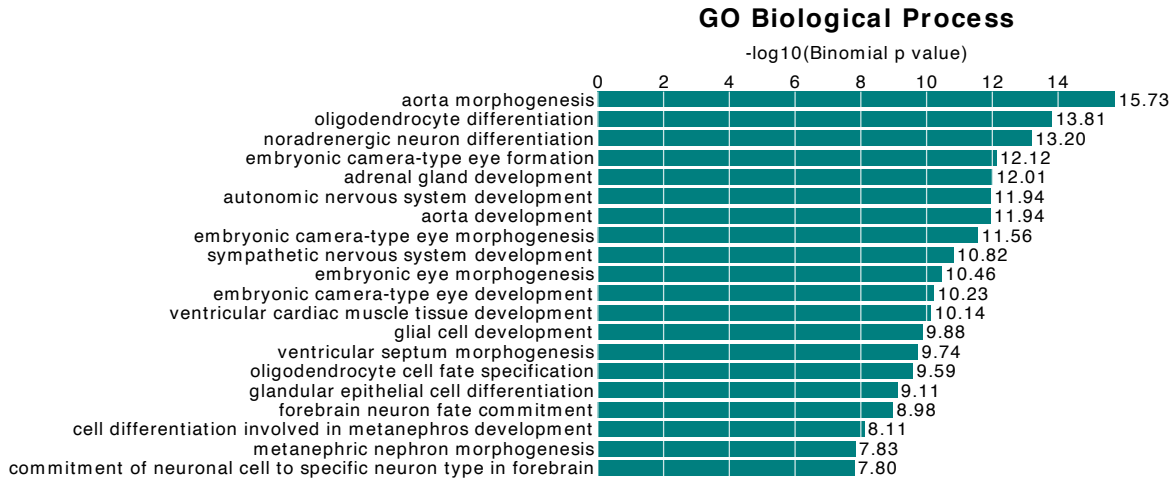

Figure 4.14: Neuronal regions are less accessible in SK-N-BE(2)c ASCL1 KO cells. GREAT software was utilised to perform GO analysis on the top regions that were recognised as less accessible in ASCL1 KO cells. GREAT analysis identified biological processes associated with the genomic regions.

4.4 Discussion

4.4.1 Summary of Results

The results of RNA-Seq analyses show that after ASCL1 removal, the ASCL1 KO lines are transcriptionally more similar to each other than to their parental lines. GO analysis on the genes that are downregulated following ASCL1 KO shows they are associated with neuronal differentiation and development (Figure 4.6-4.8). ATAC-Seq analysis shows that the accessibility of the chromatin is altered between parental and ASCL1 KO lines. The hierarchal clustering pattern of parental and ASCL1 KO cells is similar to what was observed with the RNA-Seq data, ASCL1 KO lines cluster together and are distinct from the parental lines (Figure 4.10). GO analysis was performed on regions identified as less accessible following ASCL1 KO, and similarly to the results observed following RNA-Seq, many of the less accessible areas are associated with neuronal differentiation (Figure 4.12-4.14).

4.4.2 ASCL1 KO Results in Transcriptional and Chromatin Accessibility Changes

ASCL1 has been described as both a master regulator of transcription and a pioneer factor. Being a master regulator of transcription in this case means that the expression of ASCL1 in a variety of cell types can induce the transcription of specific neuronal genes, resulting in differentiation or reprogramming into mature sympathetic neurones (Vasconcelos and Castro., 2014; Chan et al., 2013). Pioneer factors are able to bind to and remodel closed chromatin leading to a more accessible landscape that other transcription factors can access (Zaret and Carroll 2011). ASCL1 exhibits pioneer factor properties in many different cell types including fibroblasts, neuroblastoma and glioblastoma cells (Wapinski et al., 2017, Park et al., 2017). Taking both of these things into account, the transcriptional and chromatin accessibility differences observed in neuroblastoma cells following ASCL1 KO cells reflect typical functions of ASCL1.

Removing ASCL1 results in changes to both the transcriptome and the permissiveness of the chromatin state. When interrogating the RNA-Seq data, the most significantly changed genes are predominantly less expressed following ASCL1 KO (Figure 4.3-4.5). This is to be expected following the removal of a key transcriptional regulator. The ATAC-Seq data shows that there are a lot of genes that are less accessible following ASCL1 KO. Again, this is to be expected following the removal of a key pioneer factor. Assigning the accessible regions with their genomic annotations shows 40%

of accessible areas are distil intergenic, 20% are intronic and 20% are within 1kb of a TSS (Figure 4.11). This is typical of an ATAC-Seq distribution, where most open regions are observed in enhancer areas (Yan et al., 2020).

4.4.3 ASCL1 Maintains Neuroblastoma Cells in a State Primed for Neuronal Differentiation

The regions that are most downregulated transcriptionally and less accessible following ASCL1 KO are associated with neuronal development and accompanying processes (Figure 4.6-4.8). This suggests that in SH-SY5Y, IMR32 and SK-N-BE(2)c cells ASCL1 is maintaining the transcription of neuronal associated genes and supporting a state that may already be primed for differentiation. The removal of ASCL1 is therefore resulting in a less neuronal and less committed transcriptional state.

Neuroblastomas arise from neural crest cells and are thought to be stalled in a proliferative developmental precursor state (Jansky et al., 2021; Kildisiute et al., 2021). Adrenergic (ADRN) neuroblastoma cells are a more differentiated cell type than the mesenchymal (MES) cells which resemble a less differentiated neural crest cell (Van Groningen et al., 2017, Boeva et al., 2017). ASCL1 is only present in ADRN cells (Wang et al., 2019). ASCL1 is a pro-neural transcription factor and could be maintaining ADRN cells in a more developmentally mature state, one that is primed for neuronal differentiation and removing it results in a less primed chromatin accessibility landscape and transcriptome.

ASCL1 is required for differentiation of neuroblastoma cells, ASCL1 must be present and downregulated to allow differentiation. When neuroblastoma cells are treated with retinoic acid (RA) they differentiate. However, cells lacking ASCL1 or cells where ASCL1 expression has been silenced do not differentiate in response (Ichimiya et al., 2001; Kasim et al., 2016). When treated with the cyclin dependant kinase inhibitor (CDKi) Palbociclib (Pb), SH-SY5Y, IMR32 and SK-N-BE(2)c parental cells differentiate and the presence of many neuronal processes can be observed. As a CDKi, Pb inhibits the cyclin dependant kinases (CDK) 4 and 6 (Rihani et al., 2015). CDK4 and CDK6 are known to phosphorylate ASCL1, so the inhibition of these proteins will lead to a build-up of the dephosphorylated form of ASCL1, allowing the un(der)phosphorylated form to bind and transcribe genes involved in neuronal differentiation (Rihani et al., 2015). When the ASCL1 KO cells are treated with Pb they do not differentiate, showing the importance of ASCL1, specifically dephosphorylated ASCL1 in the differentiation of neuroblastoma cells (Figure 4.15) (Chaytor et al., Unpublished). This

finding is in line with previous publications and taken together these results strengthen the theory that ASCL1 must be present in neuroblastoma cells to allow differentiation to occur.

The ATAC-Seq and RNA-Seq results following ASCL1 KO could further explain why the ASCL1 KO cells do not differentiate in response to RA or Pb. In fibroblasts, introducing ASCL1 can remodel the chromatin allowing a chromatin state permissive for differentiation. In neuroblastoma cells, differentiating with RA results in a similar occurrence and the chromatin landscape alters to enable genes associated with neuronal differentiation to be accessed (Wapinski et al., 2013, Raposo et al., 2015). In the ASCL1 KO lines, the chromatin appears to be in a less primed state for differentiation. In addition to this, the ASCL1 KO lines are lacking ASCL1 protein which has the ability to remodel the closed chromatin around neuronal targets making them more accessible. The combination of both the less primed chromatin landscape and the lack of ASCL1, a key TF involved in making the chromatin more accessible for differentiation, could help understand on a chromatin accessibility and transcriptional level why ASCL1 KO cells do not respond as well to differentiation agents.

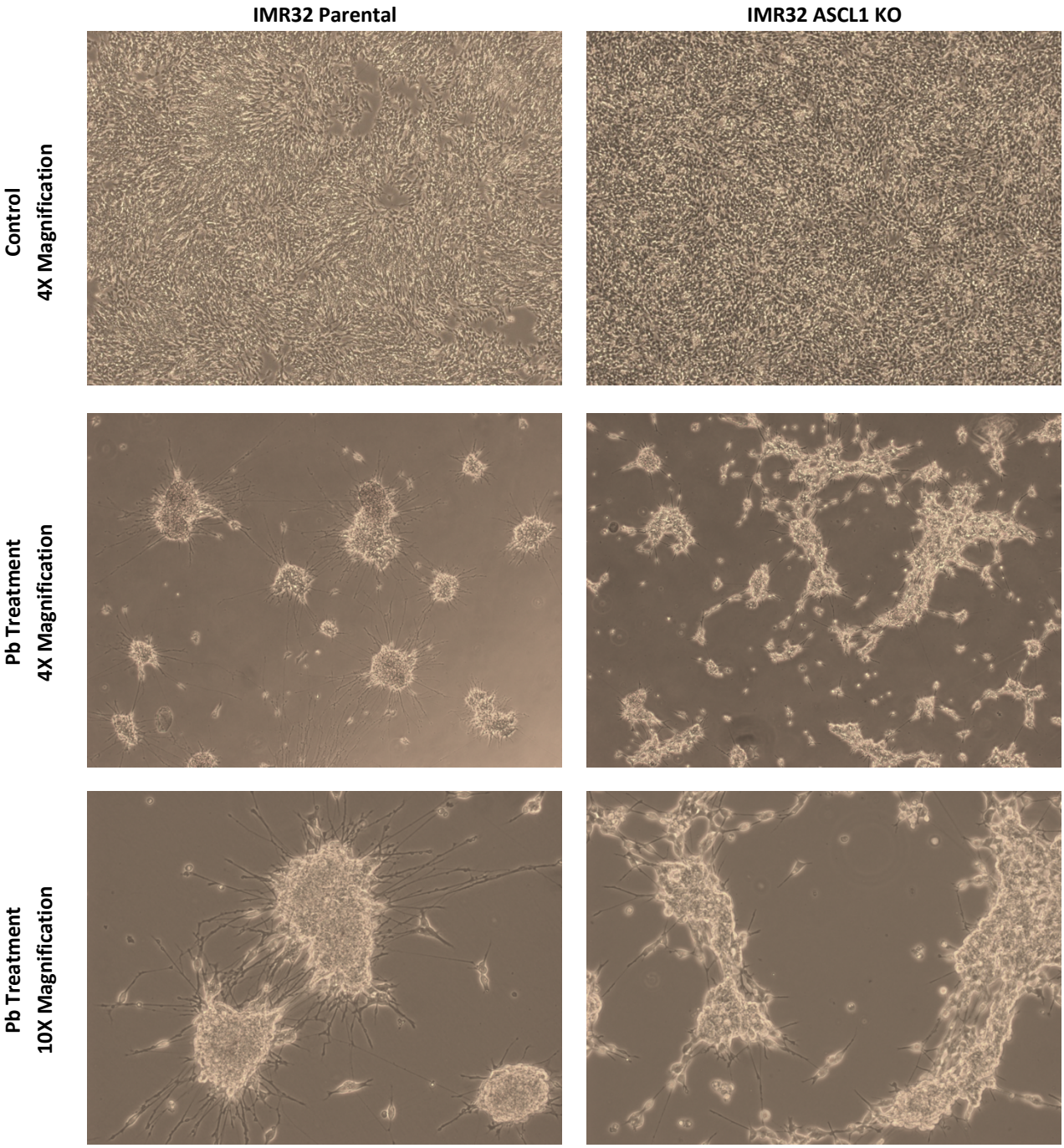

Figure 4.15: Treating IMR32 parental and ASCL1 KO cells with Palbociclib. IMR32 parental and ASCL1 KO cells were observed following 5 days of 1 µM Palbociclib treatment. Phase-contrast microscopy shows IMR32 parental and IMR32 CRISPR 1 under control conditions (top) and following 5 days Palbociclib treatment (4X, middle and 10X bottom). Experiment completed by Dr Lewis Chaytor.

Chapter 5

Reintroducing ASCL1 into Knockout Lines

5.1 Introduction

The phenotypes observed following ASCL1 knockout (KO) can all be explained by the typical functions of ASCL1 during development. The changes observed following ASCL1 KO include a reduction of proliferation (described in Chapter 2), lower transcription of neuronal targets and less accessible chromatin around neuronal targets (described in Chapter 4). ASCL1 is known to have a role in maintaining the precursor pool in development and transcribes genes involved in driving the cell cycle such as E2F1 and Tead1/2 (Castro et al., 2011). ASCL1 is also a proneural transcription factor, responsible for cell cycle exit and upregulating of genes involved in differentiation (Guillemot and Hassan, 2017, Castro et al., 2011). ASCL1 is known to be able to open closed chromatin and function as a pioneer factor, promoting chromatin accessibility around key neuronal genes (Raposo et al., 2015, Wapinski et al., 2017).

Following CRISPR gene editing there is the possibility that off-target effects could be affecting the phenotypes observed following ASCL1 KO. The sgRNA used for ASCL1 KO was gifted from Professor Steve Pollard's lab in Edinburgh who had previously used it. They did not report any off-target effects. In addition to this, multiple tools were used to check that the sgRNA did not target other locations in the genome. However, there is still the possibility that small mis-matches between the sgRNA and DNA could occur, meaning DNA damage and repair and therefore mutations could occur at the wrong site.

This work in this chapter was completed with the intention to confirm that the effects observed following ASCL1 KO were due to the absence of ASCL1 and not as a result of any off-target effects following the CRISPR gene editing process. This was achieved by reintroducing ASCL1 into SH-SY5Y ASCL1 KO cells, termed 'rescue' cells as the idea was to rescue the parental phenotype. Lentiviruses were used to transduce the ASCL1 KO cells with ASCL1 under the control of the TET3G promoter.

This meant the expression of ASCL1 was inducible and expression levels were tuneable. Various assays were undertaken to confirm the main phenotypes altered following ASCL1 KO had been restored. Fractionation and western blot were completed to determine if the chromatin binding of key TFs, such as PHOX2B and MYC/MYCN, had been reinstated. RNA-Seq was also carried out to determine whether following ASCL1 induction the transcriptome returned to a more parental state.

5.2 Results

5.2.1 Reintroducing Inducible ASCL1 into SH-SY5Y ASCL1 Knockout Lines

ASCL1 was reintroduced into KO lines in an inducible manner, allowing expression to be switched on when required. This was achieved by using two viral vectors, one containing the tetracycline controlled transactivator (TCT) and the second containing the ASCL1 gene under the control of the tetracycline response element (TRE) promoter. The TRE promoter contains a sequence that is recognised by the TCT. The TCT is constitutively produced but has no effect until cells are treated with doxycycline. Doxycycline binds the TCT, causing a conformational change enabling the TCT to bind the TRE promoter and transcribe ASCL1.

To determine the success of the viral transduction, and to ensure the rescue cells express ASCL1, the presence of ASCL1 following doxycycline treatment was initially determined by western blot. Following confirmation ASCL1 reintroduction into KO cells had been successful, the concentration of doxycycline was titrated to ensure a level of ASCL1 similar to endogenous was being induced. The concentration of doxycycline was titrated from 3 ng/µl to 1 µg/µl and as expected, the amount of ASCL1 induced in the rescue cells is directly correlated with the concentration of doxycycline cells are treated with. An example western blot where rescue cells were treated with concentrations of doxycycline from 3-10ng/µl is shown in Figure 5.1. The chosen doxycycline concentrations to treat rescue cells with to induce an endogenous level of ASCL1 ranged from 4 ng/µl to 6.5 ng/µl, these concentrations were used for all further experiments (Figure 5.1 C).

For experiments to determine the effect of reintroducing ASCL1, rescue cells were treated with doxycycline every 24 hours. This was to ensure the levels of ASCL1 remained constant in the rescue cells and to avoid the possibility of doxycycline degradation affecting the expression.

5.2.2 Continued ASCL1 Induction Alters Morphology

Initially, rescue cells were treated with doxycycline to determine the effect of ASCL1 reintroduction the morphology. When ASCL1 is removed from cells, there is no change to the morphology (Figure 2.6) so reintroducing ASCL1 into KO lines was expected to have no effect. However, after treating rescue cells with doxycycline every 24 hours for five days, the cells started to look less neuronal and instead looked flatter with less defined edges, a morphology associated with the mesenchymal (MES)-type neuroblastoma cells. Considering removing ASCL1 from cells has no effect on

A

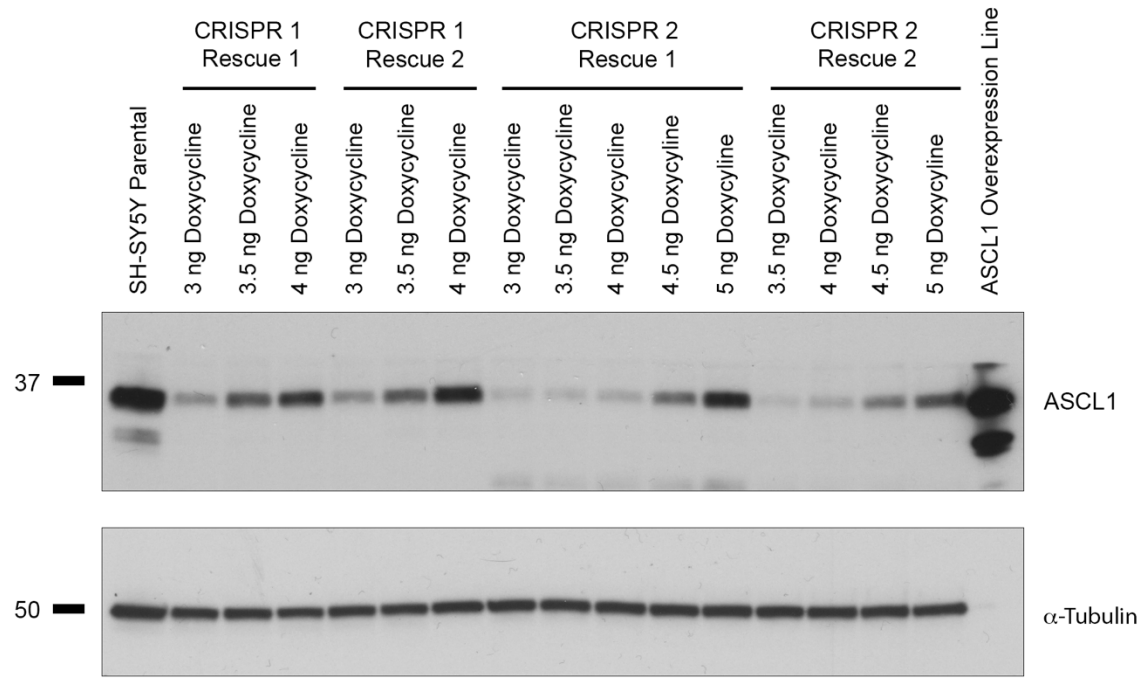

B

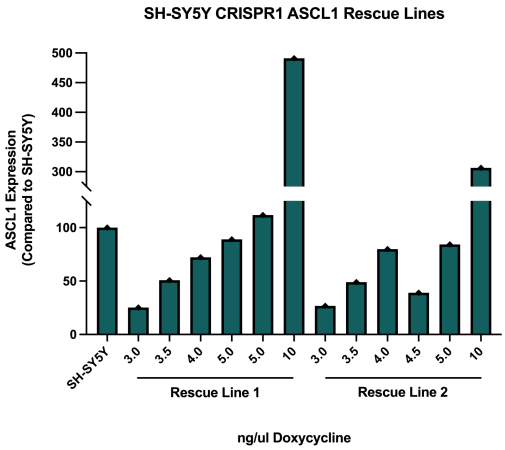

C

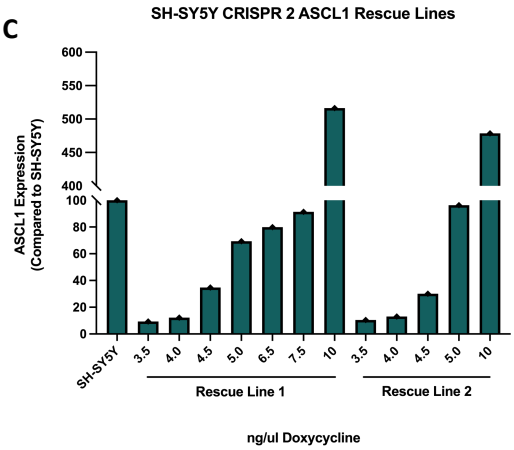

D

SH-SY5Y ASCL1 KO Line	Rescue Line	Concentration of Dox to Induce Endogenous Levels of ASCL1
CRISPR 1	1	4 ng/µl
	2	4 ng/µl
CRISPR 2	1	6.5 ng/µl
	2	5 ng/µl

Figure 5.1: Determining the doxycycline concentration to induce endogenous levels of ASCL1. Cells were treated with doxycycline for 7 days and expression confirmed by western blot (A, quantitation shown in B and C). Following multiple doxycycline titrations, a concentration that induced a protein level resembling endogenous ASCL1 was chosen (D).

morphology, this was an unexpected result. Next, it was determined if the prolonged expression of ASCL1 in the rescue cells was responsible for the changed morphology. To investigate this, rescue cells were treated with doxycycline for five days before treatment was removed. After treating the rescue cells every 24 hours for five days, cells take on the altered phenotype (Figure 5.2 A and 5.3 A). Following the removal of doxycycline, the cells were observed every 24 hours. 48 hours after removing doxycycline from the rescue cells, the morphology begins to revert back to that of parental cells and untreated ASCL1 KO cells (Figure 5.2 B and 5.3 B). 72 hours after removing doxycycline from the rescue cells, most of the cells resembled a more neuronal phenotype and only a few cells had the flatter, morphology (Figure 5.2 C and 5.3 C). This indicated that the sustained expression of ASCL1 at an endogenous level in the rescue cell lines was causing the change in morphology.

To establish how ASCL1 protein levels in the rescue lines were changing after doxycycline withdrawal, a western blot was run. The protein levels of ASCL1 begin to drop 48 hours after removing doxycycline and continue to decrease at 72 hours, further supporting the hypothesis that continuous expression of ASCL1 was causing the rescue cells to adopt an altered morphology (Figure 5.4).

5.2.3 ASCL1 Expression is Heterogeneous in Neuroblastoma Cells

When reintroducing ASCL1 into ASCL1 KO cells, multiple doxycycline titrations were completed to ensure the induced levels of ASCL1 were comparable to the endogenous levels in SH-SY5Y. It was then surprising to see that reintroducing an endogenous level of ASCL1 into the ASCL1 KO lines resulted in morphological changes, as it was expected cells would retain the ADRN phenotype of the parental line. ASCL1 is known to oscillate in neural stem cells (Imayoshi et al., 2013). While this has not been documented for neuroblastoma cells, it was reasoned that the unexpected phenotype seen in the ASCL1 rescue lines with constitutive ASCL1 expression may be because oscillations of endogenous ASCL1 expression, which happens in parental cells, does not occur in this rescue system. Confocal microscopy was completed on cells stained for ASCL1 to visualise changes in protein expression levels between cells. The levels of ASCL1 expressed is different between cells, and it does not look like ASCL1 is present in all cells at the same time (Figure 5.5). This could point to ASCL1 oscillation in neuroblastoma cells and explain why inducing a constant level of ASCL1 was resulting in the rescue cells changing morphology.

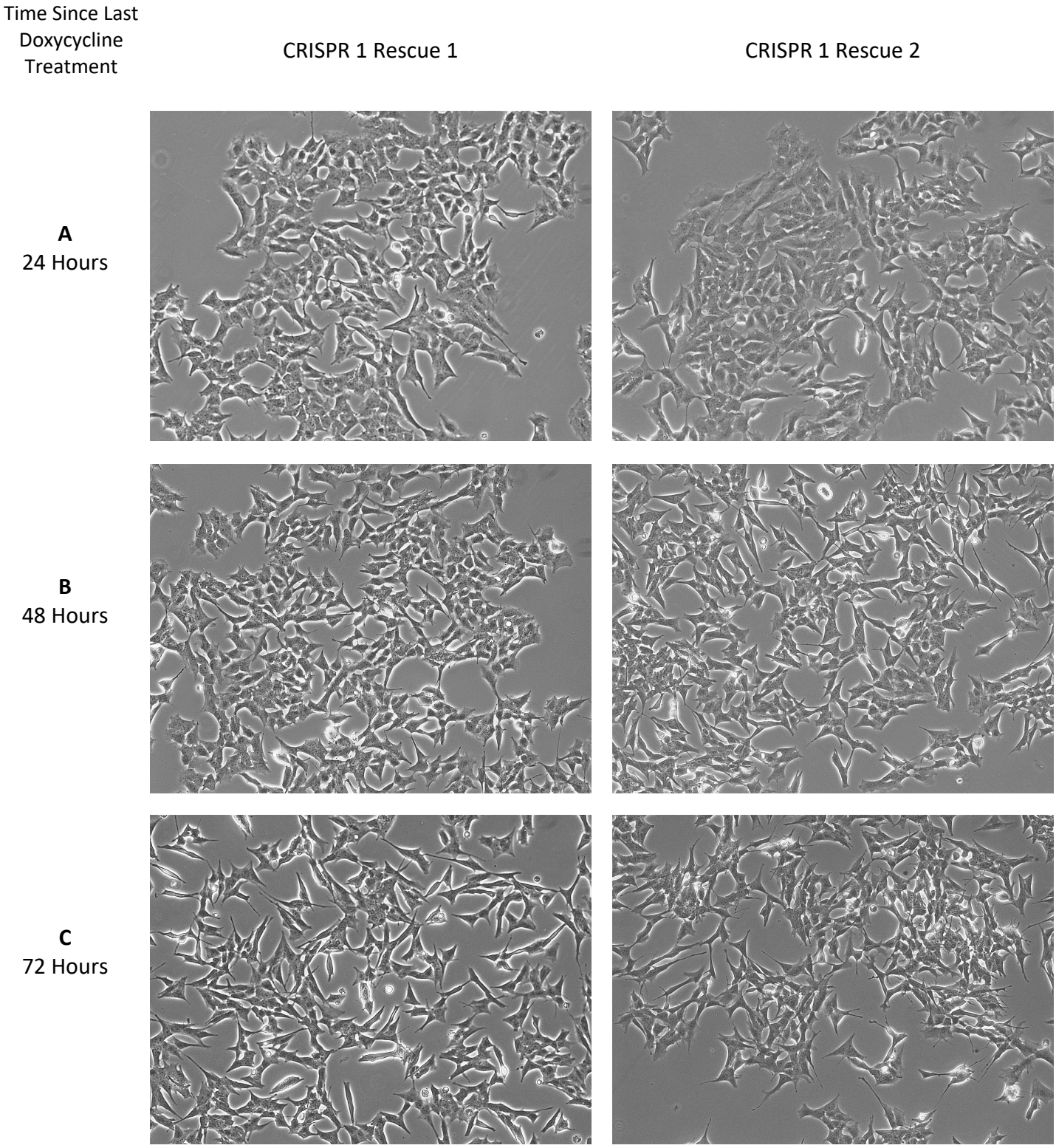

Figure 5.2: Morphology of CRISPR 1 rescue cells is altered following ASCL1 induction. Rescue cells were continually treated with doxycycline for five days (A). Doxycycline treatment was withdrawn from culture conditions for 48 hours (B) or 72 hours (C). Phase-contrast Microscopy images at 10X.

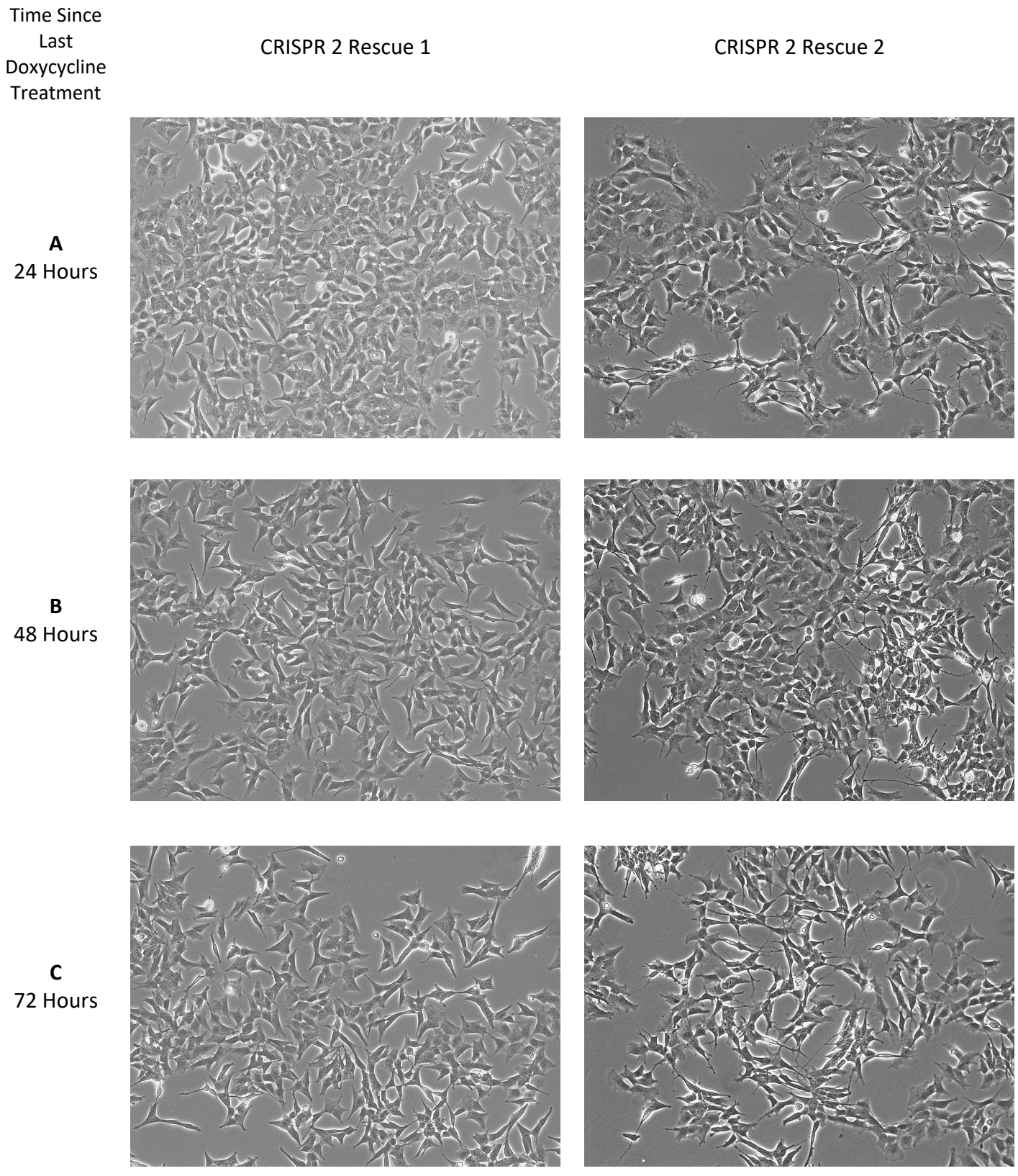

Figure 5.3: Morphology of CRISPR 2 rescue cells is altered following ASCL1 induction. Rescue cells were continually treated with doxycycline for five days (A). Doxycycline treatment was withdrawn from culture conditions for 48 hours (B) or 72 hours (C). Phase-contrast Microscopy images at 10X.

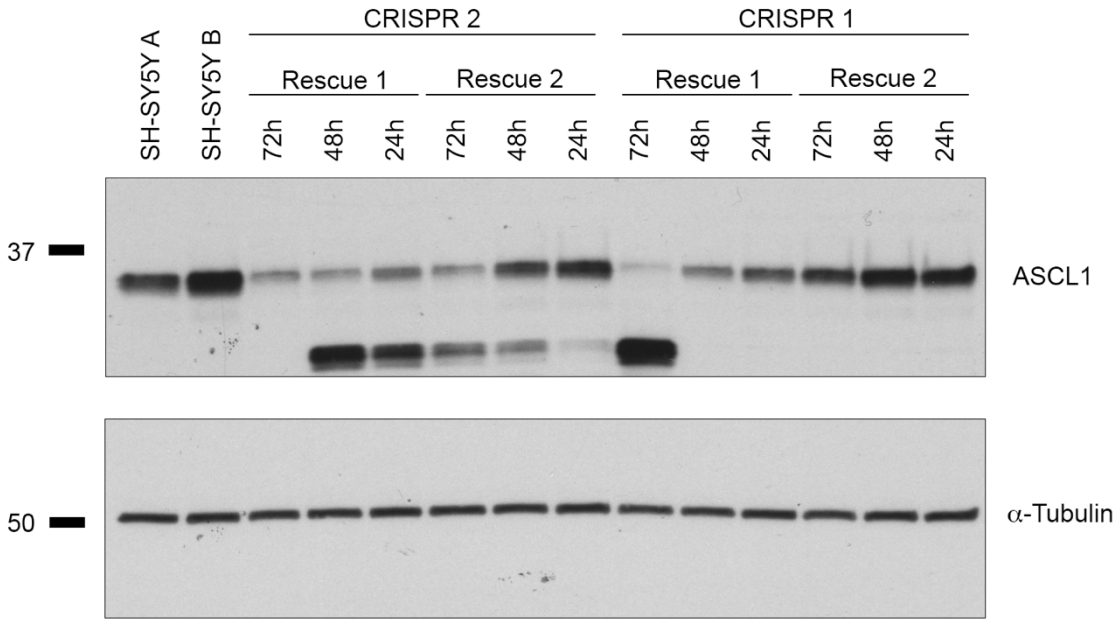

Figure 5.4: ASCL1 protein levels decrease when doxycycline treatment is withdrawn. ASCL1 expression following withdrawal of doxycycline treatment determined by western blot. The amount of time stated represents the amount of time since last treatment.

5.2.4 Reintroducing ASCL1 Reinstates Transcription Factor Binding

When ASCL1 is removed from neuroblastoma cells, one of the most striking effects is the reduction of ADRN transcription factors and MYC binding to the chromatin (Figure 3.18-3.21). Next it was investigated whether ASCL1 reintroduction could restore the chromatin binding of PHOX2B and MYC. ASCL1 was induced for one week, the rescue cells were harvested and fractionation was carried out. The chromatin fraction was then run on a western blot to compare PHOX2B and MYC levels bound in parental, uninduced and induced rescue lines.

When looking at MYC, three of the four uninduced rescue lines have much lower MYC chromatin binding than the ASCL1 induced lines, the level of MYC binding in the uninduced lines is similar to what was observed in the ASCL1 KO lines (Figure 3.21). The binding of PHOX2B to the chromatin is around 50% of the SH-SY5Y parental cells, which again is similar to the levels observed following ASCL1 KO (Figure 3.19). However, chromatin binding of MYC and PHOX2B in the uninduced CRISPR 2 rescue 1 line is much higher than what was observed in the CRISPR 2 KO line and is very similar to the levels bound to the chromatin in parental lines. As the same high level is seen for both transcription factors and is not seen for the other CRISPR 2 rescue line, this could be due to 'leakiness' where some ASCL1 is being expressed before doxycycline treatment. This small amount of ASCL1 could be enough to permit chromatin binding again (Figure 5.6 B).

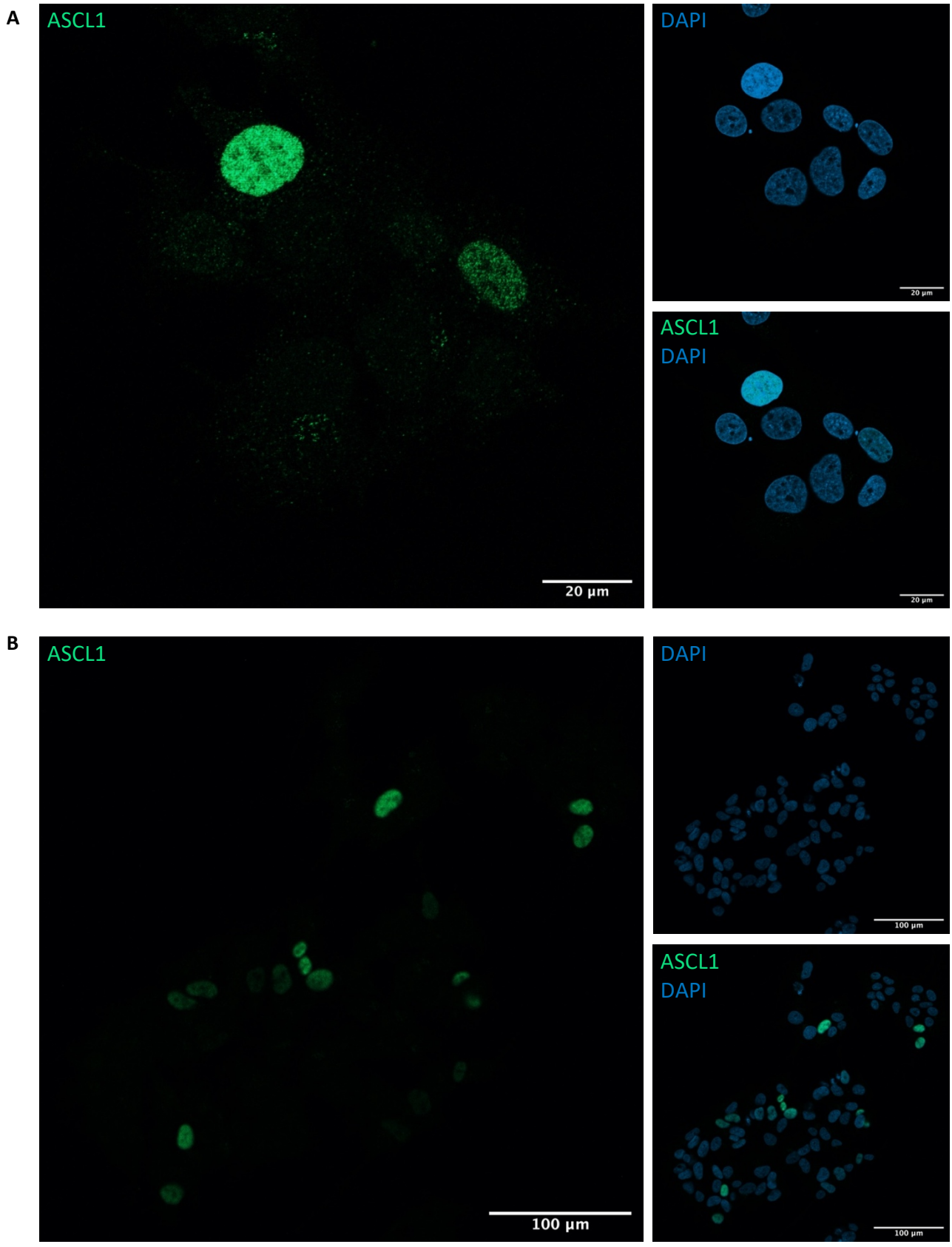

Figure 5.5: Confocal microscopy imaging shows ASCL1 expression is not consistent between cells. Immunofluorescence staining and imaging to show the presence of ASCL1. SH-SY5Y cells were stained with ASCL1 (green) and DAPI (blue). Images were taken on the Zeiss 980 Airyscan2 at 60X (A) or 20X (B).

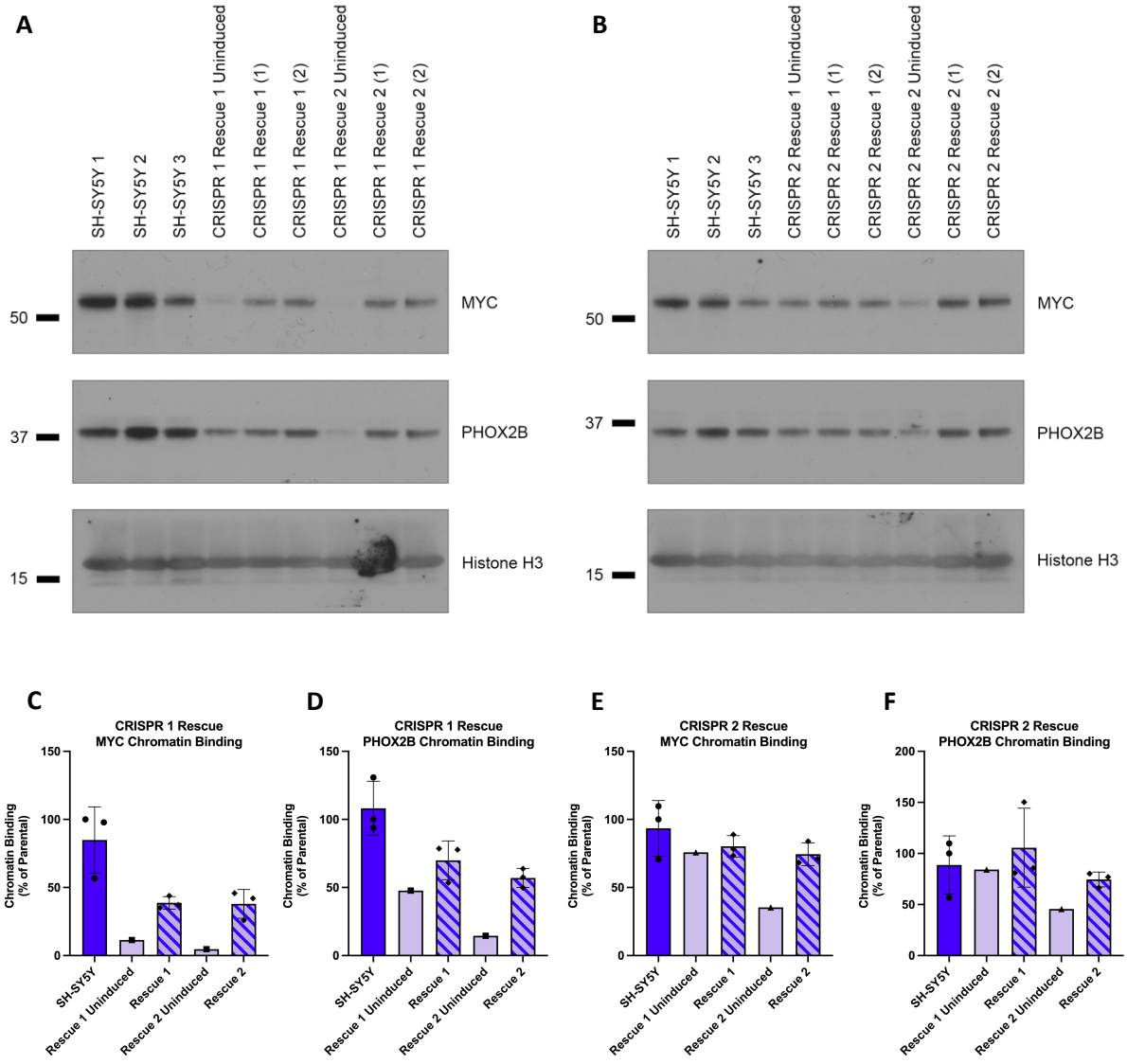

Figure 5.6: Chromatin binding of MYC and PHOX2B is restored in rescue lines. Cells were harvested and subject to the subcellular fractionation protocol, followed by western blot. Chromatin fractions of SH-SY5Y parental, uninduced rescue and ASCL1 induced rescue lines were run on a western blot and analysed for chromatin bound MYC and PHOX2B (A-B). The western blots were quantitated, and the amount of chromatin bound protein was calculated as a percentage of the chromatin bound protein in parental cells (C-F).

When the rescue lines are treated with doxycycline, the levels MYC bound to chromatin increases. For the CRISPR 1 rescue lines, levels of MYC binding chromatin are around 50% of the parental levels and for the CRISPR 2 rescue lines MYC binding is around 80% of parental levels following ASCL1 induction. For PHOX2B, the level bound to the chromatin following ASCL1 induction reaches around 70% of the parental level for the CRISPR 1 rescue lines and 85% for the CRISPR 2 rescue 2 line. The CRISPR 2 rescue 1 line shows the same level of PHOX2B binding as SH-SY5Y parental, although this line has increased binding before ASCL1 induction. These results show inducing ASCL1 partially restores the chromatin binding of key transcription factors (Figure 5.6 A-B).

5.2.5 Clustering of RNA Seq Data

To determine the gene expression changes after ASCL1 reintroduction into ASCL1 KO cells, RNA-Seq was completed. Cells were induced with doxycycline for 24 hours, 72 hours or 7 days. At 24 hours the changes observed are more likely be due to direct ASCL1 mediated effects, whereas changes at 72 hours and 7 days could be the result of downstream effectors, rather than direct ASCL1 targets. The RNA-Seq was completed alongside SH-SY5Y parental and ASCL1 KO RNA-Seq so the cell lines could be compared. PCA plots were produced to visualise how the different conditions cluster. All five replicates for each time point cluster together. Following 24 hours or 72 hours of ASCL1 induction in rescue cells, samples are more closely matched on the PCA1 axis which shows most variance. Following 24 hours or 7 days ASCL1 induction in KO cells, samples are more closely related on the PCA2 axis (Figure 5.7A). This shows that the time points are all distinct from each other and ASCL1 reintroduction causes cells to change transcriptome over the course of treatment.

MA plots are a way to visualise the differences in gene expression between datasets. They show the log fold change on the y-axis and mean counts on the x-axis. More points closer to 0 mean there is less variation, more spread indicates more variation between samples. MA plots are shown following normalisation. When comparing 24 hours and 72 hours of ASCL1 expression in ASCL1 KO cells, the points are more clustered around 0 showing less variability between samples. The points are much more dispersed when comparing 24 hours and 7 days induction, indicating there is more transcriptional change following 7 days ASCL1 expression (Figure 5.7 B).

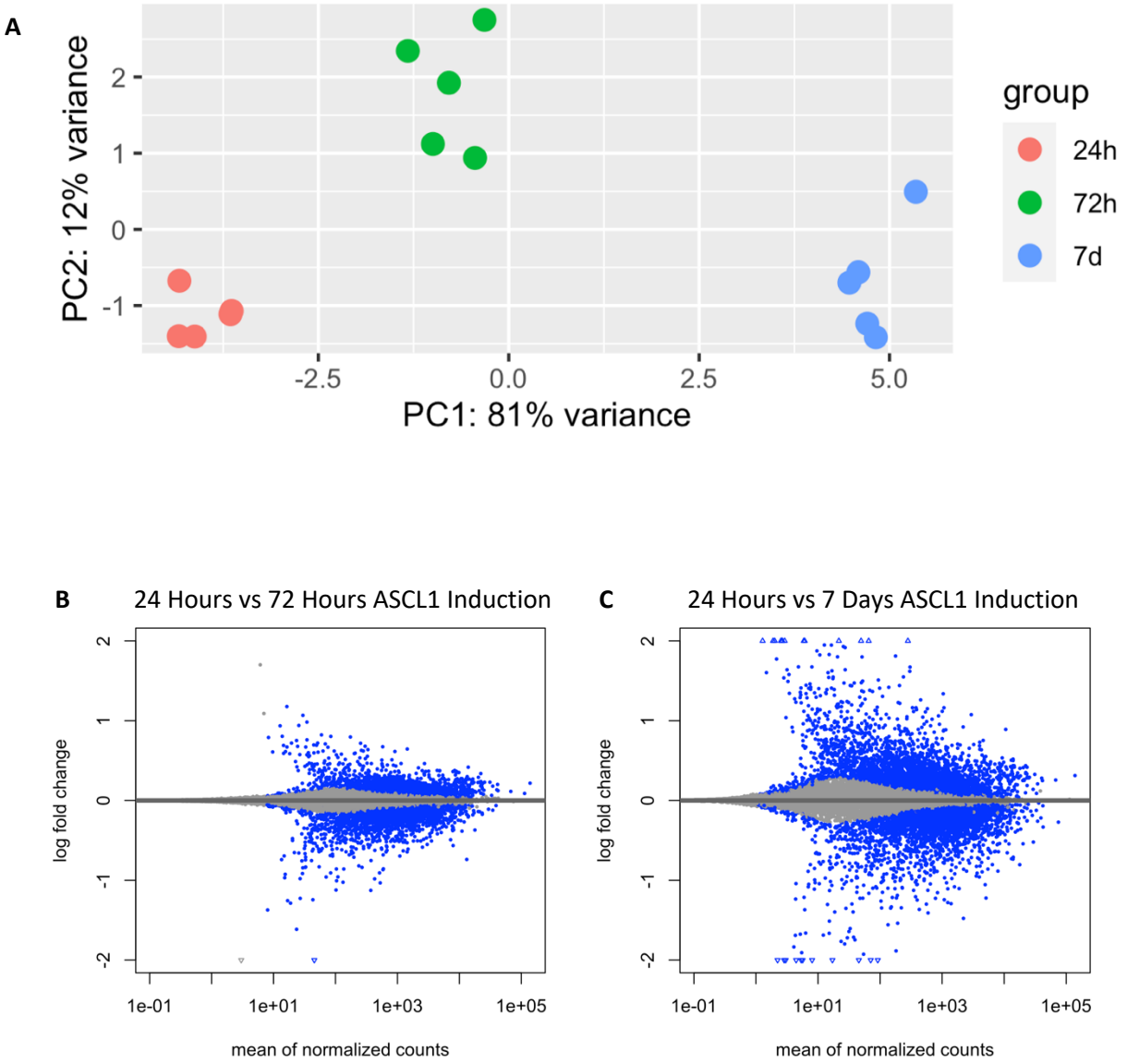

Figure 5.7: Visualisation of SH-SY5Y Rescue RNA-Seq data. PCA plots to show the variation and clustering of RNA-Seq data between 24 hour, 72 hour and 7 day ASCL1 induction into rescue lines (A). MA plots were produced to show the difference in transcription following ASCL1 reintroduction. 24 hours vs 72 hours induction (B) and 24 hours vs 7 days induction (C) are shown. Blue points represent significantly changed values ($p < 0.05$).

5.2.6 GO Analysis Shows Higher Expression of Neuronal Differentiation Genes in Parental Lines

To determine which gene sets changed between ASCL1 KO cells and the rescue cells Gene Ontology (GO) analysis was completed following DESeq2 analysis. Previously it was shown that removing ASCL1 resulted in neuronal targets being suppressed (Section 4.2), so it was anticipated that reintroducing ASCL1 would stimulate the transcription of these genes. When comparing rescue lines to the ASCL1 KO lines, following 24 or 72 hours of ASCL1 expression, genes associated with neuronal pathways such as neuron projection, the dendritic tree and genes associated with the synapse and synaptic transmission were expressed at a higher rate than in the ASCL1 KO lines (Figure 5.8 A,B). Following 7 days of ASCL1 induction, the neuronal differentiation associated genes are no longer identified as the most changed between the two cell types (Figure 5.8 C).

When comparing the rescue lines to each other, the neural differentiation genes described are not identified as being significantly changed between 24 hours and 72 hours (Figure 5.8 A). However, following 7 days of ASCL1 induction these neuronal targets are expressed at a lower rate. Genes associated with neuron projection, the dendritic tree, synapse and synaptic signalling are more highly expressed at both 24 hours and 72 hours when comparing to 7 days ASCL1 induction (Figure 5.9 B,C). Interestingly, genes associated with extracellular matrix organisation, cell motility and cell migration are more highly expressed after induction for 7 days when compared to 72 hours (Figure 5.9 C). These are genes that would be expected to be more prominent in a MES type cell, so the RNA-Seq data was then analysed to determine the expression of ADRN and MES specific genes.

5.2.7 Continued ASCL1 Induction Leads to MES Gene Upregulation

As previously described, when continually treated with doxycycline to maintain an endogenous expression level of ASCL1, cells take on a morphology resembling a ‘MES-like’ cell. To identify whether cells were taking on a more MES-like transcriptional state, RNA-Seq data was interrogated to assess the effects of ASCL1 induction on MES and ADRN genes. The Van Groningen MES and ADRN gene signatures were used to do this, this list comprises of 485 MES genes and 369 ADRN genes (Van Groningen, 2017).

DESeq Analysis was completed to identify significantly changed genes, this dataset was compared to the MES and ADRN gene lists to produce a list of significantly changed ADRN and MES genes. There is not a clear distinction between MES and ADRN targets between the 24 and 72 hour timepoints (Figure 5.10 A,B). There is a much clearer difference when looking at the cells induced with ASCL1 for 7 days. After 7 days, the expression of the ADRN targets is much lower when comparing to the 24

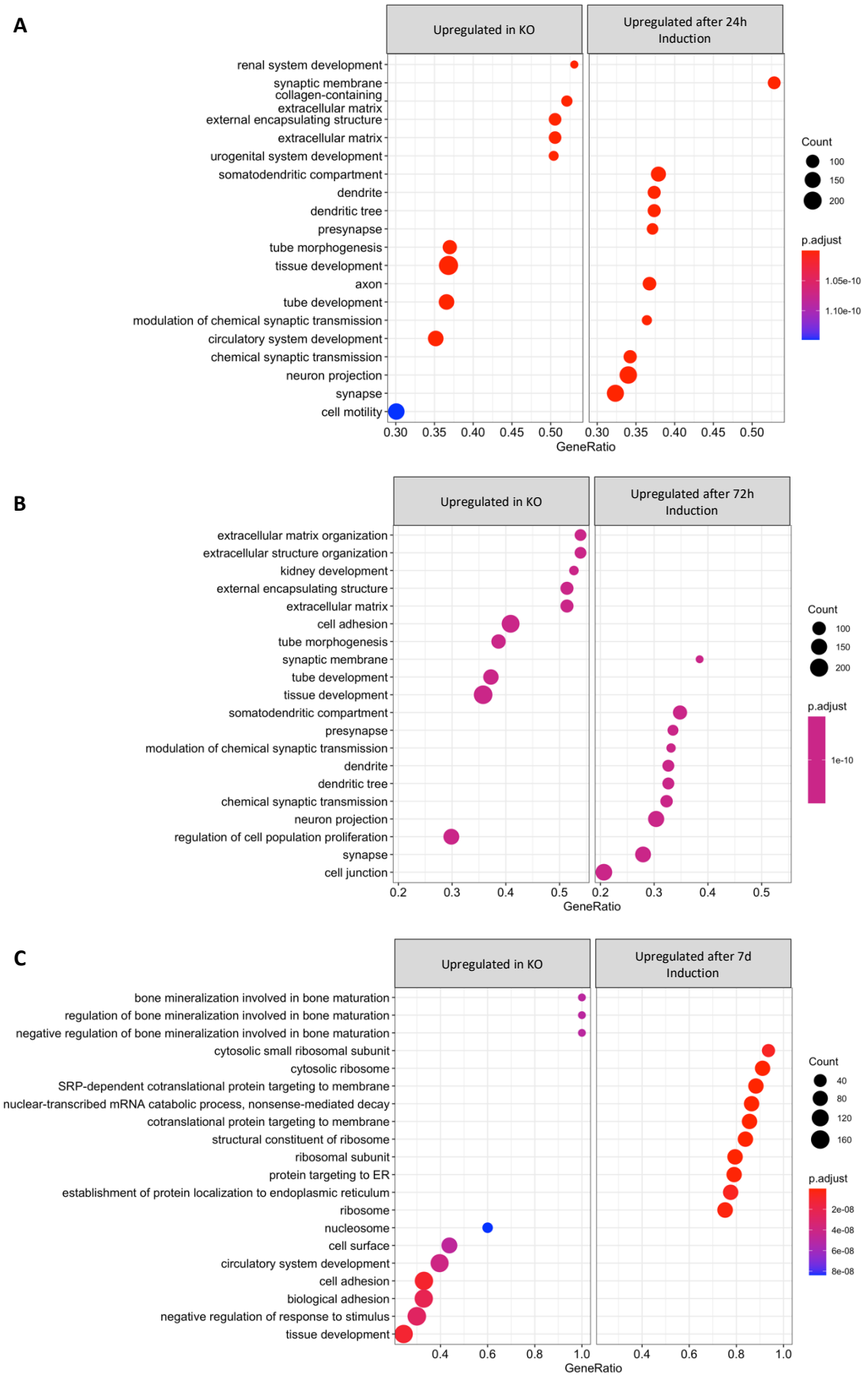

Figure 5.8: GO analysis comparing RNA-Seq data from ASCL1 KO cells with ASCL1 rescue cells. GO terms significantly changed between SH-SY5Y ASCL1 KO and 24 hours ASCL1 induction (A), ASCL1 KO and 72 hours induction (B) and ASCL1 KO and 1 week induction (C).

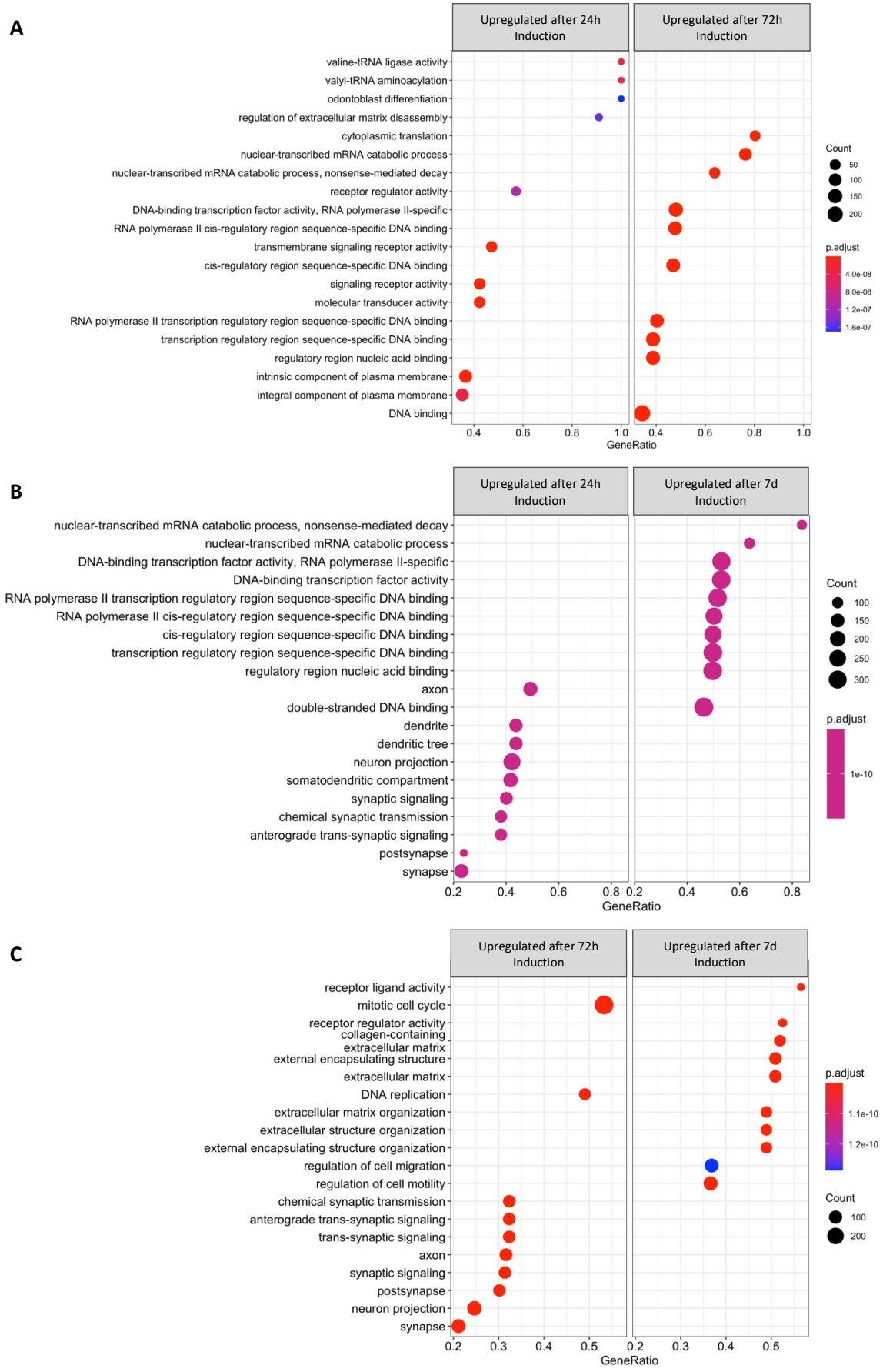

Figure 5.9: GO Analysis comparing RNA-Seq data following 24h, 72h and 1 week ASCL1 induction. GO terms significantly changed between SH-SY5Y ASCL1 KO and 24 hours ASCL1 induction (A), ASCL1 KO and 72 hours induction (B) and ASCL1 KO and 1 week induction (C).

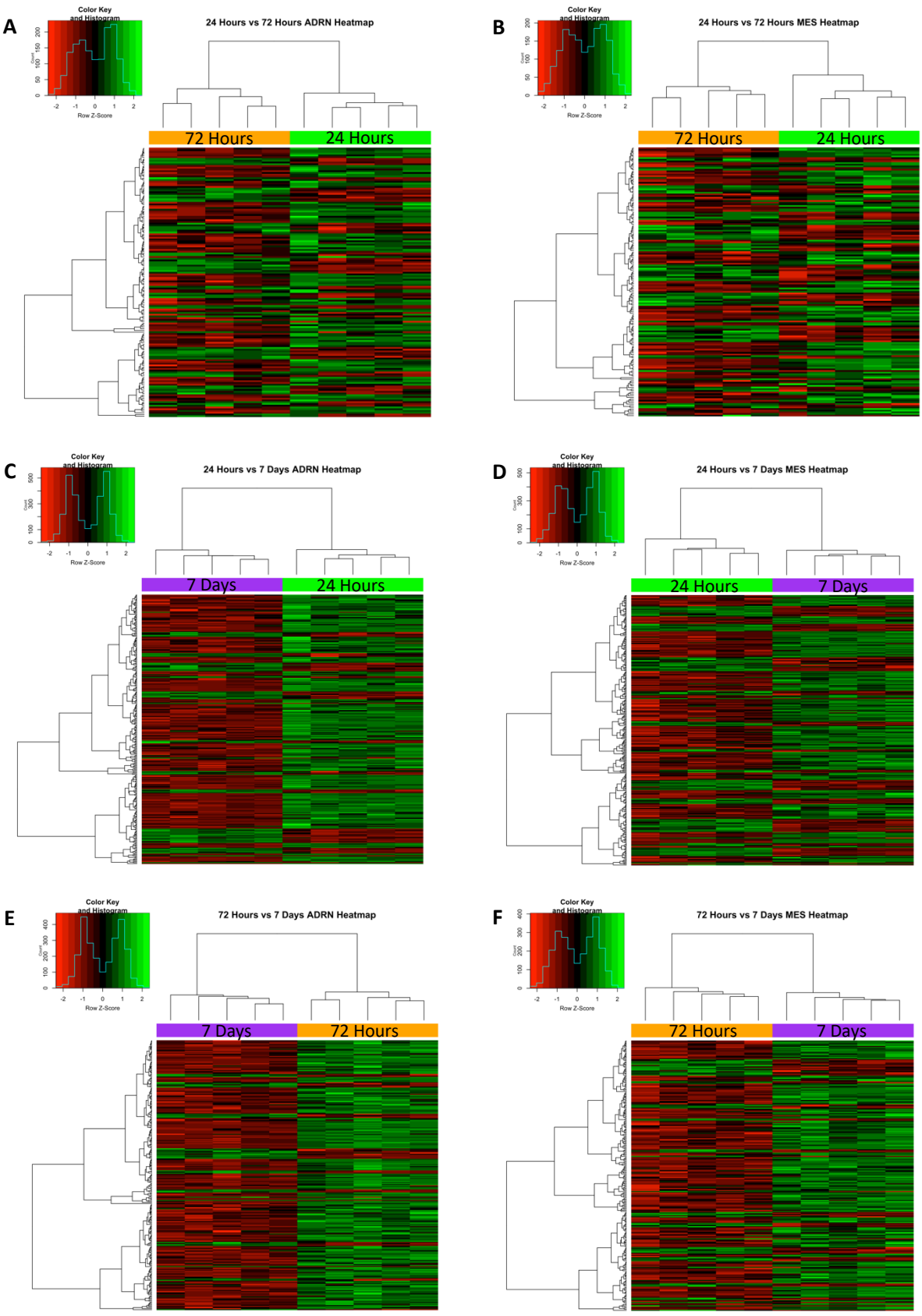

Figure 5.10: Heatmaps to show the abundance of ADRN and MES targets following ASCL1 induction. DESeq identified significantly changed ADRN and MES genes. The differences in transcription of ADRN and MES targets at 24 hours vs 72 hours (A,B), 24 hours and 7 days (C,D) and 72 hours and 7 days (E,F) are shown. Red bars represent downregulated genes and green bars represent upregulated genes in the comparison.

		Number of Differentially Expressed Genes		
	Total Genes	24 Hours vs 72 Hours	24 Hours vs 7 Days	72 Hours vs 7 Days
ADRN	369	154	281	257
MES	485	163	291	246

Table 5.1: Differentially Expressed ADRN and MES Genes. Number of ADRN or MES genes recognised as significantly different between ASCL1 induction conditions. The total number of ADRN and MES genes identified by Van Groningen is also stated (van Groningen et al., 2017).

hour or 72 hour ASCL1 induction samples (Figure 5.10 C,E). When looking at the MES gene set, it is the opposite result. The MES genes are more highly expressed following 7 days of ASCL1 induction and are at a much lower levels in the 24 and 72 hour samples (Figure 5.10 D,F). The cells look like they have a more 'MES' morphology following continual ASCL1 induction, and these results indicate the cells are moving towards a MES transcriptional state too.

5.2.8 Reintroducing ASCL1 and Treating with NOTCH Inhibitor Prevents the MES Transition

The transition from an ADRN to MES state can be forced by the introduction of NOTCH3 intracellular domain. This transition can be prevented by treating with γ-secretase inhibitor which inhibits the NOTCH signalling pathway (Van Groningen et al., 2019). If the flatter, less defined morphology of cells following continual ASCL1 induction is due to cells becoming more MES-like, it was then explored whether treatment with doxycycline, to induce ASCL1, in combination with the NOTCH inhibitor would prevent the transition.

The morphology following 24 hours of ASCL1 induction in rescue cells was similar to ASCL1 KO cells. The morphology begins to change at 48 hours and looks quite different to the untreated cells following 72 hours of ASCL1 induction. Inducing ASCL1 for 48 or 72 hours results in cells that have less apparent β-III-Tubulin, a neuronal marker which is expressed at a higher level in ADRN cells than MES cells (Figure 5.11 A-D). When cells are treated with a combination of doxycycline and the NOTCH inhibitor for 72 hours cells do not exhibit the MES-like phenotype. Instead, the presence of many neuronal processes can be observed following β-III-Tubulin staining (Figure 5.11 E). When treating with the NOTCH inhibitor alone, the cells retain their ADRN phenotype and show the presence of some neuronal processes, but it appears the combination of inducing ASCL1 and treating with the notch inhibitor is more efficient at pushing cells down a morphological differentiation pathway (Figure 5.11 F).

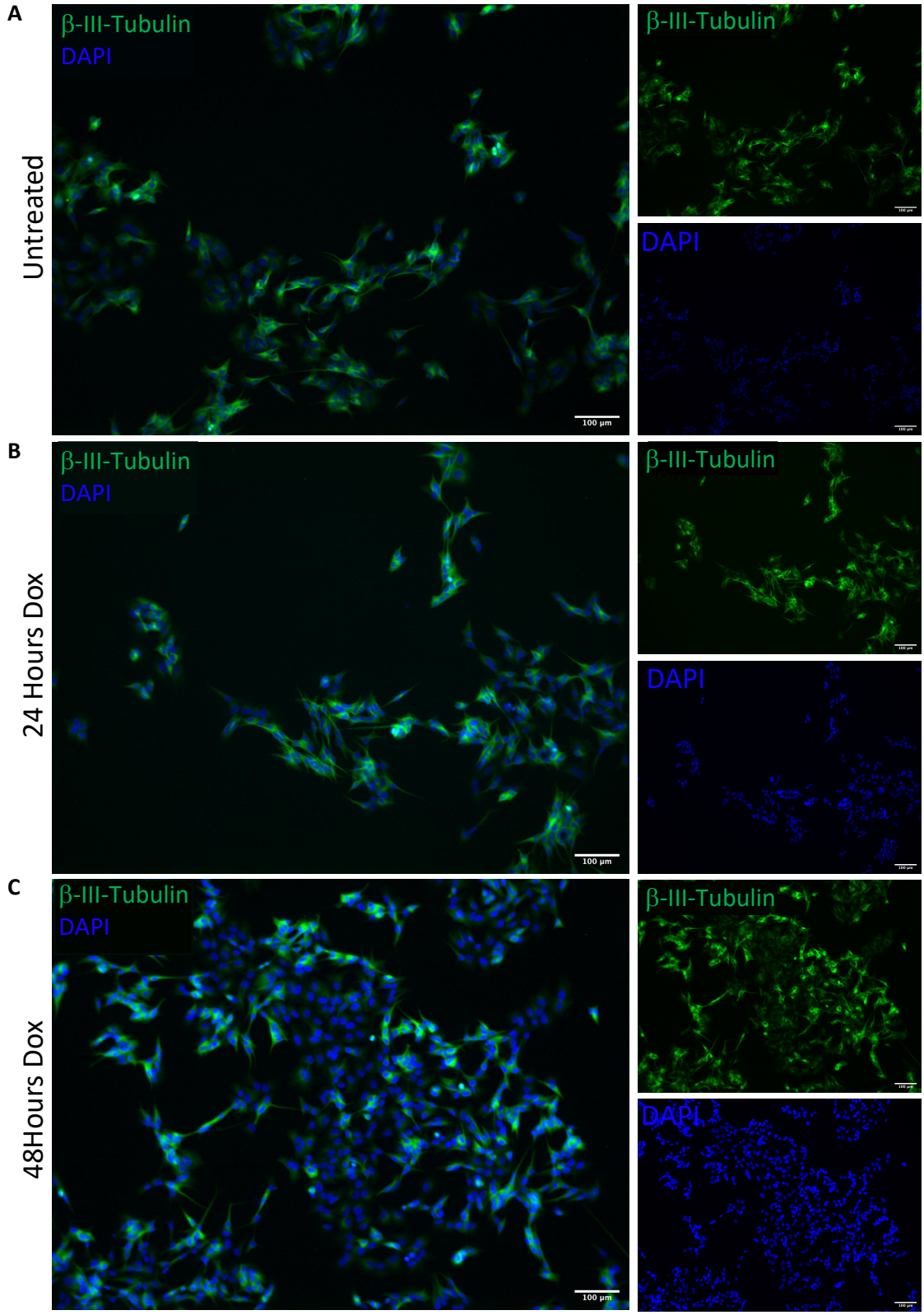

Figure 5.11: The morphology of rescue lines following treatment with doxycycline and NOTCH pathway inhibitors. Immunofluorescence staining and imaging to show the distribution of β–III-Tubulin (green) following no doxycycline induction (A), induction for 24 hours (B), 48 hours (C) or 72 hours (D). Cells were treated with doxycycline and the NOTCH inhibitor for 72 hours (E) or just NOTCH inhibitor for 72 hours (F). Images were taken on the Zeiss 4000 at 4X magnification.

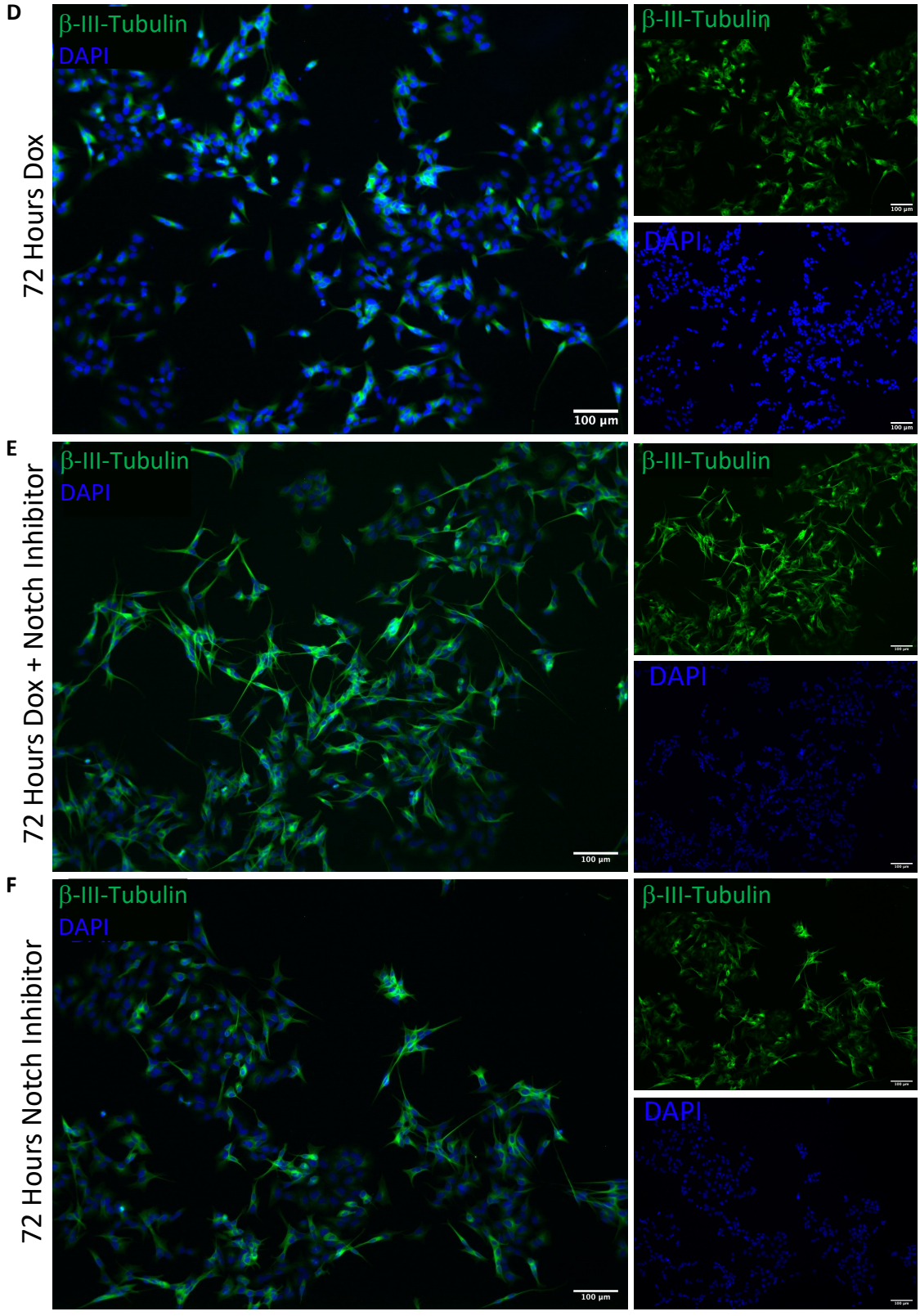

Figure 5.11 (continued): The morphology of rescue lines following treatment with doxycycline and NOTCH pathway inhibitors. Immunofluorescence staining and imaging to show the distribution of β-III-Tubulin (green) following no doxycycline induction (A), induction for 24 hours (B), 48 hours (C) or 72 hours (D). Cells were treated with doxycycline and the NOTCH inhibitor for 72 hours (E) or just NOTCH inhibitor for 72 hours (F). Images were taken on the Zeiss 4000 at 4X magnification.

5.3 Discussion

Removing ASCL1 from neuroblastoma cells results in multiple effects. Cells grow at a slower rate, key ADRN targets bind to the chromatin less, neuronal genes are transcribed at lower levels and the areas around these neuronal genes are not as accessible. Reintroducing ASCL1 into knockout lines was completed in an attempt to rescue the phenotypes observed and confirm removal of ASCL1 was responsible for the changes.

5.3.1 Summary of Results

ASCL1 was successfully reintroduced into KO cells in an inducible manner. The doxycycline treatment concentration was titrated and ASCL1 level confirmed by western blot to ensure that the level of ASCL1 being induced in rescue cells was similar to endogenous levels in parental SH-SY5Y cells (Figure 5.1). Following continuous ASCL1 induction in rescue cells, the morphology of cells changes and resembles a 'MES-like' phenotype. This is a reversible change and when doxycycline treatment is removed, the rescue cells revert back to the ADRN phenotype and resemble a more neuronal cell (Figure 5.2 and 5.3). RNA-Seq analysis indicated the rescue cells were taking on a more MES transcriptional state following 7 days doxycycline treatment, transcription of ADRN genes was lower and transcription of MES genes was higher after 7 days of sustained ASCL1 induction than when ASCL1 was induced for 24 hours or 72 hours (Figure 5.10). When rescue cells were treated with doxycycline and a NOTCH pathway inhibitor, the change to a MES-like morphology is not observed, and instead cells begin to show the presence of neuronal processes (Figure 5.11).

5.3.2 Sustained ASCL1 Expression is not Typical for Neuroblastoma Cells

A constant level of ASCL1 was being maintained in the rescue cells when they were observed to change morphology. This was determined to not be representative of normal culture conditions following IF and confocal microscopy of SH-SY5Y cells (Figure 5.5). The observation that ASCL1 levels are variable between different parental neuroblastoma cells could explain why inducing and maintaining a constant level of ASCL1 in the rescue cells resulted in the altered morphology. Oscillation of ASCL1 has been described in oligodendrocyte precursor cells and neural stem cells in the developing nervous system and in the adult brain (Imayoshi et al., 2013, Urban et al., 2016, Sueda et al., 2021). In neural progenitor cells, ASCL1 oscillation helps maintain the progenitors in a proliferative state. Continuous, non-oscillatory ASCL1 expression in this context leads to cell cycle

exit and differentiation (Imayoshi et al., 2013, Imayoshi et al., 2015). Oscillation of ASCL1 has not been described for neuroblastoma cells. It would be interesting to fluorescently tag endogenous ASCL1 in parental neuroblastoma lines to enable protein expression to be tracked over time and determine whether ASCL1 is oscillating. It would also be interesting to establish how long ASCL1 is present in cells for and to see how many of the cells express ASCL1 at any one time.

5.3.3 Sustained ASCL1 Expression is Not Permissive for Differentiation

Differentiation targets are upregulated at 24 and 72 hours of ASCL1 induction in rescue lines but downregulated following 7 days induction (Figure 5.8 and 5.9). This supports the theory that ASCL1 is required for the initiation of neuronal differentiation and must be downregulated before cells are able to differentiate. Previous studies have shown ASCL1 protein levels are downregulated following retinoic acid treatment and sustaining ASCL1 expression prevents differentiation (Ichimiya et al., 2001; Kasim et al., 2016). A similar phenomenon could be happening here. ASCL1 induction in the rescue lines is upregulating genes involved in the neuronal differentiation process, but the constant and sustained ASCL1 expression is blocking differentiation from occurring. To determine if this is what is happening, it would be informative to treat cells with doxycycline for 24-72 hours to induce the differentiation genes, then remove doxycycline treatment and supplement growth media with neuronal development factors to determine if the initial burst of ASCL1 and upregulation of differentiation genes is enough to begin the differentiation process.

5.3.4 Sustained ASCL1 Expression Leads to a MES-like State

ASCL1 is a member of the ADRN CRC, meaning it cooperates with other members of the CRC to support its own expression and expression of other ADRN targets (Wang et al., 2019). Therefore, sustained expression of ASCL1 would be expected to result in upregulation of members of the CRC, maintaining and strengthening ADRN identity. However, this is not what is happening here. It is thought that cells convert to a MES state under stress, for example, as a way to evade treatments. The cells could be identifying the sustained level of ASCL1 as a stressor and then transitioning to a MES state as a protective response. The reason for the altered phenotype cannot be confirmed, but it is an unexpected response to ASCL1 induction.

Inducing MES specific genes into ADRN cells can induce a MES cell phenotype, genotype and H3K27ac landscape (van Groningen et al., 2019, Huang et al., 2021). One of the pathways shown to be important in this transition is the NOTCH pathway. Using the γ-secretase inhibitor, a NOTCH pathway inhibitor, the MES transition is prevented (van Groningen et al., 2019). A similar outcome

was observed when rescue cells were treated with doxycycline to induce ASCL1 and also treated with the NOTCH inhibitor. Treating with both agents meant the change to a MES-like morphology was not observed and instead the cells took on a more differentiated phenotype. This is a result of the combination of ASCL1 induction and NOTCH pathway inhibition, as inhibiting the NOTCH pathway alone does not lead to as many neuronal processes.

It is well documented that inducing ASCL1 can result in differentiation of neuroblastoma cells, neuronal progenitor cells and fibroblasts (Wapinski et al., 2013, 2017, Ali et al., 2020). As described, the transition to a MES state protects the cell from stresses (Boeva et al., 2017; van Groningen et al., 2017). The transition in this case could be as a protection from differentiation, so when constant ASCL1 expression is withdrawn, cells are able to revert back to the ADRN state and continue to proliferate. Therefore, if cells are treated simultaneously with doxycycline and the γ-secretase inhibitor, they are blocked from becoming MES-like allowing ASCL1 to begin to induce a more differentiated neuronal phenotype instead.

In summary, reintroducing ASCL1 into ASCL1 KO cells partially rescued the parental phenotype, but there was also some unexpected results following ASCL1 reintroduction. Understanding the change in ASCL1 expression levels in neuroblastoma in normal circumstances is required to fully understand mechanisms behind this.

Chapter 6

Conclusions and Future Work

Neuroblastoma is a tumour of improper development and neuroblastoma cells resemble immature, poorly differentiated neurones (Ratner et al., 2016). Genes and pathways implicated in neuroblastoma are synonymous to those involved in the normal development of sympathetic neurones and represent many different stages of sympathetic nervous system (SNS) development. For example, genes involved in epithelial to mesenchymal transition such as PRRX1, VIM and SNAI2, genes responsible for proliferation and maintenance of the neuronal precursor pool such as MYCN and ASCL1 and genes involved in the differentiation pathway can all be found to be perturbed in neuroblastomas (Anastassiou et al., 2011; Otte et al., 2021; Van Groningen et al., 2017; Wylie et al., 2015). Some of these genes and proteins are maintained at a high level leading to the continued proliferation of cells and formation of neuroblastoma tumours, whereas genes involved in differentiation, and mature neuronal markers are likely to be absent. Therefore, studying proteins involved in the normal differentiation process and understanding how they may have become deregulated can be informative in understanding neuroblastoma initiation and progression and identifying new treatment targets.

For this project, the proneural transcription factor (TF) ASCL1 was chosen as the focus. ASCL1 has a role in SNS development, aiding both the proliferation of the neuronal precursor pool of cells and in initiating neuronal differentiation (Ali et al., 2014; Castro et al., 2011). ASCL1 should be transiently upregulated during development when the precursors are in the highly proliferative state. In this case, ASCL1 promotes growth by transcribing pro-proliferative genes such as E2F1 and Cyclin D1 which are involved in progression of the cell cycle (Castro et al., 2011). The presence of ASCL1 is also required for cells to differentiate, but once this process has begun, ASCL1 should be downregulated in order for cells to fully develop into mature neurones (Wylie et al., 2015; Ichimiya et al., 2001; Kasim et al., 2016).

In many high-risk neuroblastomas, ASCL1 is maintained at a high level (Wylie et al., 2015). The Philpott lab has an abundance of work to understand the role of ASCL1 in both the normal

development process and in neuroblastoma. The post-translational control of ASCL1 has been a large focus, specifically the phospho-regulation of ASCL1 in normal development and more recently how phosphorylation status effects ASCL1 activity in neuroblastoma cells (Ali et al., 2020, 2014; Wylie et al., 2015). Previous work has helped understand how a single transcription factor (TF) can influence and control growth and differentiation, two such contrasting roles. This project was aimed at building on the work already accomplished. The aim was to gain a deeper understanding of the role that ASCL1 plays in neuroblastoma, specifically, what happens when ASCL1 is no longer present in cells.

In chapter 2, the process of removing functional ASCL1 from neuroblastoma cell lines using CRISPR/Cas9 technology was completed. ASCL1 was successfully knocked out of three neuroblastoma cell lines, validated by sequencing and western blot. The neuroblastoma cell lines chosen exhibit different ASCL1 expression levels and different MYC/MYCN statuses. Despite the genetic differences displayed by the cell lines, the removal of ASCL1 resulted in all cells growing at a slower rate. This implies neuroblastoma cells do not require ASCL1 to survive. Instead ASCL1 contributes to the highly proliferative state, as cells lacking ASCL1 display the slower growth phenotype.

In chapter 3, the effect of ASCL1 knockout (KO) on the core regulatory circuitry (CRC) of transcription factors was investigated. Initially it was suspected that the slower growth was a result of lower expression of key TFs in ASCL1 KO cells. Interestingly, when the adrenergic (ADRN) targets and MYC/MYCN were interrogated, it was found that the TFs were still expressed at the same level in ASCL1 KO cells as they were in the parental. This was an intriguing result, ASCL1 is known to have a role in promoting the ADRN network, so it would have been expected that its absence would alter the expression of these factors (Wang et al., 2019). This slower growth phenotype instead was attributed to the suppressed ability of these TFs to bind to the chromatin. As the TFs are still expressed in cells at the same level as in the parental, ASCL1 must be involved in supporting their chromatin binding. Two possible mechanisms were hypothesised for this; ASCL1 could be recruiting TFs to the chromatin, or ASCL1 could be maintaining the chromatin in an accessible state. Wang and colleagues completed ChIP-Seq on ASCL1 and other members of the ADRN CRC and demonstrated that ASCL1 and ADRN TFs bind the chromatin at the same location around key genes (Wang et al., 2019). RIME analysis confirmed ASCL1 was co-binding some of these TFs on the chromatin (Ali et al., unpublished). In other studies, the combination of this evidence, alongside the observation that the knockout lessens chromatin binding has been sufficient evidence to propose ASCL1 is recruiting TFs

to the chromatin (Fueyo et al., 2018; Wapinski et al., 2017). This additional ChIP-Seq and RIME data strengthens the hypothesis that ASCL1 is actively recruiting a selection of TFs to the chromatin.

To further understand why these core TFs are less able to bind chromatin in the absence of ASCL1, their binding partners could be investigated. Co-Immunoprecipitation and Mass Spectrometry could be completed to look at the chromatin-bound and non-chromatin-bound PHOX2B, GATA3 and MYC/MYCN in parental and ASCL1 KO cells to identify what is bound to proteins in each state, aiding understanding of differences between parental and KO. For example, a particular protein that is upregulated by ASCL1 could be associated with MYC on the chromatin in parental cells and have a role in assisting MYC chromatin binding. The loss of protein in this case would mean MYC chromatin binding is suppressed, when ASCL1 is absent. Alternatively, detecting proteins associated with non-chromatin-bound TFs could identify potential proteins that are inhibiting chromatin binding.

Due to the role of ASCL1 as both a transcriptional regulator and pioneer factor, chapter 4 explored genome-wide changes following ASCL1 KO. RNA-Seq and ATAC-Seq data shows that there are significant changes to the transcriptome and chromatin accessibility landscape following ASCL1 KO. Visualising the changes shows that the KO lines are more similar to each other, cluster together and are quite distinct from the parental. The RNA-Seq data shows that following ASCL1 KO, genes are associated with neuronal differentiation are downregulated. This is mirrored in the ATAC-Seq data, the regions which are less accessible following ASCL1 KO are also associated with differentiation processes.

These results suggest ASCL1 is maintaining the cells in a state primed for neuronal differentiation. ADRN cells have a more neuronal, differentiated status and this is key in their neuroblastoma identity. PHOX2B, GATA3 and MYCN are integral TFs in the neuronal differentiation process and also in maintaining the identity of ADRN neuroblastoma cells. One of the roles of ASCL1 in neuroblastoma could be to maintain the neuronal state. If ASCL1 is lost, cells are missing a driver of the neuronal phenotype and so lose their more differentiated ADRN identity. PHOX, GATA and MYC(N) are a key part of this network so may bind to the chromatin less as a result.

The predicted ability of ASCL1 to support the neuronal identity of neuroblastoma cells also explains why cell lines lacking ASCL1 are not as sensitive to differentiation agents. When treated with Palbociclib or Retinoic Acid, ASCL1 KO lines do not show the same level of differentiation as parental when analysing number of neuronal processes and transcription of neuronal targets (Chaytor et al.,

unpublished). The chromatin in ASCL1 KO cells is not as accessible around genes involved in neuronal differentiation. This closed chromatin landscape is less permissive for TF binding, therefore induction and transcription of differentiation associated genes will be suppressed.

In chapter 5, ASCL1 was reintroduced to try and restore the characteristics that were lost following ASCL1 KO. Inducible ASCL1 was successfully reintroduced into KO lines, and an endogenous level of induction achieved. After 24 and 72 hours ASCL1 induction cells began to restore the parental transcriptome, and RNA-Seq analysis showed the upregulation of neuronal differentiation genes which were downregulated following ASCL1 KO. Following continuous ASCL1 induction for 7 days, unexpectedly, the cells displayed an altered morphology and begun to acquire a more MES-like appearance and transcriptional state. It was found that the sustained ASCL1 expression is not typical of neuroblastoma cells and variable levels of ASCL1 are expressed in parental cells. It is known that neuroblastoma cells revert to the MES-like state under stress and/or in order to preserve tumorigenicity. In the ADRN state, the potentially non-physiological pattern of ASCL1 expression could drive cell cycle exit and the differentiation of the tumour cell population. Therefore, the change to a MES state could be to evade differentiation. Cells then return to the tumorigenic ADRN state when continual ASCL1 removed. When ASCL1 is induced and the MES transition is blocked using a NOTCH pathway inhibitor, cells begin to differentiate, supporting this theory.

Following the observation that ASCL1 is not expressed at the same levels in parental lines, it would be interesting to tag ASCL1 to investigate the fluctuations in neuroblastoma cells over time. In addition to this, this system could be utilised to investigate levels of endogenous ASCL1 in the differentiation process. If neuroblastoma cells are treated with a differentiation agent such as Retinoic Acid or Palbociclib the level of ASCL1 protein could be monitored from the initiation of differentiation to terminal differentiation. The point at which ASCL1 activity and expression is diminished could also be determined.

The ASCL1 KO lines could be utilised as a ‘blank-canvas’ to investigate ASCL1 activity. The work on the rescue cells described in chapter 5 was completed using endogenous levels of the wildtype (WT) form of ASCL1. Previous Philpott lab work using the WT and phospho-mutant (S-A) protein has used overexpression systems where ASCL1 is expressed at a much higher than typical level in neuroblastoma lines. In this system there may still be presence of endogenous ASCL1 protein. Using the overexpression method, it has been shown that in SH-SY5Y cells, S-A ASCL1 is more efficient at binding to and upregulating differentiation targets than WT ASCL1 when expressed at the same high

level (Ali et al., 2020). It would be interesting to reintroduce the S-A form of ASCL1 into the KO lines to determine the effect on differentiation. Firstly, the ability to reintroduce the S-A protein into a cell where ASCL1 has been removed would identify the role of the phospho-mutant protein with no interference from endogenous ASCL1. In addition to this, the ability to induce endogenous levels of S-A ASCL1 and fine tune expression could be informative in terms of the role of ASCL1 in initiating differentiation and the levels which are required to instigate the process. Using this system, it could also be determined at what stage the expression of ASCL1 needs to be downregulated in order for stable differentiation to occur.

It is known that ASCL1 is only transiently upregulated in normal development and downregulated as cells begin to differentiate. It is also understood that the maintenance of ASCL1 at a high level leads to the initiation and progression of neuroblastoma. This project has given a greater insight into the role of ASCL1 in neuroblastoma. It seems that, similarly to its role in the development of the sympathetic nervous system, ASCL1 has a multifunctional role in neuroblastoma. During neuroblastoma tumorigenesis it appears ASCL1 works alongside other pro-growth factors to promote proliferation and removing ASCL1 will result in cells growing at a slower rate. This is in line with previous publications (Wang et al., 2019). If neuroblastoma tumours are treated with differentiation agents, ASCL1 alters its function to promote cell cycle exit and differentiation and the expression of ASCL1 will be suppressed as cells begin to differentiate. This project has shown that removing ASCL1 from neuroblastoma cells results in the cells losing a transcriptome and chromatin landscape primed for differentiation and consequently, cells do not respond as efficiently to differentiation agents (Summarised in Figure 6.1).

ASCL1 has an established pro-growth function in neuroblastoma. Removing ASCL1 slows down proliferation but also results in cells taking on a less differentiated state. Therefore, targeting ASCL1 by simply removing it from neuroblastoma tumour cells may not be therapeutically beneficial. If cells are still proliferating, albeit at a slower rate following the removal of ASCL1, there is still the opportunity for cells to acquire other mutations, overcome barriers to growth and return to higher proliferative, more tumorigenic state. It may be more important to instead modulate ASCL1 activity to cause cell cycle exit, slow down cellular proliferation and induce differentiation in neuroblastoma.

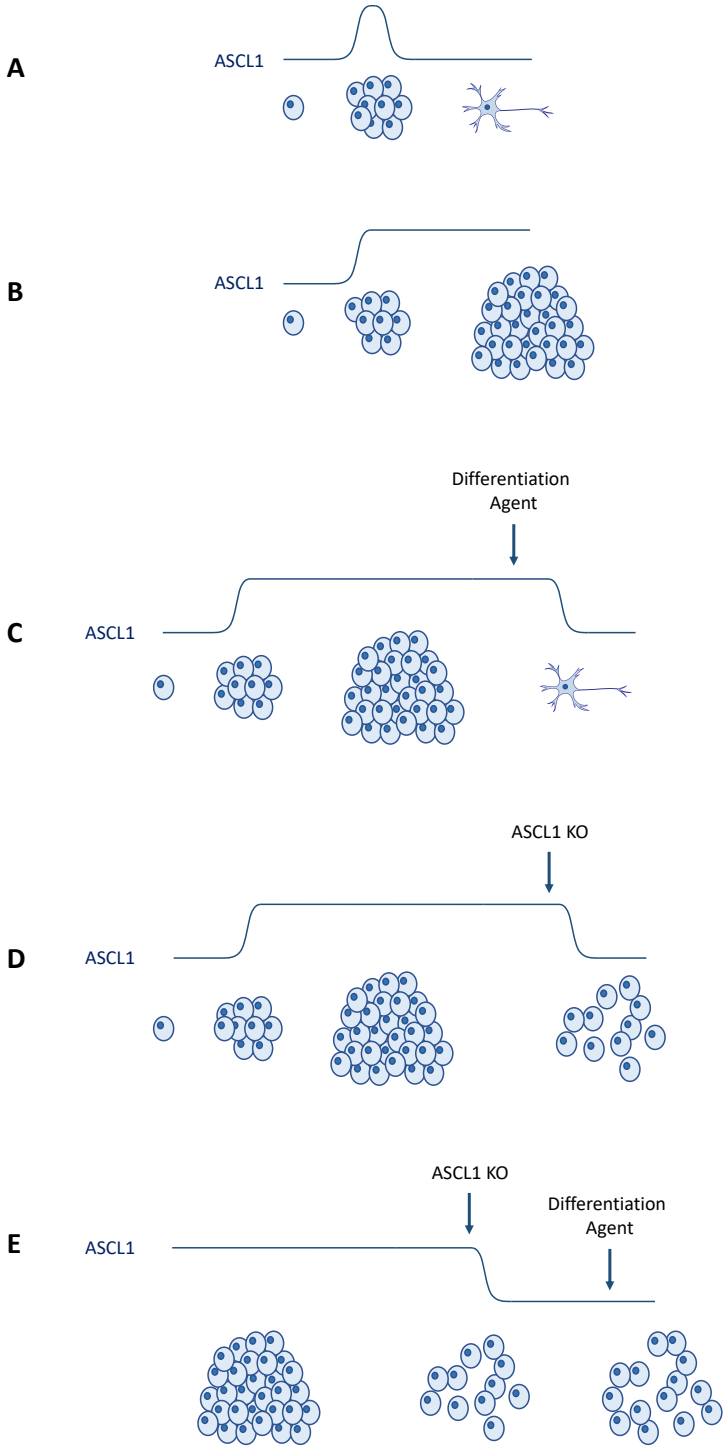

Figure 6.1: ASCL1 Levels in Development and Neuroblastoma. Building on the current proposed model for the role of ASCL1 in neuroblastoma. During normal development ASCL1 is transiently upregulated and then downregulated when cells differentiate (A), ASCL1 is maintained at a high level in neuroblastomas (B). Following treatment with a differentiation agent such as Palbociclib or Retinoic Acid, neuroblastoma cells will differentiate (C). Removing ASC1 from neuroblastoma cells makes them grow at a slower rate (D). Removing ASCL1 results in a less primed state for differentiation and renders the cells insensitive to differentiation agents (E) (Wylie et al., 2015, Chaytor et al., unpublished).

Chapter 7

Materials and Methods

7.1 Materials

7.1.1 Solutions and Buffers

Cell Culture	
Cell Growth Medium	Used to culture neuroblastoma cells. DMEM-F12 (Gibco) supplemented with 10% FBS (Sigma) and 1% Pen/Strep
Tet-Free Cell Growth Medium	Used to culture inducible cell lines. DMEM-F12 supplemented with 10% Tet-System-Approved FBS (Takara) and 1% Pen/Strep
Retinoic Acid Treatment Medium	Reduced serum medium. DMEM-F12 (Gibco) supplemented with 2.5% FBS (Sigma) and 1% Pen/Strep
Pen/Strep	Antibiotic. 10,000 units/mL of penicillin and 10,000 µg/mL of streptomycin (Gibco)
Freezing Media	FBS with the addition of 10% DMSO (Fisher Scientific)
Trypsin/EDTA	0.25% Trypsin EDTA (Sigma)
Doxycycline	Used to stimulate target gene expression in inducible lines
Retinoic Acid	Differentiation agent
Transfetion Reagents	
Opti-MEM	Reduced serum medium used for transfection (Gibco)
Lipofectamine 2000	Transfection reagent (Thermo Fisher)
Viral Infection	
Polybrene	Increase transduction efficiency
G418	Antibiotic for resistance screening. G418 Solution (Roche)
Puromycin	Antibiotic for resistance screening. EZSolution™ Puromycin Dihydrochloride, Sterile-Filtered (Source Bioscience)
CRISPR Screening	
Extracting gDNA from cells	Genomic DNA Purification Kit (Monarch)
Extracting DNA from gels	DNA Gel Extraction Kit (Monarch)
Q5 Polymerase	Used for the first PCR reaction. Q5 High-Fidelity DNA Polymerase (NEB)
pJet plasmid ligation	CloneJET PCR Cloning Kit (ThermoFisher)
SOC Medium	Bacterial culture medium. Prepared by Hutchison/MRC Media Unit
Ampicillin Plates	Bacterial growth plates used for selection of bacteria that express the Ampicillin resistance gene. Prepared by Hutchison/MRC Media Unit
LB Broth	Nutrient rich medium for bacterial growth. Prepared by Hutchison/MRC Media Unit
Isolating Plasmid DNA	MiniPrep Protocol (Qiagen)
Verifiation of DNA insertion into pJet	Bgl2 restriction enzyme (NEB) and NEB Buffer 2 (NEB)
FACS Analysis	
Propidium Iodide	1 mg/ml Propidium Iodide Solution in water (Sigma)

RNAse A	Prepared to 10mg/ml in 10 mM Tris-HCl (pH 7.5), heated to 95 °C, cooled to RT and stored at -20 °C (Sigma)
PI staining solution	0.2 ml PI, 0.2 ml RNase A, 0.1 ml 10% Triton-X in 9.5 ml PBS
RNA Analysis	
RNA Extraction Kit	RNeasy Mini Kit (Qiagen)
cDNA Preparation Kit	QuantiTect Reverse Transcription Kit (Qiagen)
SYBR Green	Power Up SYBR Green Master Mix (Applied Biosystems)
Protein Analysis	
RIPA Buffer	150 mM NaCl, 1.0% IGEPAL CA-630, 0.5% sodium deoxycholate, 0.1% SDS, 50 mM Tris, pH 8.0 (Sigma)
Protease Inhibitor Cocktail	cOmplete Mini EDTA-free Protease Inhibitor Cocktail (Roche)
BCA Assay	Pierce™ BCA Protein Assay Kit (Thermo Fisher)
Sample Buffer	NuPAGE LDS Sample Buffer (4X)
Western Blot Running Gels	NuPAGE™ 10%, Bis-Tris Mini Protein Gel, 10-well (InvitrogenTM) Criterion™ 4-20% TGX™ Precast Midi Protein Gel, 18 well (Bio-Rad)
Running Buffer	MOPS – NuPAGE™ MOPS SDS Running Buffer (Thermo Fisher) TrisGlycine – Tris/Glycine Running Buffer (Bio-Rad)
Protein Ladder	Precision Plus Protein™ Dual Color Standards (Bio-Rad)
Transfer Buffer	192 mM Glycine, 25 mM Tris, 20% MeOH
Nitrocellulose Membrane	Nitrocellulose membrane with 0.45 µm pore size (Bio-Rad)
Ponceau Stain	Check transfer efficiency. Ponceau S solution (Sigma)
TBST	Wash Buffer. TBS + 0.01% Tween-20. TBS (150 mM NaCl, 50 mM Tris-HCl (pH 7.6)) prepared by the Media Unit at the Hutchison/MRC Research Centre.
Blocking Solution	5% Skimmed Milk Powder (SLS) in TBST
Detection Reagent	Amersham ECL Prime Western Blotting Detection Reagent (GE Healthcare Life Sciences)
Fractionation Kit	Subcellular Protein Fractionation Kit for Cultured Cells (Thermo Fisher)
IP Buffer	50 mM Tris (pH 7.5), 150 mM NaCl, 0.5% NP40, 50 mM NaF. 1 mM DTT, 1 mM Na_3VO_{3x}, 1 mM PMSF, 1X PI added immediately before use.
Protein G Dynabeads	Thermo Fisher
Immunoflourescence	
4% PFA	4% Paraformaldehyde in PBS (Alfa Aesar)
PBS-T	PBS with 0.2% Tween-20
PBS-FBS (10%)	PBS with 10% FBS (Sigma)
PBS-FBS-T (2%)	PBS with 2% FBS and 0.2% Tween-20
DAPI	DAPI DNA staining solution (abcam)
ATAC	
TDE1	Nextera Tn5 Transposase (Illumina)
TD Reaction Buffer	Tagment DNA Buffer (Illumina)
Resuspension Mixture (per reaction)	50 µl RSB containing 0.1% NP-40, 0.1% Tween-20 and 0.01% digotinin
RSB-T	RSB with the addition of 0.1% Tween 20
Transposition Mixture (per reaction)	16.5 µL PBS, 25 µL 2X TD reaction buffer, 2.5 µL TDE1, 0.5 µL digitonine (1%), 0.5 µL Tween-20 (10%), 5 µL nuclease-free H2O
DNA Elution Kit	DNA Clean & Concentrator™-5 w/ Zymo-Spin™ IC Columns
NEBNext® High-Fidelity 2X PCR Master Mix	PCR Mastermix (NEB)
Evagreen	DNA binding dye for qPCR (Biotium)

AMPure XP Beads	ATAC size selection (Beckman Coulter)
Other	
PBS	137 mM NaCl, 2.7 mM KCl, 10 mM Na_2HPO_4, 1.8 mM KH_2PO_4 (Prepared by the Media Kitchen at the Hutchison/MRC research centre and Jeffrey Cheah Biomedical Centre)
Methanol	Fisher Scientific LTD
Ethanol	Sigma Aldrich
β-Mercaptoethanol	Therno Fisher
Tween-20	Sigma Aldrich
Agarose	Sigma Aldrich

Table 7.1: Solutions and Buffers.

7.1.2 Antibodies

7.1.2.1 Western Blot Primary Antibodies

Antibody	Source	Species	Dilution
ASCL1	abcam	Rabbit (mAb)	1:1000
α–Tubulin	abcam	Mouse	1:5000
C-MYC	abcam	Rabbit	1:10,000
GAPDH	PROTEINTECH	Mouse	1:5000
GATA3	CST	Rabbit	1:1000
H3	abcam	Rabbit	1:30,000
H3K27ac	abcam	Rabbit	1:10,000
LaminB	abcam	Rabbit	1:500
MYCN	Santa Cruz	Mouse	1:250
PHOX2A	Santa Cruz	Mouse	1:250
PHOX2B	Santa Cruz	Mouse	1:250

Table 7.2: Western Blot Primary Antibodies

7.1.2.2 Western Blot Secondary Antibodies

	Species	Source
Mouse	Sheep	GE Healthcare
Rabbit	Donkey	GE Healthcare

Table 7.3: Western Blot Secondary Antibodies

7.1.3 Primers

7.1.3.1 CRISPR Sequencing Primers

These primers were designed to amplify the region around the CRISPR target site. Figure 7.1 shows the location of the sgRNA and both sets of sequencing primers.

Primer Name	Forward	Reverse	Length of Amplicon
CRISPR 1	CCCGCAGCCTGTTTCTTTG	TTGACCAACTTGACGCGGTT	328 bp
CRISPR 2	AGCCTGTTTCTTTGCCACG	CTCATCTTCTTGTTGGCCGC	382 bp

Table 7.4: CRISPR Sequencing Primers

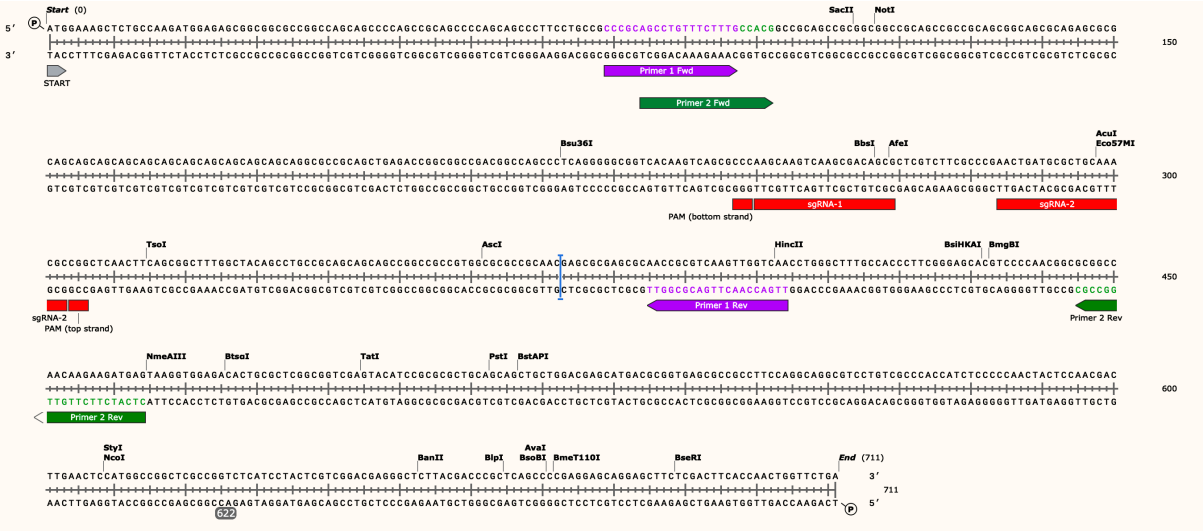

Figure 7.1: Location of the sgRNA and CRISPR Sequencing Primer Target Sites. The location of the sgRNA target site is shown in red. Two sets of primers were used for the sequencing assay, they are shown in purple and green.

7.1.3.2 RT-qPCR Primers

Gene	Forward	Reverse
GATA3	CCAGCACAGAAGGCAGGGAGT	CTGTCCGTTCATTTTGTGATAGAGCC
MYC	CTGGTGCTCCATGAGGAGA	CCTGCCTCTTTTCCACAGAA
MYCN	GAGAGGACACCCTGAGCGATT	TGGGACGCACAGTGATGGTGAAT
NTRK1	TTGCCTGCCTCTTCCTTTCTAC	ATTGTGGGTTCTCGATGATGTG
PHOX2A	GGCTCCTCCAACTGCGCACTT	AAACGCGCTCCAGCTCCTTGAG
PHOX2B	TTCACCAGTGCCCAGCTCAAAGA	TTGCCCGAGGAGCCGTTCTTG
TBP	GAGCTGTGATGTGAAGTTTCC	TCTGGGTTTGATCATTCTGTAG

Table 7.5: RT-qPCR Primer Sequences.

7.1.3.3 ATAC i7 Primers

Primer	Sequence	Index
Ad2.1	CAAGCAGAAGACGGCATACGAGATTCGCCTTAGTCTCGTGGGCTCGGAGATGT	TAAGGCGA
Ad2.2	CAAGCAGAAGACGGCATACGAGATCTAGTACGGTCTCGTGGGCTCGGAGATGT	CGTACTAG
Ad2.3	CAAGCAGAAGACGGCATACGAGATTTCTGCCTGTCTCGTGGGCTCGGAGATGT	AGGCAGAA
Ad2.4	CAAGCAGAAGACGGCATACGAGATGCTCAGGAGTCTCGTGGGCTCGGAGATGT	TCCTGAGC
Ad2.5	CAAGCAGAAGACGGCATACGAGATAGGAGTCCGTCTCGTGGGCTCGGAGATGT	GGACTCCT
Ad2.6	CAAGCAGAAGACGGCATACGAGATCATGCCTAGTCTCGTGGGCTCGGAGATGT	TAGGCATG
Ad2.7	CAAGCAGAAGACGGCATACGAGATGTAGAGAGGTCTCGTGGGCTCGGAGATGT	CTCTCTAC
Ad2.8	CAAGCAGAAGACGGCATACGAGATCCTCTCTGGTCTCGTGGGCTCGGAGATGT	CAGAGAGG
Ad2.9	CAAGCAGAAGACGGCATACGAGATAGCGTAGCGTCTCGTGGGCTCGGAGATGT	GCTACGCT
Ad2.10	CAAGCAGAAGACGGCATACGAGATCAGCCTCGGTCTCGTGGGCTCGGAGATGT	CGAGGCTG
Ad2.11	CAAGCAGAAGACGGCATACGAGATTGCCTCTTGTCTCGTGGGCTCGGAGATGT	AAGAGGCA
Ad2.12	CAAGCAGAAGACGGCATACGAGATTCCTCTACGTCTCGTGGGCTCGGAGATGT	GTAGAGGA
Ad2.13	CAAGCAGAAGACGGCATACGAGATATCACGACGTCTCGTGGGCTCGGAGATGT	GTCGTGAT
Ad2.14	CAAGCAGAAGACGGCATACGAGATACAGTGGTGTCTCGTGGGCTCGGAGATGT	ACCACTGT
Ad2.15	CAAGCAGAAGACGGCATACGAGATCAGATCCAGTCTCGTGGGCTCGGAGATGT	TGGATCTG
Ad2.16	CAAGCAGAAGACGGCATACGAGATACAAACGGGTCTCGTGGGCTCGGAGATGT	CCGTTTGT
Ad2.17	CAAGCAGAAGACGGCATACGAGATACCCAGCAGTCTCGTGGGCTCGGAGATGT	TGCTGGGT
Ad2.18	CAAGCAGAAGACGGCATACGAGATAACCCCTCGTCTCGTGGGCTCGGAGATGT	GAGGGGTT
Ad2.19	CAAGCAGAAGACGGCATACGAGATCCCAACCTGTCTCGTGGGCTCGGAGATGT	AGGTTGGG
Ad2.20	CAAGCAGAAGACGGCATACGAGATCACCACACGTCTCGTGGGCTCGGAGATGT	GTGTGGTG
Ad2.21	CAAGCAGAAGACGGCATACGAGATGAAACCCAGTCTCGTGGGCTCGGAGATGT	TGGGTTTC
Ad2.22	CAAGCAGAAGACGGCATACGAGATTGTGACCAGTCTCGTGGGCTCGGAGATGT	TGGTCACA
Ad2.23	CAAGCAGAAGACGGCATACGAGATAGGGTCAAGTCTCGTGGGCTCGGAGATGT	TTGACCCT
Ad2.24	CAAGCAGAAGACGGCATACGAGATAGGAGTGGGTCTCGTGGGCTCGGAGATGT	CCACTCCT

Table 7.6: ATAC i7 Primer Sequences

7.1.3.4 ATAC i5 Primers

Primer	Sequence	Index
i5.3	AATGATACGGCGACCACCGAGATCTACACTATCCTCTTCGTCGGCAGCGTCAGATGTGTAT	TATCCTCT
i5.4	AATGATACGGCGACCACCGAGATCTACACAGAGTAGATCGTCGGCAGCGTCAGATGTGTAT	AGAGTAGA

Table 7.7: ATAC i5 Primer Sequences

7.2 Methods

7.2.1 Cell Culture

7.2.1.1 Maintaining Cells

Neuroblastoma cell lines were maintained at 37 °C with 5% CO2. Cells were grown until they reached 80–90% confluency. At this point medium was removed and cells were washed twice with PBS. Cells were detached from the surface by adding an appropriate volume of trypsin and incubating at 37 °C for 5 minutes. The trypsin reaction was quenched using cell growth medium and cells were split into a new flask to continue growing. Aliquots of cells at this stage were also taken for plating, cell growth analysis or protein analysis.

7.2.1.2 Freezing and Thawing Cells

Prior to freezing, cells were trypsinised and resuspended in culture medium (as above). Following this, cells were centrifuged (500 xg, 5 minutes) to pellet them. The medium was removed and cells were resuspended in an appropriate volume of freezing medium. Cells were cooled to −80 °C at a rate of 1 °C per minute using a Biocision CoolCell. Once cells were frozen, they were transferred to LN2 for long-term storage.

When cells were required, they were thawed in a 37 °C water bath and added to 5 ml of culture medium. Cells were pelleted by centrifuging (500 xg, 5 minutes) and the supernatant was removed. Cells were resuspended in culture medium and placed at 37 °C with 5% CO2 to grow. After 24 hours the medium was changed.

7.2.1.3 Counting Cells

Cell number was determined by diluting cells 1:1 in Trypan Blue cell stain and counted using a Cell Countess II Automated Cell Counter (Thermo Fisher).

7.2.1.4 Incucyte Confluency Analysis

Cell confluency was analysed using the Incucyte Zoom 2016B. Cells were plated in a 24-well plate at $1.5x10^5$ cells/well and allowed to settle overnight. During Incucyte analysis, cells were maintained at 37 °C with 5% CO2. A confluence mask was prepared for each cell line to be analysed. The Incucyte imaged at set time-points (usually 2 hours) and the pre-prepared confluence mask estimated the confluence of a well at a particular time-point.

7.2.1.5 Doxycycline Treatment

Doxycycline was prepared at 10 mg/ml in DMSO and aliquots stored at −20 °C. On the day of treatment, the required concentration of Doxycycline was added to Tet-Free Medium. The culture medium was removed from the cells and replaced with treatment medium. Fresh treatment medium was prepared and the cell culture refreshed every 2 days.

7.2.1.6 Retinoic Acid Treatment

Cells were plated in a 6-well plate at $1.5x10^5$ cells/well and left overnight to settle. Cells were cultured in RA treatment medium, with the addition of RA at a concentration of 10 µM for SK-N-BE(2)c and IMR32 cells and 20 µM for SH-SY5Y cells. The RA containing medium was changed every 2–3 days. Untreated cells were also cultured in RA treatment medium to ensure that the reduced serum alone was not having an effect on the cells.

7.2.2 CRISPR

7.2.2.1 CRISPR Transfection

CRISPR Cas9 and sgRNA plasmids were kindly gifted by Raul Bressan (Steve Pollard's Lab, Edinburgh). The Cas9 plasmid also contained a GFP marker. Two sgRNA plasmids were provided that targeted the ASCL1 gene in different locations.

sgRNA 1: CGCTGTCGCTTGACTTGCTTggg
sgRNA 2: AACTGATGCGCTGCAAACGCcgg

24 hours before transfection, cells were plated in a 24-well plate at densities of $3 x10^4$, $5x10^4$, $7x10^4$ and $1x10^5$ cells per well. On the day of transfection, wells at 70% confluency were picked for treatment.

For transfection the Lipofectamine 2000 protocol was followed. For each lipofection reaction 2 µg Lipofectamine 2000 was added to 50 µl OptiMEM medium. A second tube was prepared for the plasmids; 1 µg Cas9 plasmid and 1 µg sgRNA plasmid were added to 50 µl OptiMEM medium. The two solutions were left to incubate at room temperature. After 5 minutes the two solutions were combined and mixed by pipetting. This mixture was left at room temperature for 20 minutes. During the 20-minute incubation, the medium from each well to be treated was removed and replaced with 250 µl fresh medium. 100 µl of the Lipofectamine + Plasmid + OptiMEM mixture was then added

dropwise to each well. The 24-well plate was incubated for 6 hours at 37 °C and then 150 µl medium was added to each well.

7.2.2.2 FACS Sorting and Expansion

The cells were checked for GFP expression 24 hours after Lipofectamine treatment. If the cells were positive for GFP, they were FACS sorted, one cell per well into a 96-well plate containing 100 µl pre-warmed medium. Cells were left to grow at 37 °C for 4 weeks. After this time the plates were checked for colonies. Cells were grown and expanded in a T-25 flask until they were confluent. At this stage cells were taken for sequencing analysis and harvested for protein extraction and western blot analysis.

7.2.2.3 CRISPR Sequencing Assay

gDNA was extracted from cells using the Monarch Genomic DNA Purification Kit. Briefly, cells were trypsinised and centrifuged to pellet (500 xg, 5 minutes). Cells were resuspended in 100 µl ice-cold PBS. To the resuspended cells 1 µl proteinase K and 3 µl RNase A were added and the solution was vortexed. 100 µl gDNA cell lysis buffer was then added and the samples vortexed and heated to 56 °C for 5 minutes. During this time, samples were vortexed every minute.

Next, 400 µl gDNA binding buffer was added and the sample was pulse-vortexed for 10 seconds. The whole sample was then added to the gDNA purification column and centrifuged (1,000 xg, 3 minutes) and then immediately centrifuged again at a higher speed (12,000 xg, 1 minute). Each sample was washed twice by adding 500 µl gDNA wash buffer and centrifuged (12,000 xg, 1 minute). The gDNA was eluted into a clean Eppendorf by adding 100 µl pre-warmed gDNA elution buffer. gDNA was quantified using a Nanodrop (Thermo Fisher). A PCR reaction was then completed to amplify regions around the CRISPR target location. The PCR set-up and reaction conditions were as follows:

PCR Set-up

Reagent Amount Per Reaction	(µl)
Q5 2X Mastermix	12.5
Forward Primer (10 µM)	1.25
Reverse Primer (10 µM)	1.25
ddH2O	3
gDNA	7

Table 7.8: CRISPR PCR Setup

PCR Conditions

Temperature	Time
98 °C	30 Seconds
98 °C	10 Seconds
66 °C	20 Seconds
72 °C	20 Seconds
72 °C	10 Seconds
4 °C	∞

Table 7.9: CRISPR PCR Conditions

To verify that the PCR had worked, PCR products were run on a 1% agarose gel for 1 hour at 120 V. If the presence of a band could be visualised under UV light, the band was carefully cut out using a scalpel and DNA extracted using the Monarch DNA Gel Extraction Kit protocol. Briefly, the gel slice was weighed and 4X the weight of Gel Dissolving Buffer was added. The buffer and gel were incubated at 55 °C for 5 minutes, with frequent vortexing, to dissolve the gel in the buffer. Once dissolved, the sample was added to a spin column and centrifuged (16,000 xg, 1 minute). The sample was then washed twice by adding 200 µl wash buffer and centrifuging (16,000 xg, 1 minute). The column was then placed into a fresh tube and sample eluted by adding 10 µl elution buffer, incubating for 1 minute and then centrifuging (16,000 xg, 1 minute). The sample was then sent for Sanger sequencing. If the results showed two overlapping sequence-traces, then two alleles were present.

If two sequence-traces were observed, the purified PCR product was ligated into the pJet plasmid, following the CloneJET PCR Cloning Kit protocol. For the ligation reaction, all components were added, vortexed and incubated at room temperature for 5 minutes. The blunt-end cloning protocol was used because the Q5 polymerase used in the initial PCR reaction produces a blunt-ended product.

Following the ligation, the plasmid was used to transform competent E. coli. 2 µl pJet plasmid was added to 50 µl competent cells and left on ice for 30 minutes. The reaction was heat-shocked at 42 °C for 45 seconds and then placed on ice for 2 minutes. 450 µl SOC medium was then added and the bacteria were left to recover at 37 °C for no longer than 60 minutes. The transformation reaction was then transferred to Ampicillin plates. 80 µl was plated on one plate and the remaining reaction on to a second plate. The plates were then transferred to 37 °C to allow colonies to grow overnight. The next day 5 single colonies were picked from each plate and grown overnight in 6 ml LB broth. The following day plasmid DNA was isolated following the QIAgen Miniprep protocol. The product of the Miniprep protocol was then verified for the insertion of the PCR product into the pJet vector by

digesting with the restriction enzyme BglII. 500 ng of the Miniprep product was used for the verification step and the reaction set up as follows:

Reagent	Volume Added (µl)
500 ng Miniprep Product	7
NEB Buffer 2	2.5
Water	15
Bgl2	1.5

The reaction was incubated at 37 °C for 30 minutes and then run on a 2% agarose gel to verify the presence of the plasmid and the insertion. If the product was present, 10 µl of the pJet plasmid at 100 ng/µl was prepared for sequencing analysis. The sequence was then aligned to the human ASCL1 sequence to observe if CRISPR gene-editing had been successful.

In addition to the sequencing assay, CRISPR cell samples were taken to prepare protein and run on western blots to detect ASCL1. Cells were also harvested to immunoprecipitate (IP) ASCL1; IP achieves a higher sensitivity by enriching for ASCL1 to ensure its detection.

7.2.3 Producing ASCL1 Inducible Cell Lines

7.2.3.1 Lentivirus Infection

To prepare the inducible cell lines, cells were infected with two viruses, one containing the tetracycline controlled transactivator (TCT) and the second containing the ASCL1 gene under the control of the tetracycline response element (TRE) promoter, which contains a sequence that is recognised by the TCT. The TCT is constitutively produced but has no effect until cells are treated with doxycycline. Doxycycline binds the TCT, causing a conformational change enabling the TCT to bind the TRE promoter and transcribe ASCL1.

24 hours before infection, cells were plated at $5x10^5$ cells/well in a 24-well plate. On the day of infection, virus infection medium containing polybrene was prepared. Because endogenous levels of ASCL1 are required, cells were treated with a MOI of 0.3 to try and ensure that no more than one copy of the virus infects each cell.

Viral particle (µ) = (Number of cells x Number of wells x MOI)/viral titer

For each well to be treated, 300 µl of virus infection medium, including the virus, was prepared. The culture medium was removed and replaced with 300 µl of the virus infection medium. After 6 hours the medium was topped up to 500 µl. The following day the virus-containing medium was removed and the cells were washed three times with Tet-Free Medium. The cells were then left for 2 days to allow the production of antibiotic resistance genes.

7.2.3.2 Lentivirus Selection

The cells were infected with two viruses with two different resistance genes, so two rounds of selection were completed using G418 and Puromycin. Before selection, cells were washed twice with Tet-Free Medium. Cells were treated with 0.5 µg/ml G418 medium. Control (uninfected) cells all died after 4 days of treatment, so infected cells were selected with G418 for 6 days. Following G418 selection, cells were left for 2 days to recover from the first round of selection. Cells were then treated with 1 µg/ml Puromycin. Control cells all died after 5 days, so infected cells were selected with Puromycin for 1 week.

To select the cell lines and Doxycycline concentration to proceed with, cells were treated with a Doxycycline concentration titration. Western blots and qPCR were completed using the parental cell line as a control for the endogenous levels of ASCL1 required.

7.2.4 Protein Analysis

7.2.4.1 Harvesting Cells and Preparing Protein for Western Blot

Plated cells were harvested by scraping them into 1 ml ice-cold PBS. Cells were pelleted (500 xg, 5 minutes, 4 °C) and the supernatant removed. Cell pellets were washed twice by resuspending in PBS and centrifuging (500 xg, 5 minutes, 4 °C). The supernatant was removed and cell pellets were frozen on dry ice and stored at −80 °C until needed.

To prepare protein, cell pellets were resuspended in 40 µl RIPA buffer supplemented with protease inhibitor cocktail (PIC) and incubated on ice for 20 minutes. Samples were centrifuged (16,000 xg, 10 minutes, 4 °C) and the supernatant transferred to a fresh tube and stored at −80 °C.

Protein was quantified using the BCA assay. BSA standards were prepared at concentrations of 0, 1, 2, 5, 10 and 15 mg/ml. Protein samples to be tested were made with 4 µl protein diluted in 26 µl water. To each standard and sample, 250 µl BCA reagent (BCA Reagents A + B prepared in a 50:1 ratio) was added and samples were incubated at 37 °C for 30 minutes. Protein concentration was

determined using a Nanodrop. Protein samples were prepared by diluting in water and adding LDS sample buffer (to a final concentration of 1X) and β-mercaptoethanol (to a final concentration of 2.5%). Samples were then heated at 70 °C for 10 minutes.

7.2.4.2 Western Blot Protocol

Protein samples were run on Invitrogen or BioRad PAGE gels alongside dual colour protein ladder (Bio-Rad). Protein samples were run at 150 volts until separated or until the dye had reached the bottom of the gel.

Protein was transferred onto a nitrocellulose membrane using a Bio-Rad Criterion Blotter set, using the wet transfer western blotting method. Transfer was completed at 4 °C and run for 1 hour at 100 volts. Transfer efficiency was checked using the Ponceau stain. Membranes were rinsed in TBS-T and then blocked for at least 1 hour in blocking solution. Membranes were washed in TBS-T before being incubated with primary antibody (diluted in 1% blocking solution) overnight at 4 °C. Following primary antibody incubation, membranes were washed three times in TBS-T. Secondary antibody incubation took place for 1 hour at room temperature, followed by three washes in TBS-T. Visualisation took place by incubating membranes in ECL western blotting detection reagent or West Pico PLUS Chemiluminescent Substrate for 5 minutes before being exposed to X-ray film (Scientific Laboratory Supplies).

7.2.4.3 Immunoprecipitation

For each IP, 1 x 10 cm plate was required. Cells were harvested by scraping (as described in section 7.2.4.1). Cell pellets were resuspended in 500 µl IP buffer and rotated for 2 hours at 4 °C. Following this the solutions were sonicated (high setting, cycles of 30 seconds on, 30 seconds off) for 15 minutes. The protein concentration of the lysate was calculated using the BCA assay and quantification completed on a Nanodrop.

Samples were normalised and prepared to a final volume of 500 µl in IP buffer. Antibody was added and samples rotated overnight at 4 °C. Antibody–protein conjugates were captured using Protein G Dynabeads. Before adding the beads, they were placed on a magnetic stand to enable the storage solution to be aspirated. The beads were washed three times and resuspended in IP buffer at a 1:1 ratio. The conjugates were captured by adding 30 µl Protein G beads and rotated for 3 hours at 4 °C, then the bead–antibody–protein complex was washed five times in IP buffer. The antibody–protein conjugate was released from the beads by using 40 µl 2X LDS sample buffer with the addition of

0.5 µl β-mercaptoethanol, vortexed and heated at 70 °C for 10 minutes. The samples were then placed on a magnetic stand to enable the supernatant to be taken for western blot analysis (as described in section 7.2.4.2).

7.2.5 RNA Analysis

RNA was harvested following the Qiagen RNeasy Mini Kit Part 1 protocol. Briefly, cells for RNA analysis were cultured in a 6-well plate and lysed using 350 µl RLT buffer with the addition of 10 µl β-mercaptoethanol.

350 µl 70% ethanol was added to the RLT and samples pipetted up and down to mix. Samples were transferred to a spin column and centrifuged (8000 xg, 30 seconds). Following this 700 µl RW1 buffer was added to the spin column, which was then centrifuged (8000 xg, 30 seconds). Two wash steps were then completed with 500 µl RPE buffer and samples centrifuged at 8000 xg for 30 seconds (wash 1) and then 2 minutes (wash 2). RNA was eluted in 40 µl RNase-free water by centrifuging (8000 xg, 1 minute). RNA was quantified using a Nanodrop and stored at −80 °C.

cDNA was prepared using the QuantiTect Reverse Transcription Kit (Qiagen). RNA was diluted to a concentration of at least 600 ng diluted in a final volume of 12 µl. 2 µl gDNA wipeout was added to diluted RNA and samples were incubated at 42 °C for 2 minutes. 6 µl RT mastermix (1 µl RT enzyme, 1 µl RT primers, 4 µl RT buffer) was added and the mixture incubated at 42 °C for 15 minutes. The enzyme was inactivated by heating the mixture at 95 °C for 3 minutes. cDNA was then diluted 1:5 with RNase-free water and stored at −20 °C. Gene expression was analysed by RT-qPCR using an Agilent StepOnePlus instrument and software. Each qPCR reaction was set up in a total volume of 10 µl (as below). Gene expression was analysed using the StepOnePlus software and calculated using the $\Delta\Delta C_T$ method.

Reagent	Amount Per Reaction (µl)
2X SYBR Power Up MasterMix	5
Forward Primer (10 µM)	0.25
Reverse Primer (10 µM)	0.25
ddH_2O	2.5
cDNA	2

Table 7.10: RT-qPCR Setup

Temperature (°C)	Time (Seconds)	
95	20	
95	3	40 Cycles
60	30	
25	∞	

Table 7.11: RT-qPCR Conditions

7.2.5.1 RNA Preparation for RNA-Seq

To prepare RNA for RNA-Seq, the DNase step from the RNeasy Part 2 protocol was included. The DNase treatment was completed following the first centrifugation step. Briefly; the DNase stock solution was first prepared by adding 550 ml water to the DNase I. For each RNA sample, 10 µl DNase stock solution was added to 70 µl RDD buffer.

To perform the DNase step, 350 µl RW1 buffer was added to the column and centrifuged (8,000 xg, 30 seconds). The 80 µl DNase dilution was added to the column and incubated at room temperature for 15 minutes. 350 µl RW1 was then added to the column and centrifuged (8,000 xg, 30 seconds). The RNA extraction protocol was then followed.

7.2.6 Immunofluorescence (IF)

For each IF, cells were plated in 24-well plates at 1x105 cells/well. Cells were left until they reached 50% confluency. To fix the cells, half of the growth medium was removed and replaced with 4% PFA to produce a final concentration of 2% PFA in cell growth medium, and cells were left for 5 minutes at 37 °C. All the medium was then removed and 300 µl 4% PFA was added and cells were fixed for 10 minutes at room temperature. Fixed cells were washed twice in 500 µl PBS.

Cells were permeabilised by adding 300 µl PBS-T (0.2%) and gently rocking for 10 minutes at room temperature. Unspecific sites were blocked by adding 400 µl PBS-FBS (10%) and gently rocked for 1 hour at room temperature. Primary antibody was diluted in PBS-FBS-T and cells were incubated in 300 µl of the primary antibody solution for 1 hour at room temperature. Cells were then washed three times in PBS-T. Secondary antibody was diluted in PBS-FBS-T and cells were incubated in 300 µl of the secondary antibody solution for 1 hour at room temperature. The secondary antibody incubation and all subsequent steps were completed in the dark. Following secondary antibody incubation, cells were washed three times in PBS-T. Cells were incubated in a 1:1000 dilution of DAPI

in PBS for 20 minutes at room temperature. Cells were washed twice in PBS and visualised using the Leica DMI4000.

7.2.7 FACS Cell Cycle Analysis

Propidium iodide (PI) was used to analyse what stage of the cell cycle cells were in. PI binds DNA, and as the DNA content in a cell changes throughout the cell cycle, the PI fluorescence is directly proportional to DNA content and can be used to determine the cell cycle stage.

For the PI FACS analysis, cells were harvested when they were between 50–70% confluent to ensure that they were still in the exponential growth phase. When cells were ready to be harvested (typically from a 6-well plate), culture medium was removed and the cells trypsinised and transferred to a 15 ml falcon tube. Cells were centrifuged (1,200 rpm, 4 minutes, 4 °C) to pellet them and the supernatant removed. Cell pellets were washed twice by resuspending in 1 ml ice-cold PBS and centrifuging (1,200 rpm, 4 minutes, 4 °C). After the second wash, the cell pellets were resuspended in 150 µl ice-cold PBS. Cells were fixed by adding 350 µl ice-cold 100% ethanol, as follows: ethanol was added dropwise while continually vortexing the cells on the lowest setting. Fixed cells were either placed on ice for 15 minutes before staining or stored at 4 °C for up to 1 week. Fixed cells were pelleted by centrifugation (2,000 rpm, 4 minutes, 4 °C) and supernatant aspirated. Pellets were resuspended in 500 µl PI staining solution and incubated at 37 °C for 30 minutes. Samples were filtered and placed in a polypropylene FACS tube for analysis.

Following FACS analysis, the results were interpreted using FlowJo. The PI fluorescence was visualised using a histogram and cells grouped into two peaks, 1N, 2N and an area between. The 1N peak contains cells which are in G1 phase and the 2N peak contains cells with double the DNA content which are in G2. The area between the two peaks contains cells which are in S phase (Figure 7.2). The cells in each peak were calculated as a percentage of the whole cell count to determine the proportion of cells in each stage of the cell cycle.

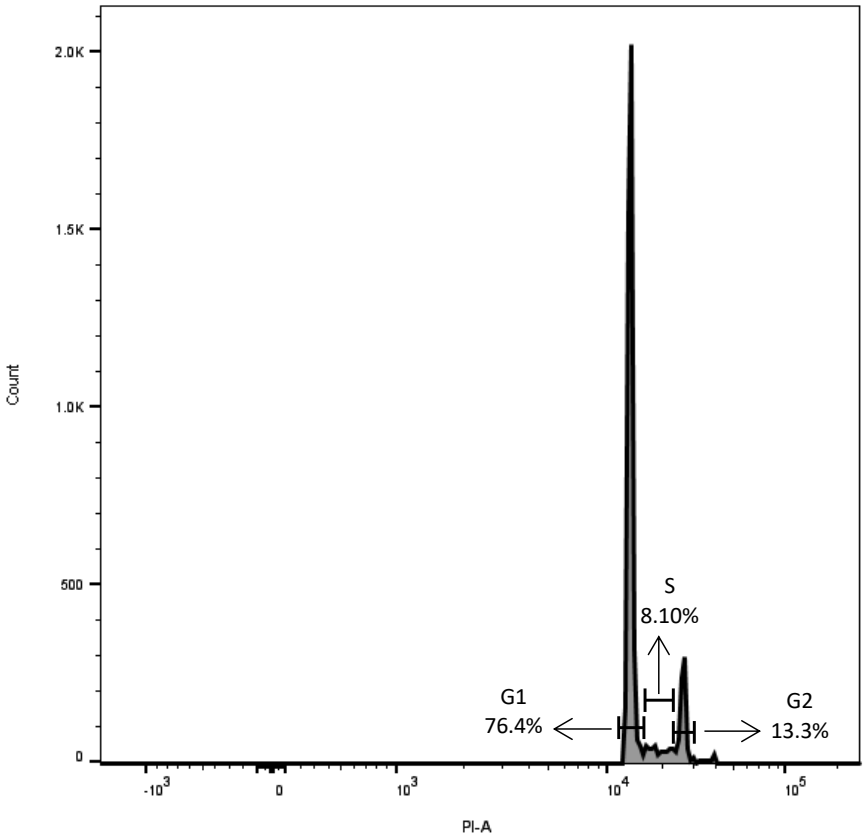

Figure 7.2: Calculating the cell cycle stage following the PI assay. A representative histogram to show how cell cycle stage was calculated following the PI assay. The 1N peak contains cells which are in G1 phase and the 2N peak contains cells with double the DNA content which are in G2. The area between the two peaks contains cells which are in S phase. The number of cells in each peak was calculated relative to the overall cell count to determine the percentage of cells in each cell cycle phase.

7.2.8 Assay for Transposase-Accessible Chromatin (ATAC)

The Omni-ATAC protocol (Corces et al., 2017) was followed, with a few minor adjustments. The Omni-ATAC protocol allows chromatin accessibility to be identified from fresh cell samples, as well as from frozen samples, and includes an additional wash step to remove the mitochondria, therefore reducing mitochondrial DNA contamination.

7.2.8.1 Nuclear Isolation and Transposition Reaction

$5x10^5$ live cells were FACS sorted and pelleted by centrifuging (500 xg, 5 minutes, 4 °C). Cell pellets were resuspended by adding 50 µl ATAC resuspension buffer and gently pipetting up and down three times. To allow the lysis to happen, cells were incubated on ice for 3 minutes. The lysis reaction was quenched by adding 300 µl RSB-T and inverting the tube three times to mix. The nuclei were pelleted by centrifuging (500 xg, 10 minutes, 4 °C) and the supernatant was carefully removed. The pellet was then resuspended in 50 µl ATAC transposition mixture by pipetting up and down six

times. This was followed by a 30-minute incubation at 37 °C, with 1000 rpm mixing throughout. The samples were then cleaned following the Zymo DNA Clean and Concentrator protocol, and eluted in 21 µl of Elution Buffer (EB).

7.2.8.2 PCR Amplification and Quantitation

The 20 µl of eluted DNA was then amplified by PCR. PCR conditions were as follows:

Reagent	Volume (µl)
Primer 1 (25 µM)	2.5
Primer 2 (25 µM)	2.5
2X NEB Next Master Mix	25
Transposed DNA	20

Table 7.12 ATAC PCR Setup

Temperature (°C)	Time	
72	5 Minutes	
98	30 Seconds	
98	10 Seconds	5 Cycles
63	30 Seconds	
72	1 Minute	
4	∞	

Table 7.13: ATAC PCR Conditions (1)

A qPCR of amplified DNA was then completed to determine how many additional cycles of PCR amplification were required. qPCR conditions were as follows:

Reagent	Volume (µl)
H_2O	2.25
Primer 1 (5 µM)	1
Primer 2 (5 µM)	1
2X NEB Next Master Mix	5
Evagreen	0.75
PCR Amplified DNA	5

Table 7.14: ATAC qPCR Setup

Temperature (°C)	Time	
72	5 Minutes	
98	30 Seconds	
98	10 Seconds	20 Cycles
63	30 Seconds	
72	1 Minute	
4	∞	

Table 7.15: ATAC qPCR Conditions

Following qPCR, the maximum fluorescence value for each sample was observed, and 1/3 of this value calculated. The cycle number where 1/3 maximum fluorescence was reached represented how many additional cycles of PCR (n) the original amplified sample required. The 45 µl remaining PCR product was then amplified for n cycles as follows:

Temperature (°C)	Time	
98	30 Seconds	
98	10 Seconds	n Cycles
63	30 Seconds	
72	1 Minute	
4	∞	

Table 7.16: ATAC PCR Conditions (2)

The samples were then cleaned following the Zymo DNA Clean and Concentrator protocol, and eluted in 20 µl of EB.

7.2.8.3 Size Selection and Sequencing Preparation

AMPure XP beads were used for the size selection protocol. To the 20 µl eluted DNA, 180 µl of EB and 110 µl AMPure XP beads were added and mixed by pipetting up and down 10 times. These samples were left at room temperature for 5 minutes. The samples were then placed on a magnetic stand, left to incubate for 2 minutes and 300 µl of the supernatant was transferred to a fresh tube. 190 µl AMPure XP beads were then added to the samples and left to incubate at room temperature for 5 minutes. The samples were then placed on a magnetic stand, left to incubate for 2 minutes and the supernatant discarded. The beads were then washed twice with 200 µl freshly prepared 80%

ethanol. Following the second wash, any ethanol remaining in the tube was carefully removed using a P20 pipette. Beads were then left to air-dry on a magnetic stand for five minutes. Beads were then resuspended in 20 µl EB by pipetting up and down 10 times. The samples were incubated at room temperature for 2 minutes and then placed on a magnetic stand for 2 minutes. The supernatant contained all the size-selected DNA and 17 µl of this supernatant was then transferred to a fresh tube.

The size of fragments following the size selection protocol was then visualised using the Bioanalyser and samples were quantified using the tape station. Samples were pooled and sequenced on the NovaSeq (Illumina) at a depth of 50 million reads.

References

Ajiki, W., Tsukuma, H., Oshima, A., Kawa, K., 1998. Effects of mass screening for neuroblastoma on Incidence, mortality, and survival rates in Osaka, Japan.

Ali, F., Hindley, C., McDowell, G., Deibler, R., Jones, A., Kirschner, M., Guillemot, F., Philpott, A., 2011. Cell cycle-regulated multi-site phosphorylation of Neurogenin 2 coordinates cell cycling with differentiation during neurogenesis. Development 138. https://doi.org/10.1242/dev.067900

Ali, F.R., Cheng, K., Kirwan, P., Metcalfe, S., Livesey, F.J., Barker, R.A., Philpott, A., 2014. The phosphorylation status of Ascl1 is a key determinant of neuronal differentiation and maturation in vivo and in vitro. Development 141. https://doi.org/10.1242/dev.106377

Ali, F.R., Marcos, D., Chernukhin, I., Woods, L.M., Parkinson, L.M., Wylie, L.A., Papkovskaia, T.D., Davies, J.D., Carroll, J.S., Philpott, A., 2020. Dephosphorylation of the Proneural Transcription Factor ASCL1 Re-Engages a Latent Post-Mitotic Differentiation Program in Neuroblastoma. Molecular Cancer Research 18. https://doi.org/10.1158/1541-7786.MCR-20-0693

Almutairi, B., Charlet, J., Dallosso, A.R., Szemes, M., Etchevers, H.C., Malik, K.T.A., Brown, K.W., 2019. Epigenetic deregulation of GATA3 in neuroblastoma is associated with increased GATA3 protein expression and with poor outcomes. Scientific Reports 9. https://doi.org/10.1038/s41598-019-55382-6

Anastassiou, D., Rumjantseva, V., Cheng, W., Huang, J., Canoll, P.D., Yamashiro, D.J., Kandel, J.J., 2011.Human cancer cells express Slug-based epithelial-mesenchymal transition gene expression signature obtained in vivo. BMC Cancer 11. https://doi.org/10.1186/1471-2407-11-529

Aydin, B., Kakumanu, A., Rossillo, M., Moreno-Estell.s, M., Garipler, G., Ringstad, N., Flames, N., Mahony, S., Mazzoni, E.O., 2019. Proneural factors Ascl1 and Neurog2 contribute to neuronal subtype identities by establishing distinct chromatin landscapes. Nature Neuroscience 22. https://doi.org/10.1038/s41593-019-0399-y

Baca, S.C., Takeda, D.Y., Seo, J.-H., Hwang, J., Ku, S.Y., Arafeh, R., Arnoff, T., Agarwal, S., Bell, C., O'Connor, E., Qiu, X., Alaiwi, S.A., Corona, R.I., Fonseca, M.A.S., Giambartolomei, C., Cejas, P., Lim, K., He, M., Sheahan, A., Nassar, A., Berchuck, J.E., Brown, L., Nguyen, H.M., Coleman, I.M., Kaipainen, A., de Sarkar, N., Nelson, P.S., Morrissey, C., Korthauer, K., Pomerantz, M.M., Ellis, L., Pasaniuc, B., Lawrenson, K., Kelly, K., Zoubeidi, A., Hahn, W.C., Beltran, H., Long, H.W., Brown, M., Corey, E., Freedman, M.L., 2021. Reprogramming of the FOXA1 cistrome in treatment-emergent neuroendocrine prostate cancer. Nature Communications 12. https://doi.org/10.1038/s41467-021-22139-7

Baine, M.K., Hsieh, M.-S., Lai, W.V., Egger, J. v., Jungbluth, A.A., Daneshbod, Y., Beras, A., Spencer, R., Lopardo, J., Bodd, F., Montecalvo, J., Sauter, J.L., Chang, J.C., Buonocore, D.J., Travis, W.D., Sen, T., Poirier, J.T., Rudin, C.M., Rekhtman, N., 2020. SCLC Subtypes Defined by ASCL1, NEUROD1, POU2F3, and YAP1: A Comprehensive Immunohistochemical and Histopathologic Characterization. Journal of Thoracic Oncology 15. https://doi.org/10.1016/j.jtho.2020.09.009

Baker, D.L., Schmidt, M.L., Cohn, S.L., Maris, J.M., London, W.B., Buxton, A., Stram, D., Castleberry, R.P., Shimada, H., Sandler, A., Shamberger, R.C., Look, A.T., Reynolds, C.P., Seeger, R.C., Matthay, K.K., 2010. Outcome after Reduced Chemotherapy for Intermediate-Risk Neuroblastoma. New England Journal of Medicine 363. https://doi.org/10.1056/NEJMoa1001527

Barrallo-Gimeno, A., Nieto, M.A., 2005. The Snail genes as inducers of cell movement and survival: implications in development and cancer. Development 132. https://doi.org/10.1242/dev.01907

Bertrand, N., Castro, D.S., Guillemot, F., 2002. Proneural genes and the specification of neural cell types. Nature Reviews Neuroscience 3. https://doi.org/10.1038/nrn874

Bhatt, S., Diaz, R., Trainor, P.A., 2013. Signals and Switches in Mammalian Neural Crest Cell Differentiation. Cold Spring Harbor Perspectives in Biology 5. https://doi.org/10.1101/cshperspect.a008326

Blom, T., Lurvink, R., Aleven, L., Mensink, M., Wolfs, T., Dierselhuis, M., van Eijkelenburg, N., Kraal, K., van Noesel, M., van Grotel, M., Tytgat, G., 2021. Treatment-Related Toxicities During Anti-GD2 Immunotherapy in High-Risk Neuroblastoma Patients. Frontiers in Oncology 10. https://doi.org/10.3389/fonc.2020.601076

Boeva, V., Louis-Brennetot, C., Peltier, A., Durand, S., Pierre-Eugène, C., Raynal, V., Etchevers, H.C., Thomas, S., Lermine, A., Daudigeos-Dubus, E., Geoerger, B., Orth, M.F., Grünewald, T.G.P., Diaz, E., Ducos, B., Surdez, D., Carcaboso, A.M., Medvedeva, I., Deller, T., Combaret, V., Lapouble, E., Pierron, G., Grossetête-Lalami, S., Baulande, S., Schleiermacher, G., Barillot, E., Rohrer, H., Delattre, O., Janoueix-Lerosey, I., 2017. Heterogeneity of neuroblastoma cell identity defined by transcriptional circuitries. Nature Genetics 49. https://doi.org/10.1038/ng.3921

Borromeo, M.D., Savage, T.K., Kollipara, R.K., He, M., Augustyn, A., Osborne, J.K., Girard, L., Minna, J.D., Gazdar, A.F., Cobb, M.H., Johnson, J.E., 2016. ASCL1 and NEUROD1 Reveal Heterogeneity in Pulmonary Neuroendocrine Tumors and Regulate Distinct Genetic Programs. Cell Reports 16. https://doi.org/10.1016/j.celrep.2016.06.081

Brodeur, G.M., Bagatell, R., 2014. Mechanisms of neuroblastoma regression. Nature Reviews Clinical Oncology 11. https://doi.org/10.1038/nrclinonc.2014.168

Brodeur, G.M., Nakagawara, A., Yamashiro, D.J., Ikegaki, N., Liu, X.-G., Azar, C.G., Lee, C.P., Evans, A.E., 1997. Expression of TrkA, TrkB and TrkC in human neuroblastomas. Journal of Neuro-Oncology 31. https://doi.org/10.1023/A:1005729329526

Brodeur, G.M., Seeger, R.C., Schwab, M., Varmus, H.E., Michael Bishop, J., 1984. Amplification of N-myc in Untreated Human Neuroblastomas Correlates with Advanced Disease Stage, New Series.

Buenrostro, J.D., Wu, B., Chang, H.Y., Greenleaf, W.J., 2015. ATAC-seq: A Method for Assaying Chromatin Accessibility Genome-Wide. Current Protocols in Molecular Biology 109. https://doi.org/10.1002/0471142727.mb2129s109

Castro, D.S., Martynoga, B., Parras, C., Ramesh, V., Pacary, E., Johnston, C., Drechsel, D., Lebel-Potter, M., Garcia, L.G., Hunt, C., Dolle, D., Bithell, A., Ettwiller, L., Buckley, N., Guillemot, F., 2011. A novel function of the proneural factor Ascl1 in progenitor proliferation identified by genome-wide characterization of its targets. Genes & Development 25. https://doi.org/10.1101/gad.627811

Chanda, S., Ang, C.E., Davila, J., Pak, C., Mall, M., Lee, Q.Y., Ahlenius, H., Jung, S.W., Südhof, T.C., Wernig, M., 2014. Generation of Induced Neuronal Cells by the Single Reprogramming Factor ASCL1. Stem Cell Reports 3. https://doi.org/10.1016/j.stemcr.2014.05.020
Cheung, N.-K. v., Cheung, I.Y., Kushner, B.H., Ostrovnaya, I., Chamberlain, E., Kramer, K., Modak, S., 2012.

Murine Anti-GD2 Monoclonal Antibody 3F8 Combined With Granulocyte-Macrophage Colony-Stimulating Factor and 13- Cis -Retinoic Acid in High-Risk Patients With Stage 4 Neuroblastoma in First Remission. Journal of Clinical Oncology 30. https://doi.org/10.1200/JCO.2011.41.3807

Corces, M.R., Trevino, A.E., Hamilton, E.G., Greenside, P.G., Sinnott-Armstrong, N.A., Vesuna, S., Satpathy, A.T., Rubin, A.J., Montine, K.S., Wu, B., Kathiria, A., Cho, S.W., Mumbach, M.R., Carter, A.C., Kasowski, M., Orloff, L.A., Risca, V.I., Kundaje, A., Khavari, P.A., Montine, T.J., Greenleaf, W.J., Chang, H.Y., 2017. An improved ATAC-seq protocol reduces background and enables interrogation of frozen tissues. Nature Methods 14. https://doi.org/10.1038/nmeth.4396

Cotterman, R., Knoepfler, P.S., 2009. N-Myc Regulates Expression of Pluripotency Genes in Neuroblastoma Including lif, klf2, klf4, and lin28b. PLoS ONE 4. https://doi.org/10.1371/journal.pone.0005799

D'Angio, GiulioJ., Evans, AudreyE., Koop, C.E., 1971. SPECIAL PATTERN OF WIDESPREAD NEUROBLASTOMA WITH A FAVOURABLE PROGNOSIS. The Lancet 297. https://doi.org/10.1016/S0140-6736(71)91606-0

de Preter, K., Vandesompele, J., Heimann, P., Yigit, N., Beckman, S., Schramm, A., Eggert, A., Stallings, R.L., Benoit, Y., Renard, M., de Paepe, A., Laureys, G., Påhlman, S., Speleman, F., 2007. Erratum to: Human fetal neuroblast and neuroblastoma transcriptome analysis confirms neuroblast origin and highlights neuroblastoma candidate genes. Genome Biology 8. https://doi.org/10.1186/gb-2007-8-1- 401

Decaesteker, B., Denecker, G., van Neste, C., Dolman, E.M., van Loocke, W., Gartlgruber, M., Nunes, C., de Vloed, F., Depuydt, P., Verboom, K., Rombaut, D., Loontiens, S., de Wyn, J., Kholosy, W.M., Koopmans, B., Essing, A.H.W., Herrmann, C., Dreidax, D., Durinck, K., Deforce, D., van Nieuwerburgh, F., Henssen, A., Versteeg, R., Boeva, V., Schleiermacher, G., van Nes, J., Mestdagh, P., Vanhauwaert, S., Schulte, J.H., Westermann, F., Molenaar, J.J., de Preter, K., Speleman, F., 2018. TBX2 is a neuroblastoma core regulatory circuitry component enhancing MYCN/FOXM1 reactivation of DREAM targets. Nature Communications 9. https://doi.org/10.1038/s41467-018-06699-9

Decock, A., Ongenaert, M., de Wilde, B., Brichard, B., Noguera, R., Speleman, F., Vandesompele, J., 2016. Stage 4S neuroblastoma tumors show a characteristic DNA methylation portrait. Epigenetics 11. https://doi.org/10.1080/15592294.2016.1226739

di Lascio, S., Saba, E., Belperio, D., Raimondi, A., Lucchetti, H., Fornasari, D., Benfante, R., 2016. PHOX2A and PHOX2B are differentially regulated during retinoic acid-driven differentiation of SK-N-BE(2)C neuroblastoma cell line. Experimental Cell Research 342. https://doi.org/10.1016/j.yexcr.2016.02.014

Durbin, A.D., Zimmerman, M.W., Dharia, N. v., Abraham, B.J., Iniguez, A.B., Weichert-Leahey, N., He, S., Krill-Burger, J.M., Root, D.E., Vazquez, F., Tsherniak, A., Hahn, W.C., Golub, T.R., Young, R.A., Look, A.T., Stegmaier, K., 2018. Selective gene dependencies in MYCN-amplified neuroblastoma include the core transcriptional regulatory circuitry. Nature Genetics 50. https://doi.org/10.1038/s41588- 018-0191-z

Fraser, J.A., Sutton, J.E., Tazayoni, S., Bruce, I., Poole, A. v., 2019. hASH1 nuclear localization persists in neuroendocrine transdifferentiated prostate cancer cells, even upon reintroduction of androgen. Scientific Reports 9. https://doi.org/10.1038/s41598-019-55665-y

Fueyo, R., Iacobucci, S., Pappa, S., Estarás, C., Lois, S., Vicioso-Mantis, M., Navarro, C., Cruz-Molina, S., Reyes, J.C., Rada-Iglesias, Á., de la Cruz, X., Martínez-Balbás, M.A., 2018. Lineage specific transcription factors and epigenetic regulators mediate TGFβ-dependent enhancer activation. Nucleic Acids Research 46. https://doi.org/10.1093/nar/gky093

Gillotin, S., Davies, J.D., Philpott, A., 2018. Subcellular localisation modulates ubiquitylation and degradation of Ascl1. Scientific Reports 8. https://doi.org/10.1038/s41598-018-23056-4

Guglielmi, L., Cinnella, C., Nardella, M., Maresca, G., Valentini, A., Mercanti, D., Felsani, A., D'Agnano, I., 2014. MYCN gene expression is required for the onset of the differentiation programme in neuroblastoma cells. Cell Death & Disease 5. https://doi.org/10.1038/cddis.2014.42

Guillemot, F., Hassan, B.A., 2017. Beyond proneural: emerging functions and regulations of proneural proteins. Current Opinion in Neurobiology 42. https://doi.org/10.1016/j.conb.2016.11.011

Guillemot, F., Lo, L.-C., Johnson, J.E., Auerbach, A., Anderson, D.J., Joyner, A.L., 1993. Mammalian achaete-scute homolog 1 is required for the early development of olfactory and autonomic neurons. Cell 75. https://doi.org/10.1016/0092-8674(93)90381-Y

Gupta, K., Gupta, S., 2017. Neuroendocrine differentiation in prostate cancer: key epigenetic players. Translational Cancer Research 6. https://doi.org/10.21037/tcr.2017.01.20

Henrich, K.-O., Bender, S., Saadati, M., Dreidax, D., Gartlgruber, M., Shao, C., Herrmann, C., Wiesenfarth, M., Parzonka, M., Wehrmann, L., Fischer, M., Duffy, D.J., Bell, E., Torkov, A., Schmezer, P., Plass, C., Höfer, T., Benner, A., Pfister, S.M., Westermann, F., 2016. Integrative Genome-Scale Analysis Identifies Epigenetic Mechanisms of Transcriptional Deregulation in Unfavorable Neuroblastomas. Cancer Research 76. https://doi.org/10.1158/0008-5472.CAN-15-2507

Hero, B., Simon, T., Spitz, R., Ernestus, K., Gnekow, A.K., Scheel-Walter, H.-G., Schwabe, D., Schilling, F.H., Benz-Bohm, G., Berthold, F., 2008. Localized Infant Neuroblastomas Often Show Spontaneous Regression: Results of the Prospective Trials NB95-S and NB97. Journal of Clinical Oncology 26. https://doi.org/10.1200/JCO.2007.12.3349

Higashi, M., Kolla, V., Iyer, R., Naraparaju, K., Zhuang, T., Kolla, S., Brodeur, G.M., 2015. Retinoic acid-induced CHD5 upregulation and neuronal differentiation of neuroblastoma. Molecular Cancer 14. https://doi.org/10.1186/s12943-015-0425-y

Hnisz, D., Abraham, B.J., Lee, T.I., Lau, A., Saint-André, V., Sigova, A.A., Hoke, H.A., Young, R.A., 2013. Super-Enhancers in the Control of Cell Identity and Disease. Cell 155. https://doi.org/10.1016/j.cell.2013.09.053

Howard, M.J., 2005. Mechanisms and perspectives on differentiation of autonomic neurons. Developmental Biology 277. https://doi.org/10.1016/j.ydbio.2004.09.034

Huang, Y., Tsubota, S., Nishio, N., Takahashi, Y., Kadomatsu, K., 2021. Combination of tumor necrosis factor-α and epidermal growth factor induces the adrenergic-to-mesenchymal transdifferentiation in SH-SY5Y neuroblastoma cells. Cancer Science 112. https://doi.org/10.1111/cas.14760

Ichimiya, S., Nimura, Y., Seki, N., Ozaki, T., Nagase, T., Nakagawara, A., 2001. Downregulation of hASH1 is associated with the retinoic acid-induced differentiation of human neuroblastoma cell lines. Medical and Pediatric Oncology 36. https://doi.org/10.1002/1096-911X(20010101)36:1<132::AID- MPO1031>3.0.CO;2-A

Imayoshi, I., Isomura, A., Harima, Y., Kawaguchi, K., Kori, H., Miyachi, H., Fujiwara, T., Ishidate, F., Kageyama, R., 2013. Oscillatory Control of Factors Determining Multipotency and Fate in Mouse Neural Progenitors. Science 342. https://doi.org/10.1126/science.1242366

Ioka, A., Inoue, M., Yoneda, A., Nakamura, T., Hara, J., Hashii, Y., Sakata, N., Yamato, K., Tsukuma, H., Kawa, K., 2016. Effects of the Cessation of Mass Screening for Neuroblastoma at 6 Months of Age: A Population-Based Study in Osaka, Japan. Journal of Epidemiology 26. https://doi.org/10.2188/jea.JE20150054

Jansky, S., Sharma, A.K., Körber, V., Quintero, A., Toprak, U.H., Wecht, E.M., Gartlgruber, M., Greco, A., Chomsky, E., Grünewald, T.G.P., Henrich, K.-O., Tanay, A., Herrmann, C., Höfer, T., Westermann, F., 2021. Single-cell transcriptomic analyses provide insights into the developmental origins of neuroblastoma. Nature Genetics 53. https://doi.org/10.1038/s41588-021-00806-1

Jiang, T., Collins, B.J., Jin, N., Watkins, D.N., Brock, M. v., Matsui, W., Nelkin, B.D., Ball, D.W., 2009. Achaete-Scute Complex Homologue 1 Regulates Tumor-Initiating Capacity in Human Small Cell Lung Cancer. Cancer Research 69. https://doi.org/10.1158/0008-5472.CAN-08-2762

Johnsen, J.I., Dyberg, C., Wickström, M., 2019. Neuroblastoma—A Neural Crest Derived Embryonal Malignancy. Frontiers in Molecular Neuroscience 12. https://doi.org/10.3389/fnmol.2019.00009

Kaneko, Y., Suenaga, Y., Islam, S.M.R., Matsumoto, D., Nakamura, Y., Ohira, M., Yokoi, S., Nakagawara, A., 2015. Functional interplay between MYCN, NCYM, and OCT4 promotes aggressiveness of human neuroblastomas. Cancer Science 106. https://doi.org/10.1111/cas.12677

Kasim, M., Heß, V., Scholz, H., Persson, P.B., Fähling, M., 2016. Achaete-Scute Homolog 1 Expression Controls Cellular Differentiation of Neuroblastoma. Frontiers in Molecular Neuroscience 9. https://doi.org/10.3389/fnmol.2016.00156

Kildisiute, G., Kholosy, W.M., Young, M.D., Roberts, K., Elmentaite, R., van Hooff, S.R., Pacyna, C.N., Khabirova, E., Piapi, A., Thevanesan, C., Bugallo-Blanco, E., Burke, C., Mamanova, L., Keller, K.M., Langenberg-Ververgaert, K.P.S., Lijnzaad, P., Margaritis, T., Holstege, F.C.P., Tas, M.L., Wijnen, M.H.W.A., van Noesel, M.M., del Valle, I., Barone, G., van der Linden, R., Duncan, C., Anderson, J., Achermann, J.C., Haniffa, M., Teichmann, S.A., Rampling, D., Sebire, N.J., He, X., de Krijger, R.R., Barker, R.A., Meyer, K.B., Bayraktar, O., Straathof, K., Molenaar, J.J., Behjati, S., 2021. Tumor to normal single-cell mRNA comparisons reveal a pan-neuroblastoma cancer cell. Science Advances 7. https://doi.org/10.1126/sciadv.abd3311

Kim, C., Choi, Y.B., Lee, J.W., Yoo, K.H., Sung, K.W., Koo, H.H., 2018. Excellent treatment outcomes in children younger than 18 months with stage 4 MYCN nonamplified neuroblastoma. Korean Journal of Pediatrics 61. https://doi.org/10.3345/kjp.2018.61.2.53

Kin Chan, S.S., 2013. What is a Master Regulator? Journal of Stem Cell Research & Therapy 03. https://doi.org/10.4172/2157-7633.1000e114

Kramer, M., Ribeiro, D., Arsenian-Henriksson, M., Deller, T., Rohrer, H., 2016. Proliferation and Survival of Embryonic Sympathetic Neuroblasts by MYCN and Activated ALK Signaling. The Journal of Neuroscience 36. https://doi.org/10.1523/JNEUROSCI.0183-16.2016

Ladenstein, R., Pötschger, U., Valteau-Couanet, D., Luksch, R., Castel, V., Yaniv, I., Laureys, G., Brock, P., Michon, J.M., Owens, C., Trahair, T., Chan, G.C.F., Ruud, E., Schroeder, H., Beck Popovic, M., Schreier, G., Loibner, H., Ambros, P., Holmes, K., Castellani, M.R., Gaze, M.N., Garaventa, A., Pearson, A.D.J., Lode, H.N., 2018. Interleukin 2 with anti-GD2 antibody ch14.18/CHO (dinutuximab beta) in patients with high-risk neuroblastoma (HR-NBL1/SIOPEN): a multicentre, randomised, phase 3 trial. The Lancet Oncology 19. https://doi.org/10.1016/S1470-2045(18)30578-3

Laverdière, C., Liu, Q., Yasui, Y., Nathan, P.C., Gurney, J.G., Stovall, M., Diller, L.R., Cheung, N.-K., Wolden, S., Robison, L.L., Sklar, C.A., 2009. Long-term Outcomes in Survivors of Neuroblastoma: A Report From the Childhood Cancer Survivor Study. JNCI: Journal of the National Cancer Institute 101. https://doi.org/10.1093/jnci/djp230

le Dréau, G., Escalona, R., Fueyo, R., Herrera, A., Martínez, J. D., Usieto, S., Menendez, A., Pons, S., Martinez-Balbas, M. A., & Marti, E. (2018). E proteins sharpen neurogenesis by modulating proneural bHLH transcription factors' activity in an E-box-dependent manner. *ELife*, *7*. https://doi.org/10.7554/eLife.37267

Lee, V.M., Hernandez, S., Giang, B., Chabot, C., Hernandez, J., de Bellard, M.E., 2020. Molecular Events Controlling Cessation of Trunk Neural Crest Migration and Onset of Differentiation. Frontiers in Cell and Developmental Biology 8. https://doi.org/10.3389/fcell.2020.00199

Lo, L.C., Johnson, J.E., Wuenschell, C.W., Saito, T., Anderson, D.J., 1991. Mammalian achaete-scute homolog 1 is transiently expressed by spatially restricted subsets of early neuroepithelial and neural crest cells. Genes & Development 5. https://doi.org/10.1101/gad.5.9.1524

Lochmann, T.L., Powell, K.M., Ham, J., Floros, K. v., Heisey, D.A.R., Kurupi, R.I.J., Calbert, M.L., Ghotra, M.S., Greninger, P., Dozmorov, M., Gowda, M., Souers, A.J., Reynolds, C.P., Benes, C.H., Faber, A.C., 2018. Targeted inhibition of histone H3K27 demethylation is effective in high-risk neuroblastoma. Science Translational Medicine 10. https://doi.org/10.1126/scitranslmed.aao4680

Love, M.I., Huber, W., Anders, S., 2014. Moderated estimation of fold change and dispersion for RNA-seq data with DESeq2. Genome Biology 15. https://doi.org/10.1186/s13059-014-05508

Maris, J.M., 2010. Recent Advances in Neuroblastoma. New England Journal of Medicine 362. https://doi.org/10.1056/NEJMra0804577

Martik, M.L., Bronner, M.E., 2017. Regulatory Logic Underlying Diversification of the Neural Crest. Trends in Genetics 33. https://doi.org/10.1016/j.tig.2017.07.015

Matthay, K.K., Maris, J.M., Schleiermacher, G., Nakagawara, A., Mackall, C.L., Diller, L., Weiss, W.A., 2016. Neuroblastoma. Nature Reviews Disease Primers 2. https://doi.org/10.1038/nrdp.2016.78

Matthay, K.K., Reynolds, C.P., Seeger, R.C., Shimada, H., Adkins, E.S., Haas-Kogan, D., Gerbing, R.B., London, W.B., Villablanca, J.G., 2009. Long-Term Results for Children With High-Risk Neuroblastoma Treated on a Randomized Trial of Myeloablative Therapy Followed by 13- cis -Retinoic Acid: A Children's Oncology Group Study. Journal of Clinical Oncology 27. https://doi.org/10.1200/JCO.2007.13.8925

Matthay, K.K., Villablanca, J.G., Seeger, R.C., Stram, D.O., Harris, R.E., Ramsay, N.K., Swift, P., Shimada, H., Black, C.T., Brodeur, G.M., Gerbing, R.B., Reynolds, C.P., 1999. Treatment of High-Risk Neuroblastoma with Intensive Chemotherapy, Radiotherapy, Autologous Bone Marrow Transplantation, and 13- cis -Retinoic Acid. New England Journal of Medicine 341. https://doi.org/10.1056/NEJM199910143411601

Mohammed, H., Taylor, C., Brown, G.D., Papachristou, E.K., Carroll, J.S., D'Santos, C.S., 2016. Rapid immunoprecipitation mass spectrometry of endogenous proteins (RIME) for analysis of chromatin complexes. Nature Protocols 11. https://doi.org/10.1038/nprot.2016.020

Molenaar, J.J., Domingo-Fernández, R., Ebus, M.E., Lindner, S., Koster, J., Drabek, K., Mestdagh, P., van Sluis, P., Valentijn, L.J., van Nes, J., Broekmans, M., Haneveld, F., Volckmann, R., Bray, I., Heukamp, L., Sprüssel, A., Thor, T., Kieckbusch, K., Klein-Hitpass, L., Fischer, M., Vandesompele, J., Schramm, A., van Noesel, M.M., Varesio, L., Speleman, F., Eggert, A., Stallings, R.L., Caron, H.N., Versteeg, R., Schulte, J.H., 2012. LIN28B induces neuroblastoma and enhances MYCN levels via let-7 suppression. Nature Genetics 44. https://doi.org/10.1038/ng.2436

Monclair, T., Brodeur, G.M., Ambros, P.F., Brisse, H.J., Cecchetto, G., Holmes, K., Kaneko, M., London, W.B., Matthay, K.K., Nuchtern, J.G., von Schweinitz, D., Simon, T., Cohn, S.L., Pearson, A.D.J., 2009. The International Neuroblastoma Risk Group (INRG) Staging System: An INRG Task Force Report. Journal of Clinical Oncology 27. https://doi.org/10.1200/JCO.2008.16.6876

Morikawa, Y., Zehir, A., Maska, E., Deng, C., Schneider, M.D., Mishina, Y., Cserjesi, P., 2009. BMP signaling regulates sympathetic nervous system development through Smad4-dependent and -independent pathways. Development 136. https://doi.org/10.1242/dev.038133

Mosse, Y.P., Laudenslager, M., Khazi, D., Carlisle, A.J., Winter, C.L., Rappaport, E., Maris, J.M., 2004. Germline PHOX2B Mutation in Hereditary Neuroblastoma. The American Journal of Human Genetics 75. https://doi.org/10.1086/424530

Naftali, O., Maman, S., Meshel, T., Sagi-Assif, O., Ginat, R., Witz, I.P., 2016. PHOX2B is a suppressor of neuroblastoma metastasis. Oncotarget 7. https://doi.org/10.18632/oncotarget.7056

Nakagawara, A., Li, Y., Izumi, H., Muramori, K., Inada, H., Nishi, M., 2018. Neuroblastoma. Japanese Journal of Clinical Oncology 48. https://doi.org/10.1093/jjco/hyx176

Narayanan, A., Gagliardi, F., Gallotti, A.L., Mazzoleni, S., Cominelli, M., Fagnocchi, L., Pala, M., Piras, I.S., Zordan, P., Moretta, N., Tratta, E., Brugnara, G., Altabella, L., Bozzuto, G., Gorombei, P., Molinari, A., Padua, R.-A., Bulfone, A., Politi, L.S., Falini, A., Castellano, A., Mortini, P., Zippo, A., Poliani, P.L., Galli, R., 2019. The proneural gene ASCL1 governs the transcriptional subgroup affiliation in glioblastoma stem cells by directly repressing the mesenchymal gene NDRG1. Cell Death & Differentiation 26. https://doi.org/10.1038/s41418-018-0248-7

Nuchtern, J.G., London, W.B., Barnewolt, C.E., Naranjo, A., McGrady, P.W., Geiger, J.D., Diller, L., Schmidt, M. lou, Maris, J.M., Cohn, S.L., Shamberger, R.C., 2012. A Prospective Study of Expectant Observation as Primary Therapy for Neuroblastoma in Young Infants. Annals of Surgery 256. https://doi.org/10.1097/SLA.0b013e31826cbbbd

Olsen, R.R., Ireland, A.S., Kastner, D.W., Groves, S.M., Spainhower, K.B., Pozo, K., Kelenis, D.P., Whitney, C.P., Guthrie, M.R., Wait, S.J., Soltero, D., Witt, B.L., Quaranta, V., Johnson, J.E., Oliver, T.G., 2021. ASCL1 represses a SOX9 + neural crest stem-like state in small cell lung cancer. Genes & Development 35. https://doi.org/10.1101/gad.348295.121

Olsen, R.R., Otero, J.H., García-López, J., Wallace, K., Finkelstein, D., Rehg, J.E., Yin, Z., Wang, Y.-D., Freeman, K.W., 2017. MYCN induces neuroblastoma in primary neural crest cells. Oncogene 36. https://doi.org/10.1038/onc.2017.128

Osada, H., Tatematsu, Y., Yatabe, Y., Horio, Y., Takahashi, T., 2005. ASH1 Gene Is a Specific Therapeutic Target for Lung Cancers with Neuroendocrine Features. Cancer Research 65. https://doi.org/10.1158/0008-5472.CAN-05-1404

Otte, J., Dyberg, C., Pepich, A., Johnsen, J.I., 2021. MYCN Function in Neuroblastoma Development. Frontiers in Oncology 10. https://doi.org/10.3389/fonc.2020.624079

Oue, T., Inoue, M., Yoneda, A., Kubota, A., Okuyama, H., Kawahara, H., Nishikawa, M., Nakayama, M., Kawa, K., 2005. Profile of neuroblastoma detected by mass screening, resected after observation without treatment: results of the Wait and See pilot study. Journal of Pediatric Surgery 40. https://doi.org/10.1016/j.jpedsurg.2004.10.062

Pang, Z.P., Yang, N., Vierbuchen, T., Ostermeier, A., Fuentes, D.R., Yang, T.Q., Citri, A., Sebastiano, V., Marro, S., Südhof, T.C., Wernig, M., 2011. Induction of human neuronal cells by defined transcription factors. Nature 476. https://doi.org/10.1038/nature10202

Park, N.I., Guilhamon, P., Desai, K., McAdam, R.F., Langille, E., O'Connor, M., Lan, X., Whetstone, H., Coutinho, F.J., Vanner, R.J., Ling, E., Prinos, P., Lee, L., Selvadurai, H., Atwal, G., Kushida, M., Clarke, I.D., Voisin, V., Cusimano, M.D., Bernstein, M., Das, S., Bader, G., Arrowsmith, C.H., Angers, S., Huang, X., Lupien, M., Dirks, P.B., 2017. ASCL1 Reorganizes Chromatin to Direct Neuronal Fate and Suppress Tumorigenicity of Glioblastoma Stem Cells. Cell Stem Cell 21. https://doi.org/10.1016/j.stem.2017.06.004

Parlier, D., Ariza, A., Christulia, F., Genco, F., Vanhomwegen, J., Kricha, S., Souopgui, J., Bellefroid, E.J., 2008. Xenopus zinc finger transcription factor IA1 (Insm1) expression marks anteroventral noradrenergic neuron progenitors in Xenopus embryos. Developmental Dynamics 237. https://doi.org/10.1002/dvdy.21621

PENG, H., KE, X.-X., HU, R., YANG, L., CUI, H., WEI, Y., 2015. Essential role of GATA3 in regulation of differentiation and cell proliferation in SK-N-SH neuroblastoma cells. Molecular Medicine Reports 11. https://doi.org/10.3892/mmr.2014.2809

Powers, J.T., Tsanov, K.M., Pearson, D.S., Roels, F., Spina, C.S., Ebright, R., Seligson, M., de Soysa, Y., Cahan, P., Theißen, J., Tu, H.-C., Han, A., Kurek, K.C., LaPier, G.S., Osborne, J.K., Ross, S.J., Cesana, M., Collins, J.J., Berthold, F., Daley, G.Q., 2016. Multiple mechanisms disrupt the let-7 microRNA family in neuroblastoma. Nature 535. https://doi.org/10.1038/nature18632

Raabe, E.H., Laudenslager, M., Winter, C., Wasserman, N., Cole, K., LaQuaglia, M., Maris, D.J., Mosse, Y.P., Maris, J.M., 2008. Prevalence and functional consequence of PHOX2B mutations in neuroblastoma. Oncogene 27. https://doi.org/10.1038/sj.onc.1210659

Raffaghello, L., Prigione, I., Bocca, P., Morandi, F., Camoriano, M., Gambini, C., Wang, X., Ferrone, S., Pistoia, V., 2005. Multiple defects of the antigen-processing machinery components in human neuroblastoma: immunotherapeutic implications. Oncogene 24. https://doi.org/10.1038/sj.onc.1208594

Rajakulendran, N., Rowland, K.J., Selvadurai, H.J., Ahmadi, M., Park, N.I., Naumenko, S., Dolma, S., Ward, R.J., So, M., Lee, L., MacLeod, G., Pasiliao, C., Brandon, C., Clarke, I.D., Cusimano, M.D., Bernstein, M., Batada, N., Angers, S., Dirks, P.B., 2019. Wnt and Notch signaling govern self-renewal and differentiation in a subset of human glioblastoma stem cells. Genes & Development 33. https://doi.org/10.1101/gad.321968.118

Rao, Z., Wang, R., Li, S., Shi, Y., Mo, L., Han, S., Yuan, J., Jing, N., Cheng, L., 2021. Molecular Mechanisms Underlying Ascl1-Mediated Astrocyte-to-Neuron Conversion. Stem Cell Reports 16. https://doi.org/10.1016/j.stemcr.2021.01.006

Rapa, I., Ceppi, P., Bollito, E., Rosas, R., Cappia, S., Bacillo, E., Porpiglia, F., Berruti, A., Papotti, M., Volante, M., 2008. Human ASH1 expression in prostate cancer with neuroendocrine differentiation. Modern Pathology 21. https://doi.org/10.1038/modpathol.2008.39

Rapa, I., Volante, M., Migliore, C., Farsetti, A., Berruti, A., Vittorio Scagliotti, G., Giordano, S., Papotti, M., 2013. Human ASH-1 Promotes Neuroendocrine Differentiation in Androgen Deprivation Conditions and Interferes With Androgen Responsiveness in Prostate Cancer Cells. The Prostate 73. https://doi.org/10.1002/pros.22679

Raposo, A.A.S.F., Vasconcelos, F.F., Drechsel, D., Marie, C., Johnston, C., Dolle, D., Bithell, A., Gillotin, S., van den Berg, D.L.C., Ettwiller, L., Flicek, P., Crawford, G.E., Parras, C.M., Berninger, B., Buckley, N.J., Guillemot, F., Castro, D.S., 2015. Ascl1 Coordinately Regulates Gene Expression and the Chromatin Landscape during Neurogenesis. Cell Reports 10. https://doi.org/10.1016/j.celrep.2015.02.025

Ratner, N., Brodeur, G.M., Dale, R.C., Schor, N.F., 2016. The “neuro” of neuroblastoma: Neuroblastoma as a neurodevelopmental disorder. Annals of Neurology 80. https://doi.org/10.1002/ana.24659

Reiff, T., Tsarovina, K., Majdazari, A., Schmidt, M., del Pino, I., Rohrer, H., 2010. Neuroblastoma Phox2b Variants Stimulate Proliferation and Dedifferentiation of Immature Sympathetic Neurons. Journal of Neuroscience 30. https://doi.org/10.1523/JNEUROSCI.5368-09.2010

Rheinbay, E., Suvà, M.L., Gillespie, S.M., Wakimoto, H., Patel, A.P., Shahid, M., Oksuz, O., Rabkin, S.D., Martuza, R.L., Rivera, M.N., Louis, D.N., Kasif, S., Chi, A.S., Bernstein, B.E., 2013. An Aberrant Transcription Factor Network Essential for Wnt Signaling and Stem Cell Maintenance in Glioblastoma. Cell Reports 3. https://doi.org/10.1016/j.celrep.2013.04.021

Ribatti, D., Tamma, R., Annese, T., 2020. Epithelial-Mesenchymal Transition in Cancer: A Historical Overview. Translational Oncology 13. https://doi.org/10.1016/j.tranon.2020.100773

Rihani, A., Vandesompele, J., Speleman, F., van Maerken, T., 2015. Inhibition of CDK4/6 as a novel therapeutic option for neuroblastoma. Cancer cell international 15, 76. https://doi.org/10.1186/s12935-015-0224-y

Rudin, C.M., Poirier, J.T., Byers, L.A., Dive, C., Dowlati, A., George, J., Heymach, J. v., Johnson, J.E., Lehman, J.M., MacPherson, D., Massion, P.P., Minna, J.D., Oliver, T.G., Quaranta, V., Sage, J., Thomas, R.K., Vakoc, C.R., Gazdar, A.F., 2019. Molecular subtypes of small cell lung cancer: a synthesis of human and mouse model data. Nature Reviews Cancer 19. https://doi.org/10.1038/s41568-019-0133-9

Rufini, V., Calcagni, M.L., Baum, R.P., 2006. Imaging of Neuroendocrine Tumors. Seminars in Nuclear Medicine 36. https://doi.org/10.1053/j.semnuclmed.2006.03.007

Sato, Y., Okamoto, I., Kameyama, H., Kudoh, S., Saito, H., Sanada, M., Kudo, N., Wakimoto, J., Fujino, K., Ikematsu, Y., Tanaka, K., Nishikawa, A., Sakaguchi, R., Ito, T., 2020. Integrated Immunohistochemical Study on Small-Cell Carcinoma of the Lung Focusing on Transcription and Co-Transcription Factors. Diagnostics 10. https://doi.org/10.3390/diagnostics10110949

Schilling, F.H., Spix, C., Berthold, F., Erttmann, R., Fehse, N., Hero, B., Klein, G., Sander, J., Schwarz, K., Treuner, J., Zorn, U., Michaelis, J., 2002. Neuroblastoma Screening at One Year of Age. New England Journal of Medicine 346. https://doi.org/10.1056/NEJMoa012277

Schneider, C., Wicht, H., Enderich, J., Wegner, M., Rohrer, H., 1999. Bone Morphogenetic Proteins Are Required In Vivo for the Generation of Sympathetic Neurons. Neuron 24. https://doi.org/10.1016/S0896-6273(00)81033-8

Seeger, R.C., Brodeur, G.M., Sather, H., Dalton, A., Siegel, S.E., Wong, K.Y., Hammond, D., 1985. Association of Multiple Copies of the N- myc Oncogene with Rapid Progression of Neuroblastomas . New England Journal of Medicine 313, 1111–1116. https://doi.org/10.1056/nejm198510313131802

Shi, H., Tao, T., Abraham, B.J., Durbin, A.D., Zimmerman, M.W., Kadoch, C., Look, A.T., 2020. ARID1A loss in neuroblastoma promotes the adrenergic-to-mesenchymal transition by regulating enhancer- mediated gene expression. Science Advances 6. https://doi.org/10.1126/sciadv.aaz3440

Shyamala, K., Yanduri, S., Girish, H., Murgod, S., 2015. Neural crest: The fourth germ layer. Journal of Oral and Maxillofacial Pathology 19. https://doi.org/10.4103/0973-029X.164536

Siaw, J.T., Gabre, J.L., Uçkun, E., Vigny, M., Zhang, W., van den Eynden, J., Hallberg, B., Palmer, R.H., Guan, J., 2021. Loss of RET Promotes Mesenchymal Identity in Neuroblastoma Cells. Cancers 13. https://doi.org/10.3390/cancers13081909

Simões-Costa, M., Bronner, M.E., 2015. Establishing neural crest identity: a gene regulatory recipe. Development 142. https://doi.org/10.1242/dev.105445

Smith, S.J., Diehl, N.N., Smith, B.D., Mohney, B.G., 2010. Urine catecholamine levels as diagnostic markers for neuroblastoma in a defined population: implications for ophthalmic practice. Eye 24. https://doi.org/10.1038/eye.2010.125

Smith, V., Foster, J., 2018. High-Risk Neuroblastoma Treatment Review. Children 5. https://doi.org/10.3390/children5090114

Sommer, L., Shah, N., Rao, M., Anderson, D.J., 1995. The cellular function of MASH1 in autonomic neurogenesis. Neuron 15. https://doi.org/10.1016/0896-6273(95)90005-5

Soufi, A., Garcia, M.F., Jaroszewicz, A., Osman, N., Pellegrini, M., Zaret, K.S., 2015. Pioneer Transcription Factors Target Partial DNA Motifs on Nucleosomes to Initiate Reprogramming. Cell 161. https://doi.org/10.1016/j.cell.2015.03.017

Spix, C., Pastore, G., Sankila, R., Stiller, C.A., Steliarova-Foucher, E., 2006. Neuroblastoma incidence and survival in European children (1978–1997): Report from the Automated Childhood Cancer Information System project. European Journal of Cancer 42. https://doi.org/10.1016/j.ejca.2006.05.008

Squire, R., Fowler, C.L., Brooks, S.P., Rich, G.A., Cooney, D.R., 1990. The relationship of class I MHC antigen expression to stage IV-S disease and survival in neuroblastoma. Journal of Pediatric Surgery 25. https://doi.org/10.1016/0022-3468(90)90375-J

Stark, R., Brown, G., 2011. DiffBind: differential binding analysis of ChIP-Seq peak data.

Strother, D.R., London, W.B., Schmidt, M. lou, Brodeur, G.M., Shimada, H., Thorner, P., Collins, M.H., Tagge, E., Adkins, S., Reynolds, C.P., Murray, K., Lavey, R.S., Matthay, K.K., Castleberry, R., Maris, J.M., Cohn, S.L., 2012. Outcome After Surgery Alone or With Restricted Use of Chemotherapy for Patients With Low-Risk Neuroblastoma: Results of Children's Oncology Group Study P9641. Journal of Clinical Oncology 30. https://doi.org/10.1200/JCO.2011.37.9990

Subramanian, A., Tamayo, P., Mootha, V. K., Mukherjee, S., Ebert, B. L., Gillette, M. A., Paulovich, A., Pomeroy, S. L., Golub, T. R., Lander, E. S., & Mesirov, J. P. (2005). Gene set enrichment analysis: A knowledge-based approach for interpreting genome-wide expression profiles. *Proceedings of the National Academy of Sciences*, *102*(43), 15545–15550. https://doi.org/10.1073/pnas.0506580102

Suenaga, Y., Islam, S.M.R., Alagu, J., Kaneko, Y., Kato, M., Tanaka, Y., Kawana, H., Hossain, S., Matsumoto, D., Yamamoto, M., Shoji, W., Itami, M., Shibata, T., Nakamura, Y., Ohira, M., Haraguchi, S., Takatori, A., Nakagawara, A., 2014. NCYM, a Cis-Antisense Gene of MYCN, Encodes a De Novo Evolved Protein That Inhibits GSK3β Resulting in the Stabilization of MYCN in Human Neuroblastomas. PLoS Genetics 10. https://doi.org/10.1371/journal.pgen.1003996

Sung, K.W., Yoo, K.H., Koo, H.H., Kim, J.Y., Cho, E.J., Seo, Y.L., Kim, J., Lee, S.K., 2009. Neuroblastoma Originating from Extra-abdominal Sites: Association with Favorable Clinical and Biological Features. Journal of Korean Medical Science 24. https://doi.org/10.3346/jkms.2009.24.3.461

Thiele, C.J., 1998. Neuroblastoma Cell Lines. Masters, J. Human Cell Culture 1, 21–53.

Thomas, W.D., Raif, A., Hansford, L., Marshall, G., 2004. N-myc transcription molecule and oncoprotein. The International Journal of Biochemistry & Cell Biology 36. https://doi.org/10.1016/S1357- 2725(03)00254-1

Torper, O., Pfisterer, U., Wolf, D.A., Pereira, M., Lau, S., Jakobsson, J., Bjorklund, A., Grealish, S., Parmar, M., 2013. Generation of induced neurons via direct conversion in vivo. Proceedings of the National Academy of Sciences 110. https://doi.org/10.1073/pnas.1303829110

Trochet, D., Bourdeaut, F., Janoueix-Lerosey, I., Deville, A., de Pontual, L., Schleiermacher, G., Coze, C., Philip, N., Frébourg, T., Munnich, A., Lyonnet, S., Delattre, O., Amiel, J., 2004. Germline Mutations of the Paired–Like Homeobox 2B (PHOX2B) Gene in Neuroblastoma. The American Journal of Human Genetics 74. https://doi.org/10.1086/383253

Urbán, N., van den Berg, D.L.C., Forget, A., Andersen, J., Demmers, J.A.A., Hunt, C., Ayrault, O., Guillemot, F., 2016. Return to quiescence of mouse neural stem cells by degradation of a proactivation protein. Science 353. https://doi.org/10.1126/science.aaf4802

Valsesia-Wittmann, S., Magdeleine, M., Dupasquier, S., Garin, E., Jallas, A.-C., Combaret, V., Krause, A., Leissner, P., Puisieux, A., 2004. Oncogenic cooperation between H-Twist and N-Myc overrides failsafe programs in cancer cells. Cancer Cell 6. https://doi.org/10.1016/j.ccr.2004.09.033

van Groningen, T., Akogul, N., Westerhout, E.M., Chan, A., Hasselt, N.E., Zwijnenburg, D.A., Broekmans, M., Stroeken, P., Haneveld, F., Hooijer, G.K.J., Savci-Heijink, C.D., Lakeman, A., Volckmann, R., van Sluis, P., Valentijn, L.J., Koster, J., Versteeg, R., van Nes, J., 2019. A NOTCH feed-forward loop drives reprogramming from adrenergic to mesenchymal state in neuroblastoma. Nature Communications 10. https://doi.org/10.1038/s41467-019-09470-w

van Groningen, T., Koster, J., Valentijn, L.J., Zwijnenburg, D.A., Akogul, N., Hasselt, N.E., Broekmans, M., Haneveld, F., Nowakowska, N.E., Bras, J., van Noesel, C.J.M., Jongejan, A., van Kampen, A.H., Koster, L., Baas, F., van Dijk-Kerkhoven, L., Huizer-Smit, M., Lecca, M.C., Chan, A., Lakeman, A., Molenaar, P., Volckmann, R., Westerhout, E.M., Hamdi, M., van Sluis, P.G., Ebus, M.E., Molenaar, J.J., Tytgat, G.A., Westerman, B.A., van Nes, J., Versteeg, R., 2017. Neuroblastoma is composed of two super- enhancer-associated differentiation states. Nature Genetics 49. https://doi.org/10.1038/ng.3899

van Groningen, T., Niklasson, C.U., Chan, A., Akogul, N., Westerhout, E.M., von Stedingk, K., Hamdi, M., Valentijn, L.J., Mohlin, S., Stroeken, P., Hasselt, N.E., Haneveld, F., Lakeman, A., Zwijnenburg, D.A., van Sluis, P., Bexell, D., Adameyko, I., Jansky, S., Westermann, F., Wigerup, C., Påhlman, S., Koster, J., Versteeg, R., van Nes, J., 2021. An immature subset of neuroblastoma cells synthesizes retinoic acid and depends on this metabolite.

van Noesel, M.M., 2012. Neuroblastoma stage 4S: a multifocal stem-cell disease of the developing neural crest. The Lancet Oncology 13. https://doi.org/10.1016/S1470-2045(12)70012-8
Vasconcelos, F.F., Castro, D.S., 2014. Transcriptional control of vertebrate neurogenesis by the proneural factor Ascl1. Frontiers in Cellular Neuroscience 8. https://doi.org/10.3389/fncel.2014.00412

Vik, T.A., Pfluger, T., Kadota, R., Castel, V., Tulchinsky, M., Farto, J.C.A., Heiba, S., Serafini, A., Tumeh, S., Khutoryansky, N., Jacobson, A.F., 2009. 123 I- m IBG scintigraphy in patients with known or suspected neuroblastoma: Results from a prospective multicenter trial. Pediatric Blood & Cancer 52. https://doi.org/10.1002/pbc.21932

Viprey, V.F., Gregory, W.M., Corrias, M. v., Tchirkov, A., Swerts, K., Vicha, A., Dallorso, S., Brock, P., Luksch, R., Valteau-Couanet, D., Papadakis, V., Laureys, G., Pearson, A.D., Ladenstein, R., Burchill, S.A., 2014. Neuroblastoma mRNAs Predict Outcome in Children With Stage 4 Neuroblastoma: A European HR- NBL1/SIOPEN Study. Journal of Clinical Oncology 32. https://doi.org/10.1200/JCO.2013.53.3604

Vitali, R., Mancini, C., Cesi, V., Tanno, B., Mancuso, M., Bossi, G., Zhang, Y., Martinez, R. v., Calabretta, B., Dominici, C., Raschellà, G., 2008. Slug (SNAI2) Down-Regulation by RNA Interference Facilitates Apoptosis and Inhibits Invasive Growth in Neuroblastoma Preclinical Models. Clinical Cancer Research 14. https://doi.org/10.1158/1078-0432.CCR-07-5210

Vo, K.T., Matthay, K.K., Neuhaus, J., London, W.B., Hero, B., Ambros, P.F., Nakagawara, A., Miniati, D., Wheeler, K., Pearson, A.D.J., Cohn, S.L., DuBois, S.G., 2014. Clinical, Biologic, and Prognostic Differences on the Basis of Primary Tumor Site in Neuroblastoma: A Report From the International Neuroblastoma Risk Group Project. Journal of Clinical Oncology 32. https://doi.org/10.1200/JCO.2014.56.1621

Vrenken, K.S., Vervoort, B.M.T., van Ingen Schenau, D.S., Derks, Y.H.W., van Emst, L., Grytsenko, P.G., Middelbeek, J.A.J., van Leeuwen, F.N., 2020. The transcriptional repressor SNAI2 impairs neuroblastoma differentiation and inhibits response to retinoic acid therapy. Biochimica et Biophysica Acta (BBA) - Molecular Basis of Disease 1866. https://doi.org/10.1016/j.bbadis.2019.165644

Vue, T.Y., Kollipara, R.K., Borromeo, M.D., Smith, T., Mashimo, T., Burns, D.K., Bachoo, R.M., Johnson, J.E., 2020. ASCL1 regulates neurodevelopmental transcription factors and cell cycle genes in brain tumors of glioma mouse models. Glia 68. https://doi.org/10.1002/glia.23873

Wang, L.H., Baker, N.E., 2015. E Proteins and ID Proteins: Helix-Loop-Helix Partners in Development and Disease. Developmental Cell 35, 269–280. https://doi.org/10.1016/j.devcel.2015.10.019

Wang, L., Tan, T.K., Durbin, A.D., Zimmerman, M.W., Abraham, B.J., Tan, S.H., Ngoc, P.C.T., Weichert-Leahey, N., Akahane, K., Lawton, L.N., Rokita, J.L., Maris, J.M., Young, R.A., Look, A.T., Sanda, T., 2019. ASCL1 is a MYCN- and LMO1-dependent member of the adrenergic neuroblastoma core regulatory circuitry. Nature Communications 10. https://doi.org/10.1038/s41467-019-13515-5

Wang, Y., Gao, S., Wang, W., Xia, Y., Liang, J., 2018. Downregulation of N-Myc inhibits neuroblastoma cell growth via the Wnt/β-catenin signaling pathway. Molecular Medicine Reports. https://doi.org/10.3892/mmr.2018.8966

Wapinski, O.L., Lee, Q.Y., Chen, A.C., Li, R., Corces, M.R., Ang, C.E., Treutlein, B., Xiang, C., Baubet, V., Suchy, F.P., Sankar, V., Sim, S., Quake, S.R., Dahmane, N., Wernig, M., Chang, H.Y., 2017. Rapid Chromatin Switch in the Direct Reprogramming of Fibroblasts to Neurons. Cell Reports 20. https://doi.org/10.1016/j.celrep.2017.09.011

Wapinski, O.L., Vierbuchen, T., Qu, K., Lee, Q.Y., Chanda, S., Fuentes, D.R., Giresi, P.G., Ng, Y.H., Marro, S., Neff, N.F., Drechsel, D., Martynoga, B., Castro, D.S., Webb, A.E., Südhof, T.C., Brunet, A., Guillemot, F., Chang, H.Y., Wernig, M., 2013. Hierarchical Mechanisms for Direct Reprogramming of Fibroblasts to Neurons. Cell 155. https://doi.org/10.1016/j.cell.2013.09.028

Weiss, W.A., Aldape, K., Mohapatra, G., Feuerstein, B.G., Michael Bishop, J., 1997. Targeted expression of MYCN causes neuroblastoma in transgenic mice whether the genetic events that give rise to neuroblastoma The evidence that MYCN participates in the genesis of, The EMBO Journal.

Whittle, S.B., Smith, V., Doherty, E., Zhao, S., McCarty, S., Zage, P.E., 2017. Overview and recent advances in the treatment of neuroblastoma. Expert Review of Anticancer Therapy 17. https://doi.org/10.1080/14737140.2017.1285230

Whyte, W.A., Orlando, D.A., Hnisz, D., Abraham, B.J., Lin, C.Y., Kagey, M.H., Rahl, P.B., Lee, T.I., Young, R.A., 2013. Master Transcription Factors and Mediator Establish Super-Enhancers at Key Cell Identity Genes. Cell 153. https://doi.org/10.1016/j.cell.2013.03.035

Woods, W.G., Gao, R.-N., Shuster, J.J., Robison, L.L., Bernstein, M., Weitzman, S., Bunin, G., Levy, I., Brossard, J., Dougherty, G., Tuchman, M., Lemieux, B., 2002. Screening of Infants and Mortality Due to Neuroblastoma. New England Journal of Medicine 346. https://doi.org/10.1056/NEJMoa012387

Woods, W.G., Tuchman, M., Robison, L.L., Bernstein, M., Leclerc, J.-M., Brisson, L.C., Brossard, J., Hill, G., Shuster, J., Luepker, R., Byrne, T., Weitzman, S., Bunin, G., Lemieux, B., 1996. A population-based study of the usefulness of screening for neuroblastoma. The Lancet 348. https://doi.org/10.1016/S0140-6736(96)06020-5

Wu, Z.L., Schwartz, E., Seeger, R., Ladisch, S., 1986. Expression of GD2 ganglioside by untreated primary human neuroblastomas. Cancer research 46.

Wylie, L.A., Hardwick, L.J.A., Papkovskaia, T.D., Thiele, C.J., Philpott, A., 2015. Ascl1 phospho-status regulates neuronal differentiation in a Xenopus developmental model of neuroblastoma. Disease Models & Mechanisms 8. https://doi.org/10.1242/dmm.018630

Yamada, Y., Beltran, H., 2021. Clinical and Biological Features of Neuroendocrine Prostate Cancer. Current Oncology Reports 23. https://doi.org/10.1007/s11912-020-01003-9

Yang, L., Ke, X.-X., Xuan, F., Tan, J., Hou, J., Wang, M., Cui, H., Zhang, Y., 2016. PHOX2B Is Associated with Neuroblastoma Cell Differentiation. Cancer Biotherapy and Radiopharmaceuticals 31. https://doi.org/10.1089/cbr.2015.1952

Yu, A.L., Gilman, A.L., Ozkaynak, M.F., London, W.B., Kreissman, S.G., Chen, H.X., Smith, M., Anderson, B., Villablanca, J.G., Matthay, K.K., Shimada, H., Grupp, S.A., Seeger, R., Reynolds, C.P., Buxton, A., Reisfeld, R.A., Gillies, S.D., Cohn, S.L., Maris, J.M., Sondel, P.M., 2010. Anti-GD2 Antibody with GM- CSF, Interleukin-2, and Isotretinoin for Neuroblastoma. New England Journal of Medicine 363. https://doi.org/10.1056/NEJMoa0911123

Zanni, E. di, Bianchi, G., Ravazzolo, R., Raffaghello, L., Ceccherini, I., Bachetti, T., 2017. Targeting of PHOX2B expression allows the identification of drugs effective in counteracting neuroblastoma cell growth. Oncotarget 8. https://doi.org/10.18632/oncotarget.19922

Zeid, R., Lawlor, M.A., Poon, E., Reyes, J.M., Fulciniti, M., Lopez, M.A., Scott, T.G., Nabet, B., Erb, M.A., Winter, G.E., Jacobson, Z., Polaski, D.R., Karlin, K.L., Hirsch, R.A., Munshi, N.P., Westbrook, T.F., Chesler, L., Lin, C.Y., Bradner, J.E., 2018. Enhancer invasion shapes MYCN-dependent transcriptional amplification in neuroblastoma. Nature Genetics 50. https://doi.org/10.1038/s41588-018-0044-9

Zhang, Qitong, Zhang, Qingquan, Jiang, X., Ye, Y., Liao, H., Zhu, F., Yan, J., Luo, L., Tian, L., Jiang, C., Chen, Y., Liang, X., Sun, Y., 2019. Collaborative ISL1/GATA3 interaction in controlling neuroblastoma oncogenic pathways overlapping with but distinct from MYCN. Theranostics 9. https://doi.org/10.7150/thno.30199

Zimmerman, M.W., Durbin, A.D., He, S., Oppel, F., Shi, H., Tao, T., Li, Z., Berezovskaya, A., Liu, Y., Zhang, J., Young, R.A., Abraham, B.J., Look, A.T., 2020. Retinoic acid rewires the adrenergic core regulatory circuitry of childhood neuroblastoma.